

VILNIUS UNIVERSITY

Edvinas Orentas

Design of supramolecular tubular
structures based on bicyclo[3.3.1]nonane
framework

Doctoral dissertation
Physical sciences, chemistry (03 P)

Vilnius, 2009

The research has been carried out at the Vilnius University during the years 2005-2009.

Research supervisor:

prof. habil. dr. Eugenijus Butkus

Table of contents

List of abbreviations	5
Acknowledgements	7
1. Objectives and outline of the thesis	8
2. Synthesis and enantiomer resolution of bicyclo[3.3.1]nonane-2,6-dione	10
2.1 Introduction to bicyclo[3.3.1]nonanes	10
2.2 Baker's yeast for the reduction of bicyclic ketones	15
2.3 Large scale synthesis of bicyclo[3.3.1]nonane-2,6-dione	19
2.4 Kinetic resolution of bicyclo[3.3.1]nonane-2,6-dione	21
3. Hydrogen bonded tubular assemblies based on bicyclo[3.3.1]nonane framework	25
3.1 Hydrogen bonding	25
3.2 Tautomers in supramolecular chemistry	29
3.2.1 Introduction	29
3.2.2 2-Pyridone/2-hydroxypyridine	31
3.2.3 Phtalhydrazides	33
3.2.4 Melamine-cyanuric acid complexes	35
3.2.5 Dihydropyridines	36
3.2.6 Quadruple hydrogen bonding modules	39
3.2.7 Cyclo-tautomerism	44
3.3 Hydrogen bonded tubular assemblies	46
3.3.1 General strategies for tubular structures design.	46
3.3.2 Cyclic peptides and related structures	47
3.3.3 Carbohydrates	51
3.3.4 Calixarenes	51
3.3.5 Barrels	52
3.3.6 G-quartets and related systems	53
3.4 Design of synthons for tubular aggregation	56
3.5 1 st generation synthon	59
3.5.1 Synthesis	59
3.5.2 Aggregation studies in solution	63
3.6 2 nd and 3 rd generation synthons	73
3.6.1 Synthesis	73
3.6.2 Synthesis of 9-azabicyclo[3.3.1]nonane analogues	91
3.6.3 Tetrameric tautoleptic aggregation	97
3.6.4 Polymeric aggregation of decyl substituted tautoleptic synthon	122
3.6.5 Association studies of 4H bonding synthon	127
4. Chiroptical properties of bicyclic enones	131
4.1 Introduction	131
4.2 Synthesis of enones	132
4.3 CD spectroscopic studies	133
5. Solid state analysis	138
5.1 Introduction	138
5.2 The diol, dione and acetal	142
5.3 Unsaturated derivatives	146
6. Conclusions.	151
7. Experimental section	153

8. References	184
-------------------------	-----

List of abbreviations

AcOH	acetic acid
Boc	tert-butyloxycarbonyl
BuLi	butyl lithium
tBuLi	tert-butyl lithium
BPLED	bipolar longitudinal eddy current delay
CD	circular dichroism
CDI	carbonyl diimidazole
CE	Cotton effect
COSY	correlation spectroscopy
cryo-TEM	cryoscopic transmission electron spectroscopy
DBU	diaza(1.3)bicyclo[5.4.0]undecane
DCM	dichloromethane
DMA	dimethylacetamide
DMC	dimethylcarbonate
DMF	dimethylformamide
DMSO	dimethylsulfoxide
DNA	deoxyribonucleic acid
DOSY	diffusion-ordered spectroscopy
DP	degree of polymerization
GPC	gel permeation chromatography
IBX	2-iodoxybenzoic acid
HMPTA	hexamethylphosphorotriamide
HMBC	heteronuclear multiple bond coherence
HMQC	heteronuclear multiple quantum coherence
LiHMDS	lithium hexamethyldisilazane

MCF	methyl chloroformate
MCPBA	<i>meta</i> -chloroperbenzoic acid
MS	molecular sieves
MW	microwaves
NAD	nicotinamide adenine nucleotide
NMO	N-methylmorpholine N-oxide
NMR	nuclear magnetic resonance
NOE	nuclear Overhauser effect
NOESY	nuclear Overhauser effect spectroscopy
OXONE	potassium peroxomonosulfate
PCC	pyridinium chloroformate
PDC	pyridinium dichromate
Py	pyridine
ROESY	rotating frame Overhauser spectroscopy
RSS	residual square sum
VPO	vapour phase osmometry
VT	variable temperature
TBME	<i>tert</i> -butyl methyl ether
TFA	trifluoroacetic acid
TFAA	trifluoroacetic acid anhydride
TLC	thin layer chromatography

Acknowledgements

This research has been supported by the Lithuanian Science and Studies Foundation, Swedish Institute (New Visby programme), Swedish Foundation for Strategic Research and Nordforsk via the Nordic-Baltic Network in Crystal Engineering and Supramolecular Materials.

1 Objectives and outline of the thesis

The derivatives of bicyclo[3.3.1]nonane are known to be embodied in the structure of a diverse variety of natural products and are important intermediates in the synthesis of complex molecular structures. In contrast to rather well developed synthetic chemistry of bicyclo[3.3.1]nonanes, the examples of the application of these compounds in supramolecular chemistry are very scarce to mention lattice inclusion hosts, crown ethers, etc. The unique V-shape of the bicyclic scaffold is obtained fusing the cyclohexane rings with aromatic(heteroaromatic) units. The geometric features may be combined with the chirality of the system, resulting from the functionalization of bicyclic core at proper positions.

The aim of this thesis is to explore stereochemical multiplicity of the bicyclo[3.3.1]nonane framework for the construction of chiral, C_2 -symmetric supramolecular preprogrammed synthons containing hydrogen bonding recognition patterns at both ends of the molecule. The resulting cleft molecules would be utilized for the formation of tubular structures via end-to-end association of these synthons.

The large scale synthesis of the most affordable starting material bicyclo[3.3.1]nonane-2,6-dione is described in Chapter 2. The improved dynamic kinetic resolution of racemic compound using fermentation with Baker's yeast for sweet dough is also presented in Chapter 2 opening access to the enantiomerically pure diketone.

Chapter 3 is concerned with the synthesis of the supramolecular synthons and their association studies in solution. The numerous analytical techniques including various NMR methods, vapour pressure osmometry and UV spectroscopy are applied to reveal the mode of aggregation and the supramolecular structures of several synthons are compared.

The chiroptical properties of some bicyclic enones are the subject of Chapter 4. The synthesis of mono- and di-functionalized enones is presented and absolute configuration stated by using the octant rule.

The crystal structure of selected bicyclo[3.3.1]nonane derivatives is described in Chapter 5. The results of application of network approach for the analysis of solid state aggregation are given in this chapter.

2 Synthesis and enantiomer resolution of bicyclo[3.3.1]nonane-2,6-dione

2.1 Introduction to bicyclo[3.3.1]nonanes

The synthetic chemistry of bicyclo[3.3.1]nonanes started more than one hundred years ago and since then this type of compounds received much attention as a useful molecular scaffolds with vast potential applications.^{1,2} The structure of bicyclo[3.3.1]nonanes is encountered in many important natural products, such as huperzine A **1** and B **2**, garsubellin A **3** and many other related sesquiterpenoids **4-6**^{3,4,5} (Figure 1).

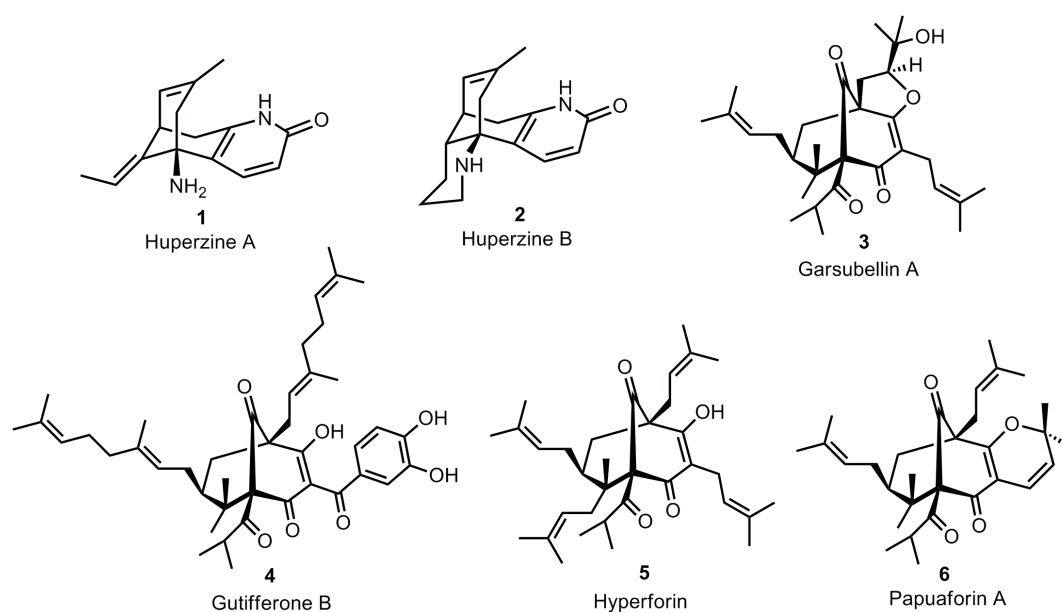


Figure 1: Naturally occurring bicyclo[3.3.1]nonane derivatives with anti-Alzheimer activity

Huperzine A and B, and garsubellin A are potent inducers of choline acetyltransferase activity in vitro at micromolar concentrations. Neurodegenerative diseases such as Alzheimer's, have been attributed to deficiencies in the levels of neurotransmitter acetylcholine. Consequently, the inducers of the enzyme, which participates in the biosynthesis of acetylcholine

have potential in developing therapeutics for treatment of Alzheimer's disease. In huperzine, the bicyclo[3.3.1]nonane framework is fused with heterocyclic pyridone moiety, while the vast majority of garsubellin related compounds belongs to a family of phloroglucin derivatives having highly oxygenated bicyclo[3.3.1]nonane-1,3,5-trione core, functionalized with one or several prenyl groups. Besides the application in treatment of neurodegenerative diseases, the terpene-like compounds incorporating bicyclo[3.3.1]nonane fragment are used as a fragrance components.⁶ A large variety of these compounds is isolated from natural sources and they are sometimes called "wood nonanes". As a consequence of frequent occurrence of this structural motif in a range of important compounds, the bicyclo[3.3.1]nonanes have been utilized as synthons to access complex ring topologies en route to many natural products, such as juvabione **7** and iophiobolin **8** (**Figure 2**).^{7,8}

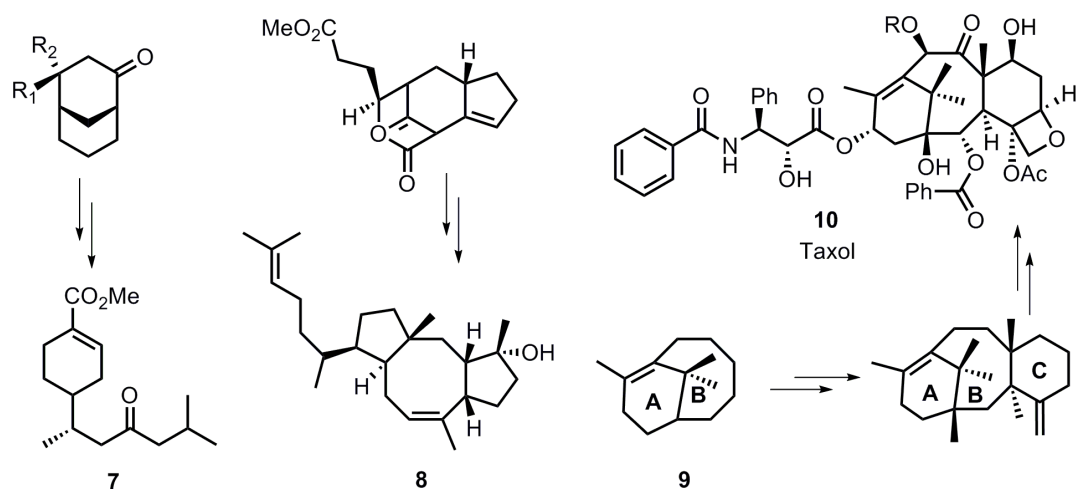


Figure 2: The application of bicyclic synthons for the synthesis of juvabione **7**, iophioboline **8**, and the AB ring system **9** of taxol.

The potential possibilities for the ring enlargement or contractions within bicyclic scaffold even more increase the value of these building blocks. For instance, the synthetic sequence leading to bicyclo[3.3.1]nonane structure has been applied in the synthesis of bicyclo[5.3.1]undecane AB fragment **9** of taxane compounds (**Figure 2**). Formation of the aforementioned bicyclic part of the taxane molecule usually presents the most difficult synthetic task.

From the theoretical point of view, bicyclo[3.3.1]nonanes are perfect model compounds for studying conformational equilibrium.^{9,10} The bicyclic skeleton is composed of two cyclohexane rings, connected together at the bridging positions. The conformational preference of one cyclohexane ring is influenced by substitution pattern not only on that particular ring, but also largely affected by substituents on the second cyclohexane ring. The bicyclo[3.3.1]nonane framework can in principle exist in three different conformations: chair-chair (cc), boat-chair (bc) and chair-boat (cb) and boat-boat (bb) (**Figure 3**).

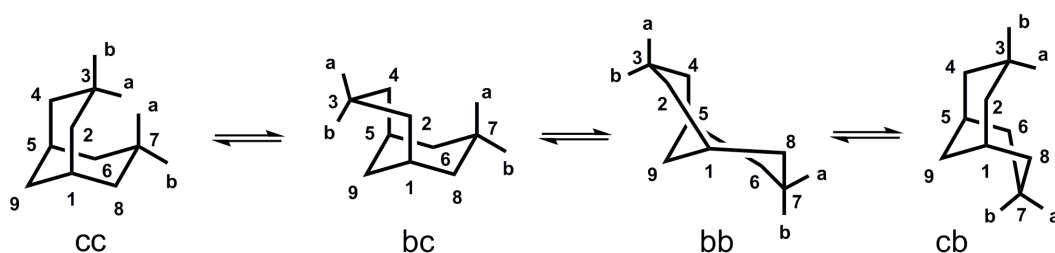


Figure 3: Conformational equilibrium of bicyclo[3.3.1]nonane; cc – chair-chair, bc – chair-boat, bb – boat-boat, cb – chair-boat.

In many cases, the double chair conformation (cc) is the most stable; however, by introducing substituents in certain positions of bicyclic structure, the conformational preference may be altered. The strongest influence is observed at the 3- and 7-positions. As fully unsubstituted bicyclo[3.3.1]nonane, the 3b-substituted or 3,7 bb-disubstituted derivatives exist mainly in cc conformation, although in the latter case significant flattening of cyclohexane ring is observed. The substitution either of 3a- or 7a-position force the substituted cyclohexane ring to adopt thermodynamically more favoured boat-chair conformation in which spatial interaction between two cyclohexane rings is reduced. When both 3a- and 7a-positions are substituted, the population of chair-boat and boat-chair conformations depends on the size of substituents. In case of bulky substituents, the boat-boat conformation predominates, whereas with small substituents the chair-boat and boat-chair conformers are major components. The conformational preference may change drastically by going from a solution to a solid state, where the most stable conformation is

determined by crystal packing forces. Since the relative arrangement of functional groups in the molecule is modified during the conformational change, the reactivity of the compound might also be changed (see chapter 3 for example). Due to the spatial proximity of different functionalities located across the bicyclic framework, these compounds display an extensive reactivity involving intramolecular ring closure as one of the steps^{11,12}.

In 1970's, the special theoretical and synthetic interests were devoted to bicyclo[3.3.1]nonane skeleton as a model compound to verify the validity of Bredt's rule.¹³ According to Bredt's rule, formation of the double bond at bridgehead position of bicyclic systems is impossible due to the strain imposed by the geometry of double bond. The unsaturated compound bicyclo[3.3.1]non-1-ene **10** was synthesized in 1967, and was shown to be the smallest "anti-Bredt" compound (**Figure 4**).^{14,15}

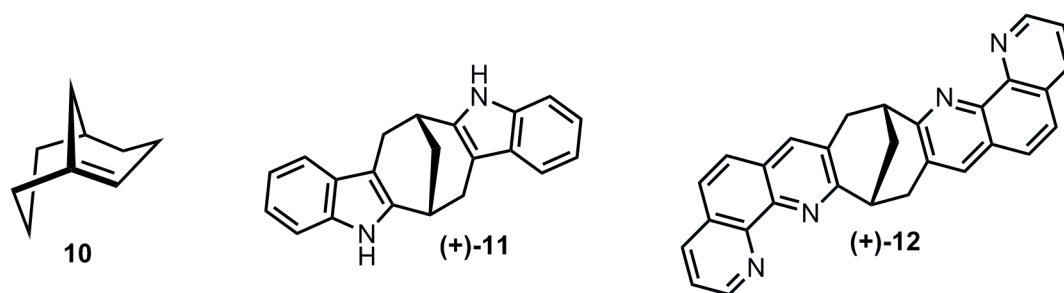


Figure 4: "anti-Bredt" molecule **10**; C₂ symmetric chiral cleft molecules (+)-**11** and (+)-**12** possessing interacting chromophores.

The bicyclo[3.3.1]nonane can be chiral by virtue of substitution pattern. The chiral derivatives of bicyclic system are of special importance, as many naturally occurring compounds exist as single enantiomers. In addition, chirality is of utmost importance when considering biological activity of these compounds. The chiral bicyclo[3.3.1]nonanes are less synthetically available and thus represent a serious synthetic challenge. The bicyclic framework offers a platform for the attachment of different chromophores for the analysis of chiroptical properties of the systems obtained. The bicyclo[3.3.1]nonane derivatives are especially attractive for multichromophoric system studies as

the contribution from conformer's distribution, interchromophoric distance or/and angle between them can be evaluated from the chiroptical properties of the molecule. For example, interaction of two chromophores through space resulted in exciton coupling in compounds (+)-**11** and (+)-**12**, as evident from their CD spectra (**Figure 4**).

The applicability of the octant rules to bicyclo[3.3.1]nonane system was tested by using a series of compound containing carbonyl chromophores.^{16,17} The recent application of bicyclic dienes as a ligand for highly enantioselective rhodium catalyzed addition of arylboronic acid to enones illustrate the potential of related structures in asymmetric synthesis.¹⁸ The fact that the chiral diene ligand was obtained by chiral HPLC separation of racemic mixture emphasizes the necessity for the convenient method allowing to obtain enantiomerically pure bicyclo[3.3.1]nonane derivatives.

Compared to its aza-cousin, Tröger's base¹⁹ **13**, the use of the carbocyclic bicyclononane analogue in supramolecular chemistry remains almost unexploited. Naemura et al.²⁰ reported the use of chiral bicyclic diols, obtained by enzymatic resolution of corresponding racemic acetates, for the synthesis of crown ethers and podands. The chiral crown ether **14** was shown to display only weak chiral discrimination of (\pm)-1,2-diphenylethylamine, whereas crown ether **15** containing bicyclo[3.3.1]nonane framework fused with aromatic moieties as an additional bulky steric barrier²¹ was by far more efficient (**Figure 5**).

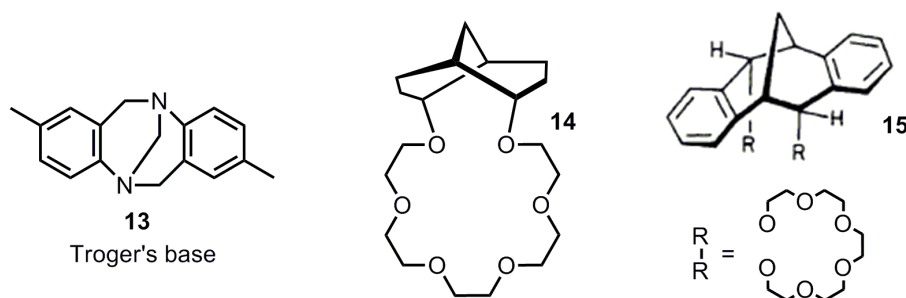


Figure 5: Chiral molecules with bicyclo[3.3.1]nonane framework used in supramolecular chemistry; Troger's base **13**, crown ethers **14** and **15**.

The bicyclo[3.3.1]nonane fused with aromatic or heteroaromatic rings undergoes a flattening of both cyclohexane rings resulting in V-shaped molecule. Unlike Tröger's base, these compounds are configurationally stable in acidic or basic solutions. The two aromatic "wings" of the molecule make almost 90° degree turn and is preorganized to form cyclic or helical aggregates provided it contains recognition patterns at both ends of the molecule. The solid state structure of bicyclo[3.3.1]nonanes fused with quinoline or quinoxaline ring **16a-b** has been reported by Bishop et al.²² The crystal structure of compounds **16a-b** is stabilized by C-H...N interaction forming molecular boxes able to encapsulate solvent molecules (**Figure 6**).

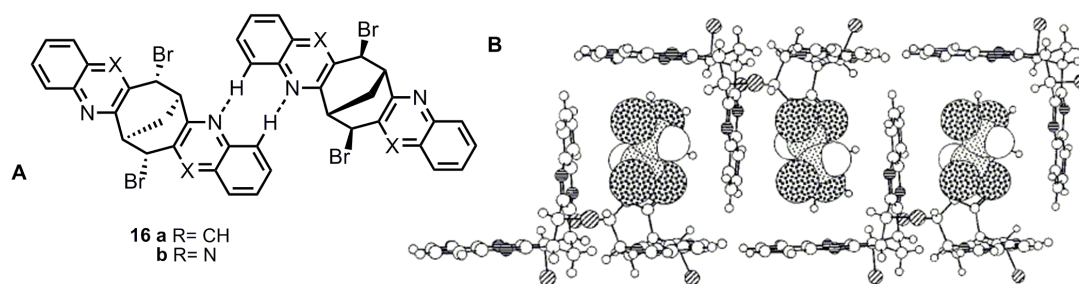


Figure 6: a) C-H...N interactions between cleft molecules **16a-b** in solid state; b) molecular boxes formed by **16b** with encapsulated solvent ($\text{CHCl}_2\text{CHCl}_2$).

2.2 Baker's yeast for the reduction of bicyclic ketones

The continuous interest in the preparation of enantiomerically enriched compounds has become even more important nowadays in relation with growing demand of single enantiomer drugs in pharmaceutical market. Together with wide arsenal of asymmetric catalysts available, the enzyme catalyzed asymmetric transformations have proved to be efficient way for creation of chiral centers in environmentally benign manner. The ability of more than two thousands enzymes to catalyze almost every known chemical reaction is highly recognized.

The microbial reduction of carbonyl compounds is classical and well documented method to prepare chiral alcohols, which are further utilized as starting materials in preparation of a range of important compound. The asymmetric reduction with fermenting yeasts (*Sacharomyces cerevisiae*) in many cases is preferred over traditional metal-based catalysts as higher enantioselectivities are obtained under milder conditions. The central microorganism in Baker's yeast usually contains a number of oxireductases and consequently, a variety of carbonyl compounds were reduced to corresponding alcohols. A highly simplified mechanism of the overall process is depicted in **Figure 7**. The enzyme catalysed reduction in the cell is mediated by NADPH dependant enzyme, and, after producing the alcohol, NAD cofactor needs to be regenerated. Although external reductants such as $\text{Na}_2\text{S}_2\text{O}_4$ or second enzyme may accomplish this task, the most common way relies on the use of metabolism of co-substrate (auxiliary substrate), e.g. sucrose or glucose. The use of large amount of co-substrate and accumulation of various metabolites produced by microorganism are the serious drawbacks associated with the use of living cells. On the other hand, the Baker's yeasts are inexpensive and are easy to use without assistance of microbiologist, the feature especially attractive for organic chemist.

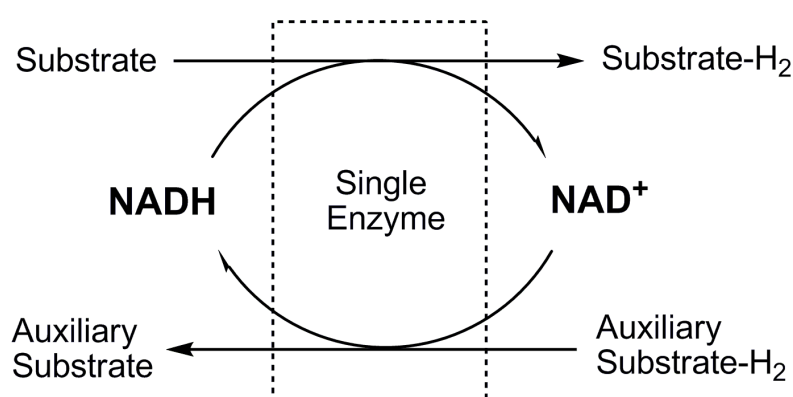


Figure 7: Simplified working mechanism of dehydrogenase enzyme in the cell of Baker's yeast.

A number of important chiral bicyclic structure are available from asymmetric reduction of corresponding ketones with Baker's yeast. The substrates having

more than one carbonyl functionality are very attractive from the synthetic point of view as the high diversity of possible transformations with the reduction product can be envisioned. The utilization of Baker's yeast reduction may be divided in two general cases depending on the structure of starting diketone. When the substrate is prochiral, e.g. contains a plane of symmetry, the mono-reduction product is a chiral molecule and the full conversion of starting material is required to get the best yield of the latter. On the other hand, when the starting dione is chiral, the compound undergoes dynamic kinetic resolution resulting in a mixture of enantiomerically enriched starting material and reduction product. Although the complete resolution is possible, in many cases one of the products has higher enantiopurity. The first approach was demonstrated by Mori et al.²³ in a series of publications describing Baker's yeast mediated reduction of prochiral bicyclo[2.2.2]octane-2,6-diones **17a-c** (**Figure 8**). The corresponding hydroxy ketones were obtained in high enantio- and diastereopurity, except the unsubstituted dione **17a**, reduction of which gave a mixture of diastereomers **18a-b**. It was found that repeated fermentation greatly improved the stereoselectivity of the reaction. The cumbersome workup due to large amount of yeast used can be obviated by application of genetically engineered yeast strains.²⁴

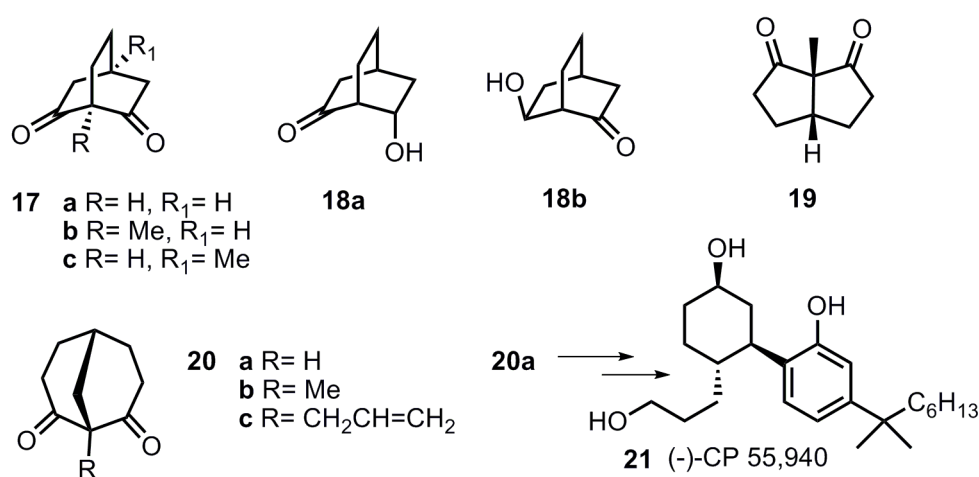


Figure 8: Prochiral bicyclic ketones reduced by Baker's yeast.

The reduction of [3.3.0] dione **19** proceeded exclusively from less hindered side with perfect enantioselectivity (**Figure 8**). The same conditions were successfully applied to the reduction of prochiral bicyclo[3.3.1]nonane-2,8-diones **20a-c**.²⁵ The enantiomerically pure hydroxy ketone, derived from the reduction of **20a**, was recently used as a starting compound for the synthesis of potent cannabinoid receptor (-)-CP 55,940 **21**.²⁶ The kinetic resolution of racemate of C_2 -symmetric bicyclic diones is also known. Racemic bicyclo[3.3.1]nonane-2,6-dione **22** was reduced by Baker's yeast and the (+)-**(1S,5S)-22** could be obtained in 24% yield (93% ee) on a small scale whereas an ee of 66% was achieved (after 2 days) on a larger scale preparation, which increased to 83% after a total reaction time of 6 days (31% yield).²⁷ **(1R,2S,5R)-22a** and **(1S,2S,5S)-22b** in an 85:15 ratio and 5% of diol were isolated. (+)-**(1S,5S)-22** of 60% ee (isolated after 18 h) was subjected to a second reduction (24h) to yield (+)-**(1S,5S)-22** of 96% ee (**Figure 9**). The more recent publication described a short time reduction (24h) of **22** on a small scale and under high dilution conditions to give (+)-**(1S,5S)-22** of 99% ee.²⁸ In the kinetic resolution of bicyclo[2.2.2]oct-7-ene-2,5-dione **23**, the 1S,5S enantiomer is reduced preferentially.²⁹

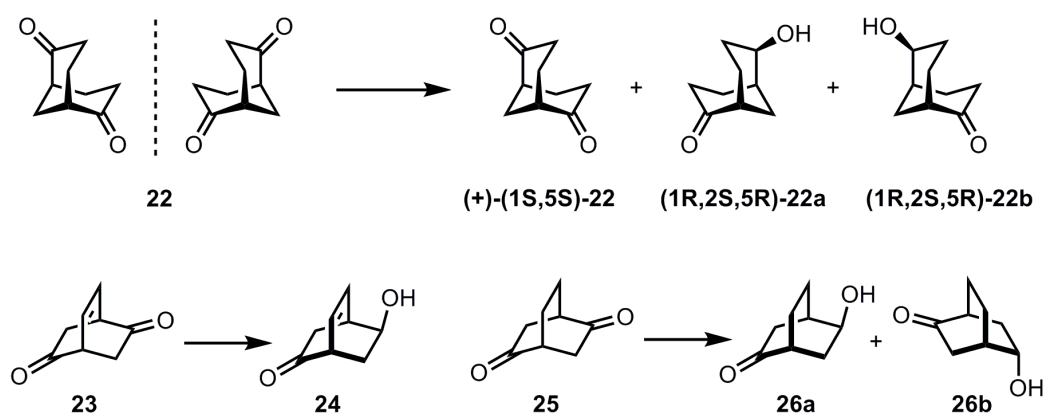


Figure 9: Chiral C_2 -symmetric bicyclic ketones reduced by Baker's yeast.

The reduced product **24** is obtained nearly enantiomerically pure and the unreacted enedione **23** has a lesser ee. In long reduction period, the unreacted enedione **23** is enantiomerically pure and hydroxy ketone has a lesser ee. The

reduction of saturated analogue **25** gave a mixture of two diastereomeric hydroxy ketones in high ee.³⁰

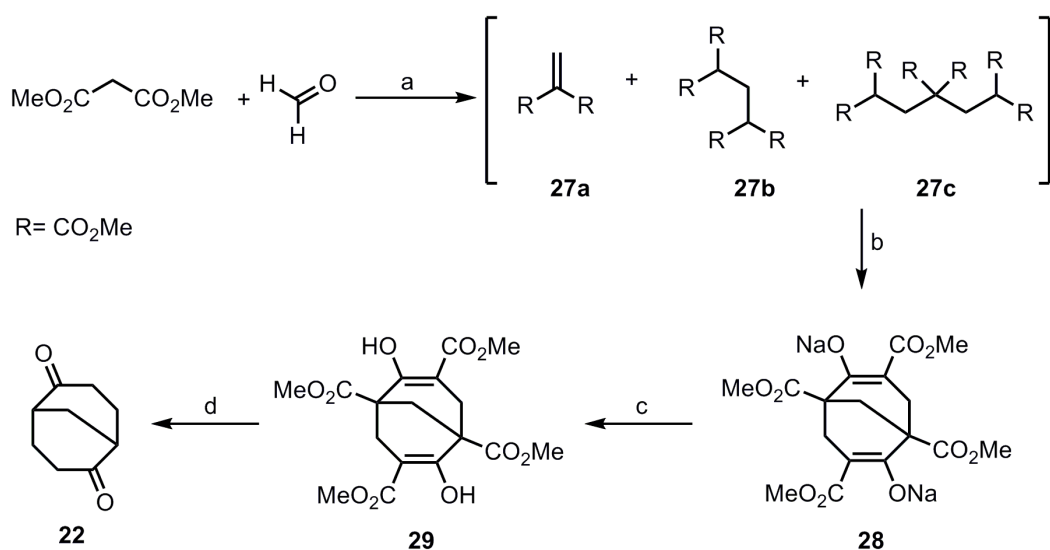
2.3 Large scale synthesis of bicyclo[3.3.1]nonane-2,6-dione

The bicyclo[3.3.1]nonane-2,6-dione **22** is perhaps the most useful and easily available starting material for the synthesis of large number of bicyclo[3.3.1]nonane derivatives. The diketone molecule **22** is C₂-symmetric and thus chiral. The synthesis of its racemate is straightforward and involves the use of simple and cheap reagents. It was reported that enantiomerically pure dione **22** can be obtained, among other methods, via kinetic resolution of racemate with Baker's yeast. An extensive utilization of this compound in our projects was the main reason for us to improve the methodology for large scale synthesis of (+)-**22**.

In 1913 Meerwein and Schurman synthesized a fascinating bicyclic compound, 2,6-dihydroxybicyclo[3.3.1]nonane-2,6-diene-1,3,5,7-tetramethylcarboxylate **29**, later known as Meerwein ester, by two step condensation of formaldehyde with dimethylmalonate.³¹ At the same time, it was realized that Meerwein ester could be converted to bicyclo[3.3.1]nonane-2,6-dione **22** by acidic hydrolysis and simultaneous thermal decarboxylation. Since then, a several improvements in the synthesis of **22** have been published and the most often employed today is the procedure developed by Schaefer and Honig.³² The reported yields for the **29** are rather scattered and varies from 8% to 67%, most frequently close to 50%. By combining different smaller variation of these syntheses together with our own experience in the preparation of **22**, we achieved 72% yield for the Meerwein ester **29**. The procedure was very reliable even on the scale up to 1.32 kg based on dimethyl malonate.

In the first step of Meerwein's ester synthesis, the dimethyl malonate is condensed with paraformaldehyde using piperidine as a base. The mixture of acyclic intermediates is formed, which results from aldol condensation of

dimethyl malonate and formaldehyde and subsequent Michael addition of another molecule of dimethyl malonate. It was found by Meerwein himself,³¹ that the major components of the mixture are compounds **27a-c** (Scheme 1). The water is formed from each aldol condensation step and needs to be removed in order to shift the equilibrium towards the formation of products. The best yields were obtained by following method of Schafer and Honig using benzene as a solvent.



Scheme 1: Reagents and conditions: a) benzene, piperidine, reflux, 26 h; b) MeOH, NaOMe, reflux, overnight; c) aq. HCl; d) AcOH, HCl, reflux, 24 h. Overall yield: 45%.

The water is efficiently removed by the aid of Dean-Stark trap. The use of less hazardous *tert*-butyl methyl ether, which also forms an azeotrope with water, was published, but the drastic decrease in yield of **29** convinced us to choose benzene as a solvent.³³ After completion of the first step, the removal of the solvent resulted in oily residue consisting of intermediates **27a-c**. In the next step, the mixture is subjected to sodium methoxide to complete the synthesis of **29** (Scheme 1). From the practical point of view, the use of commercially available sodium methoxide is preferred due to very long time required to dissolve metallic sodium (170 g for 1.32 kg scale based on dimethyl malonate). The disodium salt of Meerwein's ester **28** is very poorly soluble in methanol and can be easily isolated in high purity by simple filtration. Although it is possible to use the salt **28** directly for the next step, the higher yield is obtained

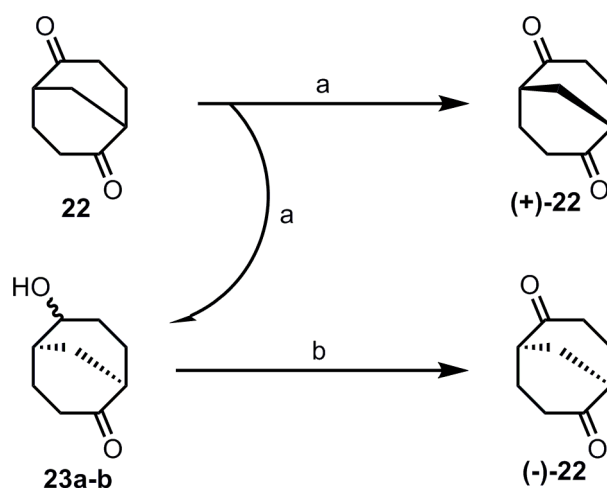
by using free **29**. The Meerwein's ester **29** was precipitated in 72% yield from aqueous solution of disodium salt **28** by addition of HCl, which we found to be more convenient than using CO₂ (g) as reported by Quast et al.³³ Following the usual decarboxylation procedure using a mixture of acetic acid and conc. HCl, **22** was isolated in overall 45% yield. We found that the crude **22**, obtained after removal of water, was rather sensitive to acid residues and gets yellow after short time. It was necessary to remove residual acid by washing solution of **22** in organic solvent with saturated NaHCO₃ solution. The pure **22** was obtained by washing crude compound with cold diethyl ether instead of crystallization. The 50% improvement compared to representative published overall yield of **22** was achieved.³⁴ The use of this procedure enabled us to synthesize **22** on a kilogram scale.

2.4 Kinetic resolution of bicyclo[3.3.1]nonane-2,6-dione

The enantiomeric enrichment of dione **22** was achieved by different methods including chromatographic resolution,³⁵ enzymatic reactions,^{36,37} desulfurization of 2-thioadamantane-4,8-dione³⁸ and by fractional crystallization.³⁹ For the synthesis of diketone **22** of high enantiomeric purity we did not find any of these routes satisfactory. For small scale enzymatic resolution, a recently published efficient procedure²⁸ for dynamic resolution with fast action Baker's yeast can be used, however when applied to larger scale, the amount of solvent necessary to ensure high dilution conditions becomes extremely large. Thus, the above mentioned procedure by Wiartalla and Hoffman²⁷ was modified and adopted for large scale synthesis. The main problem attributed to the use of more concentrated solution of substrate is the retardation of reduction rate and long reaction time as well as large amount of Baker's yeast and co-substrate needed to obtain highly enriched product. For the same reason, the fermentation process needs to be performed twice in a period of one week. In a described procedure the reaction mixture was extracted with diethyl ether using continuous extraction. From a practical point

of view, this procedure is time consuming. A common extraction with chloroform, using separatory funnel, was therefore preferred. However, after centrifugation, the fermentation mixture consists of remaining sucrose and a complex blend of cell lysate, which mainly includes lipids originating from membranes, glycolysis side products, and proteins. Due to the difficulties encountered with the workup of reaction mixture, the Baker's yeast reductions are sometimes called "intrinsically messy". The above mixture is responsible for the foam which forms upon extraction rendering separation process extremely tedious. In the wake of cumbersome workup, we envisioned that the lysis of yeast cells could be decreased by using Baker's yeast for sweet dough, which is known to have higher tolerance for osmotic pressure imposed by high sucrose concentration. Indeed, it was proved experimentally. The formation of foam was greatly suppressed and the kinetic resolution of **22** on a 10 gram scale became straightforward. However, increasing the scale even more, the formation of foam was still challenging. Attempts to precipitate the yeast proteins by changing pH or by addition of NaCl, urea, $(\text{NH}_4)_2\text{SO}_4$ or sodium dodecyl sulfate were unsuccessful. However, it was observed that when the fermentation mixture was saturated with NaCl, the formation of foam was greatly decreased during extraction. Hence, by combining the use of Baker's yeast for sweet dough in the fermentation process and saturating the reaction mixture with NaCl during workup, kinetic resolution of racemic **22** could be performed on a 90 g scale yielding 22 g of optically pure **22** (**Scheme 2**). Upon running parallel batches, it was possible to produce ~45 g of optically pure **22** ($ee > 99\%$, according to chiral GC). In addition to these improvements, Baker's yeast for sweet dough displayed rather higher activity compared to normal yeast reaching $ee > 99\%$ in 2-4 days during the second fermentation step depending on the quality of the yeast. Ordinary Baker's yeast reached the same ee value in 4-6 days. Using yeast with longer expiration date tended to reach high enantiomeric purity of (+)-**22** faster than yeast having shorter expiration date. Therefore, it was important to monitor the progress of the reaction since a

prolonged exposure of (+)-**22** to the yeast after ee>99% have been reached would have resulted in a diminished yield of (+)-**22**. The reduced compounds *endo*- and *exo*-6-hydroxybicyclo[3.3.1]nonane-2-ones **22a-b** formed in kinetic resolution of **22** are also enantiomerically enriched as a result of the process. The hydroxy ketone has higher water solubility than **22** and thus is less efficiently extracted from the mixture. Separation of **22a-b** on a large scale by chromatography is also cumbersome since an excessive amount of solvent is needed. Despite these drawbacks, the hydroxy ketone isolated from fermentation could act as a source of (-)-**22**. According to results from the work of Wiartalla and Hoffman, the hydroxy ketone had a ee of 58% using ordinary yeast. Hydroxy ketones **22a-b**, isolated from the kinetic resolution using Baker's yeast for sweet dough, were oxidized in quantitative yield using Ley-Griffith reagent as depicted in **Scheme 2**. The ee was determined to be 75%, which was a large increase in comparison to the results using normal Baker's yeast.



Scheme 2: Reagents and conditions: a) Baker's yeast for sweet dough, sucrose, yield 48%, ee>99%; b) TPAP, NMO, DCM, quantitative yield, ee= 75%.

However, as stated, (-)-**22** is only accessible in smaller amount due to incomplete extraction of hydroxyl ketones **22a-b** from water phase. The further enrichment of (-)-**22** could in principle be possible by fractional crystallization. The resolution of racemic **22** is feasible on 180 g scale

providing up to 45 g of (+)-**22**. To our knowledge this is the first kinetic resolution achieved by the use of Baker's yeast for sweet dough.

3 Hydrogen bonded tubular assemblies based on bicyclo[3.3.1]nonane framework

3.1 Hydrogen bonding

Despite the million years experience of Nature in utilizing non-covalent interactions, the chemists are only on their way to fully understand the principles that govern self-assembly, molecular recognition, energy transfer and many other fascinating processes. The supramolecular chemistry, defined as chemistry beyond the molecule, is greatly inspired by the Nature and endeavours to explore weak intermolecular forces to create functional molecular systems.⁴⁰ In molecular chemistry the molecules are assembled by creating and breaking covalent bonds, whereas in supramolecular chemistry the structures are build-up by the reversible self-assembly of molecular components. The main non-covalent bonding interactions applied in supramolecular chemistry include dipole-dipole interaction, π - π stacking and hydrogen bonding.⁴¹

Among all non-covalent interactions, hydrogen bonds are most widely used due to their strength and directionality. Many ingenious example of hydrogen bonding surround us including the structure and function of DNA and remarkable properties of water. Although the typical hydrogen bond is much weaker than covalent bond, it is comparable in strength with ion-dipole or dipole-dipole interactions.⁴² Hydrogen bonding involves interaction between electropositive hydrogen atom and electronegative atom. The strength of this bond type depends on the basicity of hydrogen acceptors (N,O,S,..) and the acidity of hydrogen donors. The strongest hydrogen bond known so far is in F-H-F⁻; the energy determined of this bonding is 163 kJ/mol.⁴³ The energy of a single hydrogen bond is generally smaller than the energetic difference between aggregation states that are formed under equilibrium conditions. To enhance the strength of interaction and promote the formation of single

construct, the multiple hydrogen bonds arranged in well-defined arrays within constituents of assembly are used. The cooperative action of single hydrogen bonds, as in β -sheets of polypeptides may also lead to a strong interaction.⁴⁴ The joint action of hydrogen bonding together with other type of non-covalent interaction is another way to reinforce the supramolecular structure.⁴⁵

Although the use of multiple hydrogen bonding in an array can ensure the strong association and directionality of bonding, the proper arrangement of hydrogen bond donors (D) and acceptors (A) also plays a significant role, as recognized by Jorgensen and coworkers.^{46,47} It was known before, that the complexes with equal number of hydrogen bond acceptors and donors might differ in stability. The complexes **30·31** and **32·33** have similar values of association constant (K_a), but the two other triply bounded complexes **34·35** and **36·37** displayed K_a values that were two orders of magnitude higher (**Figure 10**). The differences, as confirmed by theoretical calculations, were attributed to negative and positive interactions of electrostatic origin between adjacent donor and acceptor sites. Stabilization arises from the interaction of negatively and positively polarized atoms, whereas repulsion is experienced between two positively or negatively polarized atoms. In the DAD-ADA motif of complexes **30·31** and **32·33** each secondary interaction is repulsive and destabilize complex.

On the other hand, in complex DDA-AAD, the number of attractive and repulsive interactions is equal and offsets each other. Jorgensen further proposed that complex with AAA-DDD motif would experience only positive secondary interactions which has to result in extremely stable complex. This assumption was verified later by Zimmerman et al.,⁴⁸ who have shown 10^4 -fold difference in stability between ADA-DAD (**32·33**) and AAA-DDD (**38·39**) complexes. The same holds true for complexes with larger number of hydrogen bonding sites. The attempts to quantify the contribution from attractive and repulsive secondary interactions were reported by Schneider.⁴⁹ It was found that contribution to total energy is 1.9kcal/mol for each primary interaction and

± 0.69 kcal/mol for each secondary interaction, with the sign of the latter depending whether it is attractive or repulsive.

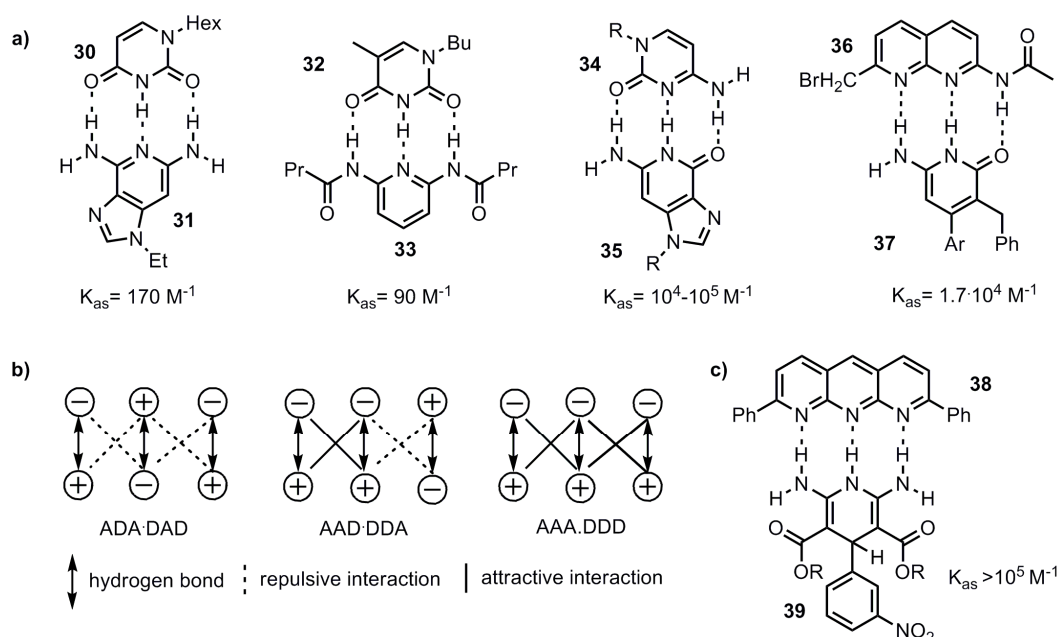


Figure 10: a) comparison of DAD-ADA and DDA-AAD complexes; b) schematic presentation of Jorgensen principle of secondary interactions in 3H-bonding modules; c) triple hydrogen bonded DDD-AAA complex.

It was long time ago recognized by Cram,⁵⁰ that for efficient binding of guest the recognition sites in the host has to be arranged in a way to maximum match the binding partner, e.g., they have to be preorganized. When the hydrogen bonding site in the array can undergo different kind of movement such as rotation about single bond or tautomeric translocation, the stability of the complex can be diminished due to improper positioning of hydrogen bond acceptors and donors. Zimmerman et al.⁵¹ have calculated that each free rotation costs ~ 1 kcal/mol of complex energy. For this reason, the majority of hydrogen bonded modules are composed of flat rigid heteroaromatic systems wherein most of the binding sites are freezed by incorporating them as constitutional parts of ring system. Meijer has attributed the higher stability of complexes **(41)**₂ and **(43)**₂ relative to **(40)**₂ and **(42)**₂ to the intramolecular hydrogen bond which retains the amide functionality preorganized for the formation of quadruple hydrogen bond.^{52,53} The other conformational issues,

even not directly related with hydrogen bonds may affect the level of preorganization. The heterodimer **44**·**45** was found to be unexpectedly loose compared to the similar **36**·**37** system.⁵⁴ The association constant for **44**·**45** was at least two orders of magnitude lower than for **36**·**37**. It was proposed that when the ethoxy group occupies the preferred orientation, the steric hindrance of this group prevents the formation of complex and the energetic penalty must be paid for conformational exchange. Incorporating the oxygen in a rigid lactone eliminated severe steric encumbrance resulting in complex **46**·**45** with $K_a > 10^4$ (**Figure 11**).⁵⁵

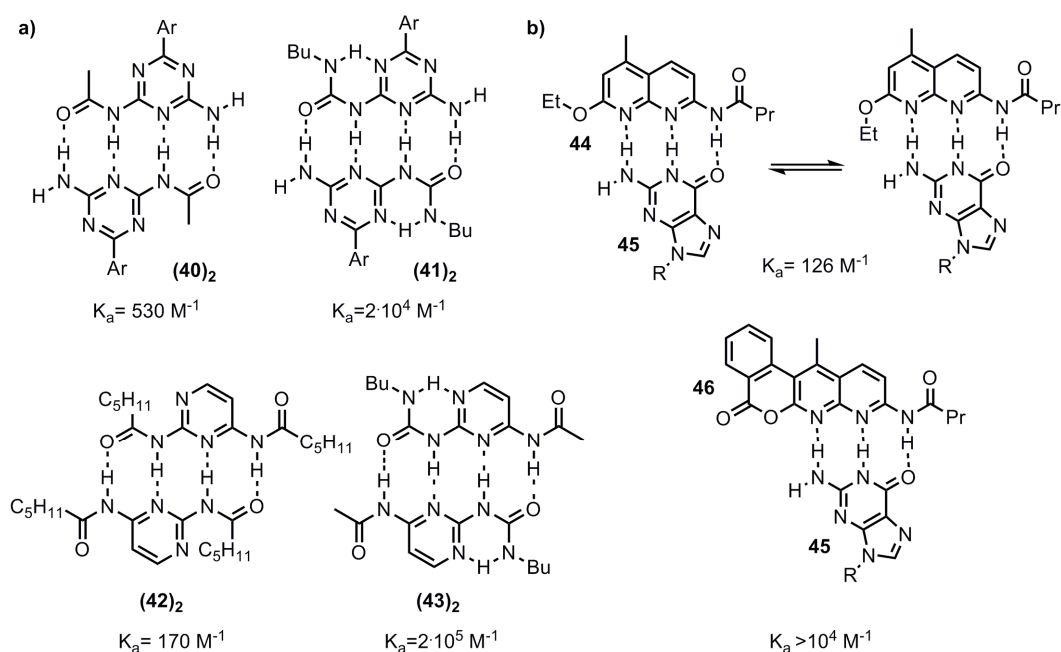


Figure 11: a) quadruple hydrogen bonded complexes with preorganizing intermolecular hydrogen bond **(41)**₂, **(43)**₂ and without **(40)**₂, **(42)**₂; b) effect of conformational freedom on complex stability.

Many other factors such as tautomeric equilibrium (*vide infra*), nature of solvent or temperature are important when considering the stability of hydrogen bonded complexes. The contribution a hydrogen bond makes to molecular interaction is, in the presence of polar solvent, limited to the extent with which the hydrogen bonding occurs within substrates or with the molecules of solvent. The polar solvent, able to act as hydrogen bond acceptor or/and donor, is therefore the competitive inhibitor of binding. For this reason,

the majority of binding studies are performed in the solvents of moderate polarity, most often, chloroform. Using even less polar solvent, such as hydrocarbons, increase the stability of aggregates even more. It should not be forgotten, that the ability of certain solvent to compete for hydrogen bonding does not always correlate with its polarity. For example, carbon tetrachloride with zero net dipole in some case leads to weaker interaction comparing to chloroform, due to the highly polarized C-Cl bond and the potential hydrogen bond acceptor nature of negatively polarized chlorine atoms. The solvation of the complex and its components is another important issue which is often disregarded when designing the components of assembly. The lesser solvation of components comparing to complex, benefits for the strength of association mainly via favorable enthalpic contribution. Nevertheless, the so-called entropically driven cases are known when more solvated substrates aggregate together with the release of excess solvent molecule thus increasing the entropy of the system.⁵⁶ The dipole moments of aggregating species and the complex may also affect complex stability as in the case of **38****39** dimer in which partial cancelation of large dipole moment of **38** and **39** occurs by forming hydrogen bonded complex. As a rule, the strength of hydrogen bond increases when the temperature is decreasing.

3.2 Tautomers in supramolecular systems

3.2.1 Introduction

In most cases, the realization of multiple hydrogen motifs is achieved by the synthesis of planar heteroaromatic units, where hydrogen bond acceptor A and donor D sites are arranged in geometrically well define arrays.⁵⁷ These modules, with some exceptions, are readily available in a few synthetic steps via known procedures using simple starting materials. Besides the hydrogen bonding motifs that are designed to form stable intermolecular complexes,

such molecules usually contain one or more intramolecular hydrogen bonds which serve as preorganizing element within the molecule to achieve particular binding mode. As a rule, the presence of multiple hydrogen bonding sites results in a mixture of different tautomers. In simplest case, when tautomerism involves the relocation of an H atom and a double bond, the term prototropic tautomerism or prototropy is sometimes used. The direction of tautomeric equilibrium is influenced by many factors such as temperature, solvent, aggregation state or by the presence of complementary hydrogen bonding partner. The rational design of supramolecules that may exist in several prototropic forms is extremely difficult due to the fact, that it is not trivial to assess the tautomeric composition. The presence of small amount of so-called parasitic tautomer, in which the hydrogen bonding sites are arranged in a way reducing the number of such sites available for the formation of intermolecular complex, could drastically decrease the association constant of complex or even prevent its formation. It is also possible to shift the tautomeric equilibria to favour one of the tautomers using different substituents having electron-accepting or electron donating properties. The steric congestion induced by substituent is another convenient mean to control tautomeric equilibrium. The subtle interplay between the tautomeric distribution and the ability to form intermolecular hydrogen bonded complex is thus a subject of prime importance in the field of supramolecular chemistry.

The presence of several constitutional isomers originated from tautomeric equilibrium has a profound effect in some important biological processes such as substitution mutagenesis of DNA. It is widely accepted that the misincorporation of tautomeric forms of natural nucleobases may be responsible for the mutation of DNA via amplification of incorrect recognition pattern during DNA replication. The “rare tautomer hypothesis” proposed by Watson and Crick⁵⁸ and later elaborated by Topal and Fresco⁵⁹ is strengthened by the fact that there is a direct correlation between the ratio of the tautomers (tautomeric constant) and the preferred nucleotide incorporation by some

polymerases. Fortunately, the tautomeric equilibrium of nucleobases favours the “right” keto and amino tautomeric forms by a ratio of 10^4 to 1 and a huge arsenal of many protecting enzymes responsible for elimination of mispaired bases makes such mutations to occur very rarely. Different tautomers may also have different pharmaceutical properties as exemplified in the case of 8-aryl-3,4-dioxo-2*H*,8*H*-6,7-dihydroimidazo[2,1-*c*][1,2,4]triazines⁶⁰ in which lactam-lactim tautomerism is possible. It has been observed that both tautomers are physiologically active; however, the type of enzyme that interacts with the compound depends on particular tautomeric form. For instance, introducing the chloro substituent in *para*-position favors the enolic form while the same substituent in *meta*-position stabilizes keto form. The *p*-Cl derivative displays a serotonergic effect and acts on some alkaloid receptors as well. On the other hand, *m*-Cl compound shows antinociceptive activity i.e. reduces sensitivity to pain. The different electronic and geometric features of two tautomers are likely to be responsible for the difference in enzyme binding (**Figure 12**).

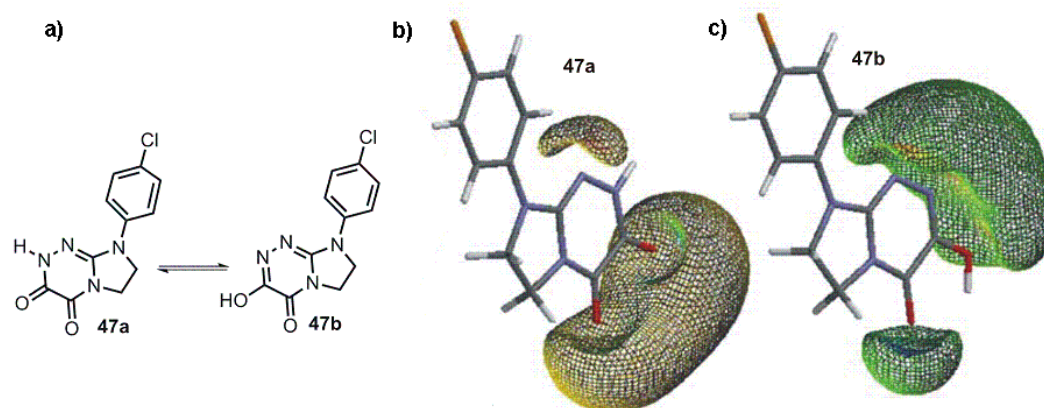


Figure 12: a) Tautomeric equilibrium of 8-(*p*-chlorophenyl)-3,4-dioxo-2*H*,8*H*-6,7-dihydroimidazo[2,1-*c*][1,2,4]triazines; Distribution of equipotential surfaces for b) keto tautomer; c) enol tautomer.

3.2.2 2-Pyridone/2-hydroxypyridine

The most famous example of heterocyclic molecule capable of forming two hydrogen bonds via AD-DA recognition pattern is 2-pyridone. It exists in tautomeric equilibrium between keto and enol forms and can form three types of hydrogen bonded dimers: a keto-keto, enol-enol or keto-enol (**Figure 13a**).

According to theoretical and experimental studies,⁶¹ the keto-keto dimer is dominant species both in a solution and in a solid state and it is commonly employed in self-assembly process as two hydrogen bonding synthon.^{62,63,64} On the other hand, the hydroxy form is slightly more stable in the gas phase. The high stability of homodimer of keto form most likely shifts tautomeric equilibrium towards its formation. It should be noted that the total number of hydrogen atoms available for complex formation is not influenced by tautomerism and both forms self-dimerize. The non-symmetrical dimerization mode is not very common and the recent calculations have shown that it is 4.8 kcal/mol less stable than corresponding symmetric keto dimer. Nevertheless, the unsymmetric dimer is unique in terms of assembly geometry; the substituents on the 6-position of pyridone ring has *cis* relationship in hetero-complex, while in the homo-complexes they are pointing towards opposite directions. It was shown by Breit et al.⁶⁵ that by introducing phosphine substituent in pyridone ring, the energetic penalty for hetero dimer formation can be compensated by chelation effect exhibited through coordination binding of metal. The chelate complex formed between rhodium and self assembled bidentatic ligand was used as a supramolecular catalyst in regioselective hydroformylation of terminal alkenes. The later example illustrates the special case of association induced tautomerism (**Figure 13b**).

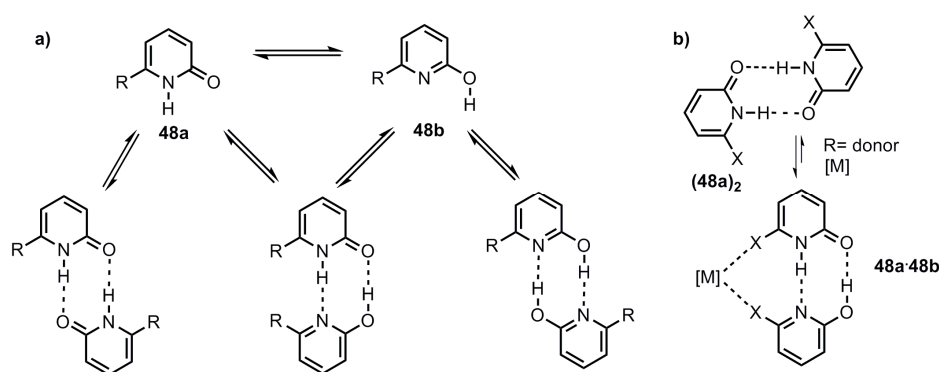


Figure 13: a) Tautomeric equilibrium of 2-pyridone and formation of homoleptic and heteroleptic dimers; b) metal complexation induced tautomeric shift.

3.2.3 Phtalhydrazides

The association process of phtalhydrazides **49** in solution has been described by Zimmerman and Lehn⁶⁶ and the aggregation of related molecules on surfaces later has been reported by Möller and Lehn.⁶⁷ Phtalhydrazide can exist in three tautomeric forms: the lactam-lactam, lactam-lactim and lactim-lactim (**Figure 14**). Although the molecule contains four hydrogen bonding sites in total, it should be regarded as two hydrogen bonding module since the linear arrangement of all sites is not feasible due to geometric constrains and exploration of all possible hydrogen bonds cannot be realized in dimeric assemblies. The two sets of hydrogen bonding motifs are positioned at 60° angle to each other. The spectroscopic studies indicate that in ethanol the most stable tautomer is lactam-lactim.⁶⁸ Lactam-lactam tautomer is the second most stable tautomer, while the contribution of lactim-lactim form can be neglected. The gas phase calculations are in line with the spectroscopic data and suggest the same trend of stability.

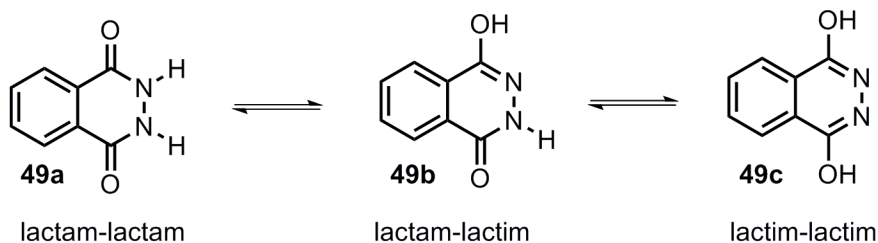


Figure 14: Tautomeric forms of phtalhydrazides showing the lactam-lactam, lactam-lactim and lactim-lactim tautomers.

The fact that the lactim-lactam form is more stable can be attributed to the repulsion in the other two tautomers involving adjacent nitrogen atoms of the same hybridization. It was shown, that in chloroform, the compound forms very stable trimeric aggregates via cooperative assembly of lactam-lactim tautomer. In this case, the lactim-lactam is preorganized to form cyclic aggregates by proper arrangement of the hydrogen bonding sites whereas the two other tautomers can only form linear assemblies. No other tautomers were observed in chloroform or toluene upon dilution, suggesting that

tautomerization is shifted by favourable interaction in trimer (**49b**)₃ via six hydrogen bonds (**Figure 15**). The same cyclic trimer in the solid state is known for luminol **50**. The addition of DMSO decreased the stability of the aggregate and the formation of mixture of different species was observed. The ability to tautomerise was further explored in order to change aggregation mode through complexation induced tautomerism. In the presence of concurrent hydrogen bonding molecule **51**, complementary to lactam-lactam tautomer of phtalhydrazide, the trimeric aggregate is dissipated and new type of mesophase is formed, most likely composed of heteroleptic tetramer (**49a**·**51**)₂. On contrary to the results obtained in solution, self-assembly on surface afforded aggregates of different type and was shown to be dependent on solvent used. Among different aggregates the linear assembly (**49b**)_n involving lactim-lactam tautomer is especially intriguing, illustrating the paramount role of packing forces for directing the molecular aggregation.

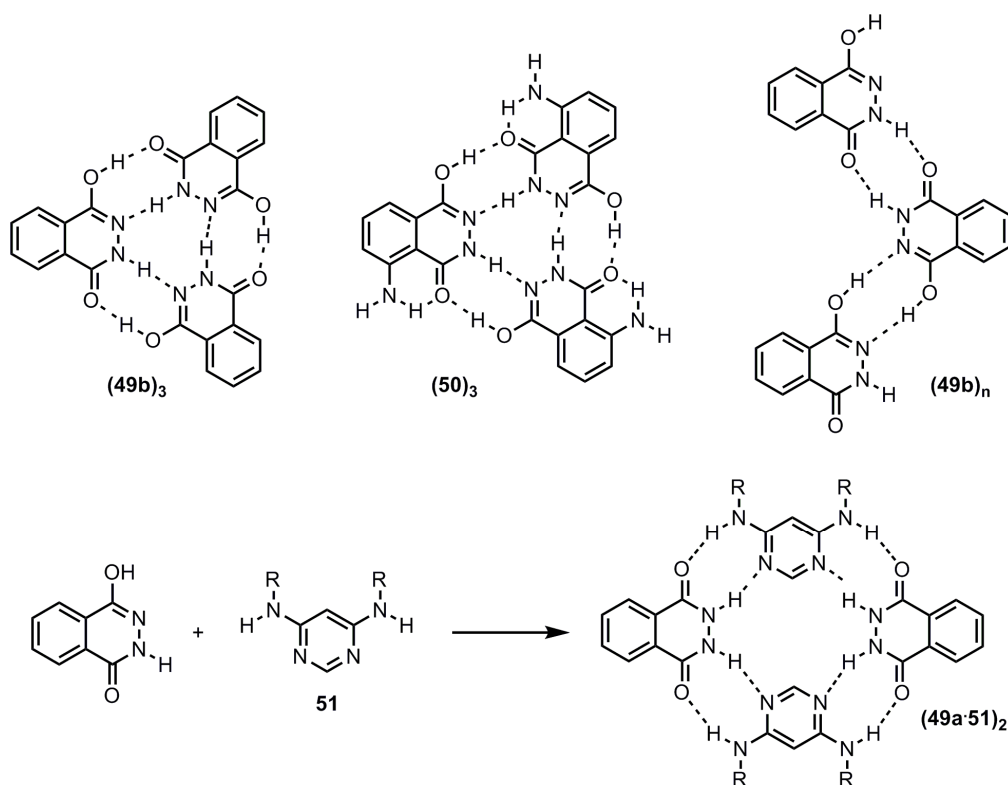


Figure 15: a) trimeric aggregates of lacim-lactam tautomers of phtalhydrazides **49b** and luminol **50**; b) tape-type aggregation of tautomer **49b**; c) tetrameric assembly of phtalhydrazides with **51**, complementary to lactam-lactam tautomer **49a**, illustrating the association induced tautomeric shift.

3.2.4 Melamine-cyanuric acid complexes

Cyanuric acid **52** may exist in four tautomeric forms: fully enolic (triazine), fully keto form (isocyanuric acid) and two intermediate tautomers consisting of both enolic and keto forms (**Figure 16**). The distribution of tautomers in water solution is pH dependent. Free cyanuric acid in crystals and in acidic solution below pH=6 exist mainly as a tri-keto form, the di-keto form dominates when pH=6 to 10.5 and the mono-keto form is found in solution above pH=11. The cyanuric acid forms an extremely stable, insoluble complex with melamine, which is held together by infinite two-dimensional network of hydrogen bonds. The stability of the complex is reflected in the old name of this complex, melamine-cyanurate, which implies the salt-like structure.

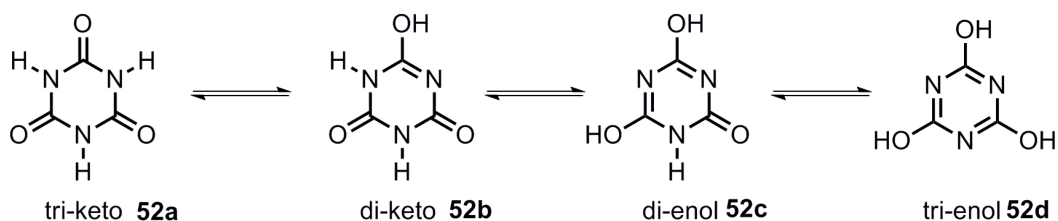


Figure 16: Tautomeric equilibrium of cyanuric acid **52a**

The formation of insoluble melamine-cyanuric acid adduct is responsible for the fatal poisoning cases, when melamine and cyanuric acid were used as a “fake” protein to increase the content of nitrogen in pets food or milk products (**Figure 17a**).^{69,70} When one of the nitrogen in cyanuric acid is substituted with sp^3 carbon, the resulting molecule (barbituric acid) possesses only two hydrogen bonding faces and the possibility to form infinite network is eliminated (at least of the same type as for **52a-53**). Likewise cyanuric acid, the barbituric acid in its most stable keto tautomer form assembles into hexameric cycles (rosettes) with melamine forming 18 hydrogen bonds. The same result can be obtained with mono-alkylated cyanuric acid (**Figure 17b**).

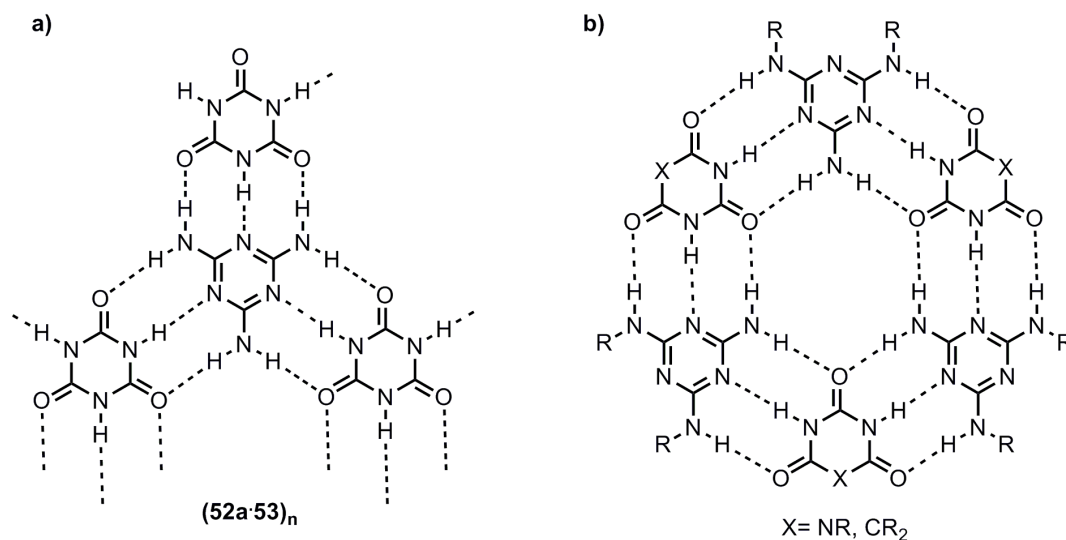


Figure 17: a) infinite hydrogen bonded network between cyanuric acid **52a** and melamine **53**; b) rosette structure formed by self-assembly between barbituric acid ($X=CR_2$) or substituted cyanuric acid ($X=NR$) and melamine

This principle was elegantly demonstrated by Whitesides et al.⁷¹ and Reinhoudt et al.⁷² by making hexameric rosettes and double rosettes, respectively. Furthermore, it is possible to control the mode of aggregation from linear tapes to crinkled tapes, by changing steric bulk of the substituent on melamine ring. Increasing the steric constraints even more favours formation of hexameric rosettes. The hexameric assembly of this type is very robust and can be decorated with additional functional groups such as porphyrins to mimic the light harvesting system in photosynthetic bacteria.⁷³

3.2.5 Triple hydrogen bonding modules

It was shown by Zimmerman et al. in 1992, that 2,6-diamino dihydropyridines depending on their tautomeric form can be used as hydrogen bonding modules with DAD or DDD sites (**Figure 18**).⁴⁸

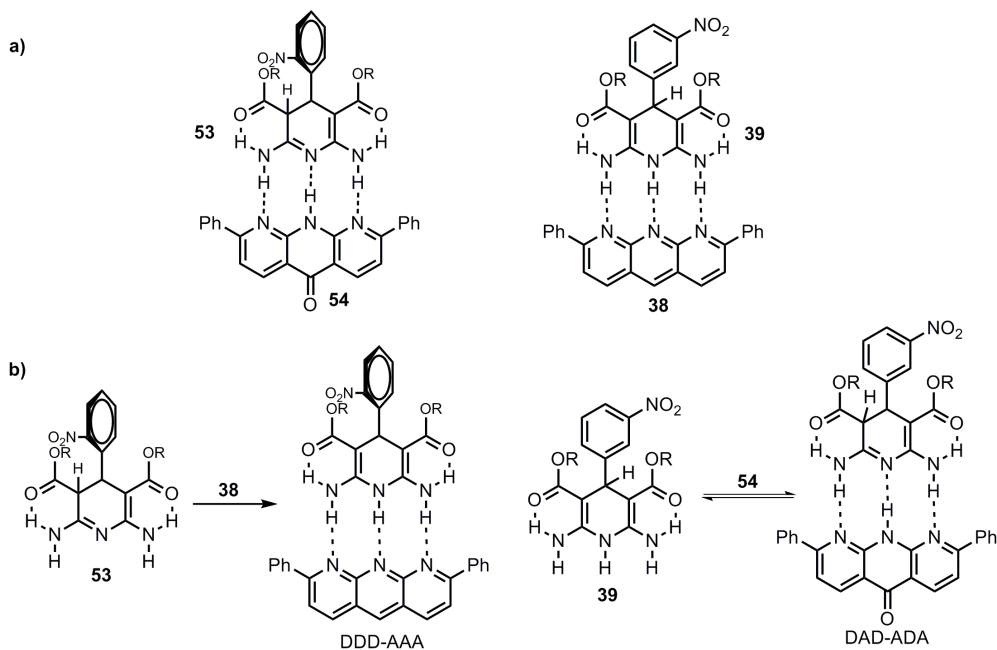


Figure 18: a) 3H bonding complexes of 3,4-dihydropyridine tautomer **53** and 1,4-dihydropyridine tautomer **39** with complementary partners; b) association-induced tautomerism of dihydropyridines **53** and **38**.

The existence of two tautomers complicates the binding studies and may result in weaker association. It was found earlier by Meyer et al.⁷⁴ that the substituent in the 4th position of dihydropyridine ring has a considerable influence on tautomeric equilibrium between 1,4-dihydropyridine and 3,4-dihydropyridine in DMF. By varying 4-substituent from 2-nitrophenyl to 3-nitrophenyl the tautomeric equilibrium could be shifted towards 1,4-dihydropyridine form. The same tendency was valid for 2-nitrophenyldihydropyridine **54** in chloroform, however, dihydropyridine **39** underwent solvent induced tautomeric shift resulting in 2:1 mixture of 1,4-dihydro and 3,4-dihydropyridines. Interestingly, the “wrong” tautomer can be converted to the desired one by tautomeric equilibrium by simple addition of excess of AAA or ADA compound. For example, after addition of tenfold excess of compound **38** to the solution of dihydropyridine **53** in chloroform, the later was fully converted to less stable 1,4-dihydropyridine tautomer. Results that are even more interesting were obtained by addition of excess of compound **54** to DDD compound **39**. The tautomeric equilibrium was shifted towards 3,4-dihydro form, though to a

lesser extent. This result shows the direct correlation between the complex stability and directing power of complementary hydrogen bonding partner.

The concept of association induced tautomeric shift was also demonstrated by Bühlmann et al.⁷⁵ in their attempts to design molecular receptor for important clinical analyte – creatinine **56** (Figure 19a). The creatinine molecule has a DAA hydrogen bonding site and can form a hydrogen bonded complex with ADD module. Instead of synthesizing molecule with fixed ADD hydrogen bonding motif, the authors tested several tautomerically labile compounds, including **55** and **57**, as possible hosts for creatinine. It was found that in the case of isocytosine host, the tautomeric equilibrium was shifted to the preference of **55b** isomer, as a result of creatine binding via three hydrogen bonds. The association process was followed by UV spectroscopy and by host mediated extraction of creatinine from water solution into organic phase. On the other hand, the change in tautomeric composition of other compounds **57** was negligible, mainly due to high energetic barrier between two tautomeric forms of host. The energy gained by hydrogen bonding with guest is simply not enough to compensate the energy penalty of the formation of thermodynamically less stable tautomer.

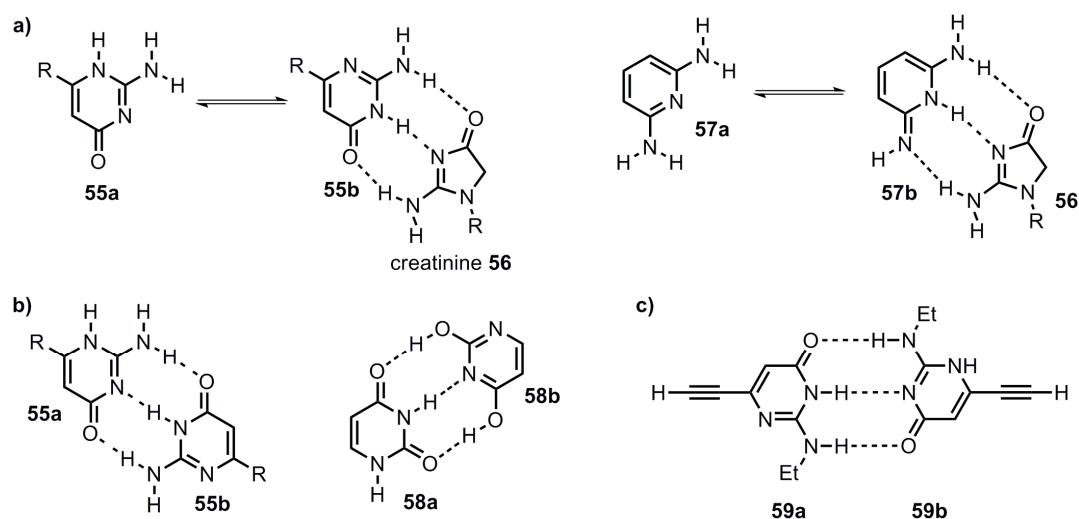


Figure 19: a) the application of association-induced tautomerism of **55** and **57** for recognition of creatinine **56**; b) self-complementarity of tautomers of **55** and **58**; c) 3H bonding module, based on self-complementarity of two tautomeric forms of **59**.

The common strategy in using hydrogen bonding modules with odd number of donor and acceptor sites is that the complementariness of such sites is fulfilled by forming heteroleptic complexes. In case where tautomeric equilibrium is not possible due to structural features of the molecules, formation of heteroleptic complex is necessary to ensure the use of all hydrogen bonding sites. The array of three hydrogen bonds is not self-complementary and thus cannot self-dimerize. However, in some cases the tautomeric equilibrium could give rise to the possibility for self-complementarity, provided there is another heteroatom in the molecule, which is not a constitutional part of hydrogen bonding module but rather serves as a reservoir to accept proton during tautomerization. The concept is illustrated in **Figure 19b** using isocytosine **55** and uracil **58** as an example

Isocytosine crystallizes in two tautomeric forms from water exactly in a 1:1 ratio.⁷⁶ X-ray analysis showed that the two tautomers of isocytosine are hydrogen bonded via triple hydrogen bond. The tautomeric distribution of isocytosine depends on media and it was shown by spectroscopic studies that in ethanol or diethyl ether N3-H tautomer dominates whereas in aqueous solution an equal amount of both tautomers co-exist. Increasing the temperature the equilibrium shifts to N1-H tautomer. The self-complementariness of tautomers of isocytosine derivatives was exploited by Inouye et al.⁷⁷ for the synthesis of new triple hydrogen-bonding module **59** (**Figure 19c**).

3.2.6 Quadruple hydrogen bonding modules

In the molecules containing quadruple hydrogen bonding moieties the number of heteroatoms increases as does the number of possible tautomers. The 2-ureido pyrimidinone compounds were first introduced by Beijer et al.⁵³ and since then they gained the reputation as one of the most versatile and reliable hydrogen bonded building blocks in supramolecular chemistry. They form very strong dimers and are perfectly suitable for the synthesis of supramolecular

polymers.⁷⁸ The ureido-pyrimidinone molecule has three tautomeric forms (**Figure 20**), two of which can self-dimerize through quadruple hydrogen bonds.

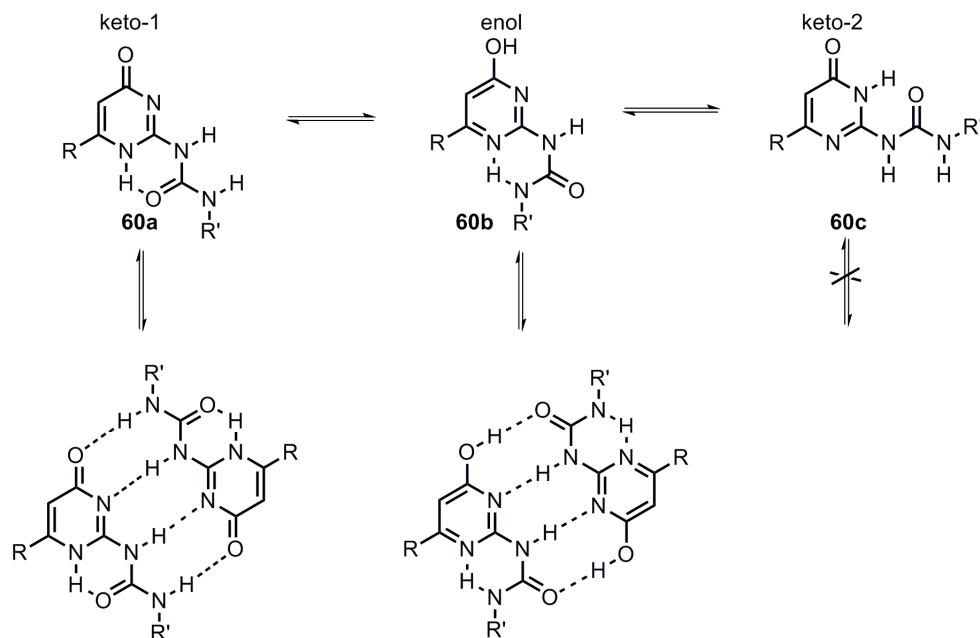


Figure 20: Tautomers of 2-ureido pyrimidinones: self-complementary keto tautomer **60a** and enol tautomer **60b** and non-dimerizing keto tautomer **60c**.

The preference of one tautomer over the other is mainly determined by solvent induced tautomerism. In chloroform, the 2-ureido-4[1H]-pyrimidinone or keto tautomeric form **60a** is strongly favoured, presumably due to strong self-dimerization. In THF and toluene, the enol tautomer 2-ureidopyrimidin-4-ol **60b** is prevalent most likely due to the polar and aromatic nature of these solvents, respectively. In DMSO, the thermodynamically most stable tautomer 4[3H]-pyrimidinone **60c** is observed. In this polar solvent, the formation of intermolecular hydrogen bonds is prevented and the contribution from association induced tautomeric shift becomes negligible. The strong dependence of tautomeric distribution on electronic nature of substituents offers an attractive mean to control aggregation. It was found that electron withdrawing groups at the 6-position of pyrimidinone ring favoured the enol tautomer, whereas electronically neutral or weakly electron-donating groups favoured the keto tautomer.

The phenomenon of association induced tautomeric shift manifests itself not only by the primary aggregation but could also be influenced by a secondary interaction of aggregating units. It was shown that stacking interactions operating in the dimer of bifunctional molecule **61** stabilize the enolic form considerably (**Figure 21**). At equilibrium, the ratio of keto-keto and keto-enol tautomers is 7 to 3 in chloroform.

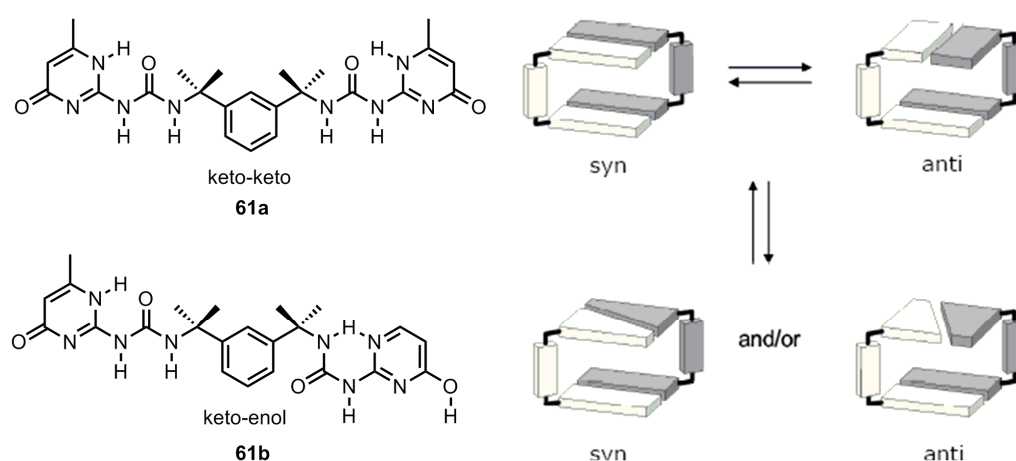


Figure 21: The tautomerism of bifunctional hydrogen bonding module **61** in stacked dimer.

Finally, the two polymorphs of ureido pyrimidinone are formed in the solid state. The needle shape crystals obtained from chloroform are composed of keto tautomer, whereas the plate shape crystals are composed of dimers in enolic form.

The presence of three different tautomeric forms of ureido pyrimidinone renders the association process more complex and eliminates one of the keto tautomers from self-dimerization equilibrium. The parasitic tautomer carries the wrong assembly instruction and thus diminishes the overall association constant. As a consequence, many efforts have been put in order to design the quadruple hydrogen bonding module irrelevant to the tautomeric distribution. The problem has been solved by Zimmerman et al.⁷⁹ by introducing additional hydrogen bond acceptor in adjacent heteroaromatic ring (**Figure 22**).

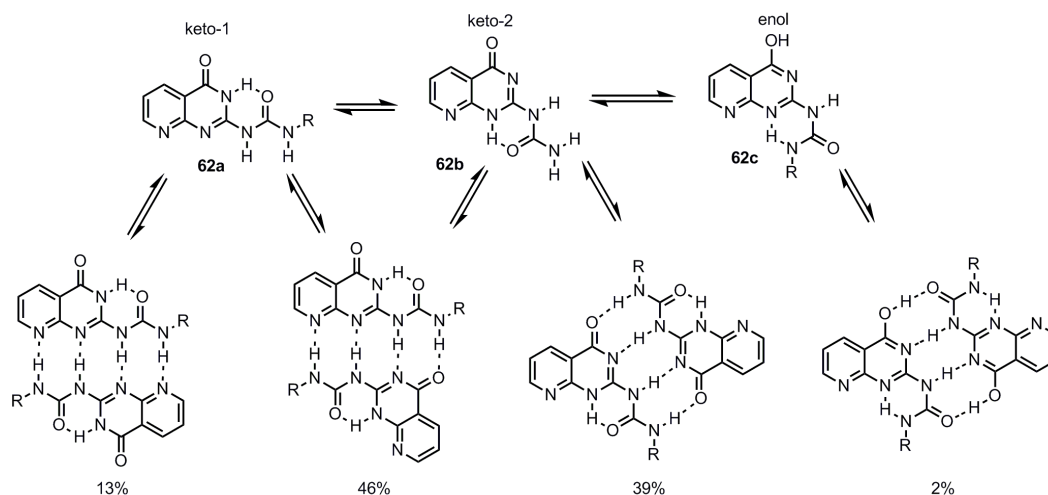


Figure 22: The tautomeric equilibrium of quadruple hydrogen bonding module **62** showing keto and enol tautomers **62a-c** and corresponding homo- and heterodimers. Relative abundance (%) of dimeric species in toluene-d₈ is given.

The obtained compound exists as a mixture of three tautomers, all of them capable of dimerizing through the formation of homo and heteroleptic complexes. An important feature of all hydrogen bonded duplexes is similar spatial arrangement of urea substituents R. Although the well-defined geometry of the dimer is not of prime importance in preparation of supramolecular polymers, it is the prerequisite for the design of more complex discrete assemblies. In non-polar solvents, the main tautomer is the keto form.

Another approach to reduce the number of tautomers is to replace NH groups in pyrimidine ring by CH groups, or by converting the NH group to NR group by alkylation. However, this may result in conformational flexibility as an important preorganizing element, intramolecular hydrogen bond, is lost. The cytosine derivative **63**, in which one of the NH group is blocked by alkylation was proposed as an alternative for ureido pyrimidinone (**Figure 23a**).⁸⁰ The compound may exist in two conformers, folded and unfolded, with the desired unfolded form stabilized by strong quadruple hydrogen bonding on dimerization. The aggregation studies in non polar solvents revealed that only unfolded dimer is present, whereas in a slightly more polar solvent chloroform a small amount of folded dimer was also detected. The quadruply hydrogen-bonded module forms the dimer in its unfolded conformation with association

constant of $9 \times 10^6 \text{ M}^{-1}$ in benzene. The corresponding bifunctional derivative behaved in a way similar to ureido pyrimidinone affording supramolecular polymers of high molecular weight. These results showed that even the modules lacking preorganization of hydrogen bonding array via intramolecular hydrogen bond might form strong quadruple hydrogen bonds. Moreover, although the folded conformer is stabilized by by intramolecular hydrogen bond, the conformational change toward less stabilized unfolded conformer occurs readily and the energy loss associated with the process is fully compensated by newly formed quadruple bond.

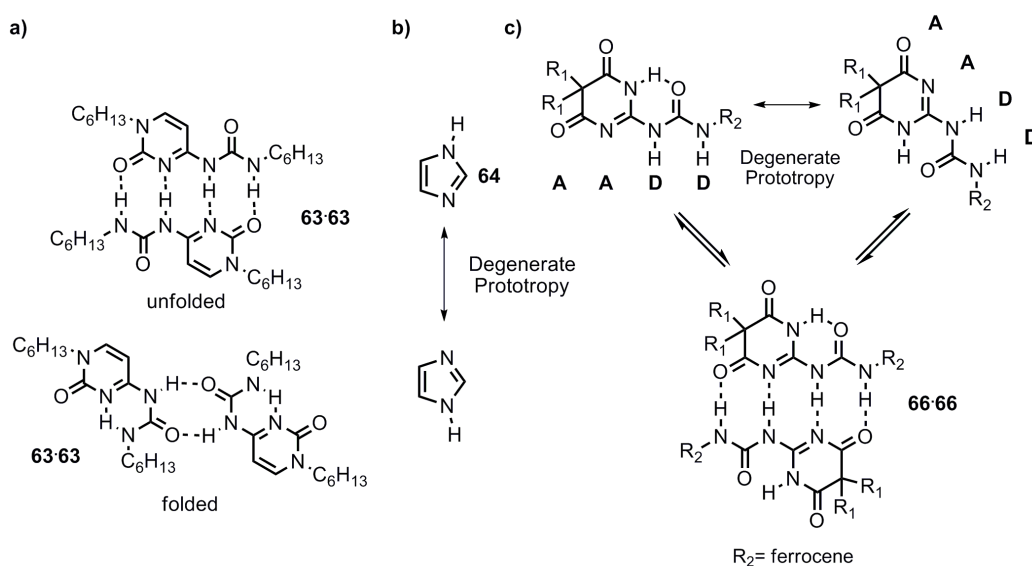


Figure 23: a) self-dimerization of cytosine derivative **63** in its unfolded and folded form; b) degenerate prototropy in imidazole **64**; c) 4H bonding module **65** capable of participating in degenerate prototropic equilibrium and its dimer.

A step further was taken by Sanjayan et al.⁸¹ by using the concept of degenerate prototropy (tautomerism), when two equilibrating tautomeric forms result in the same arrangement of hydrogen bonding sites due to the chemical equivalence of protomers. One of the simplest systems that exhibit degenerate tautomerism is imidazole wherein both protomers, formed by 1,3-annular tautomeric shift, are rendered equivalent by prototropic degeneracy (**Figure 23b**). As a proof of principle, the heterocyclic urea derivatives were obtained by acylation of 2-amino-5,5-disubstituted -1H-pyrimidine-4,6-diones, available in one step by condensation of substituted malonates with guanidine, with

corresponding isocyanates. Structural studies indeed showed that **65** forms only a single set of molecular duplex **65·65** in both solution and solid state (**Figure 23c**). The dimerization constant of **65** in chloroform was estimated to be $1.2 \cdot 10^4 \text{ M}^{-1}$, which is by two orders of magnitude lower than the corresponding value for ureido pyrimidinones. The authors did not elaborate on this issue, but the reason may lie in the reorganization of electronic density across the heterocyclic ring imposed by electron negative oxygen atom, which lowers the hydrogen bond donor potential of nitrogen and oxygen within hydrogen bonding module. In contrast to previous example, the module has preorganizing intramolecular hydrogen bond embedded in its structure. The same module anchored with two ferrocene moieties was successfully employed to probe the electronic coupling of two redox centers. It was demonstrated by Kaifer et al.⁸² that the extent of electronic communication between two electrochemically active ferrocene residues, separated by more than 10 Å within hydrogen bonded duplex, was remarkably large.

Despite the numerous attempts to reduce the number of possible tautomers in hydrogen bonding modules and thus make the association process more simple and predictable, the design of system capable of tautomerization may offer additional advantages as a mean to control self-assembly and subsequent self-organization. The change in tautomeric distribution could be employed as a switch to external stimulus for structural reorganization in order to find a new configuration of minimum energy. In addition, the switching between different tautomeric forms represents a process of dynamic combinatorial chemistry, which creates dynamic diversity through the interconversion of recognition patterns.⁸³

3.2.7 Cyclo-tautomerism

The advance in supramolecular chemistry is directly reflected in the complexity of the structures that could be assembled by using non-covalent interactions. One of the main achievements in the field is the construction of

various types of molecular receptors with concave surface for the studies of recognition processes and the reactivity of guest in the inner space of host. Over the years, Rebek et al. has reported an impressive collection of concave molecules that were able to assemble into molecular capsules with confined dimensions employing multiple hydrogen bonding between the subunits as a driving force.⁸⁴ As a result of specific spatial arrangement of hydrogen bonding sites on the rim of concave molecule or at the connecting seam between two parts of larger assembly, new phenomena such as cyclo-enantiomerism, cyclo-diastereomerism or cyclo-tautomerism have emerged. In their studies of guest encapsulation by dimeric calixarene-ureas, Rebek et al.⁸⁵ has shown that when hydrogen bonding sites, capable of interacting with each other, are connected in a cyclic array, the directionality of hydrogen bonding is created (**Figure 24**).

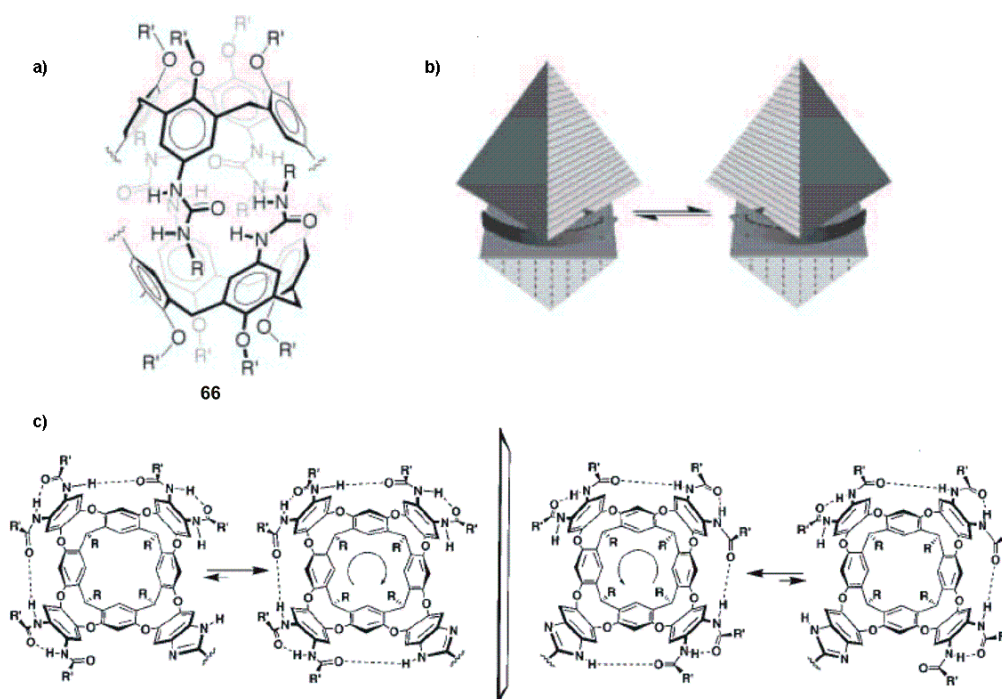


Figure 24: a) dimeric capsule **66** formed by association through hydrogen bonding urea fragments; b) the cyclo-enantiomerism resulting from the directionality of hydrogen bond of urea; c) cyclo-diastereomerism caused by two tautomeric form of benzimidazole unit.

The head-to-tail arrangement of the ureas at the equator can be clockwise or counter clock wise in respect to the pole of the capsule. The interconversion of the resulting cyclo-enantiomers occurs either through the rotation of urea

functional groups or by dissociation and recombination of monomers. Without chiral bias, the two cyclo-enantiomers form in equal amounts constituting a racemic mixture. By using chiral guest, a significant transfer of chirality was observed resulting in the enrichment with one of the cyclo-enantiomers. Even more interesting phenomenon was observed when using dimeric capsule containing benzimidazole spacer. In this case, the cyclic array of urea moieties is interrupted and the direction of hydrogen bond is governed by tautomeric form of imidazole ring.

3.3 Hydrogen bonded tubular assemblies

3.3.1 General strategies for design of tubular structures

Tubular structures are among the most versatile functional models that could be assembled in a predictable manner with the help of working principles of supramolecular chemistry.⁸⁶ The formation of tubular structures is achieved by careful design of monomeric units with inherent geometric features responsible for controlled spatial aggregation. The unique properties of such assemblies are determined by the cylindrical dimensionality in which information of directionality is encoded. Nanotubes can perform a variety of functions, such as transport of charged or neutral species, function as template for the synthesis of concave structures or nanowires and provide a nanospace with suitable dimensions for storage or catalytic purposes. The information stored in molecular building blocks, such as shape and linkage geometry as well as local solvophilicity/solvophobicity and recognition sites, can be used to generate open-ended concave tubular objects via a variety of conceptually different approaches (**Figure 25**). All approaches use a combination of both covalent and non-covalent synthesis. In first approach the covalent chain of polymer generates a helical conformation containing an internal void. In foldamers, the folding information is usually stored in the primary structure of the polymeric chain and guides the overall process.⁸⁷ The nanotube obtained has a very defined

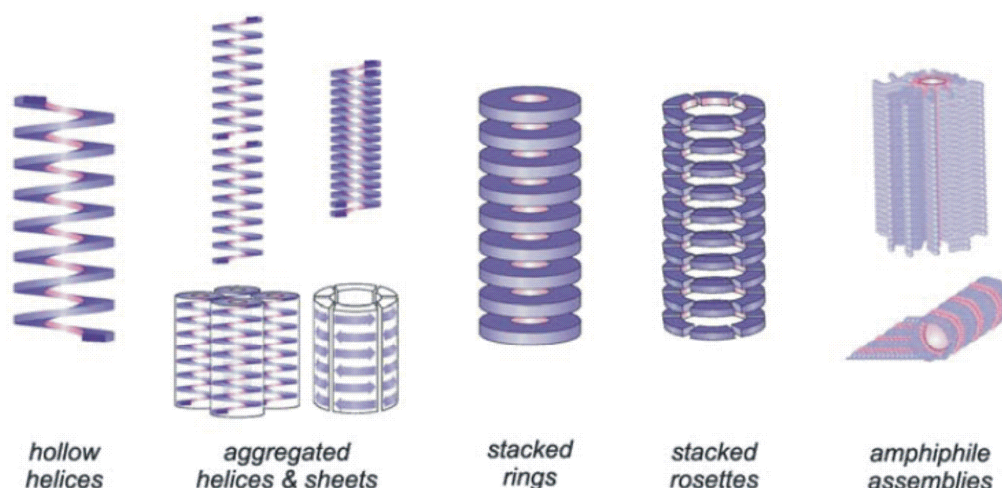


Figure 25: Cartoon representation highlighting general strategies for the design of tubular assemblies and different aggregation modes including aggregation of helices, stacked rings and rosettes and amphiphilic assemblies.

diameter and what is more important, the precise length, the characteristic difficult to attain via purely supramolecular approach. Although the folding process uses non-covalent interactions such as hydrogen bond or π - π stacking as a driving force, this type of tubular structure is not considered as completely supramolecular. If the helical arrangement of polymeric backbone is virtually divided into the stacked rings with additional recognition units on their rims, another approach towards tubular structure is envisioned. By introducing additional orthogonal interactions, the individual ring itself could be assembled from sector-shaped units. In both approaches the dimensions of internal cavity is dictated by the dimensions of macrocyclic ring. The last approach is the one with the upmost non-covalent character and relies on formation of tubular structures from micelles or rolled sheets which themselves are produced by aggregation of certain amphiphiles. In this short introduction, only nanotubes formed by hydrogen bonding between subunits are discussed.

3.3.2 Cyclic peptides and related structures

The first example of tubular structure, originating from aggregation of cyclic-(D,L)- α -peptide was described by Ghadiri et al. in 1993.⁸⁸ The work was inspired by the proposal made by DeSantis in 1974,⁸⁹ stating that peptides

composed of even number of alternating D- and L-amino acids could be in principle connected to rings, which could further aggregate to cylinders by stacking through antiparallel β -sheet hydrogen bonding. The octapeptide cyclo-[-(L-Gln-D-Ala-L-Glu-D-Ala)₂-] **67** was shown to form a stacked tube in microcrystalline aggregate obtained from careful acidification of basic solution of octapeptide (**Figure 26**).

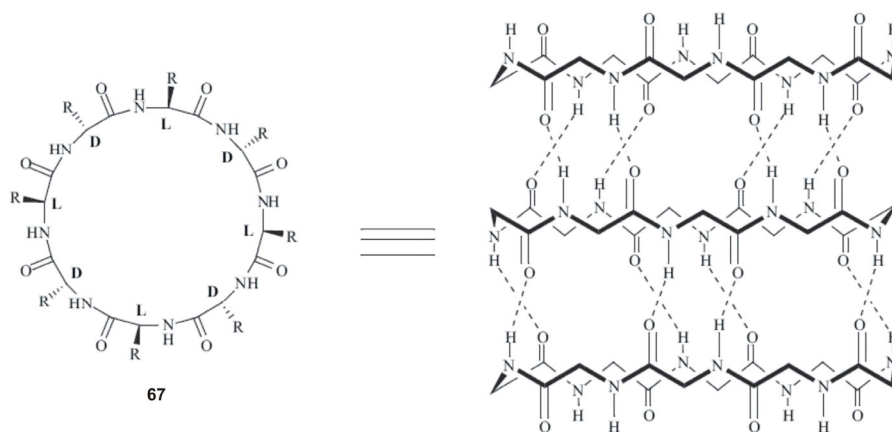


Figure 26: Ghadiri's tubular structure formed by stacking of hydrogen bonded rings of cyclooctapeptide **67**.

The tubular nature of aggregate was proved by electron microscopy, electron diffraction, IR spectroscopy and modeling. The TEM, cryo-TEM and electron diffraction studies showed that the aggregate has an inner diameter of 7 Å and 4.7 Å axial periodicity, which agree very well with the proposed stacked arrangement of cyclic oligopeptides. The versatility of this approach was further demonstrated by preparation of cyclopeptides of different size. The inner diameter of the tube was increased to 10 Å and 13 Å, by increasing the number of repeating units in covalent structure to 10 and 12, respectively. When hydrophobic chains are anchored to the microcycle, the resulting nanotube could be inserted into lipid bilayer to create transmembrane channels. It was shown, that cyclo-[-(L-Trp-D-Leu)_n-L-Glu-D-Leu-] with n=3 possessing an inner diameter of 7 Å participate in active transport of sodium ions, whereas the nanotube with n=4 and inner diameter of 10 Å showed glucose transport activity.⁹⁰ Combining this approach with the photoisomerization of an

azobenzene unit resulted in a system, which can be switched between intramolecular dimerization and linear polymerization by UV-light.⁹¹ Due to the fact that NH protons have an alternating directionality across the cyclopeptide ring, selective methylation of each second NH group could lead to dimeric stacking only, preventing higher aggregation. In a related work, Seebach et al.⁹² have found that cyclic tetramers obtained from β -amino acids such as 3-aminobutanoic acid forms tubular structures by stacking in a fashion similar to those between amide groups found in α -helix (**Figure 27**).

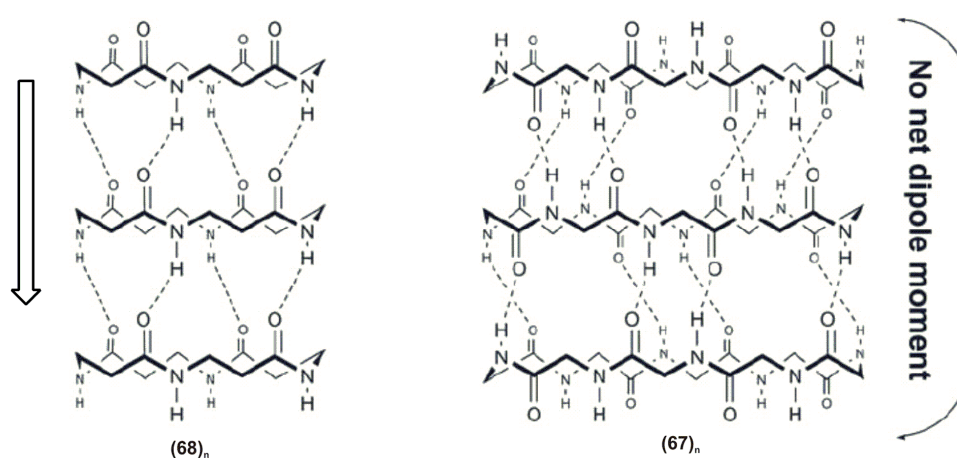


Figure 27: Comparison between tubular structures formed by cyclic tetramer of β -aminoacids **(68)_n** and octamer of α -amino acids **(67)_n**. The corresponding net dipole moment is indicated for each assembly.

The ion-channels formed by two cyclic β 3-tetrapeptides show activities similar to those of cyclic D,L- α -peptides;⁹³ on the other hand they exhibit unique and striking properties related to uniform arrangement of amide groups. As in case of biological structures, such an alignment gives rise to a macrodipole moment, which is expected to facilitate the conductance of these of, charged through the δ^- and δ^+ ends of the channel.

Due to low solubility of most of cyclic peptides, their structural studies and possible applications are challenging. Dory et al.⁹⁴ synthesized more lipophilic cyclo-(δ -amino acid)_n bearing a double bond in order to impart the necessary rigidity of the microcycle (**Figure 28a**). It was found that subtle structural variations in macrolactamic backbone may result in drastic change of the aggregation mode. The macrolactam **70** forms tubular structure in solid state,

whereas in compound **69** realization of intramolecular hydrogen bond is more preferable.

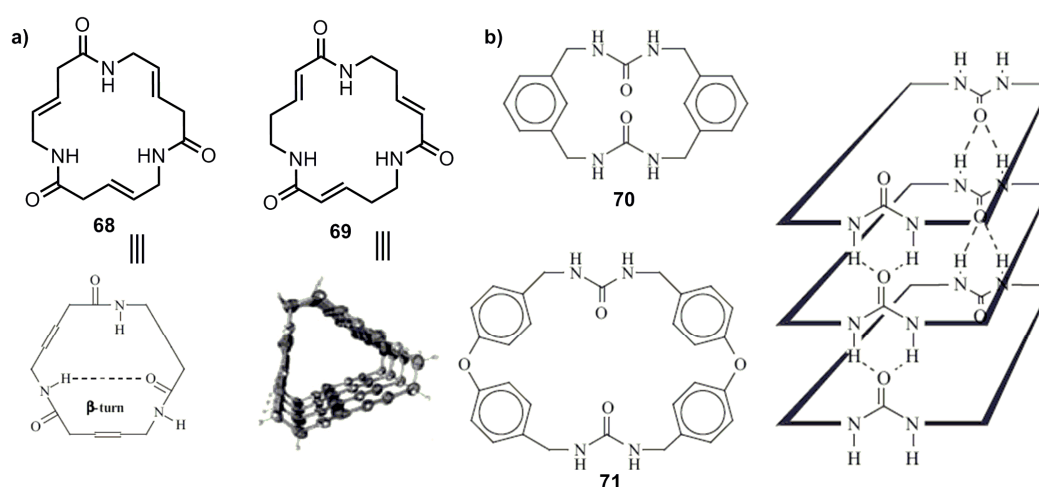


Figure 28: a) structure of cyclic unsaturated lactams **69** and **70** and their aggregation mode in solid state; b) structures of cyclic ureas **71-72** and schematic representation of the urea hydrogen bonding pattern.

The urea functionality is notorious for the large variety of supramolecular structures that could be assembled by hydrogen bonding of units incorporating this group. It was reported that the stability of the nanotube can be increased by incorporating urea motifs into the cyclic structure together with L-cystine residues.⁹⁵ The cyclic bis-ureas showed an inherent tendency to self-assemble into tube-like structures by packing atop one another. In a similar approach, the chiral C_4 symmetric cyclo tetraureas were synthesized.⁹⁶ X-ray crystallographic analysis revealed a planar conformation with all urea carbonyl groups pointing in one direction and the NH urea groups pointing in the opposite direction. As expected, the tubular structure with diameter of 3.5 Å was obtained. The utilization of urea module to construct tubular structures was very fruitful even with much simpler and easily available cyclic ureas, such as **71** and **72** (**Figure 28b-c**). The crystals of poorly soluble **71-72** were obtained from acetic acid. The crystal structure showed that the hydrogen bonding between urea groups are favoured, even in the presence of acetic acid. The tubular arrangement of individual cyclic ureas was reinforced by π - π stacking of aromatic spacers. Moreover, the crystals show stability up to 180°C both in the presence and in

absence of acetic acid. The most remarkable feature associated with these compounds are reversible hosting of guest (acetic acid) by changing the temperature. Repeating the guest loading and removal cycle for three times led to the unaffected crystal structure. The term of “organic zeolites” was used by authors to emphasize the very robust lattice structure of these compounds.

3.3.3 Carbohydrates

Stoddart et al.⁹⁷ reported the synthesis of achiral macrocyclic oligosaccharides with alternating (1→4) linked α -D- and α -L-rhamnopyranose residues. X-ray analysis of cyclic octasaccharide and decasaccharide revealed infinite stacks to form nanotubes ranging from 1.0 nm for the cyclic octasaccharide to 1.3 nm for the cyclic decasaccharide in diameter (**Figure 29**). Interestingly, the intermolecular hydrogen bonds do not connect oligosaccharide rings along the tubular axis but rather connect adjacent columns.

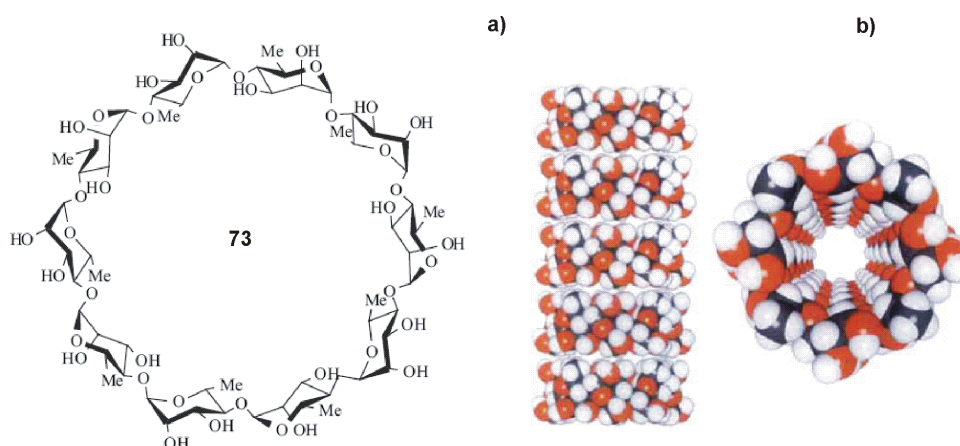


Figure 29: Space filling view of the tubular structure formed by stacking of decasaccharide **73**; a) side view; b) top view.

3.3.4 Calixarenes

Atwood et al.⁹⁸ reported an impressive example of controlled self aggregation of C-methylresorcin[4]arene **74**. Depending on conditions, the compound **74** forms a hexameric capsule held together by multiple hydrogen bonds or assembles into nanotube with similar arrangement of monomers **74** (**Figure 30**). It was found that using bromopyrene as a host promotes the formation of

nanotube. The polar hydrogen bonded hydroxy groups are efficiently shielded from the solvent by alkyl substituents. The alkyl chains also stabilize the tubular structure by forming a large number of van der Waals interactions between neighbouring hydrophobic chains and intercalated pyrene molecules. Unfortunately, the existence of nanotube in solution was not supported by experimental data.

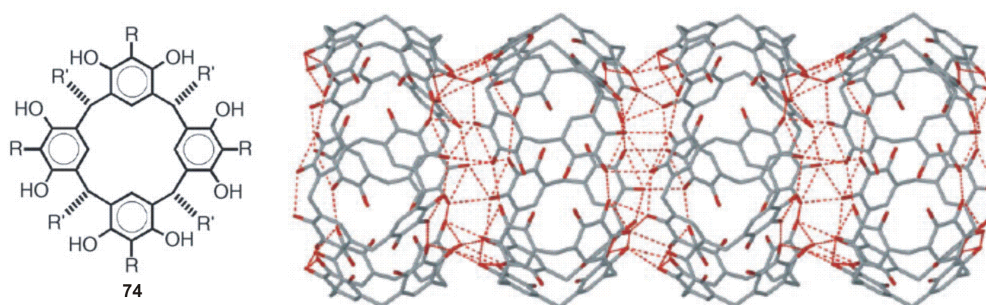


Figure 30: Tubular self-assembling of calixarene **74** in solid state via formation of multiple intra- and intermolecular hydrogen bonds.

3.3.5 Barrels

Artificial rigid-rod β barrels **75** based on stiff oligo(para-phenylene)s carrying short peptide side chains have been reported by Matille et al.⁹⁹ Covalent fixation of the stave's shape by using rigid rod like backbone combined with the formation of an interdigitating antiparallel H-bonding array between the peptide frameworks proves to be an efficient strategy for creating concave nanostructures with defined interior functionality. Most likely, hexameric barrels measuring 3.4 nm in length and ~ 1.0 nm in internal diameter are formed (**Figure 31**). The transmembrane activity of rigid-rod- β barrels has recently been exploited for designing a fluorometric detection system of enzyme activity.¹⁰⁰

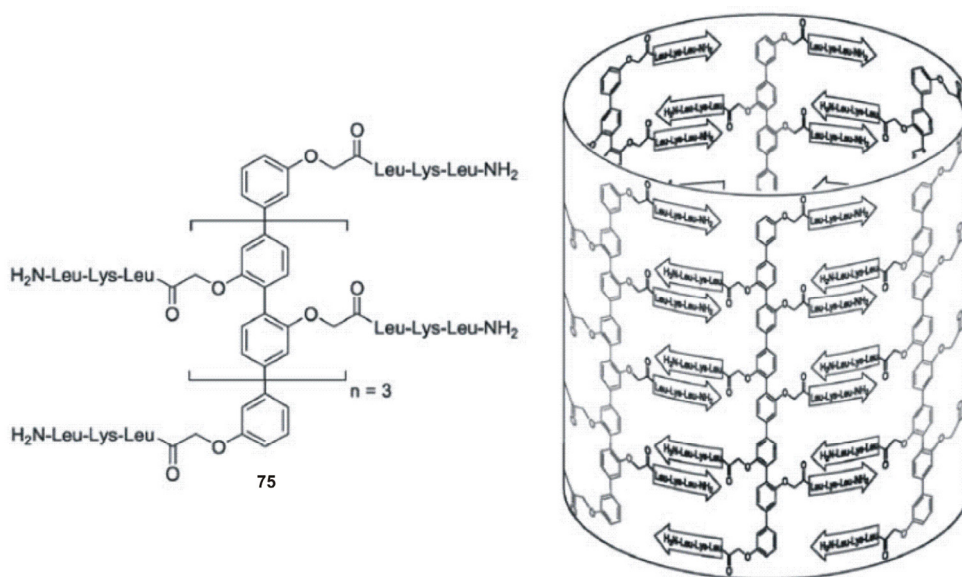


Figure 31: Matille's rigid-rod barrel **75** containing short peptide side chains attached to oligo(*para*-phenylene) and the resulting tubular structure.

3.3.6 G-quartets and related systems

The structural arrangement of hydrogen bonding arrays in guanine is predisposed to form a cyclic tetrameric rosette. The so-called G-quartets are found in G-rich sequence of both DNA and RNA and are especially abundant in tellomeric DNA.¹⁰¹ The metal cation templates the aggregation process and initiates a cascade of subsequent events such as hierarchical self-assembly of formed G-quartet-cation complex to linear polymer using π - π stacking, solvophobic or cation-dipole interactions. Gotarelli and Davis et al.¹⁰² prepared lipophilic derivative of deoxyguanosine **76** and have showed that unlike their polar counterparts in water solution, the compound **76** does not aggregate into tetrameric structure in the absence of metal ion, only by hydrogen bonds. When placed into contact with water phase containing potassium salts, the potassium cations are extracted by **76** into organic phase forming dimers of G-quartets, where potassium ion is sandwiched between two G-quartets. Increasing the concentration of potassium ions led to the formation of stacked polymer (**Figure 32**). In a very recent report, Meijer et al. has showed that the control over the extent of aggregation could be achieved by using Coulombic interaction.¹⁰³ By changing solvent polarity, it was possible to adjust the

Coulombic interaction between ions and quantitatively obtain assemblies of 8, 12, 16 and 24 guanosine molecules. It should be noted that tubular structures obtained by using G-quartets are filled with metal ions, which are essential part of the assemblies. It is not possible to create a concave structure via selective removal of the metal without disrupting the stacked column.

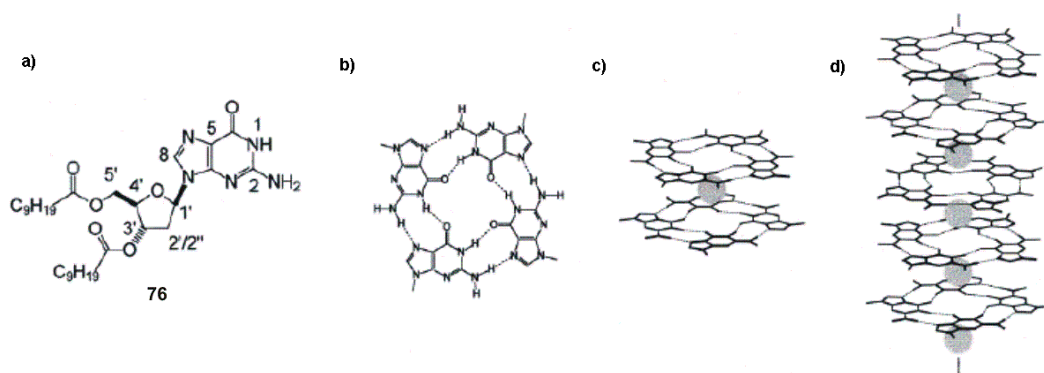


Figure 32: a) lipophilic deoxyguanine base **76**; b) G-quartet; c) octamer with sandwiched metal ion; d) metal ion stabilized polymeric stacked aggregate of G-quartets.

Another example of hierarchical assembly of planar hydrogen-bonded rosettes has been reported by Fenniri et al.¹⁰⁴ The module **77**, combining three hydrogen bonding guanine module of DDA type with complementary cytosine AAD motif was synthesized. It was shown before, that this type of bifunctional molecules forms cyclic hexamers. The methyl group was introduced to enhance the tendency for aggregation and to shield the hydrogen bonding from water molecules. The crown ether residue serves as a complexing unit, through which, chirality can be induced to the overall structure upon complexing amino acids. The stacking of rosettes occurs in water resulting in chiral tubular structure (**Figure 33**).

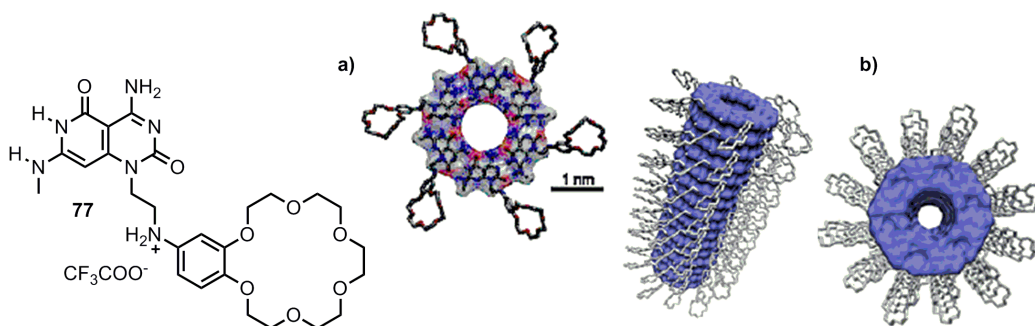


Figure 33: Fenniri's hydrogen bonding monomer **77**; a) cyclic hexameric rosette of **77**; b) tubular polymeric aggregate composed of stacked rosettes.

One of the rare examples of formation of a tubular structure without involving elements of two dimensional cyclic arrays has been reported by Sander et al. in which the α -amino acid **78** functionalized with naphthalene diimide spacer was shown to assemble in polymeric hydrogen bonded tubular structure.¹⁰⁵ The X-ray diffraction analysis revealed that the structure is held together by hydrogen bonding between carboxylate residues and the naphthalenediimide blocks constitute the walls of the tube (**Figure 34**). The same type of aggregation persists in solution, and even more, it was used to for the complexation of C_{60} inside the cavity of the tube.¹⁰⁶

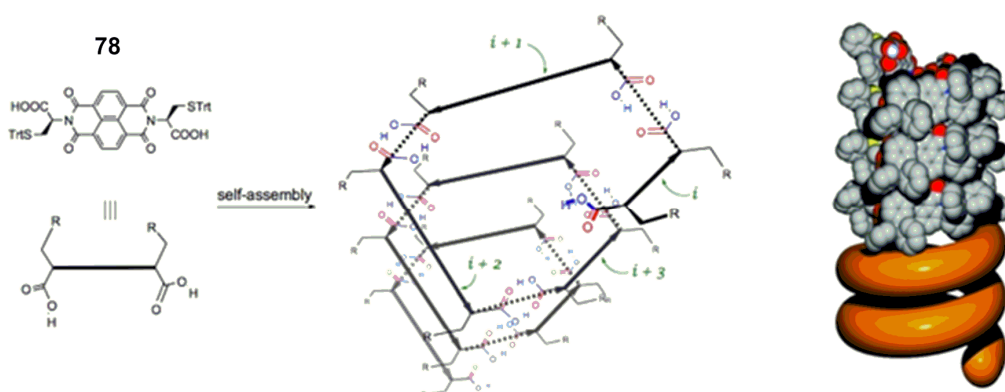


Figure 34: Tubular self-assembly of chiral amino acid with naphthalene diimide spacer.

3.4 Design of synthons for tubular aggregation

In this chapter we describe the synthesis and association studies in solution of three new chiral C_2 -symmetric hydrogen bonding supramolecular synthons **79-81** (**Figure 35**). In the first generation compound (**-**)-**79**, the rigid bicyclo[3.3.1]nonane skeleton is fused with azaindole framework, incorporating hydrogen bonding AD-DA 2-pyridone motif. According to molecular modeling, the (**-**)-**79** is expected to form tubular structure with the inner diameter of 12-14 Å. The structure is characterized by rather long distance between the hydrogen bonding units resulting in the outstretched helix in which interaction between the individual helix turns is not possible. In the second generation compounds (**+**)-**80-81**, the distance between recognition patterns is highly reduced by elimination of indole spacer. Moreover, the 3H-bonding motif of isocytosine is incorporated. The isocytosine is known to exist in solution as a mixture of two tautomers and the tautomeric composition is solvent dependent. One tautomer of isocytosine is complementary to another tautomer, similar to the heteroleptic complex of guanine and cytosine bases in DNA. Herein, we introduce a new classification for the complexes formed between two tautomeric forms of the same compound, namely the tautoleptic aggregation. In tautoleptic aggregation, the number of hydrogen bond acceptors and donors in hydrogen bonding array increases as a consequence of tautomeric equilibrium followed by amplification of the process via formation of strong AAD-DDA tautoleptic dimer. From this point of view, the tautoleptic aggregation may be regarded as special case of association induced tautomerism. By incorporating two isocytosine moieties into chiral bicyclic spacer, the isocytosine tautomers are preorganized for the formation of cyclic structures and, moreover, the self-assembled rings have additional hydrogen bonding sites along the rim that could be used for their further unidirectional stacking into tubular structure. The concept and the molecular modeling result for the tubular structure is illustrated in **Figure 35d-f**.

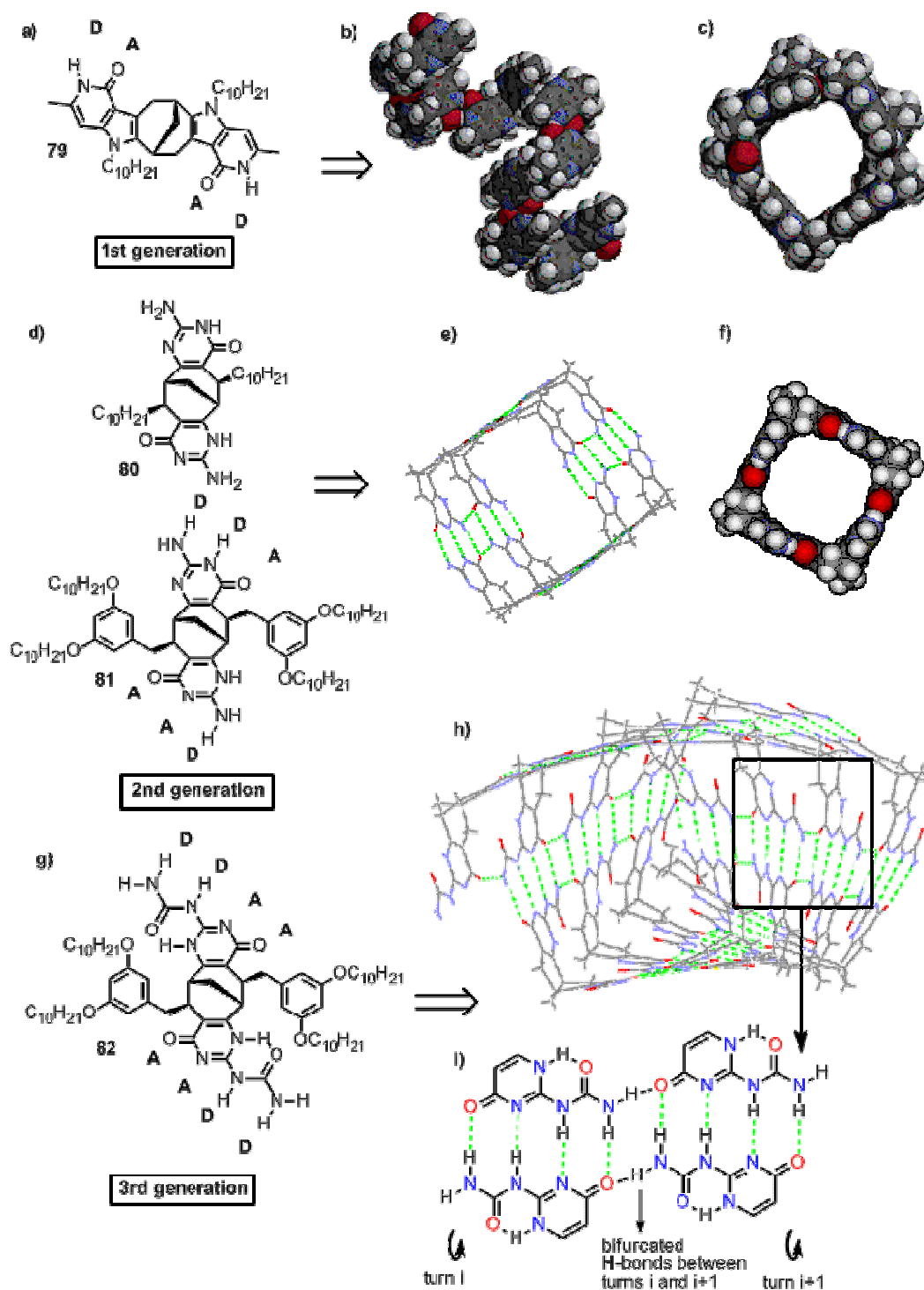


Figure 35: a) first generation cavity compound **79**, containing two hydrogen bonding 2-pyridone moiety; b) side view of proposed supramolecular helix; c) top view of proposed supramolecular helix; d) second generation of cavity compounds **80** and **81** based on tautoleptic aggregation of triple hydrogen bonding moiety of isocytosine; e) proposed tubular structure, formed by stacking of tetrameric units, depicted in f); g) third generation cavity molecule incorporating quadruple hydrogen bonding 2-ureido pyrimidinone unit; h) proposed tubular structure, stabilized by additional hydrogen bonds between the turns; i) illustration of hydrogen bonding pattern.

Finally, in the third generation synthon **(-)-82**, the 4H-bonding array is incorporated into the chiral bicyclic structure. The hydrogen bonding array is extended by using ureidopyrimidinone module in which urea -NH₂ group not only constitutes the AADD motif but also ensure the communication between the turns of helix by the mean of additional hydrogen bonding. Due to the geometric features of monomer **(-)-82**, the formation of cyclic structures is not likely to occur. The proposed mode of aggregation is depicted in **Figure 35g-i**. The helicity information of each rigid tubular structure is encoded in the building blocks and the homochiral units constitute the well-defined walls of the tubular structure. To our knowledge, the similar principles for tubular structure design have never been applied before. In addition to carbocyclic structures **79-82**, the synthesis of related azabicyclic analogues has been attempted.

3.5 1st generation synthon

3.5.1 Synthesis

The synthesis of corresponding azaindole framework from the enantiomerically pure diketone is very well documented in previous studies conducted by Stončius et al. in our group.¹⁰⁷ It was shown that unsubstituted compound (–)-**83** has a very low solubility in common solvents and the crystals obtained from acetic acid or DMF do not show the desired aggregation pattern in a solid state. It was thus anticipated that improving the solubility of supramolecular synthon by introducing solubilizing chains via alkylation of indole nitrogen could benefit not only for the further solid state studies but also exclude undesired NH hydrogen bond donor originated from indole moiety.

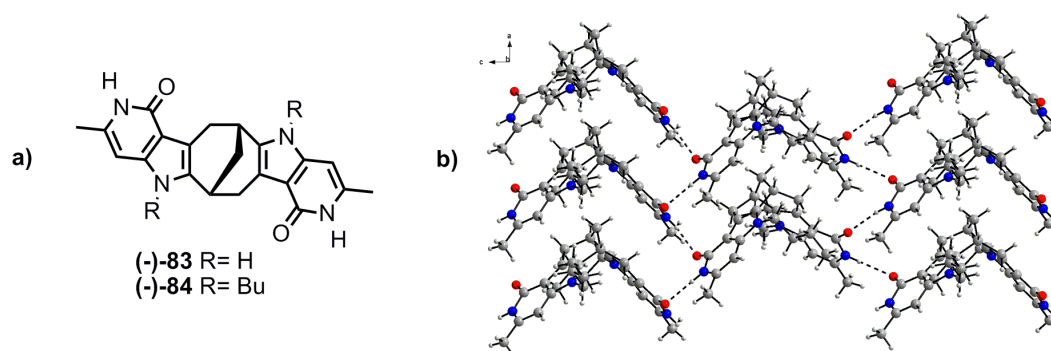


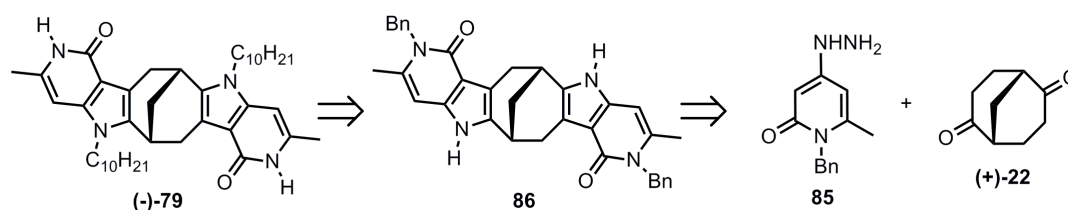
Figure 36: a) bicyclic hydrogen bonding chiral cleft molecules **83-84**, containing 2-pyridone motif; b) solid state structure of (–)-**84** showing hydrogen bonding pattern between adjacent 2-pyridone moieties.

With this intention, the more soluble chiral derivative (–)-**84** was synthesized bearing two butyl groups. Unfortunately, association of compound (–)-**84** in solid state also failed to give the expected tubular structure. Instead of forming centrosymmetric dimers between self-complementary AD-DA pyridone moieties, each pyridone motif is connected with four neighbouring molecules giving rise to hydrogen bonded network. In addition to N-H \cdots O=C hydrogen bonding, the crystal packing is assisted by the interaction of heteroaryl face with the protons of bridging methylene group. As a result, the concave molecules are stacked in rows in a shape complementary way. The crystal

packing mode is somewhat similar to that of parent 2-pyridone¹⁰⁸ and also, to the Lehn's chiral bicyclic lactam,¹⁰⁹ where the involvement of only single hydrogen bonding site of AD motif to bond a second adjacent molecule was observed.

It has occurred to us that the crystal packing forces are in favour of more dense arrangement of molecule in the solid state than if it would have resulted in case of anticipated helical architecture. Although it may be possible to find a substrate, which could co-crystallize with (-)-**84** and enforce the formation of tubular structure, we decided to investigate in depth the association of (-)-**84** in solution. For this purpose, the compound (-)-**79** bearing a longer solubilizing group was desired in order to ensure a wide range of concentrations in chlorinated solvents. The improved synthesis of compound (-)-**79** and its aggregations studies are described in this paragraph.

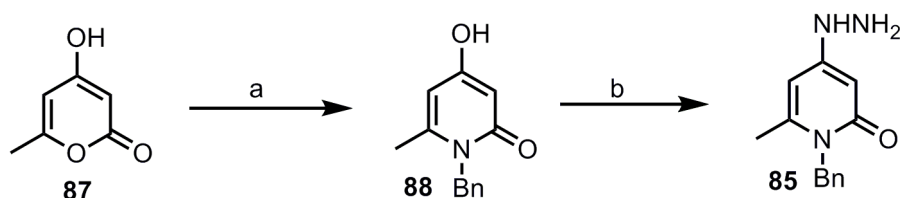
The retrosynthesis of target compound is briefly presented in **Scheme 3**. The synthesis starts with the condensation of enantiomerically pure diketone (+)-**22** with N-benzylprotected 2-pyridone hydrazine **85** to give the corresponding hydrazone, the latter subjected to thermal Fisher cyclization would afford azaindole **86**. The alkylation of compound **86** was expected to proceed smoothly at the indole nitrogen to give final compound after removal of benzyl protecting group.



Scheme 3: retrosynthetic analysis of compound (-)-**79**.

The synthesis of hydrazine **85** was accomplished by the reaction of commercially available pyrone **87** with benzyl amine in boiling water to give corresponding N-benzyl-4-hydroxy pyridone **88** in 56% yield. This transformation was previously reported in literature,¹¹⁰ however, neither the

yield of the reaction or experimental details were given. We found that the main side product was di-benzylamino substituted pyridone, the formation of which can be inhibited to some extent by using slightly less than equimolar amount of benzylamine (**Scheme 4**).

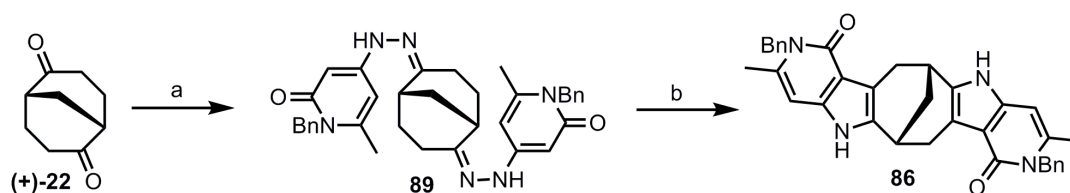


Scheme 4: *Reagents and conditions:* a) BnNH₂, H₂O, reflux, overnight; 56% b) NH₂NH₂·H₂O, MW 250W, 7min, 57%.

Nucleophilic substitution of the hydroxy group in **88** was expected to proceed readily under the conditions analogous to the synthesis of the corresponding non-*N*-benzylated hydrazine. However, all attempts to obtain hydrazine **85** directly from **88** by using an excess of the hydrazine monohydrate in boiling 2-ethoxyethanol or methanol yielded intractable mixtures. Fortunately, when the conditions of related procedure for the aminolysis of hydroxy pyridones using microwave radiation were adopted,¹¹¹ the corresponding hydrazine **85** was obtained in 57% yield. The reaction required extensive optimization and the best results were obtained under the neat conditions when the mixture of **88** and excess hydrazine hydrate was irradiated at 250 W for 7 minutes. The reaction scale was limited to few hundreds of milligrams as a consequence of high pressure that develops during irradiation due to the volatility of hydrazine hydrate. Performing the reaction in separate batches, the gram quantities of **85** were obtained (**Scheme 4**). The hydrazine **85** slightly decomposed upon exposure to silica gel during the flash chromatography, however the resulting impurity did not affect the yield of the next step. Analytically pure sample was obtained by multiple recrystallization from methanol, though with significant loss of material.

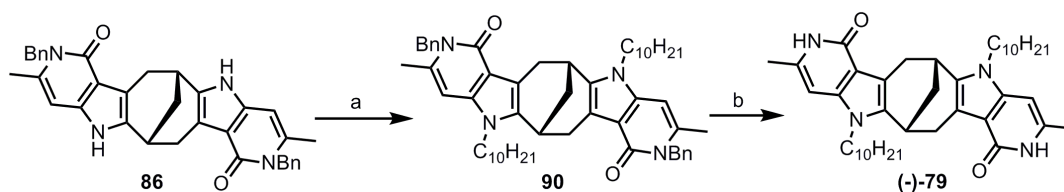
With the hydrazine **85** in hands, the formation of hydrazone **89** was accomplished under standard conditions by boiling the enantiomerically pure

diketone **22** with slight excess of hydrazine **85**. Taking advantage of low solubility of bishydrazone **89**, it was separated from the reaction mixture by simple filtration and after washing with methanol the product was obtained in 95% yield (**Scheme 5**). Subsequent thermal Fischer indole cyclization in boiling diphenyl ether afforded diindole, which was even less soluble than non-benzylated congeners, most likely due to the more efficient solid state packing via intermolecular π - π stacking of benzylic units. The harsh reaction conditions and the propensity of indole moiety for oxidation necessitated the continuous flow of argon through the mixture during the reaction. The spectral data of compound **86** was in accordance with C_2 -symmetric structure and indicated hindered rotation around C-N benzylic bond, which resulted in diastereotopicity of benzylic protons.



Scheme 5: Reagents and conditions: a) **85**, MeOH, reflux, 5 h, 95%; b) Ph₂O, reflux, 8h, 94%.

Alkylation of dianion generated from **86** using NaH as a base in dry DMF at ambient temperature with decyl iodide afforded the corresponding decyl derivative **90** in 85% yield. After numerous attempts to remove the protecting benzyl group using different procedures, the Birch reduction proved to be the method of choice. Addition of **90** to preformed solution of Na in a mixture of liquid ammonia and THF (1:1-v/v) at -45°C led to a smooth deprotection and the target compound was isolated in 83% yield (**Scheme 6**). The (-)-**79** was soluble in chlorinated solvents as expected and was used for association studies in solution.



Scheme 6: Reagents and conditions: a) NaH, DMF, C₁₀H₂₁I, rt, 24h, 83%; b) Na, NH₃(liq.):THF, 83%.

3.5 Aggregation studies in solution

NMR titration is widely used to observe and quantify the association processes by estimating the association constants of supramolecular aggregates. For an aggregate in fast exchange on the NMR time scale, the observed chemical shift of a particular proton is the weighted average of the chemical shifts in the native (nonexchanging) environments. The aggregation behavior was followed by observing the shift of NH proton of 2-pyridone moiety in CDCl₃ and CD₂Cl₂. The strong concentration dependence of a latter gave a clear indication that aggregation through the hydrogen bonding pyridone module takes place (**Figure 37**). Assuming the formation of higher than dimeric aggregates, NMR dilution titration data were analyzed by using the isodesmic model of indefinite association ($K_1 = K_2 = \dots = K_n = K_E$) for the formation of supramolecular polymers (linear aggregates).¹¹² The chemical shift δ for each of the studied proton resonances depends on the total concentration, c_t , of the monomer and the association constant, K_E , according to eq 1, where δ_m and δ_a are the chemical shifts of the studied proton resonance in the monomer and the average shift in the aggregates, respectively. By measuring the observed chemical shift(s) of the observed proton resonance(s), δ_{obs} , at different values of c_t , a data set is obtained.

$$\delta_{obs} = \delta_m + (\delta_a + \delta_m) \left(1 + \frac{1 - \sqrt{4K_E c_t + 1}}{2K_E c_t} \right) \quad (1)$$

By using a nonlinear curve fitting procedure in which the parameters δ_m , δ_a , and K_E in eq 1 are estimated to give the best fit of $\delta = f(c_t)$ to the observed data set $(\delta_{\text{obs}}, c_t)$, an estimate of K_E can be obtained.

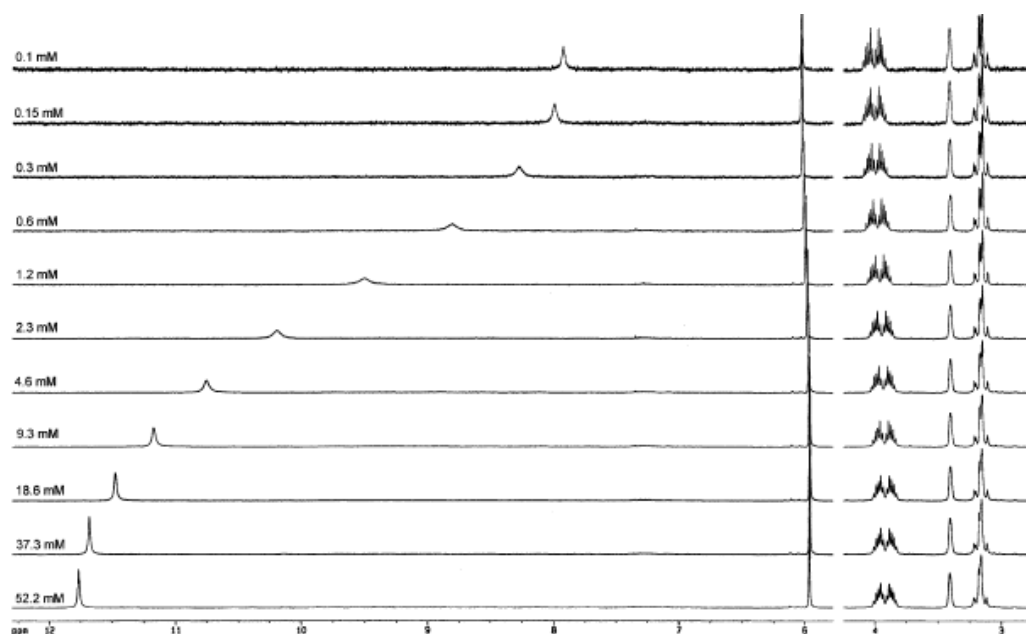


Figure 37: Parts of the ^1H NMR spectra (400 MHz), CD_2Cl_2 , 299K of $(-)\text{-79}$ at different concentrations.

We also pursued to estimate the change in enthalpy and entropy for the association of the 2-pyridone binding site in the monomer to another such site in an aggregate (polymerization) or in another monomer (dimerization) using the same model. Usually, estimates of the association constant K_E at different temperatures are used in a linear curve fitting procedure of the van't Hoff's eq 2 to give estimates of ΔH^0 and ΔS^0 .

$$\ln K_E = -\frac{\Delta H^0}{R} \frac{1}{T} + \frac{\Delta S^0}{R} \quad (2)$$

However, instead of estimating K_E values at each investigated temperature using the procedure above, *e.g.* eq 1, a globally better fit of δ to δ_{obs} can be obtained by a nonlinear curve fitting procedure. Consequently, the parameters δ_m , δ_a , ΔH^0 , and ΔS^0 in eq 3, obtained by combining eqs 1 and 2, are estimated to give the best fit of $\delta = f(c_t, T)$ to the observed data set $(\delta_{\text{obs}}, c_t, T)$. In this way,

estimation of ΔH^0 , ΔS^0 , and thus K_E at different temperatures is obtained with higher accuracy.

$$\delta = \delta_m + (\delta_a + \delta_m) \left(1 + \frac{1 - \sqrt{4c_t \exp\left(-\frac{\Delta H^0}{R} \frac{1}{T} + \frac{\Delta S^0}{R}\right) + 1}}{2c_t \exp\left(-\frac{\Delta H^0}{R} \frac{1}{T} + \frac{\Delta S^0}{R}\right)} \right) \quad (3)$$

A single set of signals corresponding to the NH proton resonance of (–)-**79** was observed throughout the concentration range with some sharpening of the signals upon dilution. In CDCl_3 , 10 different concentrations (79.0-0.667 mM) at five different temperatures (258-311 K) were investigated giving in total 50 data points.

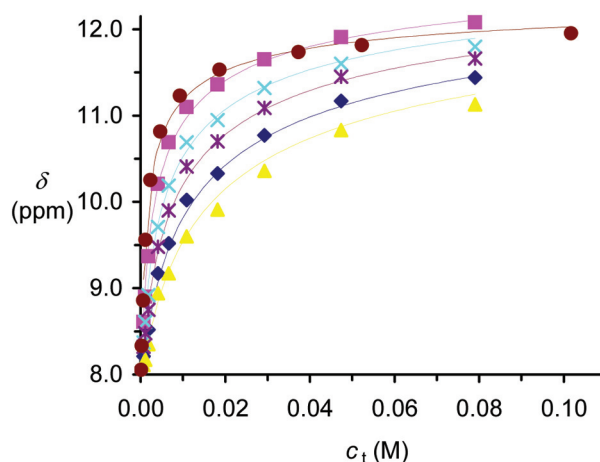


Figure 38. Observed chemical shifts of the NH proton resonance of (–)-**79** in CDCl_3 and CD_2Cl_2 , respectively, at different concentrations and temperatures. The solid lines represent the best fit of the observed data to the isodesmic model of indefinite association as expressed by Equation 3. In CDCl_3 : 258 K (■), 272 K (×), 284 K (⋈), 299 K (◆), 311 K (▲). In CD_2Cl_2 : 299 K (●).

By using non-linear data fitting to the equation 3, the corresponding values of ΔH^0 and ΔS^0 were estimated to be $-20.3 \pm 1.2 \text{ kJ mol}^{-1}$ and $29.1 \pm 4.2 \text{ J mol}^{-1} \text{ K}$, respectively. The estimated value of ΔH^0 is slightly lower than the corresponding experimental value obtained for the dimerization of 2-pyridone itself in CHCl_3 ($-24.7 \text{ kJ mol}^{-1}$),^{113,114} corresponding to twice the heat of formation of a single $\text{N-H}\cdots\text{O}=\text{C}$ hydrogen bond in CHCl_3 . This slightly lower value of ΔH^0 can be explained by some steric repulsion between the two

interacting 2-pyridone units due to the presence of the methyl group in the positions 3 and 10 in (-)-**79**. Nevertheless, the similarity of the ΔH^0 values indicates that the 2-pyridone motif of (-)-**79** is involved in self-complementary aggregation. Thus, since (-)-**79** is enantiomerically pure, the aggregate should be of a tubular helical structure of the type depicted in **Figure 35**.

By using Equation 2, K_E for each investigated temperature could be calculated from the estimated values of ΔH^0 and ΔS^0 (**Table 1**).

Table 1. Estimation of the association constant K_E for the indefinite association of (-)-**79** in CDCl_3 according to the isodesmic (equal K) model of indefinite association.^a

T (K)	K_E (M^{-1})
258	382± 60
272	235±35
284	161±21
299	105±14
311	77±10

^aThe value of K_E at each of the investigated temperature T is obtained from the ΔH^0 and ΔS^0 values using Equation 2.

According to common experience, compound (-)-**79** associates approximately 10 times stronger in CD_2Cl_2 , which is less C-H acidic compared to CDCl_3 . The upfield shift of the resonance of the NH protons from δ 11.9 to 7.93 was observed as concentration decreased from 102 to 0.102 mM (**Figure 38**). Using the non-linear curve fitting procedure based on equation 1, the association constant K_E for the aggregation of (-)-**79** in CD_2Cl_2 was calculated to be $1142 \pm 162 \text{ M}^{-1}$ at 299 K, and the chemical shifts of the NH proton resonance in free and an average of completely associated (-)-**79**, δ_m and δ_a , were calculated to be 7.34 ± 0.12 and 12.44 ± 0.08 ppm, respectively.

In order to estimate the contribution from another possible type of aggregation, such as π - π stacking, a closer inspection of the different ^1H NMR spectra obtained from the dilution titrations of (-)-**79** were undertaken. Compared to marked concentration dependence of chemical shift of pyridone NH protons,

only a small change was observed for corresponding resonance signals of heteroaromatic methine and methyl group in pyridone ring (**Figure 39**). More interesting, the concentration dependence of chemical shift of aforementioned functional groups displayed a minimum value at $c_t = 18.7$ mM. This concentration corresponds to an average degree of polymerization $DP = 5$ (*vide infra*), at which the presumed helix has completed one turn. Most likely at this point shielding/deshielding process has reversed. A very small concentration dependence of aromatic proton resonances implies that intermolecular π - π stacking is not operating in our case, supporting the proposed tubular structure as was anticipated for chiral compound (-)-**79** associating through the hydrogen bonding between pyridone motifs.

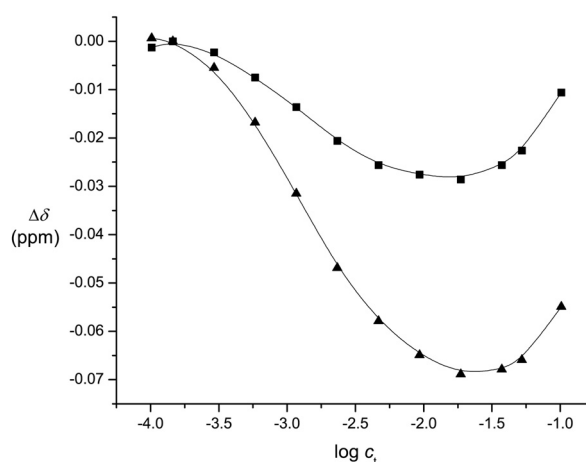


Figure 39. Concentration dependence of ^1H NMR chemical shifts of (-)-**79** in the concentration range 102-0.102 mM for heteroaromatic methine (■) and C3(10)-CH₃ (▲) proton resonances in CD_2Cl_2 at 299 K. The solid lines are to guide the eye.

The isodesmic model of infinite association expressed as a concentration dependence of δ_{obs} is indistinguishable from corresponding model describing solely the equilibrium of dimerization. The only difference being in the absolute value of dimerization constant K_2 , which in case of dimerization, would be equal $K_2 = \frac{1}{2} K_E$. Vapour pressure osmometry seemed to be a perfect independent method to differentiate between the two modes of aggregation.

Vapour pressure osmometry is based on measurement of colligative property of system, i.e., the total number of particles in solution. At a given temperature, the vapor pressure of a solution is less than that of pure solvent. In a typical

experimental setup, the solution and the pure solvent droplets are placed on two thermistors and the temperature rise caused by the release of condensation heat on the thermistor with the droplet of solution is measured with high accuracy as a difference in resistance. The calibration curve obtained by using compound of known molecular weight and not aggregating to a significant degree in given solvent is used to relate the machine readings to real molal concentration of the compound in solution. The ratio of the osmotic molality (calculated from calibration curve) and stoichiometric molality is called osmotic coefficient Φ . In case when compound does not aggregate, the osmotic coefficient is equal to $\Phi=1$. In this case, the osmotic molality is the same as the corresponding stoichiometric molality. In case when solute molecules aggregate with each other, the number of species in solution decreases and Φ is <1 . For complexes of moderate strength, the osmotic coefficient depends on concentration as the degree of association is directly related with the concentration. The concentration dependence of osmotic coefficient fitting to the appropriate mathematical model leads to the extraction of association constant and degree of association. When compound forms a strong complex of well-defined composition, the osmotic coefficient is no more sensitive to the concentration and the degree of polymerization can be obtained straightforward since $DP= 1/\Phi$. Taking into account that isodesmic (or dimerization) model fitted well for compound (–)-**79** and that association constant is only moderate, we decided to use the procedure reported by Tso and Chan.¹¹⁵ According to this method, the equation 4 that relates both association constant and the maximum number of monomers in the largest aggregate under given conditions, is derived by assuming isodesmic mode of association. The ratio Φ/γ was obtained experimentally and was plotted versus corrected molality m_1 (**Figure 40**).

$$\frac{\Phi}{\varphi} = \frac{1 - (K_E m_1)^n}{1 - K_E m_1} \quad (4)$$

The latter was obtained from stoichiometric molality and activity coefficient γ using relationship $m_1= m^* \gamma$. By fitting data obtained for seven different

concentration of (–)-79, the association constant K_E was estimated to be $120 \pm 6 \text{ M}^{-1}$ and $\gamma = 3.7 \pm 0.3$. The value of K_E obtained is in perfect agreement with the NMR titration data which gives $K_E = 77 \text{ M}^{-1}$ at 311K, the temperature at which VPO measurements were conducted. Keeping in mind relatively low sensitivity of the method and the fact that VPO generally gives higher values of K_E when the extent of aggregation is small, the agreement between two methods is even more perceptible. Furthermore, the VPO data indicated that $n > 2$ thus refuting dimerization model.

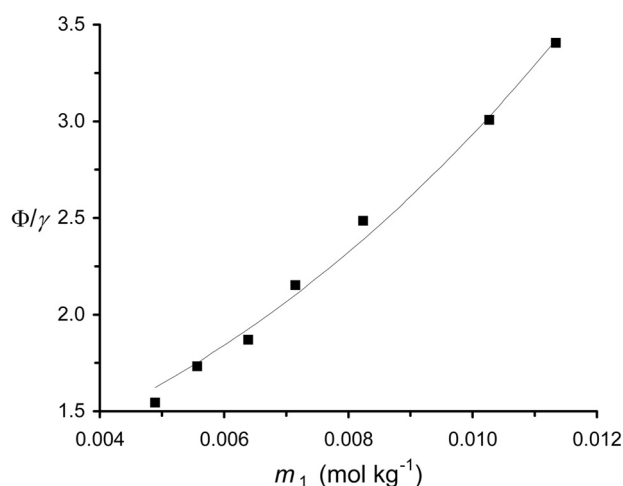


Figure 40. Observed ratio between the osmotic and activity coefficient, Φ/γ , at different true molal concentrations (activities) m_1 of (–)-79 in CHCl_3 at 313 K. The solid line represents the best fit of the observed data to the isodesmic model of indefinite association (equal K model, Equation 4).

The electronic spectroscopy is a classical technique widely used to study different kind of equilibrating systems. This analytical method is non-degrading and very sensitive provided the molecules contain good chromophore(s). When molecule possessing aromatic or heteroaromatic rings aggregates by mean of π - π stacking, the absorption bands are expected to shift, most likely hypsochromically and the concentration dependence of absorbance should significantly deviate from linearity. The UV titration was performed in CH_2Cl_2 and the spectra obtained are shown in **Figure 41a**. The absence of isosbestic points and the fact that the general image of the spectra does not

change with concentration indicate that the monomers do not interact with each other's chromophores when forming aggregates, thus suggesting the absence of π - π stacking in the concentration range studied. Furthermore, the spectra are similar to the di-*N*-benzyl-protected derivative (–)-**90** spectra meaning that the absence of hydrogen bonds does not significantly change the spectra (**Figure 41b**).

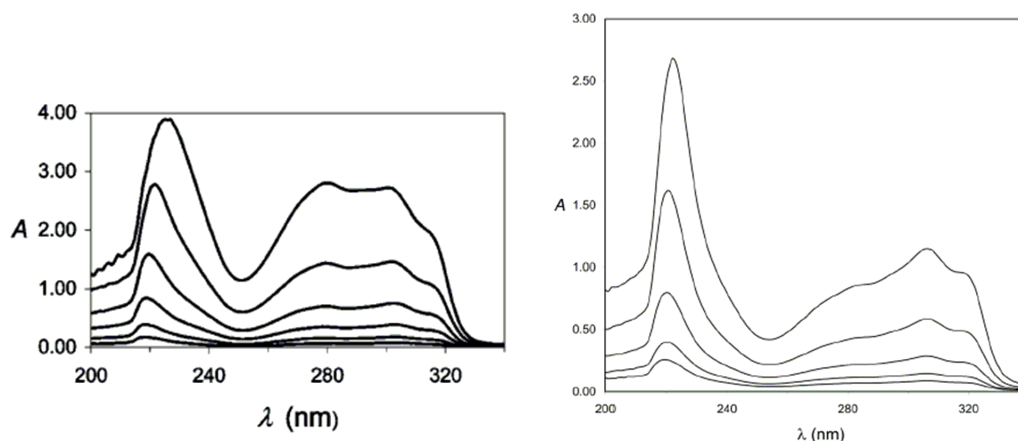


Figure 41: a) UV spectra of (–)-**79** in CH₂Cl₂ at 1.6 mM (highest absorbance) to 0.05 mM each, concentration is half of the previous higher one; b) UV spectra of **90** in CH₂Cl₂ at 0.51 mM (highest absorbance) to 0.03 mM, each concentration is half of the previous higher one.

The application of CD spectroscopy for studying molecules or molecular assemblies possessing elements of helicity is well documented.¹¹⁶ This method is especially useful when the overall helicity of the supramolecular structure is induced by “CD silent” chiral molecule.¹¹⁷ In case of compound (–)-**79**, the change in CD spectrum pattern and shift of CD bands upon dilution are expected as a consequence of reversible nature of hydrogen bonded aggregates. Indeed, the notable changes in CD spectra were evident.

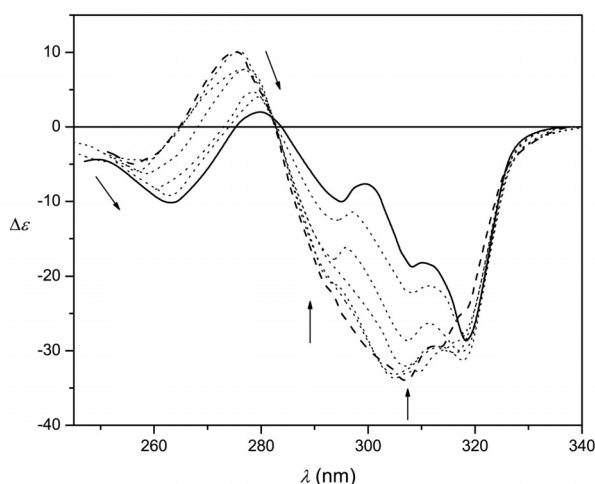


Figure 42. CD spectra of (-)-**79** in CH_2Cl_2 at concentrations from 3.3 mM (—) to 0.05 mM (---), each concentration is half of the previous higher one. Arrows indicate changes as concentration increases.

The CD spectra of compound (-)-**79** are depicted in **Figure 42**. The variation in CD spectra is definitely related with hydrogen bonding, since CD spectra of N-benzylated derivative (-)-**90** are lacking those changes over the whole range of concentration (0.5-0.032 mM). In addition, the non-linear concentration dependence of $\Delta\epsilon$ was observed. Unfortunately, it is not possible, based only on simple consideration, to decide whether the noted changes are resulted from helical arrangement of chromophores or is merely a demonstration of self-association. The issue is even more complicated by the fact, that the molecule itself has an inherent chirality, which may mask important chiroptical features of supramolecular aggregate.

Refuting the dimerization model enables calculation of the average number of monomers in the associate (polymer) obtained by self-association of (-)-**79** (the degree of polymerization, DP) from the NMR dilution titrations. For the isodesmic model of self-aggregation, DP is calculated using eq 5, where c_m is the molar concentration of free monomer, obtained from the total molar concentration of monomer, (-)-**79** in solution (free and associated), c_t , eq 6.¹¹⁸

$$DP = \frac{1}{1 - K_E c_m} \quad (5)$$

$$c_t = \sum_{i=1}^{\infty} i c_i = \sum_{i=1}^{\infty} i K_E^{-1} (K_E c_m)^i = \frac{c_m}{(1 - K_E c_m)^2} \quad \text{for } K_E c_m < 1 \quad (6)$$

The resulting curves showing DP as a function of the total molar concentration of (–)-**79**, c_t , in CDCl₃ and CD₂Cl₂, respectively, and at various temperatures are shown in **Figure 43**. As expected, the average size of the aggregate increases with decreasing temperature and in a less protic solvent (CD₂Cl₂). We can conclude from the values of DP obtained from NMR dilution titrations and from the values of n obtained from the VPO measurements that (–)-**79** forms aggregates containing only a few monomers in CDCl₃/CHCl₃ at 299 K. However, in CD₂Cl₂, at 299 K, the aggregates contain up to 11 units of (–)-**79** on an average. The relatively small extent of aggregation is related to low value of association constant. Nevertheless, the present example demonstrated the first example of tubular self-aggregation of concave chiral monomer (–)-**79** through the hydrogen bonding without the stabilization of final helical structure with additional forces, such as π - π stacking. The fact that the value of the standard enthalpy of association of compound (–)-**79** is very similar to the one of the dimerization of the 2-pyridone itself suggests that the propagation of supramolecular aggregate involves the formation of hydrogen bonds between two pyridone moieties and also shows non-cooperative interaction. The non-cooperative aggregation of monomers means that subsequent addition of monomer to the self-assembled dimer does not create any additional favorable or unfavorable interaction between the monomers and the individual interactions are contributing separately. The perfect fit of experimental data to isodesmic model in which cooperativity is not possible by definition ($K_E = K_{n-1} = K_{En}$) further supports simple association mechanism.

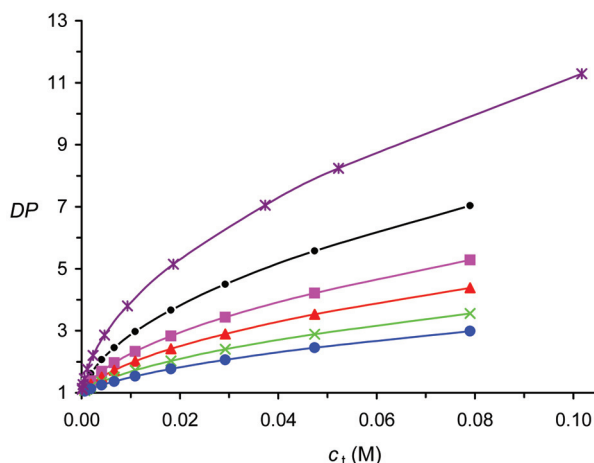


Figure 43. The average degree of polymerization, DP , as a function of the total molar concentration of (–)-**79**, c_t . In $CDCl_3$: 258 K (●), 272 K (■), 284 K (▲), 299 K (×), 311 K (●). In CD_2Cl_2 : 299 K (⋈).

The absence of cooperativity is not surprising in present case, since the supramolecular structure of helical aggregate composed of monomer (–)-**79** is very loosely packed and the interaction between individual helix turns is hardly possible.

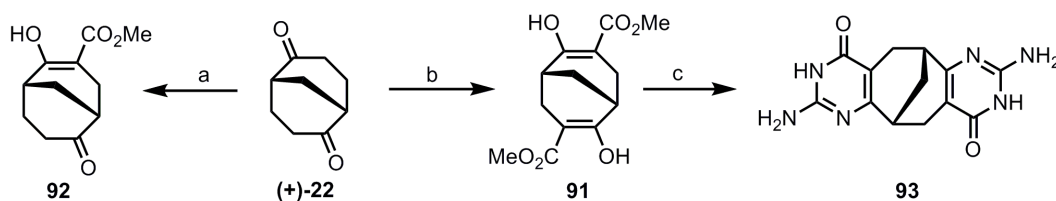
With the aim to increase the stability of tubular structure by using synthons having three and four hydrogen bonding sites, we decided to synthesize compounds (+)-**80-82** in which the fused indole ring is removed. The shorter distance between hydrogen bonding arrays within the molecule could in principle guaranty the secondary interactions between helix turns making the overall association process more energetically favourable.

3.6 2nd generation synthon

3.6.1 Synthesis

The target bicyclic isocytosines **80-81** can be synthesized from bis- β -ketoester **91** by condensation with guanidinium carbonate. Due to necessity to use chiral building blocks in order to ensure their tubular arrangement, the enantiomerically pure dione (+)-**22** was used as a starting material for all syntheses. The use of (+)-**22** instead of racemic one is also advantageous in

respect to higher solubility of the respective derivatives of the former. The synthesis of bis- β -keto ester **91** is reported in literature,^{119,31} and involves selective partial hydrolysis and decarboxylation of Meerwein ester **29** or the use of acyclic precursors. Unfortunately, none of those procedures could be applied to obtain enantiomerically pure **91**. We realized that compound **91** can be synthesized by acylation of (+)-**22** with dimethyl carbonate. Treatment of the dione with excess of NaH in THF together with dimethyl carbonate afforded only monofunctionalized derivative **92** as a major product. It appeared that the mono sodium salt of mono- β -ketoester **92** is not soluble in moderately polar solvent THF and precipitates from the reaction mixture. Under strictly controlled conditions, this reaction can be used for selective monofunctionalization of **22**. When the polarity of the reaction mixture and thereby the solubility of the sodium salt of monofunctional derivative was increased by substituting THF with DMF, the bis- β -ketoester **91** was obtained in 90% yield. The addition of dione (+)-**22** has to be as slow as possible since at higher addition rate the excess of starting material decomposed via formation of aldol-type products.



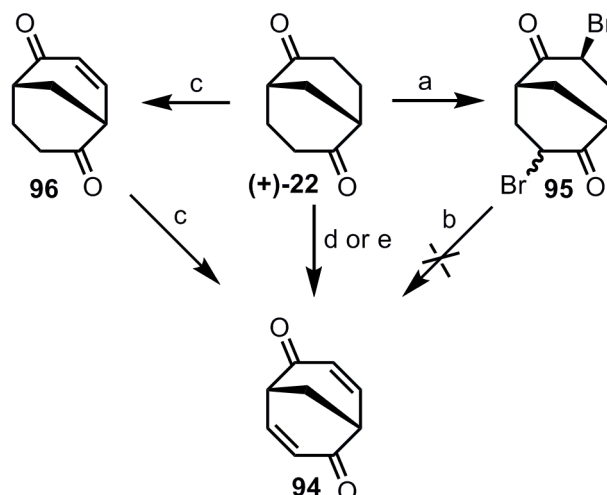
Scheme 7: Reagents and conditions: a) NaH, DMC, THF, rt; b) NaH, DMC, DMF, rt, overnight, 90%; c) guanidine carbonate, MeOH, reflux, overnight, 80%.

The obtained bis- β -ketoester was condensed with guanidinium carbonate in boiling methanol to afford isocytosine derivative **93** in 80% yield (**Scheme 7**). The compound **93** was not soluble in most of the common solvents except highly polar hot DMSO and acetic acid. By comparison with other bicyclic derivatives in which the bicyclic framework is fused with heteroaromatic rings having contiguous hydrogen bonding arrays, such as in compound (-)-**83**, the poor solubility of **93** is not very unexpected. To increase the solubility, the alkyl chains have to be attached to bicyclic skeleton. The resulting structure

would be more bulky and might resist close packing in solid state. The only sites available for the attachment of solubilizing chains without interfering with the formation of anticipated tubular aggregate are those at 4 and 8 positions on bicyclic scaffold. The *exo,exo*-selective alkylation of bicyclic dione (+)-**22** was envisioned to be achieved via Michael addition of organocopper reagents to unsaturated dione **94**. Although several syntheses of **94** from corresponding dione **22** were reported in literature,^{120,121,122} they could not be applicable to large scale synthesis. One of the methods affording highest yields comprises bromination-dehydrobromination reaction sequence; however the workup and product purification are extremely tedious, mainly due to side products formed in bromination step.¹²² During long time interest in bicyclo[3.3.1]nonane chemistry in our laboratory, it was found that the corresponding dibromo diketone **95** can be obtained almost free of other over-brominated side products by simple bromination with elemental bromine and further recrystallization of diastereomeric mixture. The subsequent attempts to accomplish dehydrobromination using DBU as milder alternative to inorganic bases were unsuccessful, producing tar-like products.

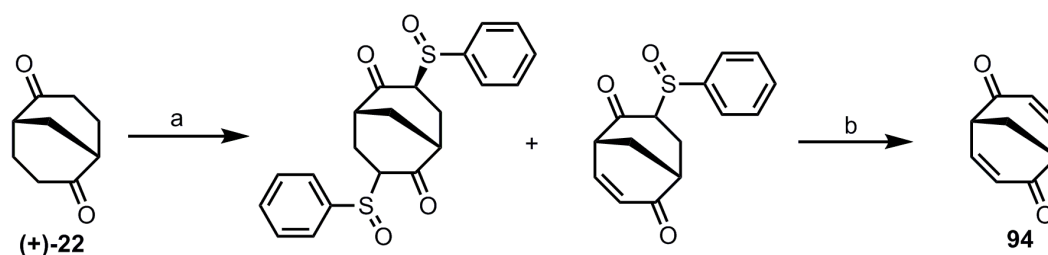
Recently, Nicolaou et al. reported unsaturation of carbonyl compounds mediated by stoichiometric amount of hypervalent iodine oxidant IBX.^{123,124} In our hands, this one-step synthesis of enones was quite rewarding with dione **22** providing dienone **94** and enone **96** in 70% and 65% yield, respectively. Nevertheless, it required a large excess of expensive IBX (4-8 eq.) and long reaction times (38-48 h) for complete conversion, and thus rendered this method unsuitable for scaling up the reaction (**Scheme 8**).

The Barton dehydrogenation procedure¹²⁵ in which the benzeneseleninic acid anhydride is generated *in situ* from catalytic amount of diphenyldiselenide and iodoxybenzene as stoichiometric oxidant, was very successful affording **94** in 90% yield. However, the explosive nature of iodoxybenzene prevented the use of this reaction for longer scale synthesis (see chapter 4 for the application of this reaction for small scale synthesis) (**Scheme 8**).



Scheme 8: Reagents and conditions: a) Br₂, CHCl₃, rt, 93%; b) DBU, toluene, rt; c) IBX, DMSO, 80°C, 20h, 65%; d) IBX, DMSO, 80°C, 48h, 70%; e) PhIO₂, cat.(PhSe)₂, cat. TsOH, toluene, reflux, 5h, 90%.

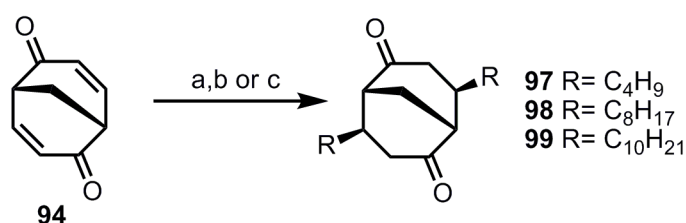
The related reaction, which relies on addition of phenyl sulphoxide group followed the thermal elimination was tested as an alternative to selenium chemistry. The treatment of diketone **22** with an excess of methyl benzenesulphinate using NaH as a base afforded diastereomeric mixture of disubstituted products with small amount of mono-unsaturated derivative. The mixture was subjected to thermal elimination directly after neutralization with acetic acid; however, the higher yield was obtained when the excess of methylphenyl sulphinate was removed before the elimination. This reaction enabled us to prepare dienone **94** in gram scale (**Scheme 9**).



Scheme 9: Reagents and conditions: a) PhSO₂Me, NaH, THF, rt, overnight; b) Na₂CO₃, toluene, reflux, 15 min. Overall yield 80%.

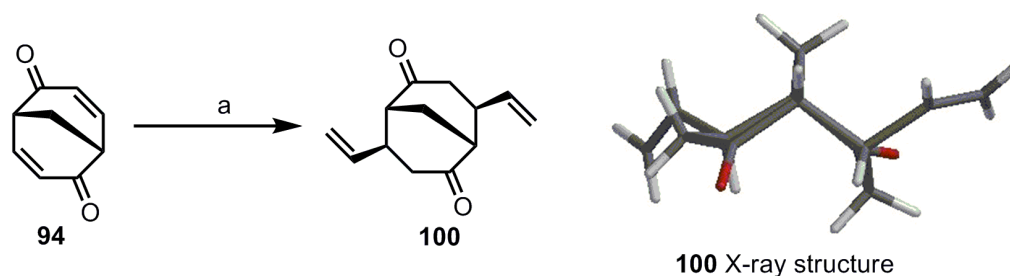
The obtained dienone subsequently was employed in Michael addition reaction, using dibutyl cuprate as a model reaction. The dibutyl ketone **96** was obtained in high yield via addition of dibutyl cuprate in THF or diethyl ether illustrating the potential of this approach (**Scheme 10**).

The butyl chain was obviously too short to provide the good solubility of the target compound and the method to introduce longer chains was sought. The higher alkyl lithium compounds can be obtained by the reaction of corresponding alkyl iodide with two equivalents of t-BuLi in diethyl ether-pentane mixture. Following this methodology, the octyl lithium was obtained and after transmetalation to Gilman cuprate, the Michael addition to dienone **94** afforded dioctyldione **98** in 83%. Despite the high yield, this method suffered one serious drawback, i.e. for 1 eq. of Michael addition product, 3 eq. of Gilman reagent was required, which in turn was obtained from 6 eq. of alkyl lithium or 12 eq. of t-BuLi and alkyl iodide. The large quantity of t-BuLi required to generate Gilman reagent made this procedure inconvenient. Therefore, the cheaper and readily available organozinc reagents were chosen to effect the same transformation. The organozinc reagents can be easily obtained by different methods using activated zinc metal and alkyl halide.^{126,127,128} The use of catalytic amount of iodine¹²⁹ to activate zinc metal was selected due to operational simplicity compared to more widely used activation with dibromoethane and TMSCl.¹³⁰ Furthermore, alkyl iodides can be substituted with cheaper bromides. When decyl bromide reacted with activated zinc in DMA for 5h at 80°C, the decylzinc bromide was obtained. The organocopper reagent was prepared by subsequent transmetalation reaction with soluble copper source (Knochel complex, CuCN·2LiCl).¹³¹ The monocuprate was not active enough to react with **94** and required activation with Lewis acid, trimethylsilyl chloride. The 1,4-addition product **99** was obtained in 95% yield (**Scheme 10**).



Scheme 10: Reagents and conditions: a) BuLi, CuCN, THF or Et₂O, -78°C, 77-85%; b) i) C₈H₁₇I, t-BuLi, Et₂O-pentane, -78°C to rt ii) CuCN, **94**, THF, -78°C, 83%; c) i) Zn, cat.I₂, C₁₀H₂₁Br, DMA, 80°C 5h ii) CuCN·2LiCl, THF iii) TMSCl, **94**, -60°C to rt, 95%.

The 1,4-addition reaction should proceed exclusively from external side of concave dienone molecule to give *exo,exo*-disubstituted product as in known precedents of the related reactions.¹³² This assumption was supported by the fact that the obtained compounds were C₂ symmetric according to ¹³C NMR, but the unambiguous assignment of *exo,exo*-substitution was not possible by the NMR spectroscopy. For this purpose, in addition to oily substituted diones **97-99**, crystalline divinyl diketone **100** was synthesized via 1,4-addition of vinyl cuprate to dienone **94**. The X-ray structure gave a direct proof of the *exo* substitution (**Scheme 11**).



Scheme 11: *Reagents and conditions:* a) i) vinyl magnesium bromide, CuCN·2LiCl, THF ii) TMSCl, **94**, THF, -60°C to rt; 70%.

With didecyl diketone **99** in hands, we concentrated our efforts towards the synthesis of the corresponding bis- β -ketoester. The enolate anion required for the transformation is ambident nucleophile and can react with electrophiles at both carbon and oxygen atoms. The acylation reaction is particularly well known for giving mixtures of O-acylated and C-acylated products depending on reaction conditions such as reactant addition order, temperature, softness and hardness of electrophile, etc.¹³³ In contrary to unsubstituted diketone **22**, the carbomethoxylation reaction of didecyl diketone with dimethyl carbonate in DMF was not successful and resulted in an inseparable mixture. All attempts to make the corresponding enamine from diketone **99** also failed. We then turned to more active acylation agent, methyl cyanofomate (Mander's reagent)¹³⁴ which is one of the most useful reagents for introducing methoxycarbonyl group, especially when high C-selectivity and mild reaction

conditions are required. After reaction of the corresponding lithium enolate, obtained from dione **99** and LiHMDS in THF, with methyl cyanofomate, only O-acylated product **101** was obtained in 80% yield (**Scheme 12**). It is known from the literature¹³⁵ that O-acylation prevails in cases where nucleophilic carbon atom is sterically hindered by substituents located in vicinity and, is also favored by using lithium complexing solvents, such as THF or HMPTA (with substrates where steric hindrance is not a problem, the use of HMPTA as additive might even be advantageous increasing the solubility of enolate. Without steric bias, the match of hardness and softness of reactive centers dominates and high C-selectivity is observed). In these solvents, lithium counterion is highly solvated by solvent molecules and dissociates from enolate oxygen atom more easily, thus making it more accessible to electrophiles. In these instances, the problem of O-acylation can normally be eliminated by the use of diethyl ether as the solvent. Diethyl ether has lower solvating strength and the lithium enolate exists mainly as a tight ion pair in this solvent. Therefore, the nucleophilicity and steric accessibility of negatively charged oxygen atom is significantly reduced, favouring C-acylation. When the acylation reaction of **99** was repeated in diethyl ether, the formation of O-acylated products were completely suppressed, however, the mono ketoester was obtained as a major product accompanied by the trace amount of desired bis ketoester **102**. The reluctance of diketone **99** to form bis- β -ketoester is expected to be of steric origin caused by the crowding in the intermediate tetrahedral adduct. In the first step, addition of methyl cyanofomate is governed by steric hindrance of alkyl substituents on the *exo* side and most likely occurs from *endo* side of the enolate (**Figure 44a**). As a result, the tetrahedral carbon center is created which blocks the *endo* side of the remaining enolate functionality (**Figure 44b**).

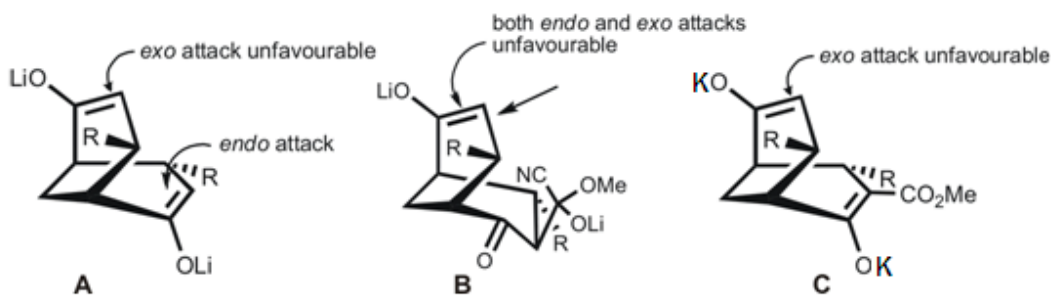
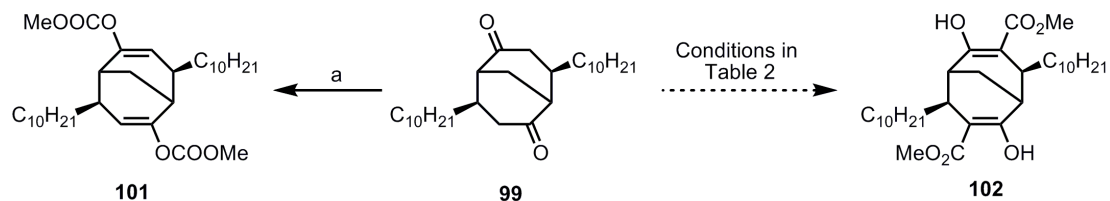


Figure 44: The possible explanation for mono selective acylation of **99** based on stereochemical considerations, a) preferable *endo*-selective attack of lithium enolate of **99** is shown; b) the illustration of the steric hindrance imposed by newly formed tetrahedral carbon center after reaction of **99** with Mander's reagent; c) flattened structure of intermediate salt of mono ketoester, formed in the reaction of **99** with DMC in toluene using KH as a base.

These results prompted us to investigate acylation reaction in more details and the different attempts are summarized in **Table 2**. Together with “direct” carbomethoxylating agents such as Mander's reagent, dimethyl carbonate and methyl chloroformate, we also tested tosyl cyanide as an electrophile. The nitrile group could serve as a surrogate for methylester group. In all cases complex mixtures were obtained, the yield of target product never exceeding 30% (determined by ^1H NMR of crude mixture). Nevertheless, one entry in the table is worth of additional comment. By conducting the reaction in boiling toluene with dimethyl carbonate and KH as a base, the mono ketoester was obtained as a sole product in 80% yield. Since no tetrahedral intermediate could form by using this reagent, the previous arguments about steric crowding of reactive centers is not valid anymore (**Figure 44c**). We believe that the reason for selective monofunctionalization lies in poor solubility of potassium salt of mono ketoester. As in the aforementioned case with NaH, switching to more polar DMF or DMA did not improve the situation. At present time, we don't have a plausible explanation for this observation. With lack of success, we also examined three new reagents **103-105** in which carbomethoxy moiety is attached to a leaving group.



Scheme 12: Reagents and conditions: a) i) LiHMDS, **99**, -78°C ii) Mander's reagent, -78°C , 80%.

Table 2: Various reaction conditions in the attempted synthesis of **102**. *General reaction conditions and reagents:* when LiHMDS was used as base, the bis-enolate was formed before the addition of the electrophile. When KH, NaH and NaOMe were used as base, **99** was added dropwise in a solution of the electrophile. Methyl chloroformate (MCF), methyl cyanoformate (Menders reagent), dimethylcarbonate (DMC) and tosyl cyanide (TsCN) were used as electrophiles.

Entry	Base	Electrophile	Solvent	Temp. ($^{\circ}\text{C}$)	Note
1	LiHMDS	MCF	Ether	-78 to rt	
2	LiHMDS	MCF	Ether	-78 to rt	inverse addition
3	LiHMDS	MCF	Ether	-98 to rt	
4	LiHMDS	Mander's	THF	-78 to rt	
5	LiHMDS	Mander's	Ether	-78 to rt	
6	LiHMDS	Mander's	Ether	-78 to rt	excess base
7	LiHMDS	Mander's	TBME	-78 to rt	
8	LiHMDS	Mander's	Ether	-78 to rt	$\text{Sc}(\text{OTf})_3$
9	LiHMDS	Mander's	Ether/THF	-78 to rt	CeCl_3
10	LiHMDS	Mander's	Ether	-78 to rt	MgBr_2
11	none	Mander's	Ether	-78 to rt	$\text{Cu}(\text{OTf})_2$
12	KH	DMC	Toluene	reflux	
13	KH	DMC	Dioxane	80	
14	KH	DMC	DMC	80	
15	NaH	DMC	DMA	100	
16	NaOMe	DMC	MeOH	reflux	
17	Et_3N	MCF	DCM	-65 to rt	TiCl_4
18	LiHMDS	Ts-CN	Ether	-78 to rt	
19	KH	Ts-CN	Toluene	80 to 100	

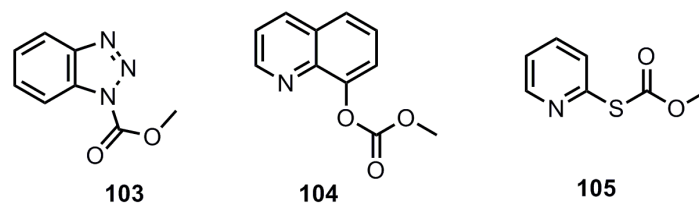
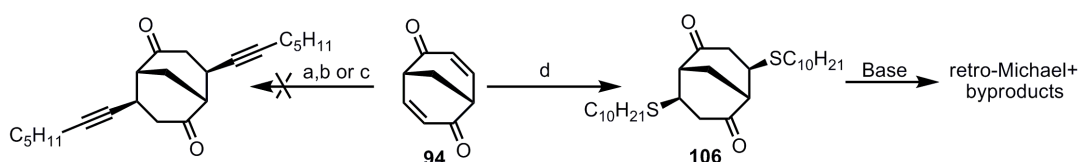


Figure 45: New carbomethoxylation agents synthesized during the course of developing C-selective acylation of **99**. Methyl (*1H*)-1,2,3-benzotriazole-1-carboxylate, methyl ester (**103**), methyl quinolin-8-yl carbonate (**104**) and O-methyl S-pyridin-2-yl carbonothioate (**105**).

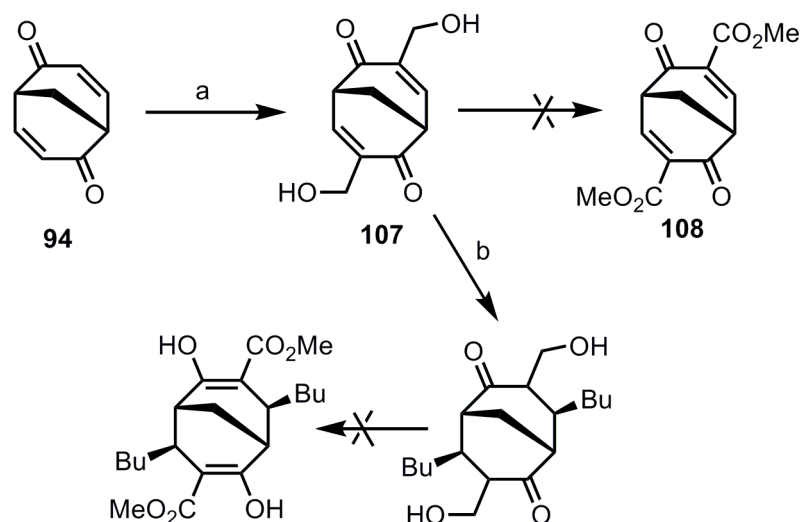
All reagents possessed the nitrogen atom in the leaving group, in order to stabilize tetrahedral intermediate, as in case of Mander's reagent(**Figure 45**). Disappointingly, the yield of the target bis- β -ketoester **102** has not been improved. It occurred to us that the steric congestion imposed by alkyl substituents has to be reduced by changing the type of solubilizing group. The alkyl chains attached to bicyclic framework are conformationally labile and effectively shields the α -carbon atom of enolate. We reasoned that exchanging the alkyl substituent with corresponding alkyne would significantly decrease the steric hindrance. In contrast to well known 1,4-addition of alkyl and alkenylcuprates to enones, the same type of reaction is almost unexploited for alkyne copper compounds. The reason for that is extremely strong bond between copper and alkyne, which results in low reactivity of those compounds towards electron deficient alkenes.¹³⁶ Despite this fact, a few methodologies have been developed for this particular task. We tried known methods using alkyne-copper^{137,138}, alkyne-aluminum¹³⁹ and alkyne-zinc¹⁴⁰ derivatives without success. (**Scheme 13**). Since the starting dienone **94** was recovered unaltered in these reactions, the problematic step obviously was 1,4- addition reaction of metal acetylide. With the same rationale, the 1,4-addition of thiols was investigated. The sulfur has a smaller van der Waals radius compared to methylene group and in addition, the C-S bond is longer than corresponding C-C bond. The both factors could make the α - carbon atom more accessible to electrophiles. The coordination of sulfur to lithium in tetrahedral intermediate of enolate-Mander's reagent adduct could favor *exo* attack of electrophile, in contrast to alkyl chain substituted enolate. The thiols in general are very

powerful nucleophiles and many protocols for 1,4-addition of these compounds are reported. In our hands, this transformation was not so trivial. After many trials, the best results (90% yield) were obtained by using proline as catalyst in MeOH¹⁴¹, whereas utilizing Lewis acid catalyst (ZnClO₄, I₂)^{142,143} or weak (Et₃N) and strong (NaH) bases gave either no product or complex mixture (**Scheme 13**). Unfortunately, it turned out that compound **106** was not stable in the presence of bases and underwent rapid retro-Michael reaction.



Scheme 13: Reagents and conditions: a) i) 1-heptyne, BuLi, Et₂O ii) CuCN iii) TMSOTf, **94**; b) 1-heptyne, BuLi, THF ii) CuI iii) TMSI, **94**; c) 1-heptyne, BuLi, THF ii) Me₃Al iii) TMSOTf, **94**; d) 1-heptyne, BuLi, Et₂O ii) ZnBr₂ iii) TMSOTf, **94**; e) C₁₀H₂₁SH, L-proline, MeOH, rt, overnight, 95%.

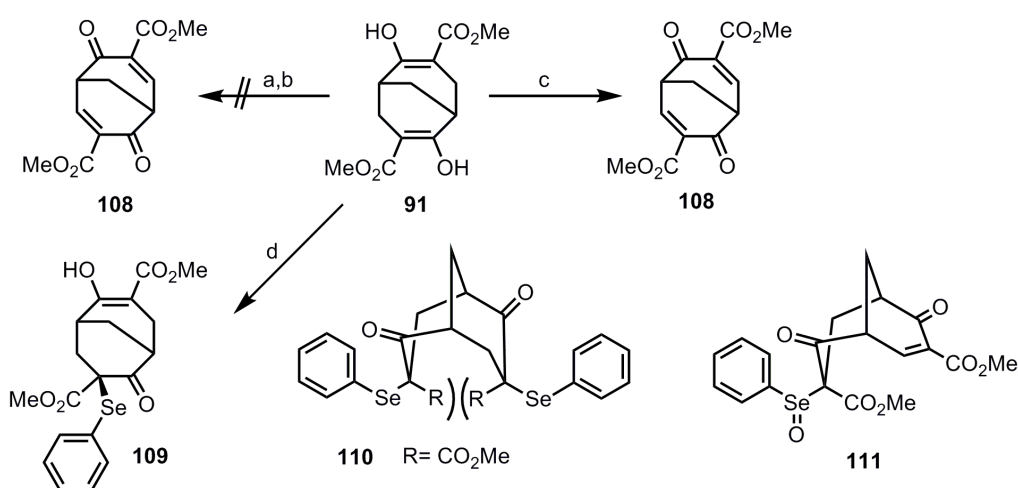
A minor detour in the synthetic plan was undertaken in order to avoid the acylation step after introducing the solubilizing chains. It was obvious that the ester functionality has to be installed prior to 1,4-addition reaction. Having a synthetic access to dienone **94**, a next logic step was to try a Baylis-Hillman reaction with formaldehyde. The resulting allylic alcohol **107** could be further oxidized to unsaturated ester **108** or the oxidation of alcohol could follow 1,4-addition step. The best results were obtained with aqueous formaldehyde and tributylphosphine as catalyst.¹⁴⁴ The product was obtained in moderate 50-60% yield. To our surprise, all attempts to oxidize this alcohol failed. The 1,4-addition of dibutyl cuprate to dienone **107** gave a quantitative yield of diastereomeric alcohols, however, the conversion of the latter to corresponding bis-ketoester failed (**Scheme 14**). Thus, this alternative was abandoned.



Scheme 14: Reagents and conditions: a) formaldehyde, cat. Bu_3P , $\text{MeOH}/\text{CHCl}_3$, rt, overnight, 50-60%; b) i) BuLi , THF , -78°C ii) **107**, THF , -78°C ; quantitative yield.

With the focus on unsaturated bis- β -ketoester **108** as a key synthon, we continued our synthetic endeavor based on direct oxidation of saturated precursor **91**. The oxidation of this compound with IBX in DMSO resulted in full conversion, but the desired product was not isolated. The DDQ oxidation in benzene or toluene at ambient temperature or at reflux returned unaltered starting material. Bis- β -ketoester was treated with an excess of phenylselenenyl chloride in THF with NaH or NEt_3 as base or in DCM with pyridine as base. In all cases the mono functionalized **109** and not the expected di-functionalized derivative **110** was obtained. The reason for this is believed to be the steric crowding that arises between the ester groups upon the second addition of phenylselenenyl group from the *exo* side (**Scheme 15**). The energetic barrier is just too high for the diselenide to form. The Barton dehydrogenation reaction resulted in complete consumption of starting material, but again, TLC indicated only the presence of very polar products. The reason for this might be the instability of the unsaturated product under rather harsh reaction conditions (boiling toluene and excess of oxidant) and the low nucleophilicity of bis- β -ketoester enolate towards phenylselenenic acid anhydride. We thus repeated the same reaction using stoichiometric amount of phenylselenenic acid anhydride and sodium hydride as a base in order to convert the bis- β -ketoester **91** into more nucleophilic sodium salt. Indeed, the reaction afforded desired product in

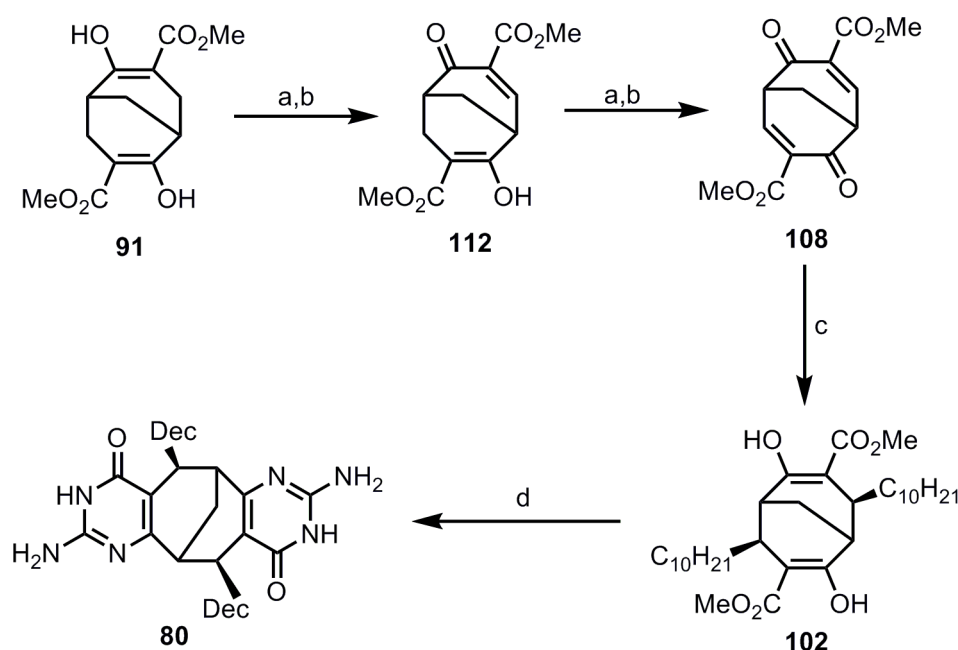
yields ranging from 70 to 30% (**Scheme 15**). The variation in yield was found to be directly related to the quality of the phenylseleninic anhydride. The latter compound is very sensitive to moisture and the content of free acid in commercial grade reagent sometimes amounts to 30%. The best yield was obtained by using reagent pre-dried in high vacuum for at least 3 h to remove the traces of free acid. The result from this set of experiments confirmed that the hypothesis about steric crowding between the positions 3 and 7 of bicyclic framework was valid. Introducing selenium in highest oxidation state ensures its immediate elimination thus avoiding the unfavourable interaction of two ester functionalities (intermediate **111**, **Scheme 15**). However, the use of anhydrous reaction conditions, strong base and expensive reagent were not optimal for scaling-up the reaction.



Scheme 15: Reagents and conditions: a) IBX, DMSO, 80°C; b) DDQ, toluene, rt or reflux; c) (PhSeO)₂O, NaH, THF, reflux, 2-6h, 30-70%; d) PhSeCl, NaH or Et₃N, THF or CH₂Cl₂, rt.

For this purpose, we tested selenation of bis-β-ketoester **91** with phenylselenenyl chloride performing the reaction stepwise. After elimination of the phenylselenoxide group from mono selenated bis-β-ketoester **109**, the addition of second phenylselenenyl moiety and subsequent oxidative elimination proceeded without problems to afford **108** in an overall 64% yield (**Scheme 16**). It is important that the crude mixture obtained after first elimination is immediately used without purification in the second step due to the low

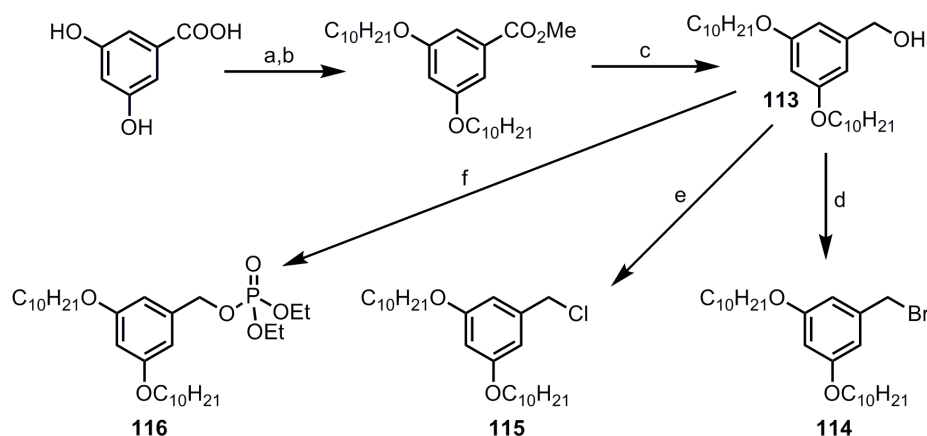
stability of monounsaturated derivative **112**. The 1,4-addition of decyl cuprate, obtained from decylzinc bromide, in the presence of TMSCl yielded 92% of desired didecyl ketoester. The condensation of the latter with guanidinium chloride using KO^tBu as a base at 100°C in MeOH in sealed tube provided isocytosine derivative (+)-**80** in 65% yield. The solubility of compound (+)-**80** in chlorinated solvents was greatly improved comparing with unsubstituted derivative **93**, but still not enough for further aggregation studies. Moreover, the compound (+)-**80** forms a gel in chloroform at very low concentrations, the phenomenon worth more detailed studies.



Scheme 16: Reagents and conditions: a) PhSeCl, Py, CH₂Cl₂, 0°C to rt, 1.5 h; b) aq.H₂O₂ (30%), CH₂Cl₂, 0°C to rt, 64% overall yield of **108** from **91**; c) i) C₁₀H₂₁Br, Zn, cat.I₂, DMA, 80°C, 5h ii) CuCN·2LiCl, THF iii) TMSCl, **108**, -60°C, 92%; d) guanidine chloride, KO^tBu, MeOH, 100°C, overnight, sealed tube, 80%.

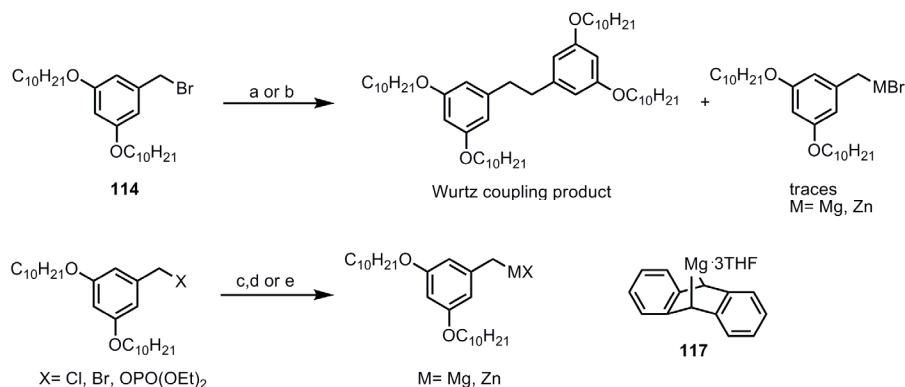
With the aim for more soluble derivative, we decided to introduce more bulky, branched substituents. The 3,5-dihydroxybenzyl moiety seemed very attractive from the synthetic point, as the alkyl chains of different length can be easily introduced in this fragment by simple alkylation. 3,5-bis(decyloxy)benzylic alcohol **113** was prepared from 3,5-dihydroxybenzoic acid in 3 steps in above 90% overall yield (**Scheme 17**) The alcohol **113** was converted to

corresponding bromide **114**, chloride **115**, and phosphate **116** in high yield. All these derivatives were used as possible precursors to obtain benzylic organometallic compounds.



Scheme 17: Reagents and conditions: a) MeOH, cat. H₂SO₄, reflux, overnight; b) C₁₀H₂₁Br, K₂CO₃, DMF, 80°C; c) LiAlH₄, THF, rt, overall yield >90%; d) PBr₃, DCM, 0°C to rt, 90%; e) cyanuric chloride, DMF, rt, quantitative yield; f) (EtO)₂POCl, DMAP, Et₃N, THF, rt, 48 h, 45% (99% brsm).

The considerable drawback of electron rich benzylic halides arises from their propensity to give Wurtz coupling products instead of organometallic compound. Indeed, when the direct insertion of zinc, activated with catalytic amount of iodine was attempted with bromide **114**, more than 60% of starting material was wasted for Wurtz coupling. The chloride **115** was inactive under the same reaction conditions. Zinc insertion, facilitated by the presence of LiCl was reported to give benzyliczinc chlorides in high yield.¹⁴⁵ In our case, only the starting material was recovered from the reaction mixture.

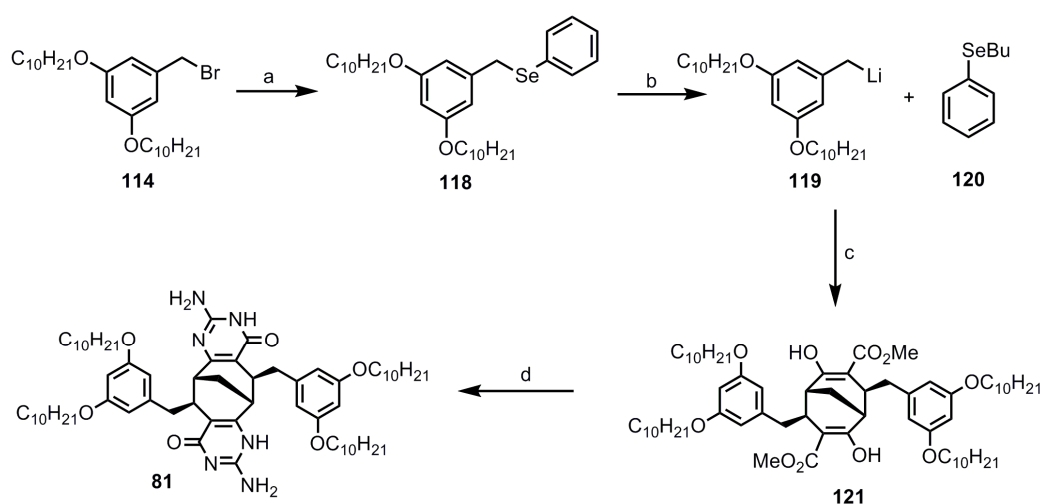


Scheme 18: Reagents and conditions: a) Zn, cat. I₂, DMA, rt; b) Mg, THF, rt; c) for X=OPO(OEt)₂: Zn, cat. I₂, LiI, DMA, 80°C; d) for X= Cl: Mg, ZnCl₂, LiCl, THF, rt; e) for X=Cl or Br: **117**, THF, rt.

The treatment of phosphate **116** with LiI and zinc did not afford organozinc derivative either. The insertion of magnesium suffered from the same type of side reaction. The magnesium-anthracene adduct **117**, known to smoothly promote formation of electron rich benzylic magnesium compounds without concomitant formation of Wurtz coupling products was inactive in the reaction with benzylic bromide **114** and chloride **115**. In addition, the most recent procedure¹⁴⁶ using magnesium together with the ZnCl₂ and LiCl did not produce organozinc compound from chloride **115** (**Scheme 18**).

The formation of corresponding benzyl lithium via halogen-lithium exchange is not possible because of the coupling of the organolithium formed with the unreacted halide.¹⁴⁷ In many cases, the selenium-lithium exchange proved to be the only method available to produce benzylic or allylic organolithiums.¹⁴⁸ In the case of unsymmetric benzylphenyl selenide, the metallation reaction (most often using BuLi) generates the organometallic species in which carbanion is expected to be the most stabilized, to produce concomitantly the new selenide (usually butyl selenide) which is regarded to be inert toward any of the organolithiums used or generated in the process. The substituted benzylphenyl selenide **118** was obtained 95% yield by reacting the benzylic bromide with excess of diphenyldiselenide in the presence of NaH (**Scheme 19**).¹⁴⁹ This reaction is a rare case where NaH acts as a reductant. Selenide **118** easily underwent lithiation with BuLi in THF at low temperature to afford the benzyllithium, which after transmetalation with CuCN, reacted with dienone ester **108** giving the 1,4-addition product. This synthetic step required extensive optimization due to the simultaneous formation of phenyl lithium as the amount of butylphenyl selenide **120** increased in the course of the reaction. Both phenyl lithium and the excess of BuLi are deleterious to the reaction yield even if they are present in small amount. All organolithium compounds react with CuCN resulting in a difficult-to-purify mixture of 1,4- addition products, containing combinations of butyl, phenyl and resorcinol chains. The phenyl lithium could form by different pathways including reaction of BuLi with

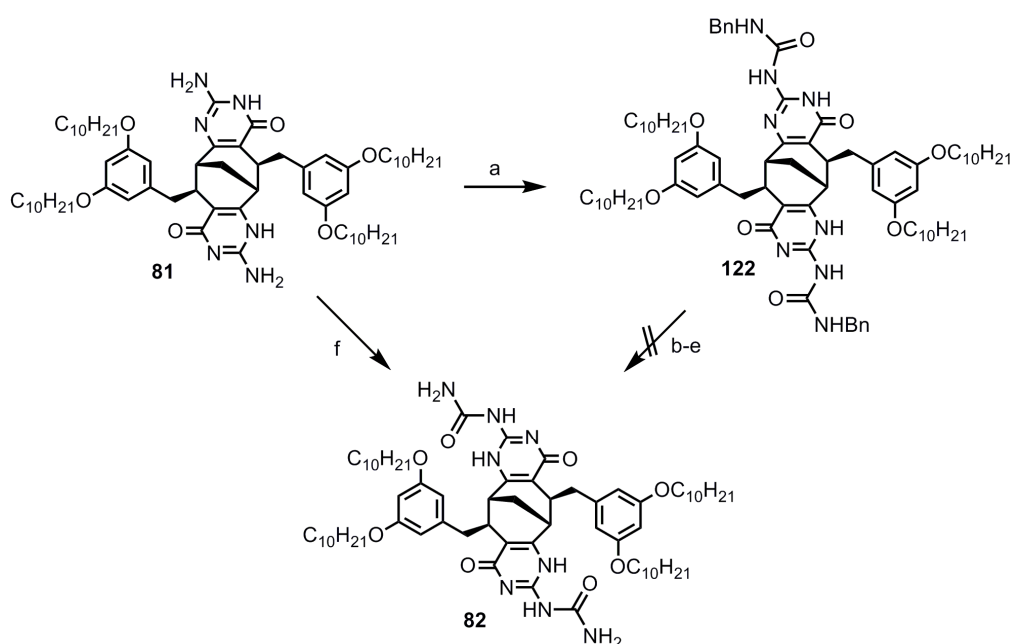
butylphenyl selenide **120**, the reaction of the same selenide with benzyl lithium or via unselective lithiation of starting electron rich benzylphenyl selenide. After fine tuning of the reaction conditions, the target compound **121** was obtained in good yield when **118** was added swiftly to a solution containing 0.8 eq. of BuLi at -110°C . The addition order when selenide is added to the solution of BuLi is essential to prevent α -lithiation of selenide. The bis- β -ketoester **121** was condensed with excess of guanidinium chloride and KO^tBu as a base in MeOH at 100°C in a sealed tube overnight. Alternatively, guanidinium carbonate can be used without decrease in yield, but the reaction time increased to 48 h (**Scheme 19**). The resulting isocytosine (+)-**81** was soluble in virtually any solvent except very polar ones and was used for further association studies in solution.



Scheme 19: Reagents and conditions: a) $(\text{PhSe})_2$, NaH, THF, reflux, 95%; b) i) BuLi, THF, -110°C ii) CuCN, THF, -78°C iii) TMSCl, **108**, THF, -78°C , 59%; d) guanidinium chloride, KO^tBu , MeOH, 100°C , overnight, sealed tube, 92%.

Finally, the isocytosine (+)-**81** was utilized for the synthesis of unsubstituted urea (-)-**82**. The benzyl urea derivative **122** was synthesized in 82% yield by treating with 3 eq. of benzylisocyanate under microwave irradiation at 120°C . The reaction was complete in 15 minutes, whereas the same transformation under thermal conditions required 48 h of heating. To our disappointment, the subsequent deprotection of benzylic groups proved to be extremely sluggish and the starting material was recovered after hydrogenolysis even at the

pressure of 80 atm. Acidic (TFA, HCOOH, TsOH)^{150,151,152} or reductive (Na/liq.NH₃, Li/NH₃)^{153,154,155} conditions for benzylic group removal were also unsuccessful. The activation of isocytosine amino group with CDI¹⁵⁶ resulted in incomplete conversion and complex mixture of products. To our delight, the *in situ* protection of isocytosine OH group with TMSCl in pyridine and activation of amino group with phenyl chloroformate followed by aminolysis afforded the urea (-)-**82** in 92% yield without chromatographic purification (**Scheme 20**).



Scheme 20: Reagents and conditions: a) BnNCO, Py, MW, 120°C, 15 min, 82%; b) H₂, Pd/C 80atm, EtOAc, AcOH; c) TFA, DCM, reflux; d) HCOOH, reflux; e) Na, NH₃(liq.)/THF; f) i) TMSCl, Py, 1.5h, rt ii) PhOCOCl, 5h, rt iii) aq. NH₃, rt, overnight, 92%.

3.6.2 Synthesis of 9-azabicyclo[3.3.1]nonane analogue

After successful elaboration of synthetic sequence leading to carbocyclic synthons **80-82**, our attention turned to the corresponding azabicyclo[3.3.1]nonane system. This type of compounds offers a unique advantage to introduce various solubilizing groups into the bicyclic framework at the position not accessible in case of carbocyclic congeners, i.e. on the apical nitrogen atom. In contrast to carbocyclic analogue, the alkyl chain or other group attached to the nitrogen occupies the radial position in respect to the bicyclic skeleton which means it is directed straight outwards (**Figure 46a**). This geometric feature could have a great influence on the type of supramolecular aggregate or even change the mode of aggregation. Moreover, the basic nitrogen atom could be protonated to produce charged species or in similar way converted to amphiphilic quarternary ammonium salt. The aggregation of the latter would definitely be of interest as this class of compounds has a very rich supramolecular chemistry (**Figure 46bc**).

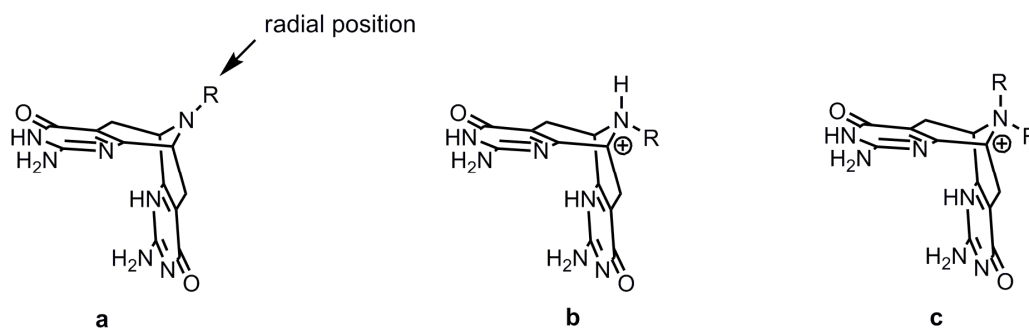


Figure 46: Structural diversity available in 9-azabicyclo[3.3.1]nonane derivatives: a) compound containing isocytosine hydrogen bonding moiety and solubilizing substituent in radial position; b) protonated form of 9-alkyl substituted derivative; c) amphiphilic quarternary salt possessing 9-azabicyclo[3.3.1]nonane framework.

From synthetic point of view, the advance in the plethora of the synthesis of 9-azabicyclo[3.3.1]nonane derivatives is important *per se*, as many natural compounds contain this fragment in their structure. For example, macroline compounds **123-124** feature a wide spectrum of biological activities, including antihypertensive and antiplasmodial properties (**Figure 47**).¹⁵⁷

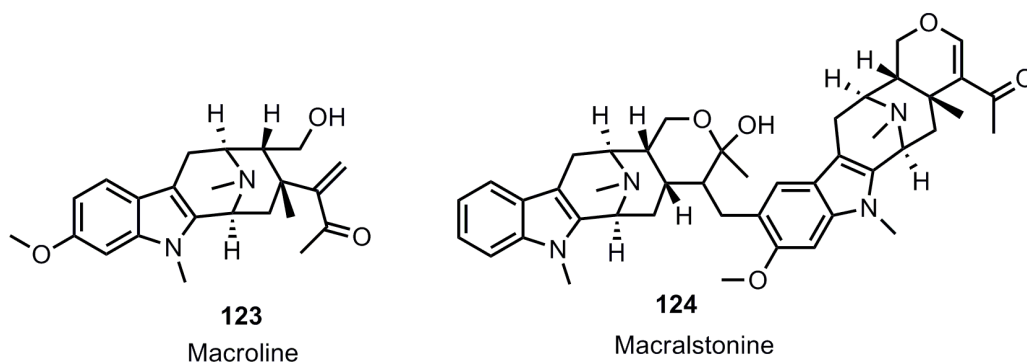
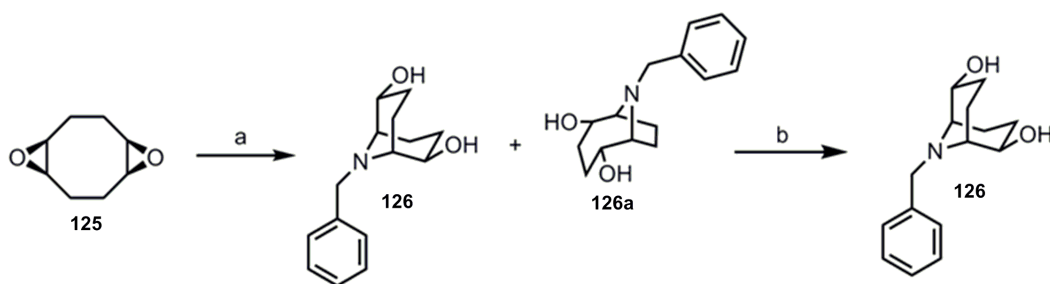


Figure 47: Examples of alkaloids **123** and **124** belonging to macroline family with 9-azabicyclo[3.3.1]nonane fragment embedded in their structure.

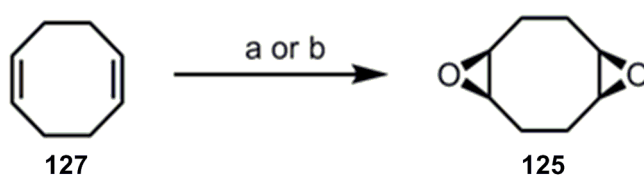
Our synthesis started with a two step conversion of syn-diepoxyde **125** to N-benzyl azadiol **126** according to the reported procedure (**Scheme 21**).¹⁵⁸



Scheme 21 Reagents and conditions: a) BnNH₂, H₂O, reflux, overnight; b) i) TFAA, DCM, -60°C ii) Et₃N, DCM, reflux, 8h iii) 2.5N NaOH, THF, rt, 95%.

In the first step, the diepoxyde **125** reacted overnight with benzyl amine in water at reflux to produce a 1:1 mixture of isomeric azadiols **126** and **126a** in quantitative yield. The interconversion of diol **126a** to desired diol **126** was accomplished by acid catalyzed isomerization of bicyclo[4.2.1]nonane skeleton. The corresponding diol was isolated in 95% overall yield solely as *diendo* diastereomer. This procedure worked well on small and on large scale providing an easy access to starting material. However, the use of rather expensive commercial diepoxyde **125** was not practical and the convenient preparation of this material from the cheap 1,5-cyclooctadiene **127** was needed. According to literature, the former compound could be synthesized by epoxidation using either peracetic acid (57% yield)¹⁵⁹ or MeReO₃/H₂O₂ (80-97% yield on a small scale).¹⁶⁰ However, none of the most used procedures was suitable for large scale synthesis since it required hazardous reagent such

as 90% H₂O₂ for peracetic acid preparation or expensive oxo-rhenium compound. Other methods including heterogeneous catalysis by hydrotalcite¹⁶¹ or sodium perborate¹⁶² mediated epoxidations also suffered from long reaction time and low yield. The epoxidation reaction with m-chloroperbenzoic acid was tested first as an alternative to the use of unstable peracetic acid. The reaction proceeded smoothly to afford the syn-diepoxide **125** as a major product in 68% yield (**Scheme 22**).

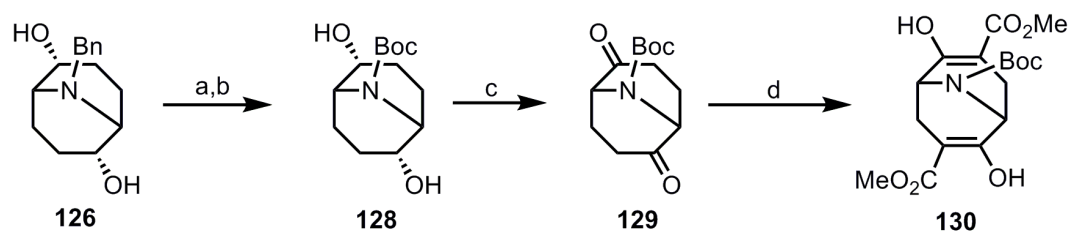


Scheme 22: Reagents and conditions: a) m-CPBA, DCM, rt, 2h, 68%; b) OXONE, NaHCO₃, EtOAc-Acetone-H₂O, rt, 2h, 77%.

The high stereoselectivity of the reaction was in accordance to the published precedents, the *syn* isomer being the major product. Nevertheless, the purification of the product involved flash chromatography, and therefore we attempted to replace m-chlorobenzoic acid with cheap and safe oxidant OXONE[®].¹⁶³ The two-phase procedure using an aqueous solution of OXONE[®] and ethyl acetate in combination with acetone¹⁶⁴ as a mediator was rewarding giving diepoxide in 77 %. The crude product was pure by TLC, showed only minute amount of impurities in NMR spectra and was used without further purification.

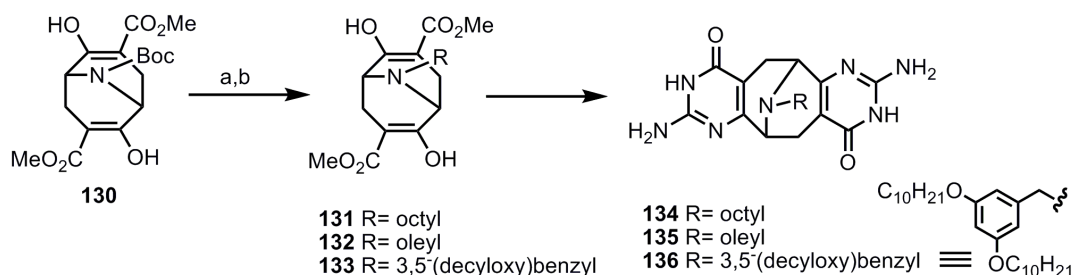
The preliminary results revealed serious difficulties encountered in the conversion of azadiol **126** to the corresponding diketone. The benzyl protecting group was therefore replaced with more convenient *tert*-butyloxycarbonyl group (Boc) following reported procedure. After testing different oxidizing agents (TPAP/NMO, Dess-Martin, PDC, PCC) the best results were obtained by using Swern oxidation or RuO₂ catalyzed oxidation with NaIO₄ (**Scheme 23**). The room temperature ruthenium catalyzed oxidation gave a higher yield and was operationally more simple than Swern oxidation and could be easily

adopted to a large-scale synthesis. To our surprise, the synthesis of the corresponding bis- β -ketoester was problematic using the conditions successfully applied previously for the preparation of carbocyclic analogue **91**. The treatment of dione **129** with NaH and dimethyl carbonate caused the decomposition of starting material. Interestingly, the utilization of Mander's reagent together with HMPTA additive provided the bis-keto ester **130** in 95% yield as a single product (**Scheme 23**). The latter result stress the importance of substitution pattern on the reactivity of bicyclo[3.3.1]nonane derivatives. As was discussed above, the introducing of carbomethoxy groups into 4,8-disubstituted dione **99** was impossible due to steric hindrance imposed by two *exo*-alkyl chains. In contrary, the substituent on the 9-position has little effect, even in case of rather bulky Boc group.



Scheme 23: Reagents and conditions: a) H₂, Pd/C, AcOH, MeOH, rt, overnight; b) Boc₂O, Et₃N, MeOH, reflux, overnight, total yield over two steps 70%; c) cat. RuO₂, NaIO₄, CCl₄-MeCN-H₂O, rt, overnight, 96%; d) i) LiHMDS, HMPTA, **129**, THF, -78°C ii) Mander's reagent, 91%.

The bis- β -ketoester **130** was deprotected by using TFA and was used directly as a salt in subsequent reaction. The reductive amination was accomplished by using sodium cyanoborohydride or triacetoxyborohydride¹⁶⁵ as a reducing agent in the presence of triethylamine. The corresponding ketoester **131** bearing the octyl group was obtained in 83% yield. The following condensation with guanidine carbonate in MeOH at 80°C in sealed tube afforded isocytosine **134** in 84% yield (**Scheme 24**).



Scheme 24: Reagents and conditions: a) TFA, DCM, rt; b) R'CHO, NaBH(OAc)₃, Et₃N, DCM, 4 MS, rt, yields: 84% of **131**, 70% for **132** and 78% for **133**.

The octyl isocytosine obtained was not soluble in chlorinated solvents and only moderately soluble in DMSO or MeOH. The octyl chain was replaced with oleyl residue, bearing Z-double bond in the chain. The zigzag chain was expected to prevent close packing of the compound **135** in the solid state and could increase the solubility. Unfortunately, the solubility was only slightly increased. The branched solubilizing 3,5-(didecyloxy)benzyl chain was introduced using the corresponding benzaldehyde under typical conditions. To our surprise, introduction of bulky chain did not increase the solubility significantly as well. It is known that enantiomerically pure bicyclo[3.3.1]nonane derivatives in general possess higher solubility comparing to racemic ones. The attempts to resolve some of the above synthesized racemic azabicyclic compounds were undertaken. The basic nature of amino alcohol **126** seemed to be perfectly suitable for diastereomeric salt formation with chiral acids. The chiral acids used are depicted in **Figure 48**.

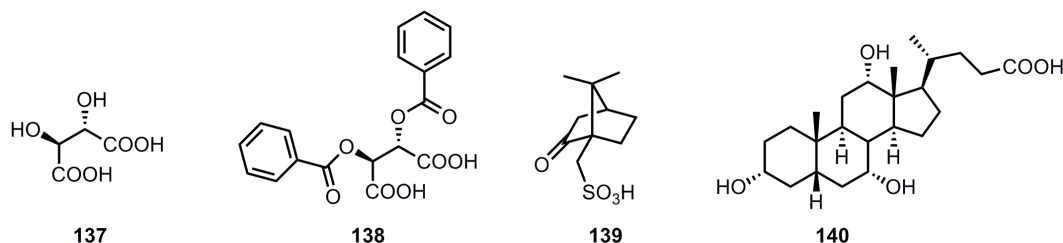


Figure 48: Chiral acid used in the attempted resolution of amino alcohol **126**; (+)-D-tartaric acid (**137**), (+)-D-dibenzoyl tartaric acid (**138**), (+)-camphorsulphonic acid (**139**), cholic acid (**140**).

All chiral acids except **140** afforded crystalline salts with amino alcohol **126**. The cholic acid **140** crystallized separately from the mixture with **126**. The

single crystallized salts **126**·**137**, **126**·**138** and **126**·**139** had the rotation angle, which did not increase further after subsequent crystallization. To our disappointment, the diastereomeric excess was below 20% in all cases (determined by chiral HPLC of free base **126**). The variation in solvent systems used for crystallization did not improve the situation. Then the covalent modification of **126** with N-benzyloxycarbonyl (Cbz) protected proline **142** and Boc-protected tryptophan **142** were attempted. The acid **142** was reported to give a good chromatographic separation of diastereomeric esters of BINOL type alcohols.¹⁶⁶ In case of **126**, the corresponding diesters were inseparable by chromatography. The same result was obtained by using Moscher's acid **143** (Figure 49).

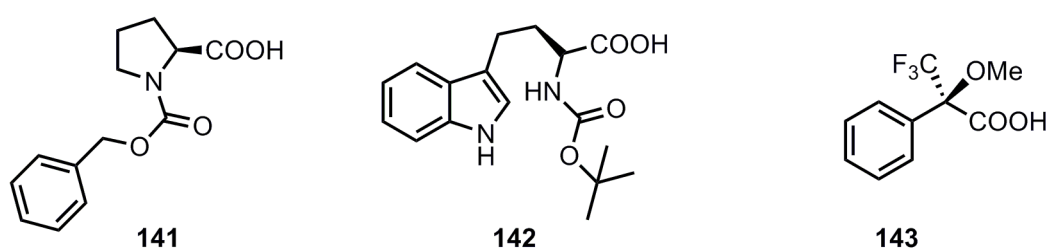


Figure 49: Chiral acids used for the preparation of diastereomeric diesters of amino alcohol **125**: N-benzyloxypyrrolidine (**141**), N-benzyloxypyrrolysine (**142**), Moscher's acid (**143**).

As a last resort, the dynamic kinetic resolution of dione **129** with Baker's yeast were tested. Despite the bulky Boc protecting group at 9-position of bicyclic framework, the rather fast reduction of dione **129** was observed resulting in mixture of keto alcohol and diol. The reaction required very careful monitoring, as the resulting enantioenriched dione (+)-**129** was further reduced by Baker's yeast. Concomitant deprotection of *tert*-butyloxycarbonyl protecting group was observed, which resulted in low recovery of the compound from water phase. Unfortunately, the ee of the recovered dione (+)-**129** was below 30% even after repeated fermentation or using high dilution conditions. As a future perspective, the extensive manipulation of protecting group is obviously needed to find the optimal conditions for highly enantiospecific reduction.

3.6.3 Tetrameric tautoleptic aggregation

The ^1H NMR spectrum of the (+)-**81** gave a first insight into the aggregation mode. The spectrum is obviously more complex than expected for a single C_2 symmetric molecule and shows at least four different NH signals indicating that the compound exists as a mixture of tautomers (**Figure 50**).

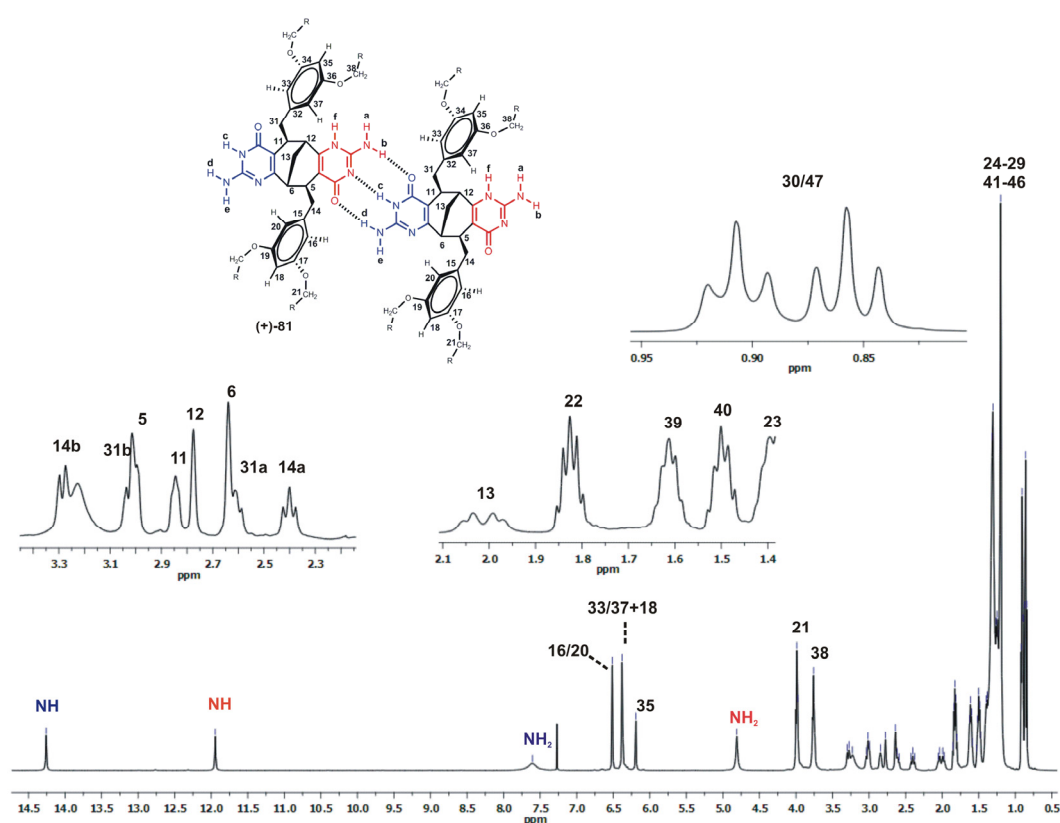


Figure 50: ^1H NMR (400 MHz) spectrum of (+)-**81** in CDCl_3 .

The ratio of the integrals of two most downfielded NH resonances at 14.27 and 11.95 ppm and those at 7.58 and 4.83 ppm, is exactly 1:2, which is consistent with the presence of equimolar amount of two tautomers. This fact and the unusually downfield position of two NH proton resonances imply that two different tautomers are hydrogen bonded via three complementary hydrogen bonds of DDA-AAD type. It should be noted that only one of two amino group protons in each tautomer is involved in hydrogen bond formation with another one being exposed to the solvent. Due to the fast rotation around C-N single

bond both hydrogen bonded and free protons are averaged resulting in broad peaks. Furthermore, dilution of the solution down to the detection limit of NMR spectrometer (400 MHz) resulted in no shift of any NH resonance signals. This indicates that monomer (+)-**81** associates strongly in CDCl₃. There are also additional evidences from ¹H NMR spectrum that support a very strong hydrogen bonding (**Figure 50**). Firstly, the proton resonances of methylene group next to the oxygen in the chains of the resorcinol unit, namely H21 and H38 are not equivalent and give rise to two sets of signals with equal intensities. These two types of protons do not correlate with each other in COSY spectrum and thus must originate from two different chains rather than from the same methylene group as a result of diastereotopicity. Surprisingly, the magnetic non-equivalence of two alkoxy chains can be observed down to the very terminus of the chain as the proton resonances of methyl group H30 and H47 are not equivalent as well. Secondly, the aromatic proton resonances H16/20 and H33/37, and also H18 and H35 are not equivalent which shows that the rotation about the bond connecting benzylic group to bicyclic framework is restricted. The full assignment of all protons was finalized using COSY, NOESY, HMQC, HMBC and ¹⁵N-¹H HMQC correlation spectroscopy.

The interactions observed in HMBC and ROESY spectra are shown in **Figure 51** and **Figure 52**, respectively.

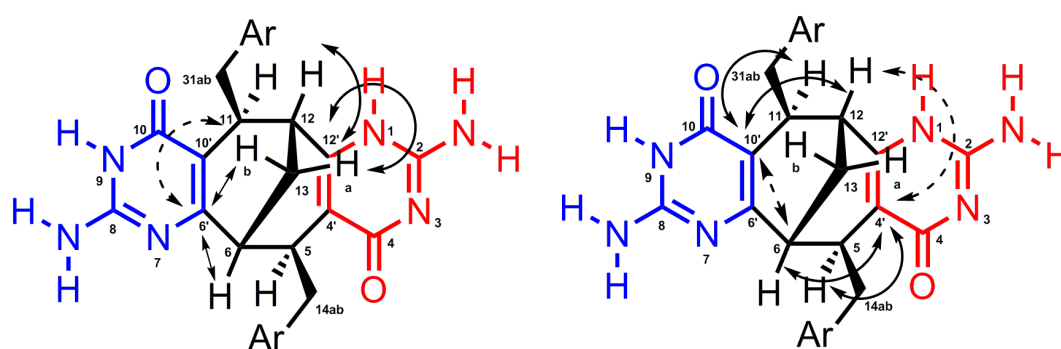


Figure 51. Assignment of cross peaks in HMBC spectrum of (+)-**81** (500 MHz, CDCl₃). Solid line arrows indicate major cross peaks, dashed arrows indicate minor cross peaks.

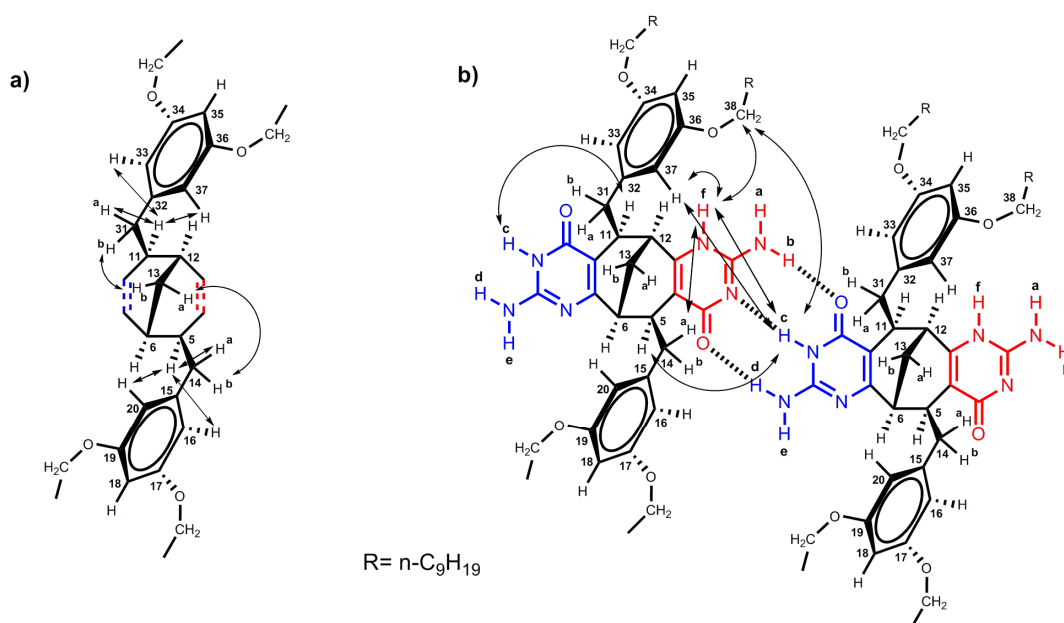


Figure 52: ROESY correlation of compound (+)-**81**; a) ROESY cross peaks of benzylic moiety; b) ROESY cross peaks of NH protons.

According to ROESY spectrum, the rotation of benzylic substituent in (+)-**81** is highly restricted and the benzylic protons are pointing toward isocytosine rings.

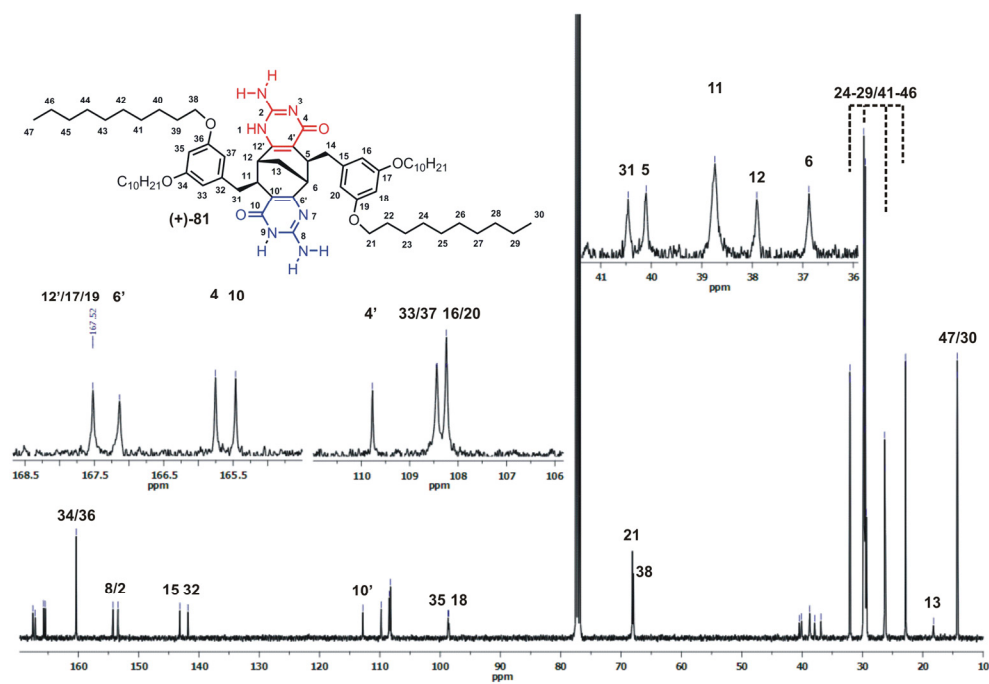


Figure 53: ¹³C NMR spectrum of (+)-**81** in CDCl₃.

Additional strong evidence for two tautomers slowly equilibrating at NMR time scale comes from the analysis of ^{13}C spectrum (**Figure 53**). It shows that most of the alkyl chain and aromatic rings signals are duplicated with very close chemical shift values resulting in so-called twin peaks of almost equal intensities. It seems that co-existence of two tautomeric forms in chloroform is closely related with their ability to form extremely strong hydrogen bonding and may result from association-induced tautomeric shift. To probe the importance of the hydrogen bonding for tautomer distribution we run NMR experiments in deuterated DMSO (in a mixture of DMSO and chloroform due to solubility reasons, the content of DMSO was kept high enough to break down all hydrogen bonds) completely suppressing hydrogen bonding. The spectrum obtained is shown in **Figure 54a**. From the spectrum it is obvious that compound (+)-**81** in DMSO exists as a single tautomer and monomeric since the spectral features, associated with supramolecular hydrogen bonded structure vanish. The NH signal is observed in the spectrum at the positions typical for isocytosine derivatives (compared with literature data and some related compounds previously made in our lab) and can be ascribed to keto-N3-H tautomer. In addition, it is known from UV spectroscopy studies¹⁶⁷ that this tautomer is dominant in DMSO. In DMSO, the spectrum is much simpler compared to chloroform solution. Both alkoxy chains on resorcinol aromatic ring are equivalent and there are only two aromatic proton resonance signals. These results confirmed that the compound is monomeric in this solvent and that aforementioned changes in spectrum pattern can be directly related to the formation of supramolecular aggregates providing a good method to sense them. The single set of signals in the ^{13}C NMR spectrum also indicated the presence of single tautomer (**Figure 54b**).

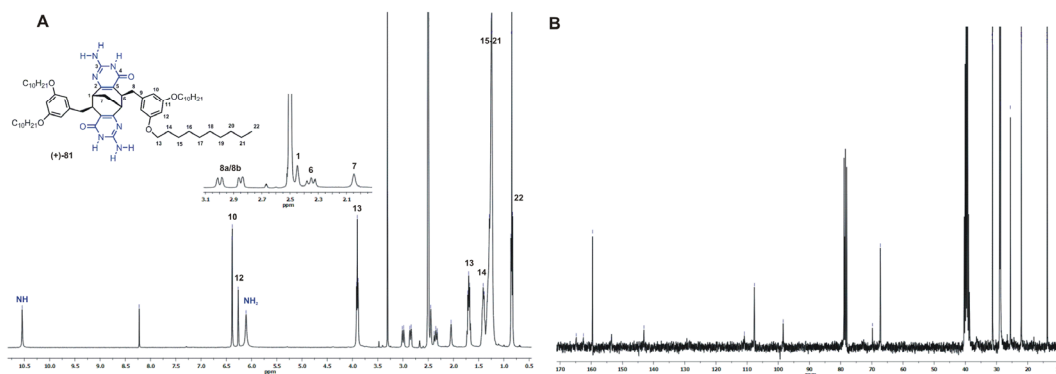


Figure 54: NMR spectra of **(+)-81** in d_6 -DMSO: a) ^1H NMR spectrum; b) ^{13}C NMR spectrum.

The entire situation described so far corresponds to self-association of either one tautomer of **(+)-81**, the DDA-AAD, or the association of a 1:1 mixture of the DDA-DDA and AAD-AAD tautomer of **(+)-81** (**Figure 55**). Tautoleptic aggregation corresponding to the self-aggregation of the DDA-AAD monomer of **(+)-81** would lead to the two unequal rims of the propagating supramolecular structure, however, there would only be one observable carbon resonance signal of the bridging methylene group, C-13. In contrast, aggregation of a 1:1 mixture of one DDA-DDA monomer **(+)-81** and one AAD-AAD monomer **(+)-81** would also lead to two unequal rims of the propagating supramolecular structure, however, there would be two carbon resonance signals of the bridging methylene group, C13' and C13''. The ^{13}C spectrum of **(+)-81** (**Figure 53**) clearly shows just one carbon resonance for carbon 13, showing that it is the DDA-AAD monomer of **(+)-81** that is aggregating.

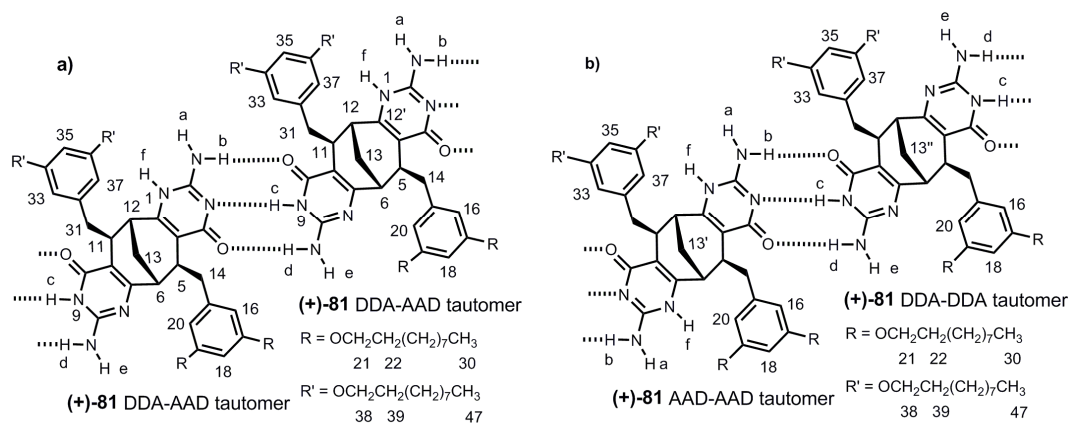


Figure 55: The monomer (+)-81 and its possible aggregation a) using one monomer having the DDA-ADD self-complementary motif; b) two different monomers each containing the same tautomer DDA-DDA and AAD-AAD respectively.

In order to prove the averaged nature of two NH₂ signals at 7.58 and 4.83 ppm and to gain more structural information we performed a variable temperature ¹H NMR experiment. Both signals were split to two decreasing the temperature to 200K, more specifically, the resonance signal at 7.58 ppm was shown to be an average value of two resonance signals at 8.54 ppm and 6.91 ppm, and the one at 4.83 ppm is composed of resonance signals at 5.00 and 5.19 ppm (at 200K). The splitting of two signals is not simultaneous in terms of the splitting temperature indicating that two hydrogen bonds between oxygen atoms and b and d protons of isocytosine tautomers are not of the same strength (**Figure 56**). This can be explained assuming a different electron distribution in tautomers, which accounts for the change in hydrogen bond acceptor and donor properties of appropriate atoms, or it is merely a consequence of non-symmetric structure of aggregate itself.

The further support for the existence of two tautomers in solution was obtained from UV-Vis spectroscopy. Several spectroscopic studies regarding the tautomeric equilibrium of isocytosine have been published.^{168,169,170} Unfortunately the use of only simple isocytosines is described, which are not soluble in many solvents, except very polar like water and ethanol or ethanol-diethyl ether mixture. The exact position of absorption bands slightly varies from one source to another, although the spectrum pattern is the same. It was

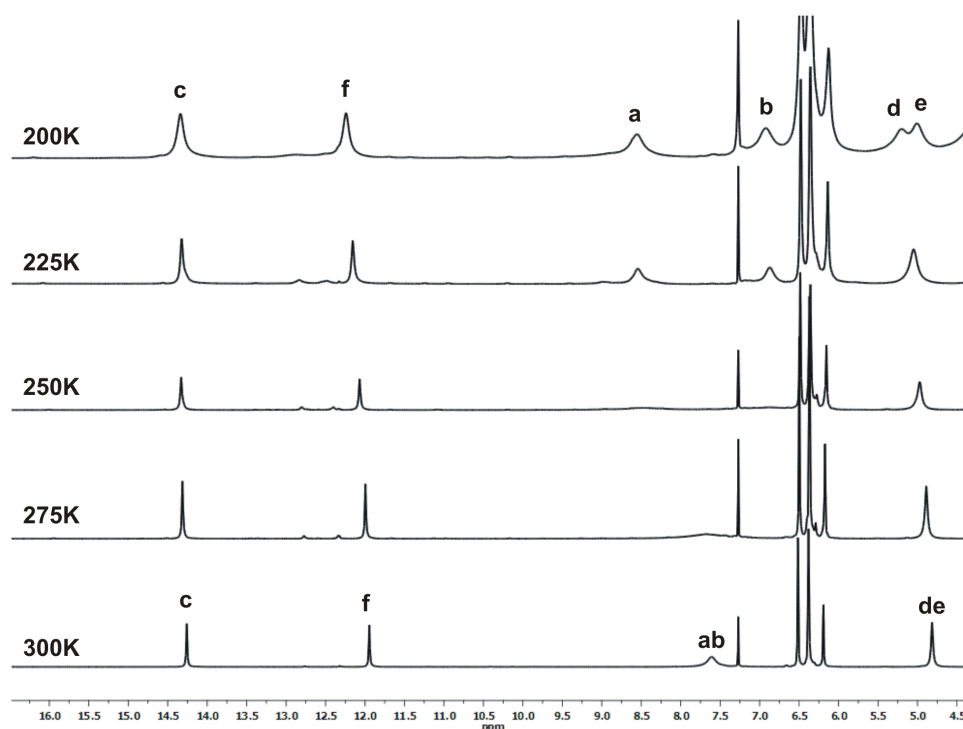


Figure 56: Variable temperature ^1H NMR spectra of (+)-**81** in CDCl_3

shown that increase of isocytosine concentration leads to a deviation from Lambert-Beer's law, what was attributed to the formation of hydrogen bonded aggregates.

The typical spectrum of isocytosine in water is shown in **Figure 57a** together with absorption spectra of individual tautomers obtained by statistical decomposition of the spectrum. The spectrum consists of two non-symmetric bands corresponding to the $\pi\text{-}\pi^*$ transitions. The short wavelength band at 205 nm is more intense and is attributed to N1-H tautomer, whereas the tautomer N3-H absorbs at both short and long wavelengths with the maximum at 220 nm and 280 nm. Nevertheless, it can be concluded that N1-H tautomer contribute mainly to short wavelength band, and N3-H tautomer is responsible for the intensity of long wavelength band. The relative intensity of these two bands is related to the amount of two tautomers in the mixture.

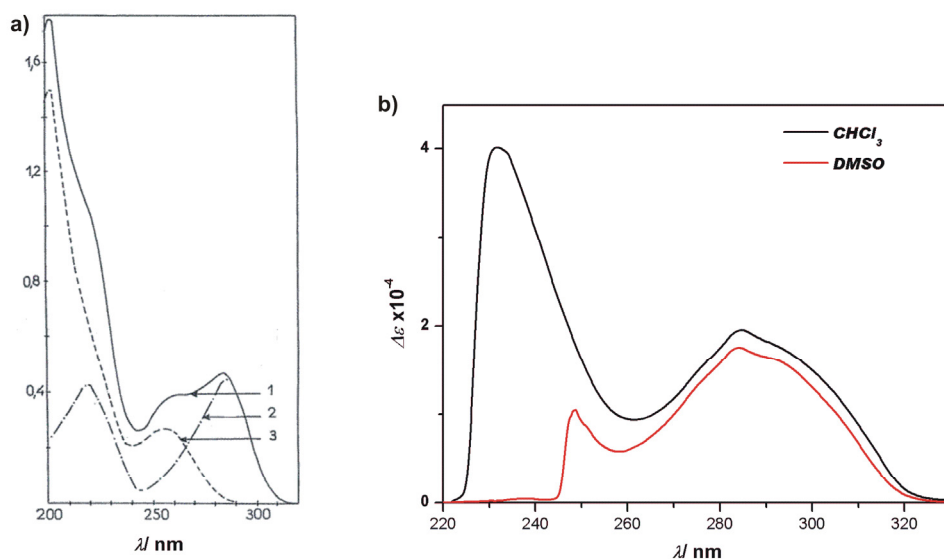


Figure 57: a) UV spectrum of unsubstituted isocytosine (3) in water showing the spectra of individual tautomers: UV spectrum of N3-H tautomer (2), UV spectrum of N1-H tautomer (1); b) UV spectra of (+)-81 in chloroform and DMSO.

The absorption spectrum of (+)-81 is composed of two broad structureless bands with the maximum at 232 and 285 nm in chloroform and 248 and 284 nm in DMSO. The relative intensity of the two bands correlates very well with the proposed change in tautomeric composition. Going from pure chloroform to DMSO, the long wavelength band intensity remains almost unchanged. This band corresponds to N3-H tautomer. The intensity of short wavelength band is very small compared to that in chloroform. Since N1-H tautomer does not absorb at long wavelength the presence of this band in the spectrum proves the existence of both tautomers in chloroform. In order to detect possible dissociation at low concentration we performed a dilution experiment in chloroform. The change of absorbance vs concentration was linear over the whole concentration range ($2.13 \cdot 10^{-4}$ - $1.10 \cdot 10^{-6}$ M) and obeyed Lambert-Beer's law (**Figure 58a**). The linear concentration dependence of absorption indicated that the association of monomers does not involve π - π stacking. A stepwise addition of DMSO to chloroform solution caused the decrease of short wavelength band intensity, which is in accordance to the tautomeric shift towards N3-H tautomer (**Figure 58b**).

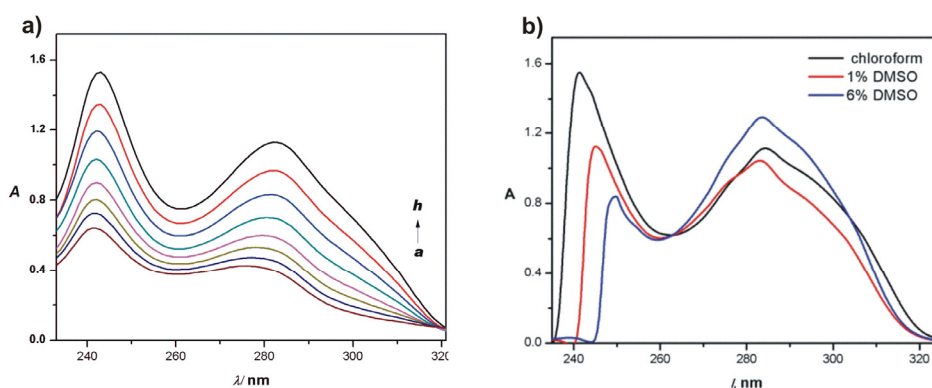


Figure 58: a) UV-dilution spectra of (+)-**81** in chloroform; b) UV spectra of (+)-**81** in chloroform with varying amount of DMSO.

The CD spectra of (+)-**81** in chloroform and DMSO, together with their UV spectra are shown in **Figure 59**.

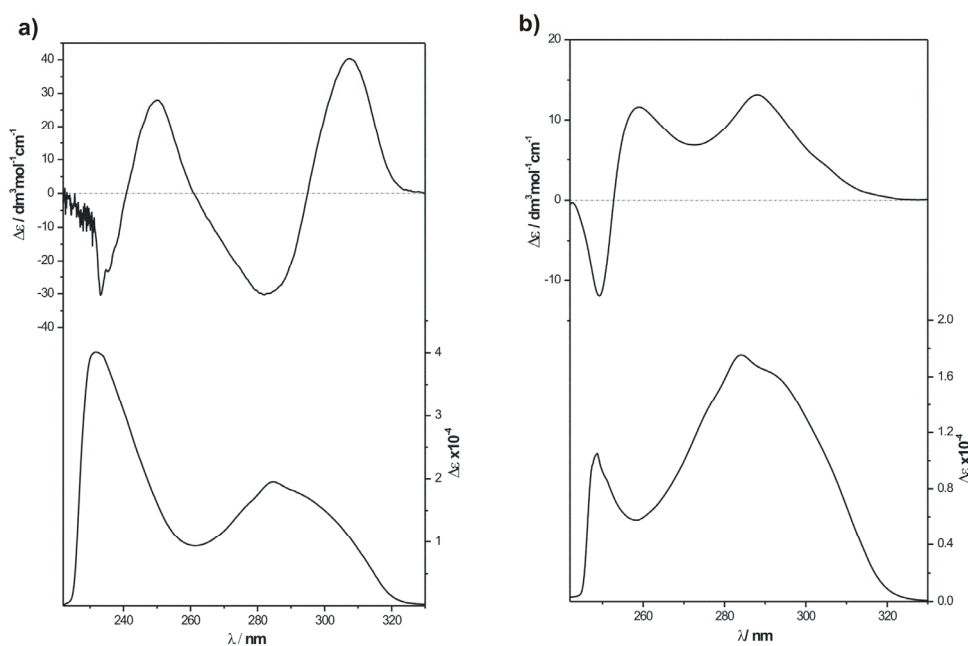


Figure 59: a) CD spectrum of (+)-**81** in chloroform; b) CD spectrum of (+)-**81** in DMSO.

The bisignate CD curve of (+)-**81** in a whole wavelength range and high $\Delta\epsilon$ values (≈ 40) are suggestive of an exciton coupling. However, the positions the curve cross the zero line do not correspond to the UV maxima. As can be seen from the spectra, the long wavelength negative band disappears in DMSO, as does the positive band above 300 nm. Whether this change is related to the changes in molecule structure (two different tautomers vs. single tautomer) or

the mode of aggregation is difficult to predict. Most likely, concerted action of both factors is operating. A stepwise addition DMSO to a chloroform solution was accompanied by the decrease of negative band with increasing amount of DMSO (**Figure 60**).

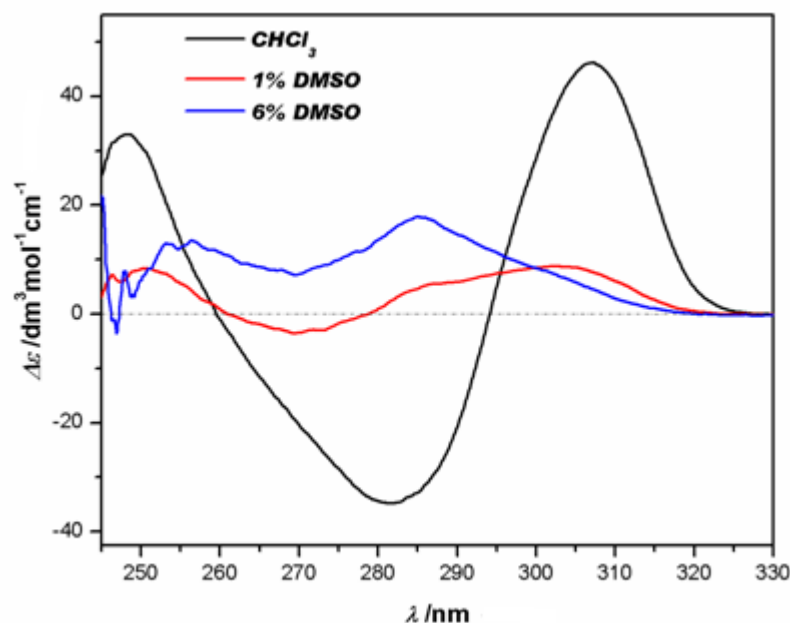


Figure 60: CD spectrum of (+)-**81** in chloroform with varying amount of DMSO.

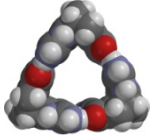
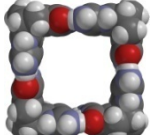
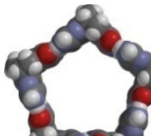
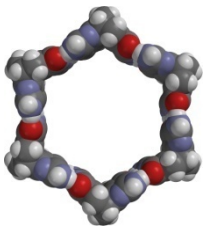
Hypsochromic shift of the negative band at 283 nm is observed after adding DMSO and the long wavelength positive band also experiences hypsochromic shift, the intensity of the bands decreasing significantly. According to ¹³C NMR, (+)-**81** exists as a mixture of two tautomers in CDCl₃-d₆-DMSO solvent system when the content of DMSO is 1% (*vide infra*), and only single tautomer is detected when DMSO content reaches 6%. CD spectra shows that addition already of 1% of DMSO has profound influence on spectrum pattern. Thus, the decrease in intensity of long and short wavelength bands can be attributed to the dissociation of supramolecular aggregate, whereas hypsochromic shift of positive long wavelength band is related to change in tautomeric composition.

The preliminary results from NMR and UV-Vis spectroscopy convincingly demonstrated that the monomer (+)-**81** is composed of two complementary tautomers of isocytosine moiety. Furthermore, due to the fact that the ¹H NMR

spectrum is very symmetric, it must be concluded that (+)-**81** forms one very well-defined supramolecular structure instead of oligomers. Such a structure is likely to be cyclic. To assess the structural nature of the discrete cyclic aggregate we performed computational modeling. We first investigated the possible geometry of **93**, as a model compound for (+)-**81**, using semiempirical (PM3^{171,172} and RM1¹⁷³), density functional theory (B3LYP¹⁷⁴/6-31G*) and ab initio (HF/6-31 G*) molecular orbital calculations. All heavy atoms of the the global minima obtained with the three different methods were superimposed. The geometries obtained with HF and DFT gave a RMS of 0.0241, which, in essence, is an exact match. Performing the same superimposition with the HF conformation and the RM1 and PM3 conformations resulted in RMS values of 0.1602 and 0.0997, respectively. Thus, both RM1 and PM3 generate conformations that are in excellent agreement with the conformation obtained by the HF and DFT methods. Accordingly, the thermodynamic stability of the supramolecular aggregates was evaluated using RM1 and PM3 methods. The global minima of cyclic n-mers was evaluated for n = 3 to n = 6 and the results are presented in **Table 3**. The RM1 method gives a larger enthalpic gain for the self-complementary association of the isocytosine derivative and therefore estimates this hydrogen bonding pattern to be stronger than the PM3 method (the strain energies of the monomers imposed by the size of the macrocyclic structure gives higher enthalpic deficit by RM1 compared to PM3). This is reflected in the Gibbs free energy (ΔG_r^0) and is the main reason for why the results by the two methods differ to such an extent. Consequently, the RM1 method predicts that the formation of all macrocycles is thermodynamically favourable. In contrast to this, the PM3 method predicts that the formation of heptamers and the hexamers is unfavourable whereas the formation of trimers and tetramers is favourable. It should be mentioned that the RM1 method is a reparametrisation of AM1 and was developed fairly recently (2005) and hence, has not been excessively employed, and thus evaluated for hydrogen bonded systems. In contrast to RM1, the PM3 method has been used successfully in

modelling supramolecular systems.¹⁷⁵ In order to evaluate which species are thermodynamically most stable and accordingly predominate in a solution it is important to compare the difference in relative Gibbs free energies ($\Delta\Delta G_{\text{rel}}^0$) given per mol monomer. The $\Delta\Delta G_{\text{rel}}^0$ obtained by both methods suggests that the tetramer is the most stable, even though all the different sized aggregates are close in relative energy.

Table 3: Standard enthalpies (ΔH_r^0) and Gibbs free energies (ΔG_r^0) of the hydrogen bond mediated macrocyclization of isocytosine (**93**) using RM1 and PM3 semi-empirical methods (RM1 / PM3). The energies were obtained by subtracting the cumulate energies of the n monomers from the energies of the macrocycles. The difference in relative Gibbs free energies ($\Delta\Delta G_{\text{rel}}^0$) are given per mol monomer and can hence be compared directly.

Macrocyclic aggregates	ΔH_r^0 (kJ/mol)	ΔG_r^0 (kJ/mol)	$\Delta\Delta G_{\text{rel}}^0$ (kJ/mol)
1 	n = 3 -231,4 / 149,0	-82,6 / -1,4	0 / 0
2 	n = 4 -322,1 / 208,4	-113,4 / 4,1	-0,8 / -0,6
3 	n = 5 -396,4 / 253,0	-127,8 / 14,7	2,0 / 3,4
4 	n = 6 -460,9 / 299,3	-136,5 / 24,7	4,8 / 4,6

Since the energy difference is just a few kJ/mol it is possible that a mixture of different sized aggregates are present in solution. However, it is obvious that the hydrogen bonding motifs in the tetramer have a more optimal spatial arrangement than in the other aggregates. In addition, ¹H-NMR only shows one set of resonances suggesting that only one type of aggregate is present. Since

theoretical calculations could not be used to predict the size of the cyclic structure unequivocally, we turned to vapour pressure osmometry (VPO). The measurements were conducted in dry chloroform at 37°C in order to directly compare with the results obtained by the NMR spectroscopy. For comparison purposes, the same measurements were done in less polar toluene solution. The average value of degree of polymerization ($\langle N \rangle$) obtained for wide range of concentration was constant within experiment error and was equal to 4.38 ± 0.087 (**Figure 61**). The insensitivity of the $\langle N \rangle$ value to the concentration of (+)-**81** served as direct proof for cyclic structures, since increase in the size of aggregates is expected at higher concentration for linear structures. The value obtained agreed well with tetrameric structure. In toluene, $\langle N \rangle$ was found to be 4.62 ± 0.092 . The higher degree of polymerization in toluene may result from the small amount of pentamers present or may be due to further aggregation of cyclic tautomers by forming stacked dimers.

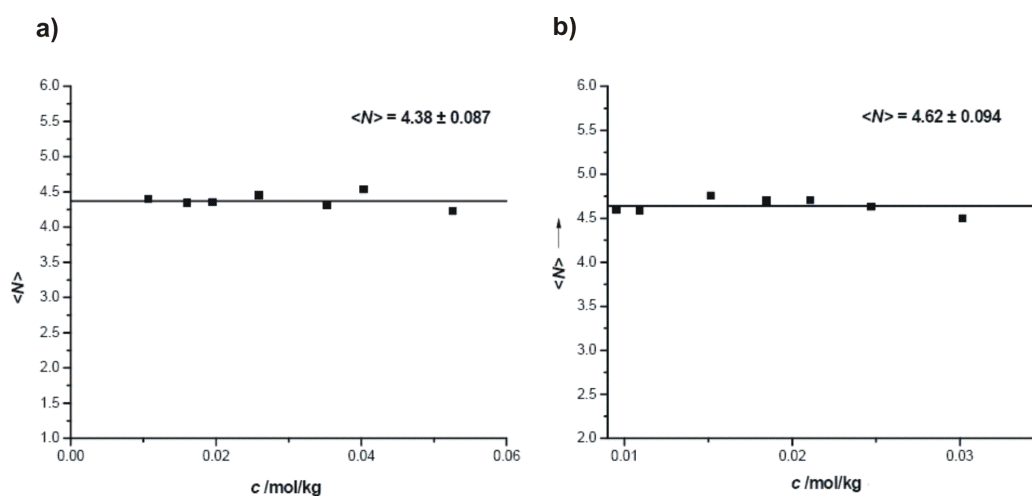


Figure 61: a) concentration dependence of degree of association of (+)-**81** in chloroform; b) concentration dependence of degree of association of (+)-**81** in toluene; the lines show average value of $\langle N \rangle$.

Further investigations on the aggregate were performed by the diffusion NMR. This is a vital technique for size determination of supramolecular entities and has gained increasing importance the last decade, even though it is still considered underused. In principle, the technique is based on the possibility to

label the position of spins by applying a linear gradient of the magnetic field. The decay of resonance intensity (I) as a function of the magnitude of the gradient is related to the diffusion coefficient (D) according to equation 7 (where g is the gradient strength, δ is the gradient pulse duration, γ is the gyromagnetic ratio and Δ is the time between the start of the first and the second gradient pulses). Diffusion NMR can be used to estimate binding and association constants, studying the encapsulation of molecular guests and to determine molecular size, shape and general self-aggregation properties.¹⁷⁶

$$I = I_0 \exp\left(-D\sqrt{2\pi\gamma g\delta}\left(\Delta - \frac{\delta}{3}\right)\right) \quad (7)$$

$$D = \frac{K_b T}{6\pi\eta R_s} \quad (8)$$

$$\sqrt[3]{\frac{M_j}{M_i}} < \frac{D_i}{D_j} < \sqrt{\frac{M_j}{M_i}} \quad (9)$$

Diffusion, i.e. the random translational motion originating from thermal energy, is related to molecular size, shape and intermolecular interactions. The hydrodynamic radius (R_s), often called the Stokes' radius, is given by the Stokes-Einstein equation 8, in which K_B is the Boltzmann constant, T the absolute temperature, D the diffusion coefficient and η is the viscosity of the solvent. However, as most molecules are not spherical certain approximations are needed to express its effective size. One such approximation that has successfully been applied is to treat the R_s as the mean of the radius in the x, y and z-direction of computationally minimized geometry of the compound. Furthermore, it has been shown that the ratio of the diffusion coefficients for two structurally related molecules is inversely proportional to the cubic root of their M_w -ratio if they are spherical molecules or to the square root if they are rod-like (eq. 9).¹⁷⁷ Thus, if supplied with a suitable reference molecule, it is possible to obtain a M_r interval for an unknown supramolecular species being

analyzed. Validation of the proposed aggregate can subsequently be achieved by comparing the experimentally obtained Stokes' radius with the calculated, as described above.

The diffusion experiments were performed at 293 K with a BPLED gradient pulse sequence and the diffusion coefficients were obtained by non-linear curve fitting using equation 7. The diffusion coefficients obtained for the isocytosine derivative were based on four different resonances and measured at three different concentrations. Normally, the diffusion coefficient is measured at such a low concentration that the intermolecular interactions can be neglected which means that the viscosity of the solution can be approximated to that of the pure solvent. When these parameters are fulfilled, the obtained Stokes' radius will only be dependent on individual molecular species. When dealing with large supramolecular aggregates it is oftentimes difficult to *a priori* know or guess at which concentration the Stokes-Einstein equation can be applied. However, if the diffusion coefficient is observed to be inversely proportional to the viscosity ($D \sim \eta^{-1}$) the accurate hydrodynamic radius can be obtained from D_0 (diffusion coefficient at infinite dilution) by simple extrapolation of the diffusion coefficients from a dilution series. The concentration dependence of the dynamic viscosity was therefore measured for (+)-**81** and up to a concentration of 35 mM, the viscosity turned out to have a linear dependence of the concentration with an intercept corresponding to that of pure solvent. Therefore, three concentrations (10, 20 and 30 mM) were chosen from this interval for diffusion NMR. The average diffusion coefficients obtained are reported in **Table 4** together with the average diffusion coefficient obtained by extrapolation to infinite dilution (D_0). As evident from **Figure 62** it was concluded that $D \sim \eta^{-1}$ which confirms the validity of the procedure. This linearity strongly supports a static system (on the NMR timescale) with only one type of supramolecular species present. In addition, $^1\text{H-NMR}$ of the solutions with different concentrations generated identical spectra which corroborate this conclusion. Furthermore, DOSY plots

showed near to identical diffusion coefficients for all present resonances which clearly indicate the presence of only one type of aggregate.

Table 4: Average diffusion coefficients (D) and average Stokes' radius (Rs) for isocytosine derivative (+)-**81** obtained from four different peaks; 14.27, 11.95, 4.84 and 3.75 ppm at three different concentrations (10, 20 and 30mM). The diffusion coefficient reported for 0 mM (D₀) was obtained by plotting D against the concentration and extrapolating to infinite dilution. Dynamic viscosities (η) were obtained experimentally.

Conc.(mM)	Average D (m ² /s)	η (pas)	Average R _s (Å)
30	2,42E-10	0,000681	13,0
20	2,50E-10	0,000654	13,2
10	2,61E-10	0,000627	13,1
0	2,71E-10	0,000589	13,5

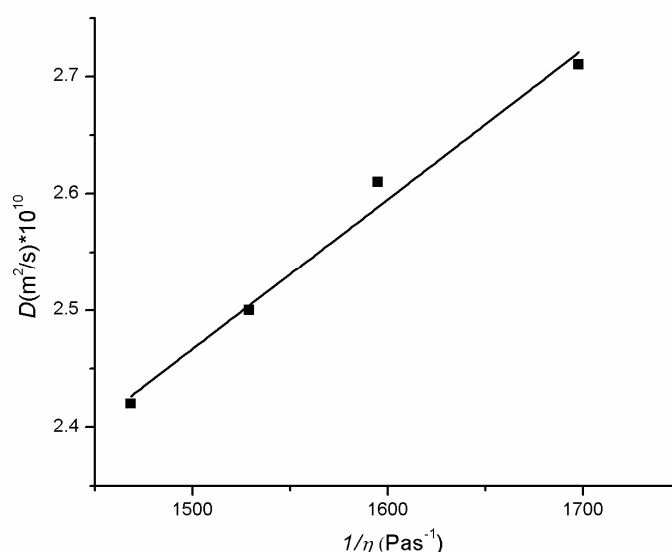


Figure 62: Linear relationship between D and η^{-1} at the concentration regime 0 – 30 mM.

With a D₀ of 2.71×10^{-10} m²/s the Stokes' radius was calculated using *eq. 8* to be 13.5 Å. Estimating the Stokes' radius for a computational minimized cyclic tetramer, in accordance with the procedure described above (the distance between the fifth carbon in the most peripheral recorsinol decyl chains was

used to approximate effective sizes in the x, y and z directions), a radius of 12.6 Å was obtained. Considering the approximations implicated in the estimation, the agreement between the observed and the calculated value is remarkable. Thus, the calculated R_s is consistent with a cyclic tetramer as aggregation state. To further strengthen the hypothesis of a cyclic tetramer as the supramolecular species, diffusion experiments were also performed on the reference molecule **121**, which has the same size and geometrical features as the monomeric isocytosine. The diffusion coefficients obtained for the reference molecule were based on three different shifts and measured at three different concentrations in accordance with the previous procedure. The average diffusion coefficients obtained are reported in **Table 5** together with the average diffusion coefficient obtained by extrapolation to infinite dilution (D_0) at the very bottom of the table. With a D_0 of $4.80 \times 10^{-10} \text{ m}^2/\text{s}$ the Stokes' radius was calculated using *eq. 6* to 7.6 Å. Applying the relationship expressed in *eq. 9* ($D_{81}/D_{121} = 1.77$), the aggregate should be either nearly a perfect spherical pentamer or a tetramer with a geometry intermediate between spherical and rod-shaped (see **Table 6**). Consequently, trimeric and hexameric aggregates can be ruled out, but it is not possible to unambiguously establish if the aggregate is tetrameric or pentameric by diffusion NMR alone. However, considering all spectroscopy studies, computational modelling and VPO data together, it is obvious that that (+)-**81** self-assembly into tautoleptic cyclic tetramers.

Table 5: Average diffusion coefficients (D) and average Stokes' radius (Rs) for reference **121** obtained from three different peaks; 12.26, 3.78 and 0.89 ppm at three different concentrations (5, 30 and 55 mM). The diffusion coefficient reported for 0 mM (D_0) was obtained by plotting D against the concentration and extrapolating to infinite dilution. Dynamic viscosities (η) were obtained theoretically.

Conc. (M)	Average D (\AA)	$\langle\eta\rangle$ (pas)	Average R_s (\AA)
0,055	3,83E-10	0,000743	7,6
0,03	4,25E-10	0,000673	7,5
0,005	4,71E-10	0,000603	7,6
0	4,80E-10	0,000589	7,6

Table 6: Cubic and square roots of the ratio between trimeric, tetrameric, pentameric and hexameric aggregates.

Aggregate	$(M_j/M_i)^{1/3}$	$(M_j/M_i)^{1/2}$
Trimer	1,45	1,75
Tetramer	1,60	2,02
pentamer	1,72	2,26
Hexamer	1,83	2,47

Aggregates of lower symmetry than the cyclic aggregate formed in chloroform, were observed in solvents with lower polarity. In order to investigate the nature of these aggregates diffusion experiments of (+)-**81** were performed in toluene. The experiments were performed at such a low concentration that the viscosity, could be rather accurately approximated to that of the pure solvent (3 mM) to give a qualitative measurement of the D_0 . It is not possible to directly compare the diffusion coefficients obtained in two different solvents. The diffusion coefficient from three resonances ($D = 2.12 \times 10^{-10} \text{ m}^2/\text{s}$) was used to calculate

the Stokes' radius which resulted at 17.2 Å. This strongly suggests that an aggregate of higher order is formed in this solvent compared to chloroform where the Stokes' radius was calculated to 13.5 Å. Roughly, the difference between the smaller symmetric aggregate in chloroform and the larger less symmetric aggregate in toluene corresponds to a prolongation of twice the length in one dimension of the smaller aggregate. Therefore, it is plausible that the cyclic tetramers observed in chloroform dimerize in solvents with lower polarity. Therefore, a less symmetric ^1H -NMR spectrum would be expected for such an aggregate. To test the possibility of higher aggregation of supramolecular tetramer, the ^1H NMR spectra of monomer (+)-**81** were recorded in various solvent of different polarity. In solvents less polar than chloroform, such as CD_2Cl_2 , deuterated benzene and toluene, complex spectra were obtained (**Figure 62-63**).

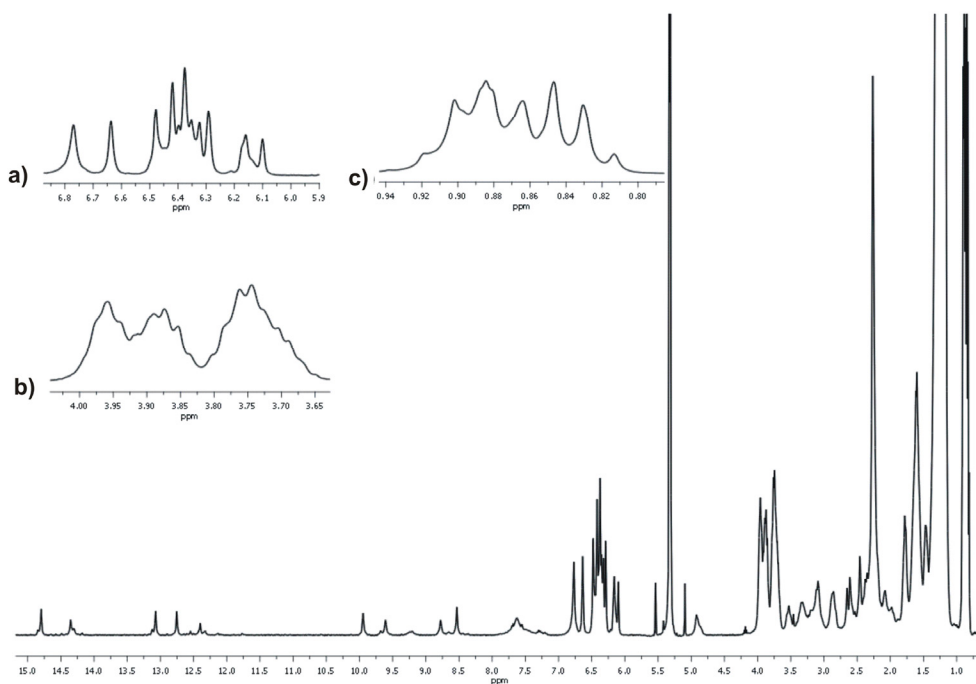


Figure 62: ^1H NMR of (+)-**81** in CD_2Cl_2 . The insets a,b and c show expanded selected regions of spectrum.

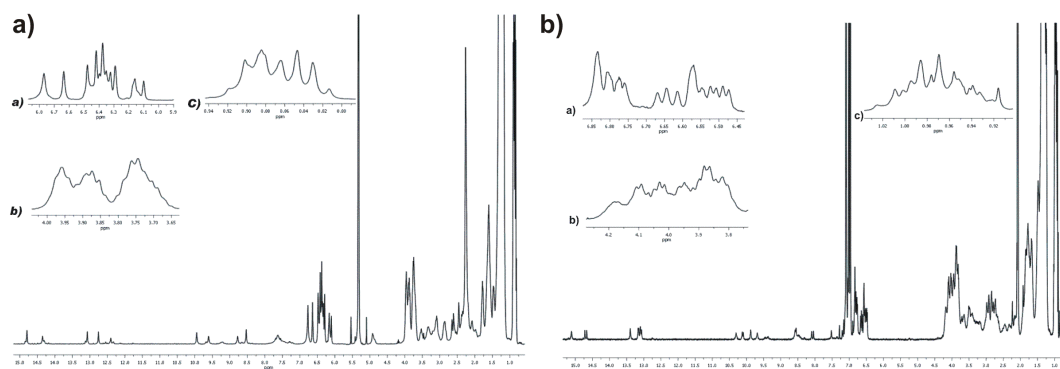


Figure 63: a) ^1H NMR spectrum of (+)-**81** in d_6 -benzene; b) ^1H NMR spectrum of (+)-**81** in d_8 -toluene. Insets show expanded selected regions of spectra.

The spectra display multiple peaks at downfield region as well as much more complex pattern of signals corresponding to protons of aromatic rings and alkoxy chains. The ^{13}C NMR indicates the presence of two tautomers in all these solvents; therefore, the complexity of the spectra most probably arises from further aggregation of supramolecular tetramers. In chloroform, the supramolecular tetramers do not associate at any noticeable degree to form higher aggregates because of steric hindrance of two resorcinol moieties that precludes the tetramers to approach each other. On the other hand, in less polar solvent, where hydrogen bonding is stronger the steric congestion can be at least partially circumvented. If the resulting mixture of tetramers and octamers are in slow equilibrium, proton NMR spectra can be rather complicated, especially if NH protons that participate in connecting two tetramers have different chemical shift comparing to outer NH protons and NH protons connecting the monomers within the tetramer. In addition, the resorcinol moieties change their conformation when going into close contact in octamer. It is evident from proton NMR spectra that there are many different resorcinol moieties. If two or more supramolecular tetramers aggregate with each other, the hydrogen bonds connecting two tetramers must be much weaker than endocyclic hydrogen bonds between constitutive parts of tetramer. When increasing the temperature of the mixture, the weaker hydrogen bonds between the tetramers should be broken first resulting in monomeric tetramers. The validation of this assumption was borne out by variable temperature NMR in

benzene (**Figure 64**). The disappearance of all downfield resonances except those belonging to tetramer is evident when increasing the temperature. The ^1H NMR spectrum of (+)-**81** at 340 K looks almost identical to one obtained in chloroform, and consists of equal amount of two tautomeric forms of isocytosine hydrogen bonding motif.

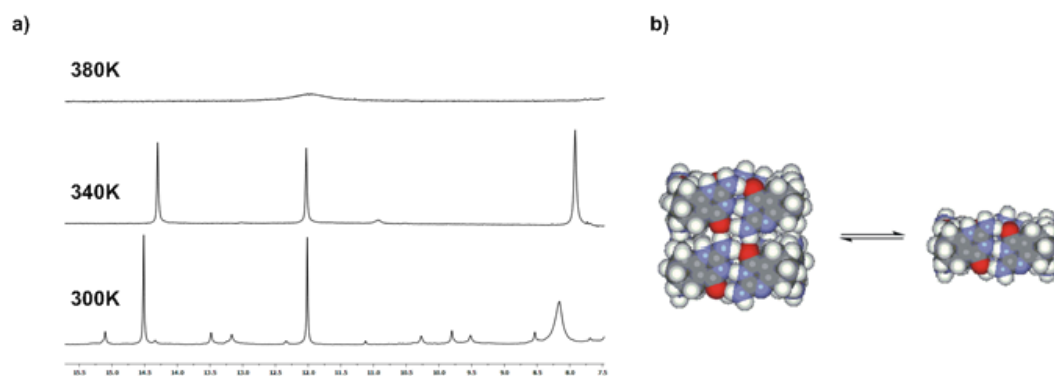


Figure 64: a) variable temperature ^1H NMR of (+)-**81** in d_6 -benzene; b) dimerization of cyclic tetramers of (+)-**81**.

The resonances of NH protons are far downfield which supports the formation of hydrogen bonded tetramer. Beside the similarity of the spectra in chloroform and in benzene at 340 K, the formation of tetramer as the most presumable species in benzene or toluene is confirmed by the DOSY data in toluene. As was mentioned above, the molecular dimensions of aggregate derived from hydrodynamic radius, agree well with the size of stacked dimer of tetramers. By increasing the temperature to 380 K, the hydrogen bonded tetramer disintegrates and the monomeric species of single tautomer (or both equilibrating very rapidly) are formed. The process is accompanied by a coalescence of two sets of NH and NH_2 proton resonances to one.

Finally, the data obtained from gel permeation chromatography (GPC)¹⁷⁸ showed the polydispersity index to be equal to 1.05, which confirms the presence of single species in chloroform. Moreover, the molecular weight obtained using polystyrene as reference, was equal to 4390, the value very close to that estimated for tetramer $M_w = 4336$.

Having the solid proof for the formation of supramolecular tetramer via very strong tautoleptic aggregation, the next step was the determination of association constant K_a . Since no changes were observed in ^1H NMR and UV spectra upon dilution of chloroform solutions, it was not possible to quantify K_a in this solvent. A common practice used to estimate the association constant for strongly bonded complexes is to add small amount of a very polar co-solvent, which competes for hydrogen bonding and decreases the stability of aggregate. DMSO was a solvent of choice because another polar solvent methanol could exchange acidic NH protons with deuterium. During the stepwise addition of DMSO into chloroform solution, the system underwent various changes resulting in complex splitting and shifts of proton resonances (**Figure 65**).

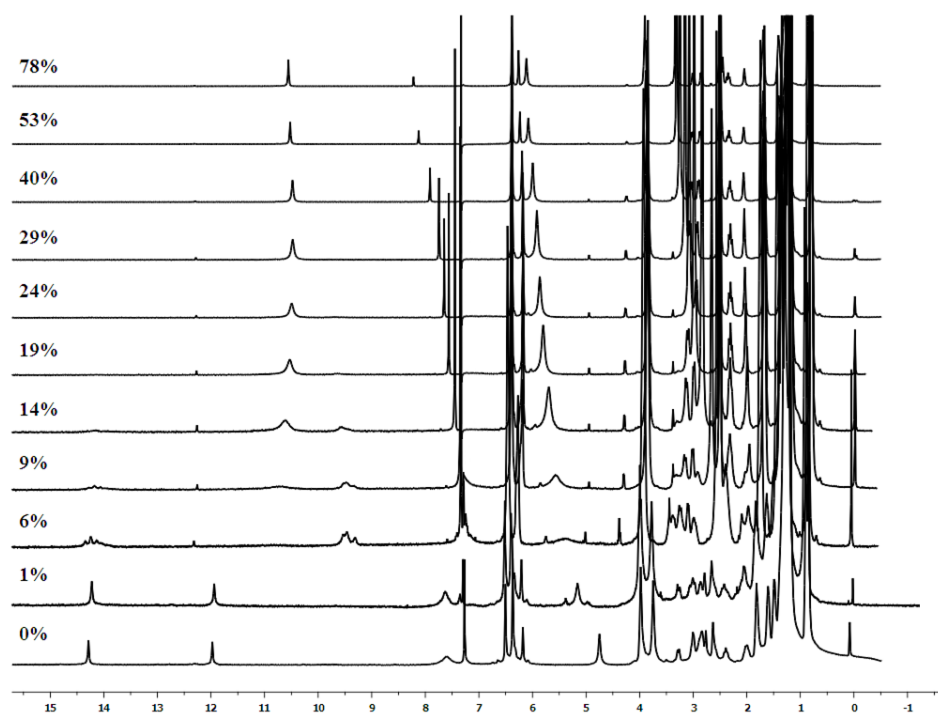


Figure 65: ^1H NMR spectra of (+)-**81** in CDCl_3 with increasing amount of DMSO (in %).

First, after addition of 1% (v/v) of DMSO, there are almost no changes observed in spectrum except that the NH_2 resonance at 4.78 is shifted to 5.20 ppm downfield, towards the position of fully solvated NH_2 group in DMSO. Most probably, the first step is partial complexation of DMSO molecules to

extra NH protons, which are pointing out from the rim of tetramer (**Figure 66a**). For some reasons, the complexation is less efficient with NH₂ group protons of N3-H tautomer than with NH₂ group protons of N1-H tautomer. The carbon NMR by adding 1% DMSO also shows twin-peaks and confirms that at this solvent composition both isocytosine tautomers are present. Further addition of DMSO complicated spectra even more. At 6% content of DMSO, the NH peaks at 12 ppm and 7.6 ppm average to multiple peaks at 9.5 ppm, while the most downfielded peak is split to multiplet with no shift in position. The complex pattern of the spectra indicates that there is a mixture of several species that does not equilibrate rapidly. The single set of signals was observed in ¹³C NMR spectrum. The (+)-**81** already exists in a single tautomeric form, though it is probably still hydrogen bonded via two hydrogen bonds forming mixture of dimer, trimer and other species (**Figure 66b**). The original tetramer is already dissociated since the methylene signals of alkoxy chains coalesce. Addition of excess DMSO up to 19% results in spectrum of purely monomeric DMSO solvated (+)-**81** (**Figure 66c**).

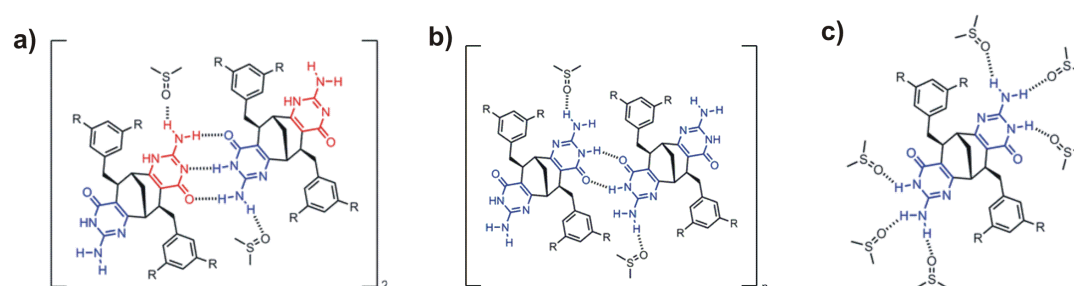


Figure 66: The suggested sequence of changes in aggregation mode of (+)-**81** in CDCl₃ with increasing amount of DMSO; a) coordination of DMSO to external NH protons of supramolecular tetramer at low DMSO content; b) the solvent-induced tautomeric switch of isocytosine moieties forming DA-AD hydrogen bonded intermediates; c) fully solvated single tautomer of (+)-**81** in CDCl₃ with high DMSO content.

From the results obtained it was clear that the evaluation of association constant is hampered by tautomeric equilibrium which not only weakens hydrogen bonding but also alters the type and geometry of supramolecular structure.

The ^1H NMR spectra in the solvents of moderate polarity were recorded in order to test the possibility to reduce the strength of hydrogen bonding. The spectrum in deuterated tetrahydrofuran is very similar to that in chloroform with few percents of DMSO. By analogy, it seems that in this solvent there is one tautomer, which remains partially hydrogen bonded. This is quite reasonable keeping in mind that tetrahydrofuran is poorer hydrogen bond acceptor compared to DMSO. In more polar pyridine and dimethylformamide only monomeric (+)-**81** is detected.

The molecular modeling of the cyclic tetramer of (+)-**81** suggested that the so formed cavity has a length of 12.6 Å from face to face and would fit one molecule of C_{60} (7.1 Å). An almost perfect match is seen taking into account the van der Waals radii (**Figure 67**).

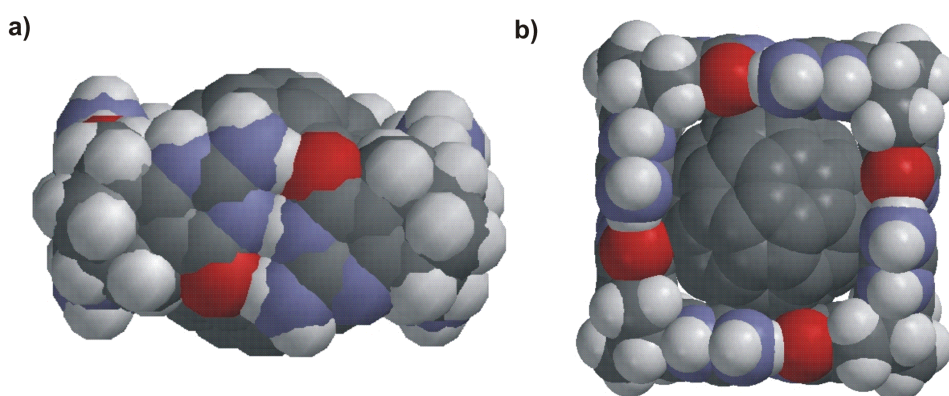


Figure 67: Space filling models of complex between (+)-**81** and C_{60} ; a) side view; b) top view.

Upon addition of a saturated solution of C_{60} in CHCl_3 into the solution of (+)-**81** in CHCl_3 , a drastic colour change from purple to light brown was observed, indicating that (+)-**81** indeed interacts with C_{60} (**Figure 68b**). The UV-Vis titration in CDCl_3 showed that the spectra of the mixture of (+)-**81** and C_{60} are not equal to the sum of spectra of two components. The corrected spectra are shown in **Figure 68a**.

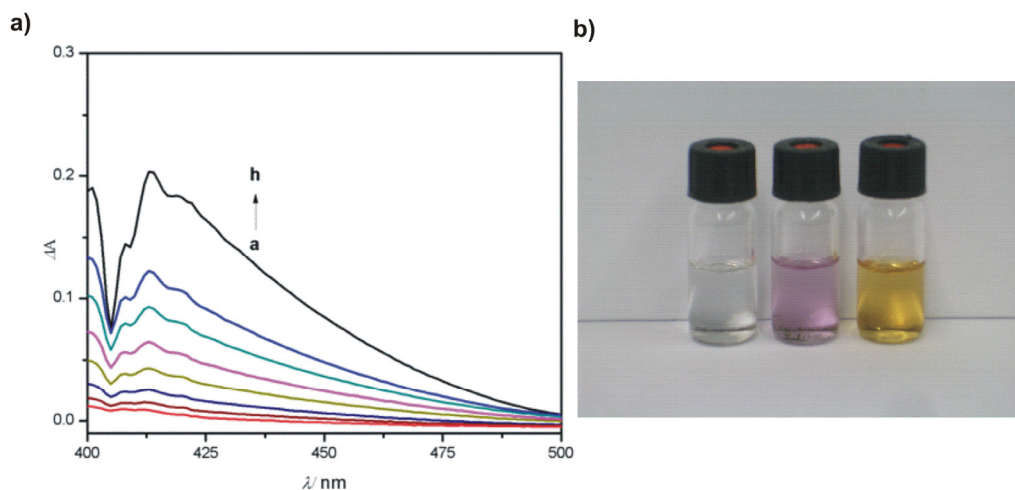


Figure 68: a) corrected spectra of C₆₀ with increasing amount of (+)-81 in chloroform; b) solutions of (+)-81 (left), C₆₀ (middle), (+)-81+C₆₀ (right) in chloroform.

Unfortunately, we were not able to determine the binding stoichiometry by using continuous variation method (Job's plot)¹⁷⁶ most likely due to concomitant formation of dimeric complexes. The data from UV titration were consistent with the 1:1 binding model, however at higher ratio of host (+)-81 to C₆₀, significant deviation occurred. The complexation is also indicated by increased solubility of C₆₀ in chloroform. Although the quantitative studies have not been conducted, the increased solubility was witnessed by dissolution of solid C₆₀ in its saturated CHCl₃ solution upon addition of excess of (+)-81. On the other hand, ¹³C NMR showed that carbon resonance of fullerene was not affected by complexation. The same was true for the ¹H NMR spectrum of monomer (+)-81 as no visible shift of proton resonance signals could be detected. The poor solubility of C₆₀ in CHCl₃ was inconvenient for the association studies and the solvent was changed to benzene. As in the previous case, the addition of (+)-81 to the benzene solution of C₆₀, colour change from purple to pale purple and then to brownish-yellow was observed (**Figure 69a**). In contrast to chloroform solution, the colour change occurred twice at the (+)-81/C₆₀ ratio of 4:1 and 8:1. The UV-Vis spectroscopy also indicated at least several species involved in host-guest equilibrium (**Figure 69b**).

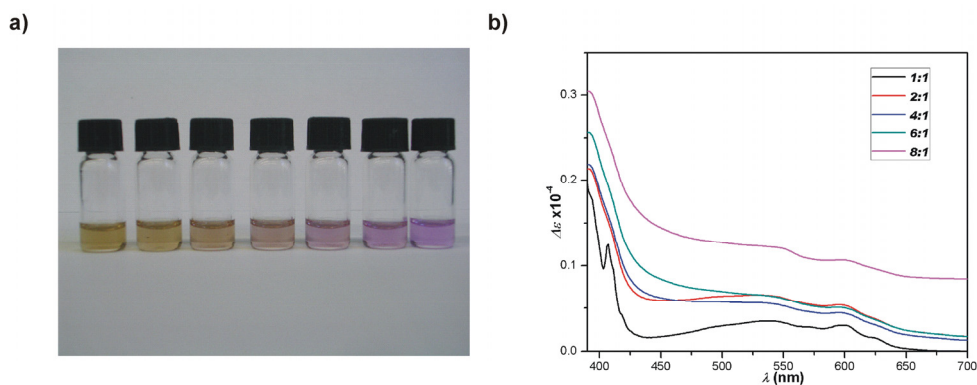


Figure 69: a) solutions of C₆₀ with increasing amount of (+)-81 (the ratio of (+)-81/C₆₀ is (from right to left) 0, 1, 2, 4, 6, 8,10); b) uncorrected UV spectra of the mixture of (+)-81 and C₆₀ at different ratios (from 1:1 to 8:1).

These findings support the formation of dimer of tetramers in benzene or toluene. The CD spectra of monomer (+)-81 at different ratio to C₆₀ failed to give proof for chirality transfer to C₆₀ as no bands in visible spectrum region were observed. The overall picture of complexation event is likely to be more complicated and involves the equilibrium between tetramers and octamers, binding of C₆₀ by tetramer or by octamer and further binding of additional tetrameric monomer to already formed complex of tetramer and C₆₀. The detailed study of C₆₀ and C₇₀ complexation by host (+)-81 will be the subject of further studies.

3.6.4 Polymeric aggregation of decyl substituted tautoleptic synthon

To the contrary to (+)-81, decyl analogue (+)-80 showed completely different aggregation behaviour. It is not soluble in polar solvents and has rather limited solubility in chlorinated solvents. The solutions of (+)-80 in chloroform are very viscous already at low concentrations which render NMR experiments more complicated or even impossible. The high viscosity of its solution can be regarded as an indication of extensive hydrogen bonding or other type of aggregation.

The ^1H NMR spectrum of (+)-**80** in chloroform shows only signals of decyl chains. The NH resonance peaks and peaks from bicyclic protons are very broad and inseparable from the baseline (**Figure 70a**). This outcome can be explained by the formation of supramolecular polymer of very high degree of polymerization.

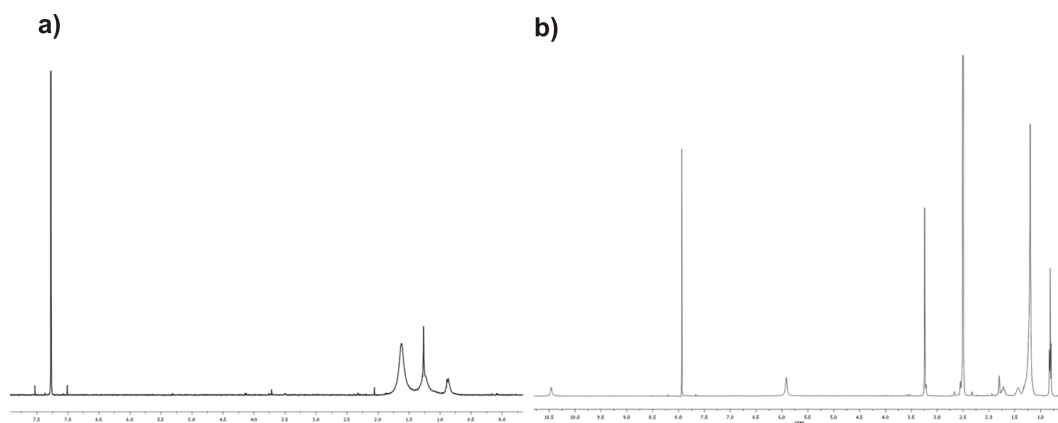


Figure 70: a) ^1H NMR spectrum of (+)-**81** in CDCl_3 ; b) ^1H NMR of (+)-**80** in CDCl_3 - d_6 -DMSO mixture.

Breaking down the supramolecular polymer by diluting with DMSO resulted in more informative spectrum with single set of NH signals as in case of compound (+)-**81** (**Figure 70b**). Unfortunately, we were not able to collect the ^{13}C NMR spectrum of saturated solution of (+)-**80** in chloroform. It was unclear if the monomer of (+)-**80** exists in chloroform as a mixture of two tautomers or not. The UV spectroscopy provided an unambiguous answer to the question. As in the case of compound (+)-**81**, the spectrum in chloroform is composed of two intense broad bands with the maximum at 231 nm and 303 nm. In DMSO, the short wavelength band at 238 nm is weak and the long wavelength band at 290 nm is of the same intensity as in chloroform (**Figure 71a**). This observation shows that in chloroform compound (+)-**80** exist as a mixture of tautomers, whereas in DMSO single tautomeric form is detected. The concentration dependence of the absorption showed that (+)-**80** obeyed Lambert-Beer's law. The linear relationship between concentration and absorption means that the association process does not involve the interaction of molecular orbitals. Thus, π - π interaction is refuted as a mean of interaction.

The stepwise addition of DMSO to a chloroform solution of (+)-**80** induced the change in tautomeric composition by increasing the polarity of the media. Addition of 1% of DMSO only slightly affected the spectrum, but further addition of DMSO resulted in hypsochromic shift of the long wavelength band. After addition of 10% of DMSO, the spectrum looks almost the same as in pure DMSO (Figure 71b).

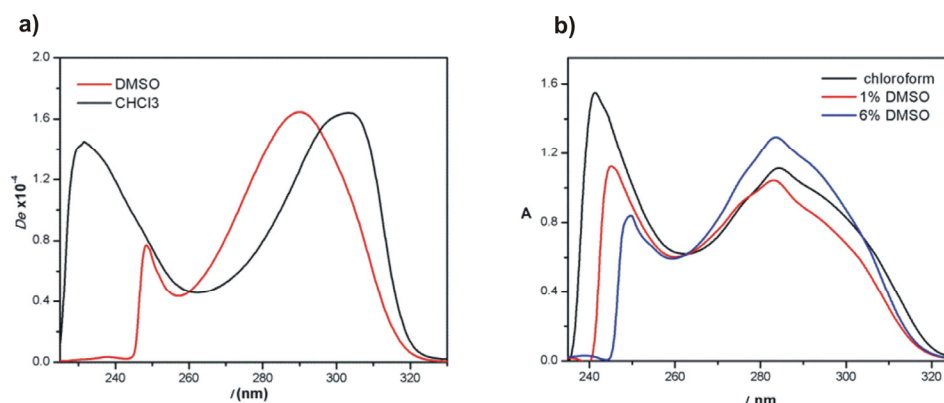


Figure 71: a) UV spectra of (+)-**80** in CHCl_3 and DMSO; b) UV spectra of (+)-**80** in CHCl_3 with increasing amount of DMSO.

The CD spectra of (+)-**80** in chloroform and DMSO are shown in Figure 72.

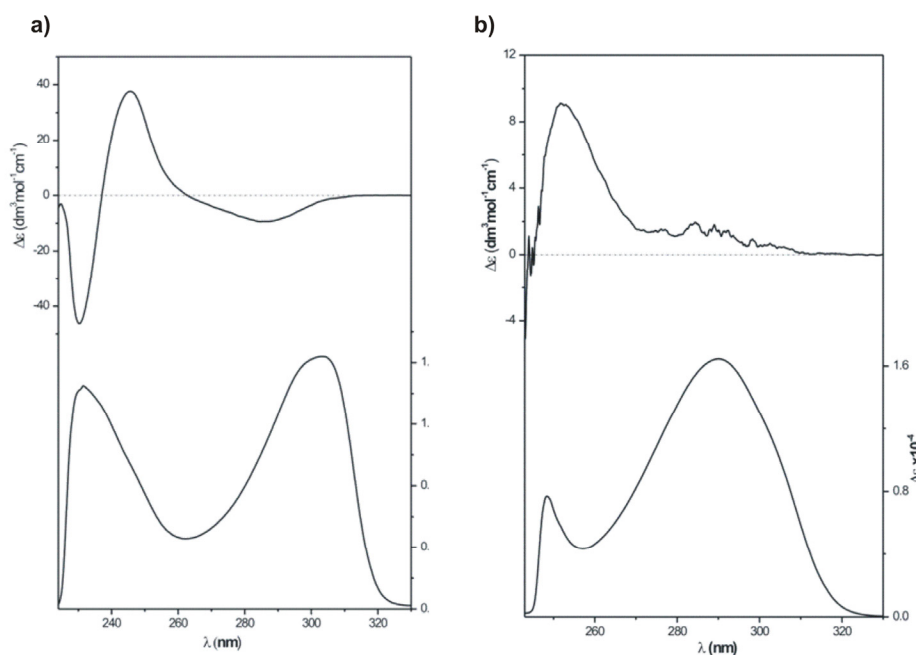


Figure 72: a) CD and UV spectra of (+)-**80** in chloroform; b) CD spectra of (+)-**80** in DMSO.

In contrast to (+)-**81**, the spectra are lacking positive long wavelength band. This band may be related with the aromatic moieties in the (+)-**81** molecule. In DMSO, the negative long wavelength band becomes a broad weak positive band, likewise in the case of (+)-**81**. Unfortunately, it is not possible to guess about the aggregation mode of (+)-**81** using CD data. The shift of tautomeric equilibrium by changing solvent composition was also demonstrated by ^1H NMR. Dilution of the solution of (+)-**80** in DMSO-chloroform mixture with chloroform caused broadening of NH and bicyclic protons signals (**Figure 73a-b**), indicating an increase of the degree of polymerization. The very high degree of aggregation and high viscosity are most likely to result from unidirectional association of tetrameric units formed from tautoleptic aggregation of monomers (+)-**80**. The stacking of tetramers is possible since the steric hindrance imposed by solubilizing decyl groups is not so significant, as compared to more bulky chain in (+)-**81**.

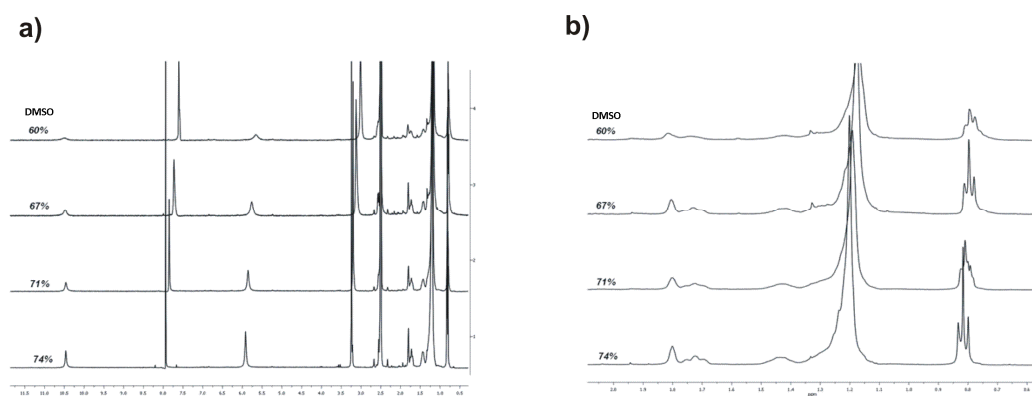


Figure 73: Parts of ^1H NMR spectra of (+)-**80** in d_6 -DMSO- CDCl_3 mixture with increasing amount of CDCl_3 .

The formation of high-molecular-weight one dimensional aggregates results in high viscous solution which upon increasing the concentration above 4 mg/ml forms a gel. It is possible that above this critical concentration, entanglement of decyl chains begins and the gel is formed. The concentration dependence of the solution viscosity provides information on the aggregation behavior of compound (+)-**80**. The plot of specific viscosity versus the concentration of

(+)-80 in chloroform together with reference molecule (+)-81 is shown in **Figure 74**.

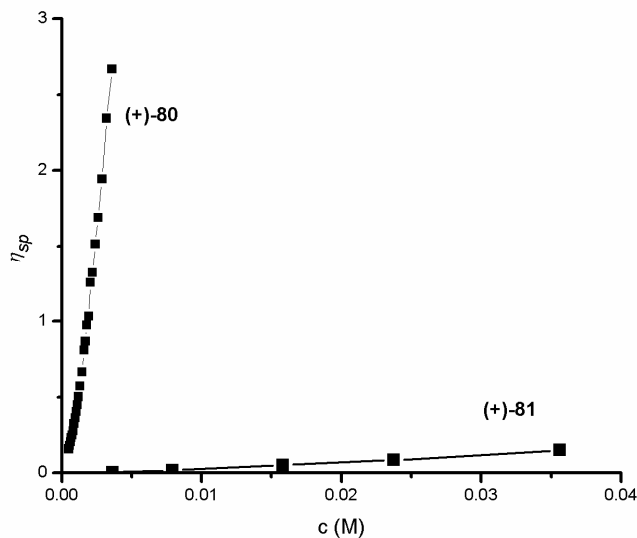


Figure 74: Concentration dependence of specific viscosity of (+)-80 and (+)-81 in chloroform.

From the plot, it is evident that compound (+)-80 displays much stronger concentration dependence of specific viscosity comparing to non-aggregating tetramer (+)-81. The double logarithmic plot gave a slope of 1.46, which agreed well with the predicted value for reversible polymers below critical overlap concentration at which the entanglement of alkyl chains begins (**Figure 75**).¹⁷⁹

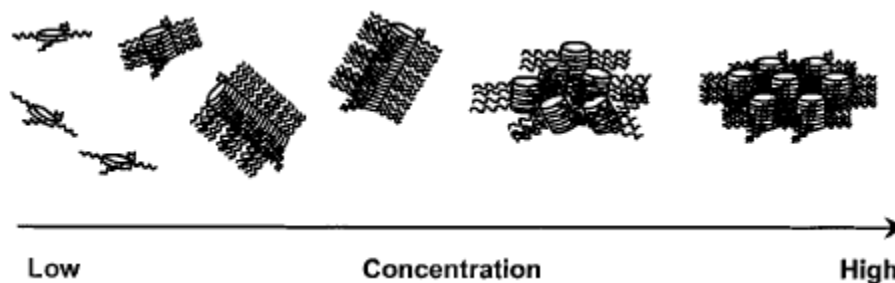


Figure 75: Concentration dependence of structural changes of molecular aggregates of (+)-80.

3.6.5 Association studies of 4H bonding synthon

The ^1H NMR spectra of urea (-)-**82** in chloroform and DMSO are shown in **Figure 76**. The spectrum in chloroform features the typical pattern of ureidopyrimidinone composed of three broad donfielded singlets corresponding to urea moiety. The chemical shift of NH protons indicates strong hydrogen bonding via four hydrogen bonds between self-complementary urea motifs.

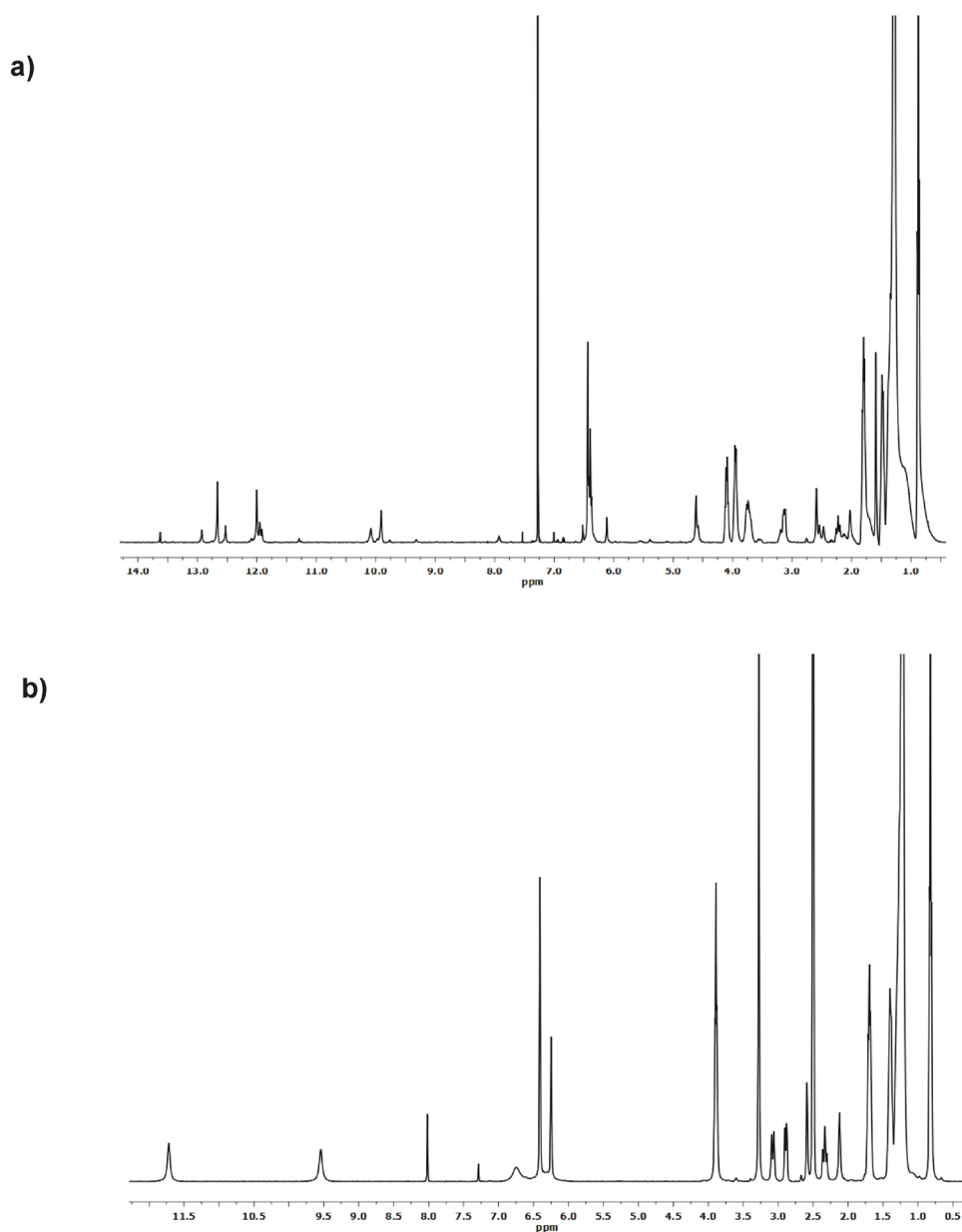


Figure 76: a) ^1H NMR spectra of (-)-**82** in CDCl_3 ; b) ^1H NMR spectra of (-)-**82** in CDCl_3/d_6 -DMSO (1:1-v/v).

The presence of small satellite peaks is also evident in spectra, which results from other tautomeric forms of (-)-**82**. In analogy to the case of isocytosine derivative (+)-**81**, the association of (-)-**82** gives rise to the splitting of proton resonances of methylene group of the alkoxy-chain, however, only single signal corresponding to terminal methyl group was observed. This indicates, that the rotation of benzylic chains are somewhat restricted in the supramolecular aggregate, but the monomers are not so tightly packed comparing to tetramer formed by (+)-**81**. The above mentioned features are lacking in ¹H NMR spectrum of (-)-**82** in DMSO (**Figure 76b**). The single resonance for methylene group is observed and the position of NH resonances moves upfield in DMSO. The data are in agreement with the presence of non-self-complementary keto tautomer (-)-**82c**, which is the most stable tautomeric form in polar solvents (**Figure 77**). The NH resonance signals did not move upon dilution of chloroform solution, although the relative amount of other tautomeric forms was slightly sensitive to concentration.

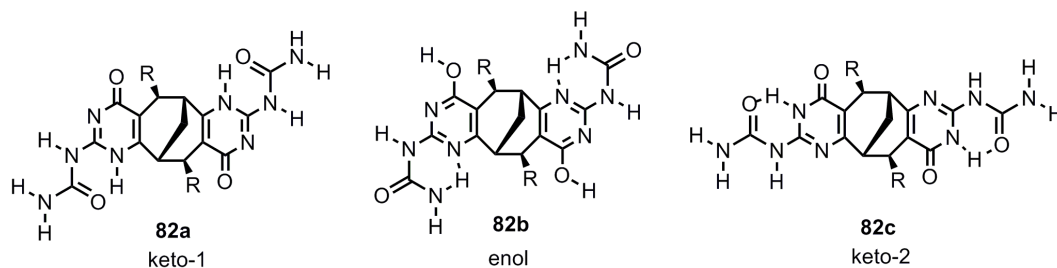


Figure 77: The tautomeric forms of (-)-**82**. Only symmetric tautomers are shown.

In order to gain more information about the degree of association and structural features of the assembly, the urea (-)-**82** was subjected to VPO analysis. The degree of aggregation $\langle N \rangle$ was constant over the whole concentration range and was found to be 3.50 ± 0.25 . The small value of $\langle N \rangle$ indicates that supramolecular polymer is not formed in chloroform; instead, smaller aggregates dominate. According to molecular modeling, formation of cyclic structure is not feasible for monomer (-)-**82** due to improper positioning of urea fragments. Thus, it is likely that the steric interaction between 3,5-

didecyloxybenzyl groups prevents the propagation of tubular supramolecular polymer and the undefined trimeric or tetrameric structures are formed. To confirm the results obtained using VPO, diffusion NMR studies were conducted. The data obtained are presented in **Tables 7-9**.

Table 7: Average diffusion coefficients (D) and average Stokes' radius (R_s) for **(-)-82** obtained from three different peaks; 12.93, 12.53 and 10.08 ppm at three different concentrations (20, 29 and 39 mM). The diffusion coefficient reported for 0 mM (D_0) was obtained by plotting D against the concentration and extrapolating to infinite dilution. Dynamic viscosities (η) were obtained theoretically

Concentration (mM)	Average D (\AA)	$\langle\eta\rangle$ (pas)	Average R_s (\AA)
39	2.533E-10	0.00075149	11.27443634
29	2.599E-10	0.00071453	11.55653371
20	2.81667E-10	0.00067612	11.26920716
0	3.08E-10	0.000589	11.8300948

Table 8: Average diffusion coefficients (D) and average Stokes' radius (R_s) for reference **120** obtained from two different peaks; 12.66, and 9.91 ppm at three different concentrations (20, 29 and 39 mM). The diffusion coefficient reported for 0 mM (D_0) was obtained by plotting D against the concentration and extrapolating to infinite dilution. Dynamic viscosities (η) were obtained theoretically.

Concentration (mM)	Average D (\AA)	$\langle\eta\rangle$ (pas)	Average R_s (\AA)
39	2.884E-10	0.00075149	9.902270196
29	2.9755E-10	0.00071453	10.09424672
20	3.134E-10	0.00067612	10.12814301
0	3.38E-10	0.000589	10.7749858

Table 9: Cubic and square roots of the ratio between trimeric, tetrameric, pentameric and hexameric aggregates

Aggregate	$(M_j/M_i)^{1/3}$	$(M_j/M_i)^{1/2}$
Dimer	1.305093808	1.490948333
Trimer	1.49395947	1.826031324
Tetramer	1.644315161	2.108519353
pentamer	1.771284812	2.357396302

The diffusion NMR shows the presence of two aggregates, one with R_s of 12 Å and one with R_s of 11 Å. The ratio of diffusion coefficients of the smaller and larger aggregates and reference molecule **121** were 1.42 and 1.56 respectively. According to equation 9 (**Table 9**), these aggregates are likely to be a dimer and a trimer. The discrepancy between the results of VPO analysis and diffusion NMR are probably related to inaccuracies in calculating hydrodynamic radius of non-symmetric acyclic aggregates. Nevertheless, both methods confirmed the low degree of aggregation and the presence of small aggregates.

4 Chiroptical properties of bicyclic enones

4.1 Introduction

The α,β -unsaturated ketone (enone) chromophore belongs to the group of chromophores that have been investigated quite extensively in recent years.¹⁸⁰ A number of sector and/or helicity rules have been proposed to correlate the sign of the CEs observed in the spectral region between 200 and 350 nm with the absolute configuration of α,β -enone molecules.¹⁸¹ These rules are derived from the observation that the CD and UV spectra of enones are affected by substituents located close to this chromophore, which alter its electronic structure.

En route to the synthesis of alkyl substituted bicyco[3.3.1]nonane-2,6-dione, the large scale synthesis of the dienone **94** was developed (vide supra). The later compound was highly UV active and was reported to undergo efficient intramolecular photochemical dimerization between two enone double bonds.¹²¹ This fact accounts for the degradation of the compound under exposure to the direct sunlight. In addition, the transannular interaction of enone chromophores in this compound has been demonstrated earlier by photoelectron spectroscopy.¹⁸² Being intrigued by these observations we decided to investigate the chiroptical properties of enantiomerically pure **93** in more details and also to compare its properties with the di- and monochromophoric reference molecules **144**, **96**, **145**, possessing only one enone functionality (**Figure 78**).

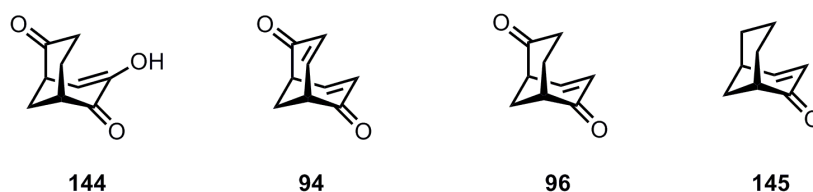
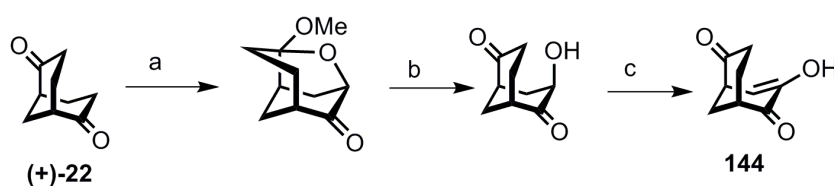


Figure 78: The structure of mono- and dienones studied by CD spectroscopy.

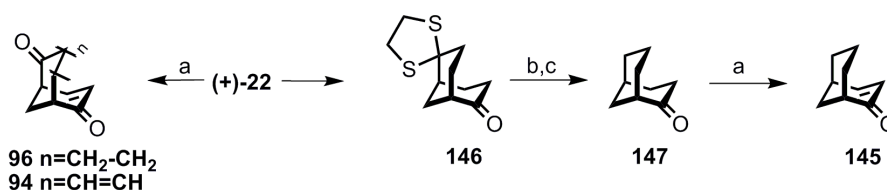
4.2 Synthesis of enones

The compound **144** was synthesized earlier in our laboratory from enantiomerically pure dione (+)-**22** by α -hydroxylation involving the use of iodine under the basic conditions and subsequent cascade-addition-cyclization reaction initiated by methoxide anion attack on the carbonyl group (Scheme 25).



Scheme 25: Reagents and conditions: a) I₂, KOH, MeOH, 0°C, 81%; b) TsOH·H₂O, acetone, rt, 90%; c) TFAA, Et₃N, DMSO, DCM, -60°C, 80%.

The dienone **94** was obtained by following Barton dehydrogenation procedure which, as was noted before, proceeded in very high yield in case of dione **22**, although was impractical for large scale preparation. However, for spectroscopic studies where only minute amounts of material are required, this procedure seemed to be very attractive since it enabled us to obtain the desired enone in a single synthetic step. The unsaturation of enantiomerically pure diketone (+)-**22** under these conditions afforded dienone **94** in 90% yield. The monounsaturations were successfully achieved by using only two equivalents of iodoxybenzene giving compound **96** in 60% yield. By analogy, enone **145** was synthesized in 95% yield from monoketone **147**, which was obtained by protection of one carbonyl group in diketone **22** with slight modification of the reported procedure (Scheme 26).¹⁸²



Scheme 26: Reagents and conditions: a) PhIO₂, cat. (PhSe)₂, cat. TsOH, toluene, reflux; 90% for **94**, 60% for **96**, 95% for **145**; b) Ra-Ni, EtOH, reflux; c) Jones reagent, rt, 74% over two step.

4.3 CD spectroscopic studies

The synthesized compounds possess enone chromophores, and among them compounds **144**, **94** and **96** are dichromophoric. The CD spectra of enones usually have two CD bands in the range 220 to 350 nm. The third short-wavelength CD band, which is found in the 200 to 220 nm spectral region, is of very small absorption intensity and is likely to be due to a π - π^* transition, though this assignment is not unequivocal.¹⁸³ The long-wavelength band is due to an n - π^* transition which appears around 350 nm. The second band, which appears between 230–260 nm, is due to a π - π^* transition polarized approximately along the line connecting the oxygen and the most remote carbon atom of the C=C bond. The bands of the n - π^* transition in the CD spectra of the studied enones are observed at ca. 340 nm for enone **145** and bis(enone) **94**, and at ca. 310 nm for ketoenone **96** and triketone **144** (Figure 79). The λ_{max} and specific rotation of these enones are presented in Table 10. The CD spectra of all compounds exhibited a positive Cotton effect. Enone **145**, containing the single chromophore, could be regarded as a reference compound for this transition.

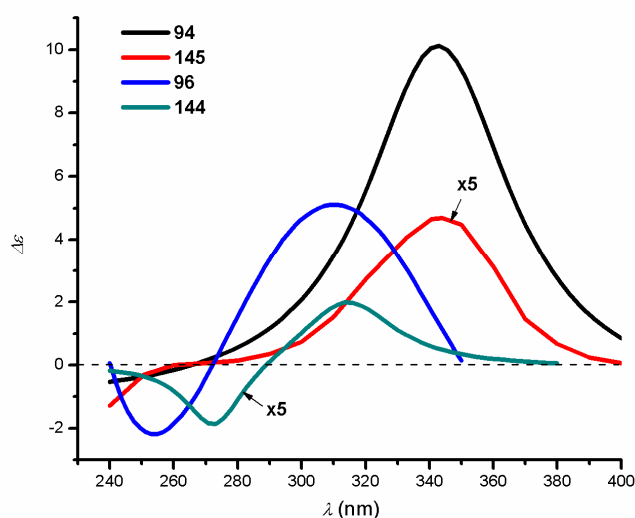


Figure 79: CD spectra of triketone **144**, ketoenone **96**, enone **145**, and dienone **94** in ethanol.

Conformational analysis by molecular mechanics and B3LYP/6-31G* calculations revealed that the cyclohexenone ring of enones **144** and **96** exists in a distorted flattened chair conformation. The enone functionality is nonplanar, and the torsional angles were found to be 4° and 5°, respectively, in minimized structures. The sector and/or helicity rules correlating the sign of the CEs that are observed in the spectral region between 200 and 350 nm with the absolute configuration of α,β -enone molecules have to be applied with caution. Recently a study on the chiroptical properties of *cisoid* enones showed that, in general, the positive (negative) sign of the CE associated with the $n-\pi^*$ transition reflects the positive (negative) enone helicity.¹⁸⁴ The sign of the torsional angles in enones **144** and **96** correlates with the long-wavelength sign of the CE in the bisignate CD curve (**Figure 79**).¹⁸⁵ The sign of the shorter-wavelength band is opposite to that of the longer-wavelength band.

Table 10: Rotation angles and λ_{\max} of enones

Compound	$[\alpha]_D$, deg cm ² g ⁻¹	CD, λ_{\max} , nm ($\Delta\epsilon$, dm ³ mol ⁻¹ cm ⁻¹)
(+)-(1 <i>S</i> , 5 <i>R</i>)- 144	+350 (EtOH, <i>c</i> 3.1, 20°C)	314 (+0.40), 273 (-0.37)
(+)-(1 <i>S</i> , 5 <i>S</i>)- 145	+115 (EtOH, <i>c</i> 0.76, 20°C)	341 (+0.95)
(+)-(1 <i>S</i> , 5 <i>S</i>)- 96	+1569 (EtOH, <i>c</i> 0.04, 20°C)	313 (+5.4), 254 (-2.4)
(+)-(1 <i>S</i> , 5 <i>S</i>)- 94	+2260 (EtOH, <i>c</i> 0.37, 20°C)	342 (+10.2)

Compound **144** possesses one band in the UV region between 200 and 360 nm (**Figure 81b**). The CD maximum is shifted to a shorter wavelength relative to that of the UV absorption of **144**. The hypsochromic shift of the $n-\pi^*$ transition in triketone **144** and ketoenone **96** is associated with the effect of neighbouring substituents. The marked difference in intensity of this transition is accounted for by the electronic effects of the carbonyl group in the next six-membered ring of ketoenone **96**, and more substantially, of the hydroxy group attached directly to the enone double bond in triketone **144**. The intensity of the CD

bands of enone **144** are ten times weaker than those of ketoenone **96**. This is due to the magnitude of the dipoles, although their orientation is nearly the same in both molecules (**Figure 80**).

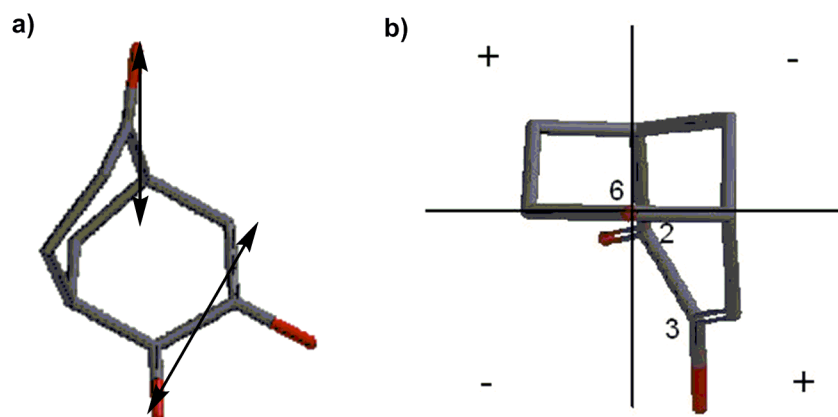


Figure 80: a) distorted cyclohexanone chair conformation (in front) and angle between planes containing chromophores in triketone **144**; b) projection of the C-6 carbonyl group in triketone (+)-**144** into octants.

We calculated the angle between the planes containing chromophores to be ca. 60° for both compounds by the B3LYP/6-31G* method. However, the dipole moment is substantially smaller in molecule **144** compared to **96** because of the electronic effects of the hydroxy group at the enone double bond, which decreases the electron density. The positive mesomeric effect of the hydroxy group and the intramolecular hydrogen bonding of the latter with the enone carbonyl group (cf. the case of 1,2-cyclohexanedione)¹⁸⁶ considerably reduce the charge separation between the carbonyl oxygen atom and the terminal carbon atom of the enone double bond, thus affecting the value of the chromophore dipole moment in compound **144**. This conclusion is strongly supported by the ^1H NMR signals of the corresponding ethylene protons in molecules **144** and **96**, 6.17 ppm and 7.12 ppm, respectively, which demonstrates the strong deshielding of the enone double bond in **96**. Accordingly, the bathochromic shift of the shorter-wavelength band in the CD spectrum of compound **144** relative to that of ketoenone **96** (**Figure 79**) is accounted for by the resulting dipole as well.

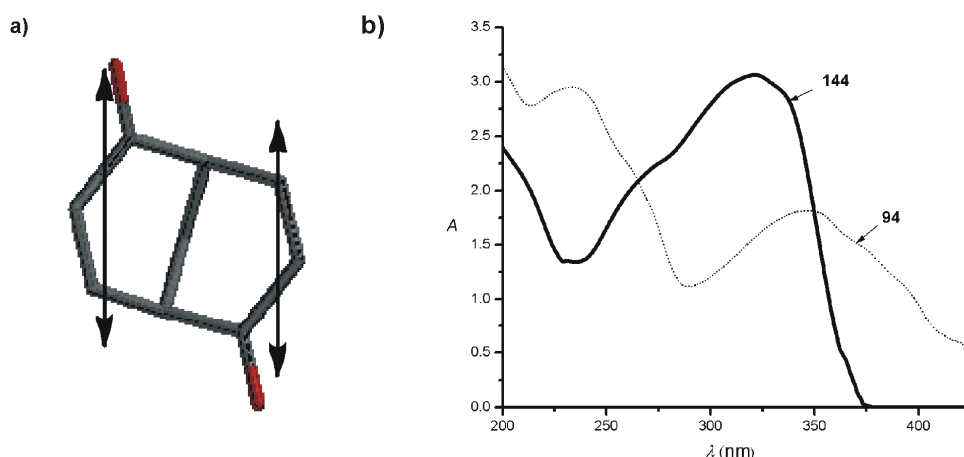


Figure 81: a) the orientation of dipoles in the minimized structure of dienone **94**; b) UV spectra of triketone **144** and dienone **94**.

We next examined the applicability of the octant rule for the correlation of the sign of the observed Cotton effect with the absolute configuration of enones containing a carbonyl chromophore in the next six-membered ring. The band of an $n \rightarrow \pi^*$ transition is ascribed to the carbonyl chromophore. In order to apply the octant rule, the triketone molecule **144** was placed into octants. The cyclohexanone ring with the carbonyl group is in a conformationally defined chair form in this molecule, and locating it into octants is straightforward. **Figure 80** shows the projection of the minimized structure (1*S*,5*R*)-**144** into octants. The hydroxyl group of the enone functional group, the C-2 carbon atom of the carbonyl group in the cyclohexenone ring and the C-8 carbon atom of the next six-membered ring are located in positive octants, while the enone carbonyl group is close to the nodal surfaces. Thus, the major input in the top left and the bottom right positive octants leads to a positive CE, which is in accordance with the experimental data. An analogous unambiguous conclusion can be reached by locating the carbonyl groups of ketoenone (1*S*,5*S*)-**96** into octants. The intensities of the $n \rightarrow \pi^*$ transition bands of compounds **144** and **94**, **96** and **145** are significantly different. For bis(enone) **94** the absorption of this transition is enhanced by an order of magnitude in comparison to enone **145**. This originates from a transannular orbital interaction of chromophores in dichromophoric bis(enone) **94**. The transannular interaction of enone

chromophores in this compound has been demonstrated earlier by photoelectron spectroscopy as well as by their chemical reactivity leading to intramolecular ring closure. In addition, the molecular structure of **94** has a slightly nonplanar arrangement of chromophores (calculated torsional angle 2°), and this helicity contributes to the intensity of the CD absorption. In bis(enone) **94** the intensity of the $n \rightarrow \pi^*$ transition band is significantly higher as a result of the orientation of dipoles which are nearly parallel (**Figure 81a**). Compound **94** possesses two bands in the UV region, maxima occurring at 350 and 230 nm (**Figure 81b**). The CD maximum corresponds to the absorption maximum in the UV spectrum. Interestingly, the polarimetric rotation angle of the bis(enone) **94** is remarkably large. The second band between 230 and 260 nm arises from a $\pi\text{-}\pi^*$ transition polarized approximately along the line connecting the oxygen atom and the most remote carbon atom of the C=C double bond, and is observed for enones **144** and **96** (**Figure 79**). Interestingly, though the exciton chirality rule is not applicable to enones **144** and **96**, a positive CD couplet could be linked to a positive angle between planes containing transition dipoles (**Figure 80a**) and vice-versa,¹⁸⁷ thus relating positive chirality with the positive first and negative second Cotton effects.

5 Solid state analysis

5.1 Introduction

The introduction of the concept of supramolecular chemistry, i.e. the chemistry beyond the molecule, was an important developing step in modern chemistry, discarding the common notion that the molecular structure of the compound already embodies all of its chemical and physical properties. This branch of chemistry is concerned with different types of weak intermolecular interactions that govern the assembly process of the molecular components. The interaction of molecules in a specific way is realized by the recognition between molecular partners through their energetic and spatial complementarity. The most fascinating consequence of self-assembly is that the properties of supramolecule are different from those possessed by its constituting parts and can be tailor-made. The overall assembly process is the result of close balance between enthalpy, which determines energy of the association, and entropy, which corresponds to the penalty of loss of degree of freedom. The reversible nature of non-covalent interactions offers another advantage of bottom-up approach of self-curing of the defects in the assembly process via the association-dissociation equilibrium until energetic minimum of the system is reached. The supramolecular structure is held together by multipoint weak intermolecular interactions acting in cooperative manner, as the single non-covalent bond is not enough to ensure high-degree of both, directionality and association strength. The understanding of the nature and strength of intermolecular forces is thus of fundamental importance in supramolecular chemistry.

The field of supramolecular chemistry has been traditionally divided in two branches- the study of supramolecules in solution and the study in crystals. The crystal can be regarded as nearly perfect periodic self-assembly of large number of molecules held together by medium and long range non-covalent

interactions that ensures very high level of molecular precision. The rational design of the crystal structure from molecular building blocks is referred to crystal engineering, the concept first introduced by Schmidt¹⁸⁸ in connection with solid state photochemical reactions of cinnamic acids. Since then, the meaning of crystal engineering has broadened and now includes many aspects of solid state supramolecular chemistry. The objective of crystal engineering is to obtain particular crystal structure by carefully designing organic or inorganic molecules. The ever-growing demand for designed solids is connected with the possible applications in catalysis, separation processes or developing of molecular-based materials. The organic solids are especially important due to their unusual magnetic, optical, or electronic properties. In addition, the crystal engineering may benefit to better understanding of the principles of weak interactions in the solid state.

As in retrosynthetic analysis of covalent molecules, the supramolecule or crystal can be mentally divided into smaller parts, so called synthons, which encodes the necessary assembly information in its structure. The term tecton instead of synthon is sometimes used to describe the building block of the structure formed in solid state. By analyzing crystal structures of structurally similar compounds (for instance, using Cambridge Crystal Database), it is often possible to identify the part of the molecule or recognition patterns, responsible for the formation of supramolecular structure. The recognition of the set of interaction that constitutes supramolecular synthon is somewhat confusing. In principle, it is possible to identify group of interactions for any crystal structure, however, such set should not be regarded as synthon if it fails to demonstrate the same type of packing when incorporated into the structure of similar molecules. The supramolecular synthon for crystal engineering thus have to be a unit providing interactions that has maximum structural information within relatively small part of molecule. The most frequently encountered synthons in solid state supramolecular chemistry are depicted in **Figure 82**. The use of supramolecular synthons in crystal engineering greatly

simplifies the crystal analysis process, as the same synthon may be present in many related compounds. However, the overall picture is more complicated as one functional group can represent many different supramolecular synthons, for instance, carboxylic acid can form hydrogen bonded dimer or tape-like structure.¹⁸⁹ The same one-to-many relationship of synthons to functional groups is responsible for the formation of polymorphs (two or more different crystal structures formed by the same compound).

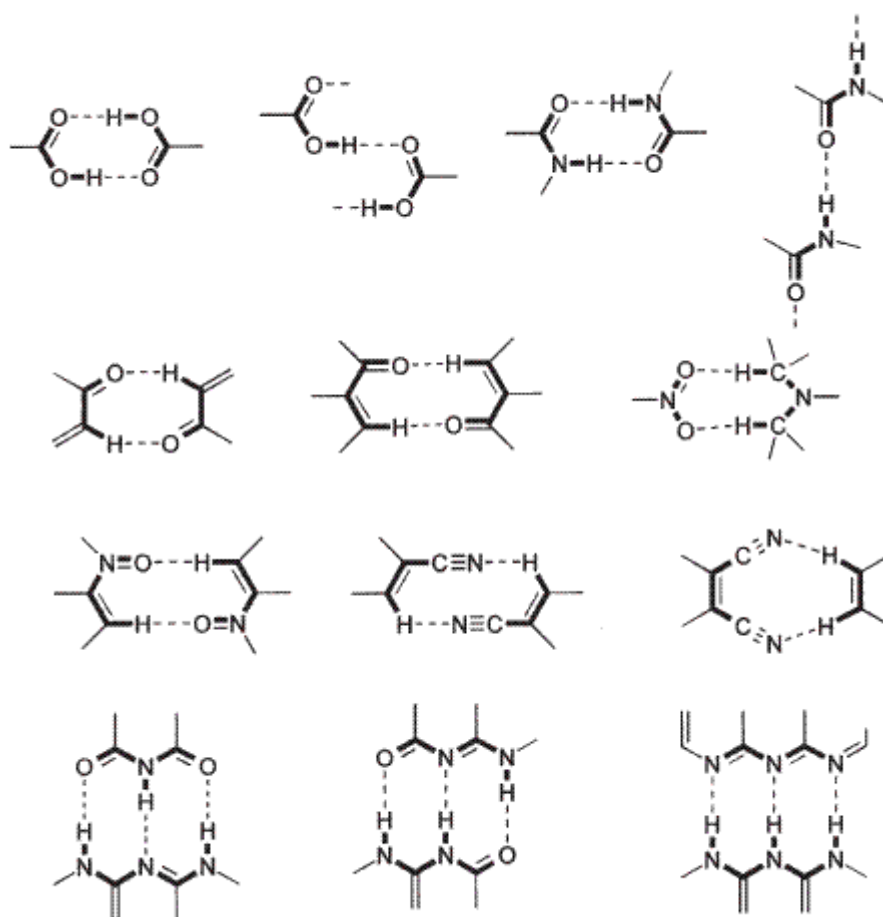


Figure 82: some supramolecular synthons used in crystal engineering.

When designing a crystal as a supramolecule, the topological features and geometric connectivities of intermolecular interactions are sought as targets. The network is composed of node (molecule) and node connectivities (supramolecular synthons). The advantage of use of network approach in

crystal engineering is that: (1) connections between molecules are easily identified; (2) comparison between seemingly different crystal structures are facilitated and instead of extensive explanation of connection pattern of molecules in the crystal, the identification of the structural network can settle the issue; (3) interference between supramolecular synthons can be minimized by analyzing crystal structure; and (4) other supramolecular synthons may be envisioned to afford the same type of connectivity.^{190,191}

Naming of networks (nets) is somewhat problematic, since no general nomenclature exists to describe them. In the simplest case, the two letters Wells notation is used, in which the description of net is given by general expression (n,p), where n is the number of nodes in the smallest ring and p is the number of connections originating from the node. The path connecting n number of nodes is called an n-circuit of ring. The simple 2D-networks with different n,p combinations are shown in **Figure 83**.

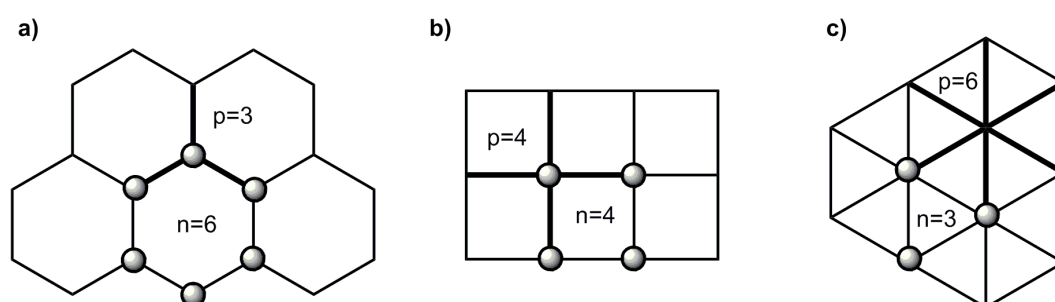


Figure 83: examples of 2D nets with different combinations of p and n; a) (6,3)-net; b) (4,4)-net; c) (3,6)-net. The grey spheres indicates node atoms which are connected in circuit and the bold lines shows connectivity at each node.

The nets designated (n,p) are sometimes called uniform nets, but often the situations arise where a network contains more than one type of n-circuit and p-node. In this case, more complicated notation is used for naming the network, which includes the matrix of all possible combinations of several n-circuits with several p-nodes. These nets are better described by Schläfli notation, a more descriptive numbering scheme, where only circuits are included. Thus, for the net composed of two circuits n and m, the Schläfli notation gives the result $m^x n^y$, where the superscript describe the number of

rings that are equal in size. In addition to Schläfli symbols, a three letter codes for the naming of nets, adopted from similar system for naming of ceolites, is used. The three letter abbreviation in most cases is derived from the known crystal structure of inorganic compounds. For example, in **Figure 84** the illustration of ideal 6^6 -**dia** and $6^6.8^2$ -**qtz** networks is given where three letter codes **dia**- and **qtz** represents crystal packing found in diamond and quartz, respectively.

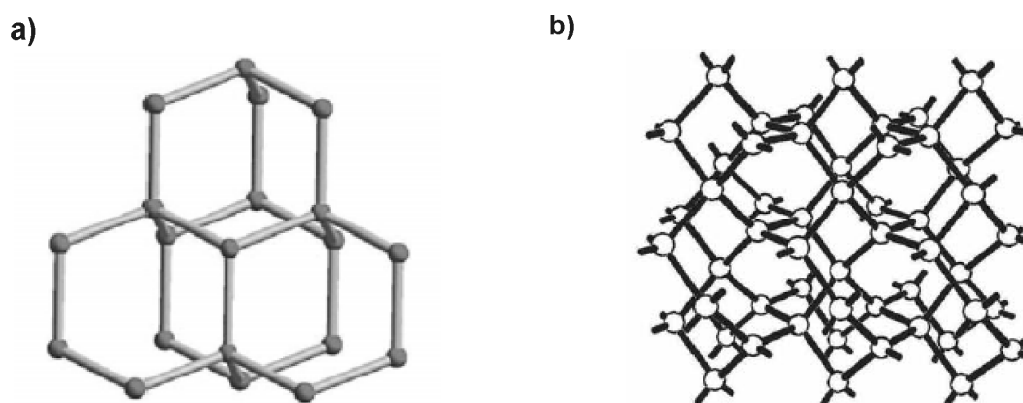


Figure 84: a) the diamond, or 6^6 -**dia** net; b) the chiral quartz, or $6^6.8^2$ -**qtz** net.

In this chapter we report an application of network approach for the analysis of crystal structures of selected bicyclo[3.3.1]nonane derivatives. The network analysis of crystal structures, held together by hydrogen bonds, is expected to provide a better understanding and facilitate the comparison of these systems.

5.2 The diol, dione and acetal

The hydrophobic bicyclic diols are known to form tubular supramolecular structures and inclusion compounds with various guest molecules.¹⁹² For this reason, they are called “tubuland diols”. On the other hand, the crystal structure of simplest diol of this series, *endo, endo*-bicyclo[3.3.1]nonane-2,6-diol **148**, was not reported so far,¹⁹³ and the analysis of crystal structure of this compound may significantly contribute to the supramolecular chemistry of

these compounds, especially in context of network analysis. For the sake of comparison, the crystal structures of two other derivatives, namely dione (+)-**22** and acetal **149** are also analyzed. The latter compounds are lacking the strong hydrogen bonding hydroxyl group, and other types of intermolecular interactions are likely to direct the crystal packing.

The diol **148** and acetal **149** were prepared by known methods.^{32 120} The crystals, suitable for X-ray analysis, were grown by slow evaporation of solvent or by cooling of saturated solutions. All attempts to grow suitable single crystals of enantiomerically pure **149** were unsuccessful because of its high solubility in all solvents explored.

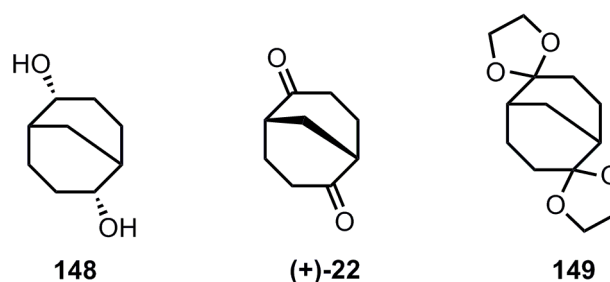


Figure 85: the bicyclic derivatives used for comparative solid state structure analysis

The *endo,endo*-bicyclo[3.3.1]nonane-2,6-diol **148** crystallizes in the chiral space group $P_41_21_2$, and forms a conglomerate by spontaneous resolution. In the so formed enantiomorphs each hydroxyl group participates in intermolecular hydrogen bonds as both donor and acceptor so that each oxygen can be regarded as a node in a three-connected, 3D-net, schematically shown in **Figure 86a**. These hydrogen bonds define helices that are interconnected by longer intramolecular links, and the complete net (see **Figure 86b**) has the unusual $(8^2.12)$ -**utg** topology, which has no known examples in any compilations or databases to date.^{194,195}

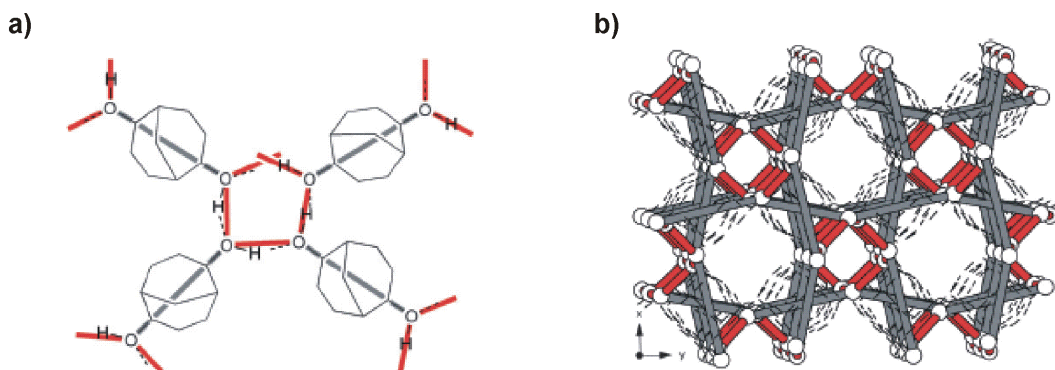


Figure 86: a) schematic representation of hydrogen bonding and nodes in the 3D-network; b) the **utg**-net in enantiomorphic **x**. Red links are hydrogen bonds and grey links are intramolecular connections.

This net is built from 8- and 12-membered rings, and is inherently chiral. Possibly, the large bulk of the bicyclic ring system prevents any of the common^{196,197} 12,13 three-connected nets from forming. The fact that **rac-148** crystallises as an enantiomorph makes it more likely that it will form a chiral net. Contrary to the case of the tubuland diols, that seem to crystallize as enantiomorphs in general, there are no voids or channels in enantiomorphic **148**.

The analysis of crystal structure of the dione (+)-**22** poses a somewhat different problem: While it is clear that strong hydrogen bonds are the dominant forces in crystal structure of **148**, it is not so clear if the weaker C-O \cdots H-C interactions in (+)-**22** and **149** will have the same influence. The question then is if a network approach is a profitable way of looking at these structures. In the crystal structure of racemic **22**122 the weak hydrogen bonds (CH \cdots O) connect the dione molecules into heterochiral parallel chains, the situation only possible with racemic **22** since the similar way of interaction cannot be realized in enantiomerically pure **22**. Indeed, it is not possible to form even a dimer using the same type of weak hydrogen bond connectivities. Consequently, the enantiomerically pure crystals of **22** adopt a different structure with every molecule forming weak C-H-O hydrogen bonds to four neighbouring molecules. This arrangement results in a (6⁴.8⁴)-**qtz** topology (**Figure 87ab**).

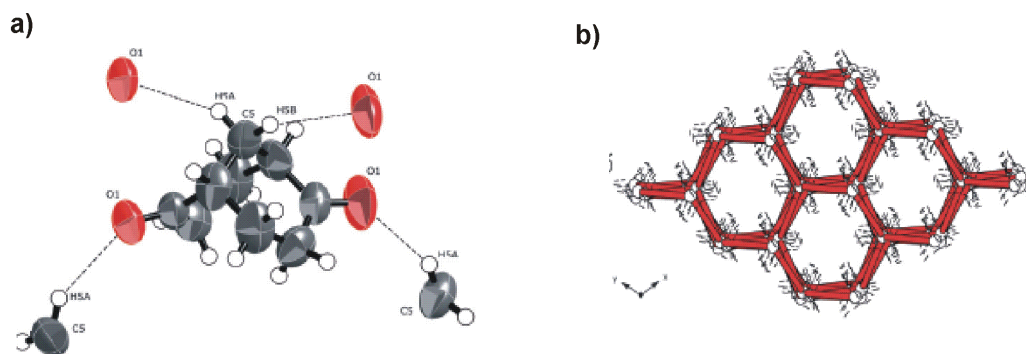


Figure 87: a) ellipsoid plot showing the four weak hydrogen bonds connecting each (+)-**22** dione to four neighbours; b) the four-connected chiral qtz-net in (+)-**22** shown in red. Nodes are placed in the centroids of bicyclononane and the network is build up from weak hydrogen bonds.

The results are not surprising as **qtz** network is one of the most abundant between chiral four-connected nets. In contrast to racemic **22**, where the formation of network is not possible, the net formation in (+)-**22** may imply that the molecules of latter are interacting stronger in the crystal. This, however, might not be true. The higher density and melting point of racemic dione **22** indicates that the molecules, in fact, are interacting more strongly in this case. Whether this is a consequence of higher number of van der Waals forces operating between the molecules of **rac-22** compared to (+)-**22** is hard to say.

The acetal **149** has four oxygen atoms, which are potential hydrogen bond acceptors. The tendency for oxygen atoms to participate in the weak hydrogen bonding is enhanced comparing to carbonyl oxygen, as the basicity of oxygen atoms are higher in the former. On the other hand, the steric crowding in the molecule of **149** may, to some extent, prevent the formation of such bonds. The effect of acetal functional group to crystal packing is thus difficult to estimate *a priori*.

By analysing the crystal structure of **149** we find no intermolecular O...H contacts shorter than 2.72 Å, indicating considerably weaker, or even non-existent, hydrogen bond interactions than in (+)-**22**. Whatever interactions there are, they seem to assemble **149** in oblong stacks that are more or less close packed and somewhat resembling the packing of the weak hydrogen

bonded chains in the crystal structure of rac-**22** containing heterochiral **22** (**Figure 88b**).

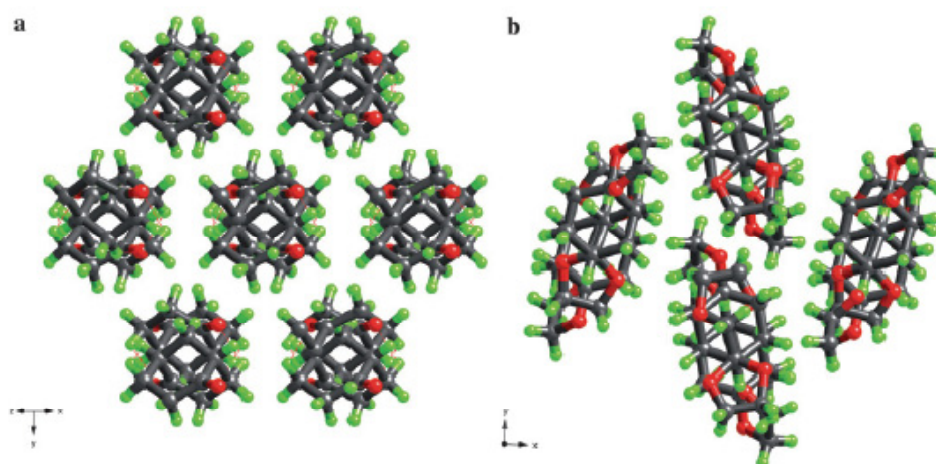


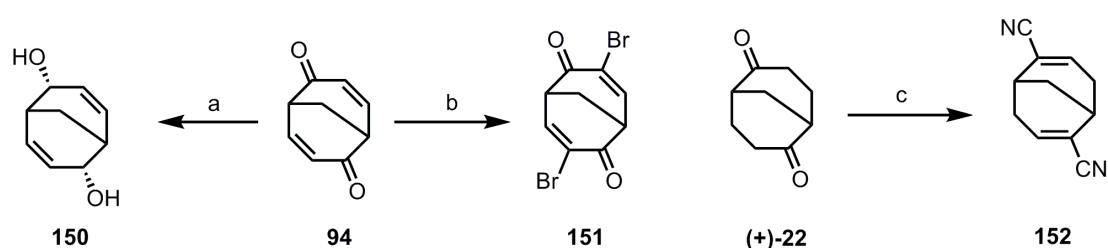
Figure 88: close packing of one-dimensional motifs in a) rac-**22** and b) acetal **148**

In summary, network analysis provides a good way to analyze the hydrogen bonded diol crystal structures, and may be profitable also for systems with weaker hydrogen bonds. However, its importance should not be exaggerated; close-packing motifs (non-directional dispersion forces etc) are probably important in the majority of structures with molecules having a dominant hydrocarbon backbone, as in **149**. The contribution of particular recognition pattern in guiding the packing process of this kind of molecules should be carefully weighted including the chirality of the compounds, as a powerful mean of control.

5.3 Unsaturated derivatives

The series of unsaturated bicyclo[3.3.1]nonane derivatives **150-152** were synthesized (**Scheme 27**) and the corresponding crystal structures were obtained as a continuation of our endeavour for more complete understanding of factors, controlling the solid state structure of this kind of compounds. The introduction of double bond into the bicyclic skeleton causes a significant flattening of the structure and, also reduces the conformational flexibility of cyclohexane rings. Moreover, the conjugation

of double bond with electronwithdrawing group increases the acidity of the vinylic hydrogens and the strength of otherwise weak C=C-H...O hydrogen bond. As can be seen from **Figure 82**, the enone and unsaturated nitrile patterns are recognized supramolecular synthons in crystal engineering. The incorporation of these synthons in bicyclic framework can result in different realization of crystal structure, compared to monofunctional derivatives. In addition, the α -bromo enone **151** was synthesized, in which the acidic hydrogens are replaced with bromine atoms, transforming the enone synthon to one, in which bromine- bromine interaction is possible.



Scheme 27: Reagents and conditions: a) NaBH₄, CeCl₃·7H₂O, MeOH, 95%; b) Br₂, Et₃N, CCl₄, 65%; c) i) TMSCN, ZnI₂, DCM ii) POCl₃, Py, 76%.

The compound **152** was synthesized using known procedures. The compound **150** and **151** were obtained by Luche reduction and bromination-elimination sequence of the enone **94**, respectively.

The hydrogen bond pattern of unsaturated diol **150** is shown in **Figure 89a**. The hydrogen bonded squares connect diols into a sheet structure, which is distinctively different from the 3D hydrogen bond nets of **148**, (8².12)-**utg**. The resulting 2D networks molecular sheets are closely packed. The topological representation of can be described as having a (8,3)-topology. In contrary to **148**, the compound **150** does not form a conglomerate and the overall structure is composed of alternating homochiral sheets.

The structure of dienone **94** is also significantly different from the structure of saturated congener **22**. The shortest intermolecular O...H-C interaction in **94** is between the protons of bridgehead methylene groups and one of the carbonyl groups. The same packing mode is observed for saturated dione **22**, however, in the latter case there are four such interaction. Based on the similarity of

interaction in **94** and **22**, the formation of homochiral chains of **94** is expected. This was indeed observed for **94**, where the single enantiomer flat helices are formed along crystallographic b-axis. In addition, the weak interaction between the enone units are observed for **94**, which results in a (6,3) 2D sheet structure. If every second interaction between bridgehead methylene group protons and carbonyl groups are disregarded, the structure is simplified and it can be described using the principles of close packing. This illustrates the difficulty drawing conclusions based on individual weak interactions.

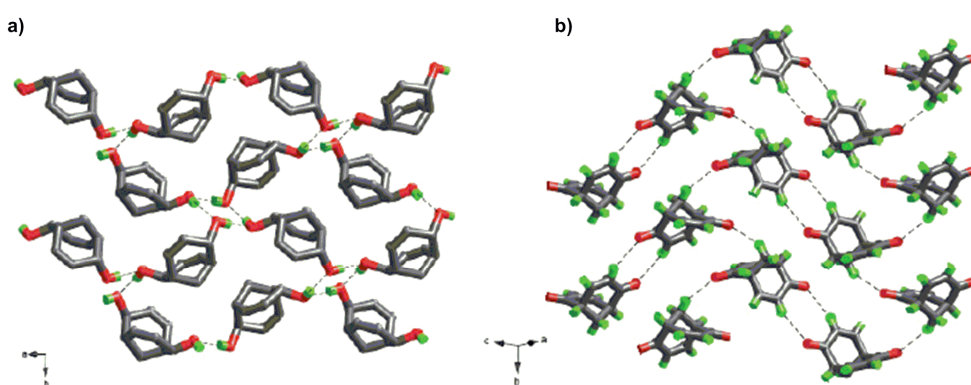


Figure 89: a) 2D nets formed by **149**; b) sheets formed by weak O...H-C interactions in **94**.

The substitution of α -hydrogen in the enone unit by bromine, the formation of weak hydrogen bonds C=C-H...O between vinylic protons and carbonyl oxygens are no longer possible and instead, the bromine-bromine interaction is expected. Two types of bromine-bromine bonds are described in literature, mainly based on the angles between bromine atoms θ_1 and θ_2 ($\theta_1 = \text{C}_1\text{-Br}_1\text{---Br}_2$, $\theta_2 = \text{Br}_1\text{---Br}_2\text{-C}_2$) as either “type-I” with $\theta_1 = \theta_2$ and usually $> 110^\circ$, or “type-II” with $\theta_1 = 180^\circ$ and $\theta_2 = 90^\circ$.¹⁹⁸ The nature of halogen-halogen bond lies in the polarization of electron density of halogen atom. The crystal structure of compound **151** is shown in **Figure 90a**. The bromine –bromine interactions of type I (3.901 Å, $\theta_1 = 145^\circ$, $\theta_2 = 140^\circ$) is evident from the structure. In addition to these interactions, the weak hydrogen bonding between β -proton of enone moiety to carbonyl oxygen is observed. This type of interaction is lacking in the crystal structure of enone **94**, and possibly, it is reinforced by the inductive effect of the bromine atom. These interactions are also stronger (2.436 Å,

3.282 Å, 143°) comparing to weak enone-enone interaction in **94**. The alternating homochiral 2D (4,4) net are interconnected via Br...CH interactions forming an overall racemic structure. The introduction of the bromine means that the molecules take on a much more specific “cleft” shape as the distance from the “peak” to the base is increased from around 2.8 Å (C...C distance) to 4.6 Å (C...Br distance). The crystal structure of **151** can be regarded as close packing of these “clefts”.

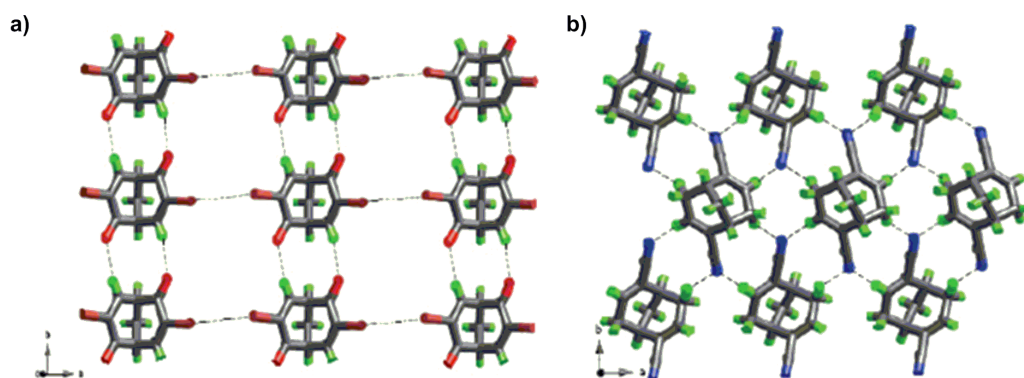


Figure 90: a) 2D nets formed by **151**; b) 2D nets formed by **152**.

The nitrogen atom in nitrile group is connected to α and β vinylic protons of neighbouring molecules giving a 2D network (**Figure 90b**). The structure of the racemate of **152** displays the same kind of weak hydrogen bonds, giving the same 2D pattern, and consequently cell parameters that are very close to the ones of (+)-**152**. The long distance between the hydrogen bonding nitrile nitrogen atom from the bicyclic core may be responsible for the flexibility of the structure and very similar packing mode in both enantiomerically pure and racemic **152**.

To conclude, the unsaturated bicyclo[3.3.1]nonane derivatives with the cleft structure are very prone to form 2D networks, which interact with each other resulting in nearly close packing of molecules. In contrast to diol **148**, the unsaturated diol **150** does not form conglomerate and the spontaneous resolution is not possible. The preference for racemate formation is likely related with more stable 2D racemic network, comparing to chiral networks.

The situation is reversed in case of **148**, where the formation of stable chiral 3D network is a driving force for conglomerate formation.

6 Conclusions

1. The synthesis of an important intermediate, bicyclo[3.3.1]nonane-2,6-dione, was improved up to 50% comparing to existing procedures and the reaction was successfully adopted to large scale preparation.
2. The large scale dynamic kinetic resolution of bicyclo[3.3.1]nonane-2,6-dione was achieved by using Baker's yeast for sweet dough overcoming difficulties associated with the use of ordinary Baker's yeast enabling the large scale synthesis of enantiomerically pure (+)-(1*S*,5*S*)-bicyclo[3.3.1]nonane-2,6-dione.
3. General synthetic strategies leading to three generations of novel chiral cleft molecules were developed by fusing bicyclo[3.3.1]nonane framework with heteroaromatic rings containing two, three and four hydrogen bonding complementary modules. In addition, the general synthetic procedure for racemic aza-bicyclo[3.3.1]nonane analogues, containing isocytosine moiety, was developed.
4. The first generation cavity compound, containing 2-pyridone hydrogen bonding unit forms tubular assemblies of moderate size (up to 10 molecules in CD₂Cl₂) in solution. The association is best described by using isodesmic model, and the association constants were estimated to be $K_E = 1142 \pm 162 M^{-1}$ and $K_E = 105 \pm 9.2 M^{-1}$ at 299K in CD₂Cl₂ and CDCl₃, respectively. The change in entropy and enthalpy of the association was estimated to be $-20.3 \pm 1.2 \text{ kJ mol}^{-1}$ and $-29.1 \pm 4.2 \text{ J mol}^{-1} \text{ K}$, respectively. The obtained values agree well with those of parent 2-pyridone, indicating non-cooperative association.
5. The second generation compound, containing isocytosine unit, forms very stable hydrogen bonded tetramers via self-complementariness of its two tautomeric forms. The new term, tautoleptic aggregation, is introduced for describing this type of aggregation. The supramolecular tetramer undergoes reversible stacking in non-polar solvents resulting in tubular structure. The preference for the formation of tetramer or stacked polymer depends on the bulkiness of substituent on the bicyclic moiety. Preliminary results show that the cavity of the tetramer is well suited to encapsulate C₆₀ molecules.
6. The aggregation of third generation compound, containing quadruple 2-ureido pyrimidinone module is limited to the formation of dimers and trimers

only. The small degree of association is attributed to steric crowding in the assembly implied by bulky solubilizing groups.

7. The CD spectroscopic studies of chiral bicyclo[3.3.1]nona-3,7-diene-2,6-dione shows that trans-orbital interaction of enone chromophores is taking place resulting in increase of $n \rightarrow \pi^*$ transition intensity. The octant rule was applied for the analysis of bicyclic enones.

8. The network approach for the analysis of the crystal structure of bicyclo[3.3.1]nonane derivatives was applied and proved to be a good method for understanding and comparing weak interactions in this type of compounds. Previously unknown type of chiral network, $(8^2.12)$ -**utg** net, was found in the crystal structure of *endo,endo*-bicyclo[3.3.1]nonane-2,6-diol. The introduction of double bond into bicyclic structures resulted in predominance of 2D networks.

7 Experimental section

Synthesis and characterization

All chemicals were used as received from commercial suppliers. All moisture sensitive reactions were carried out under an atmosphere of dry nitrogen using oven-dried glassware. Flash column chromatography was performed on Matrex (25-70 μ m). TLC was done on aluminum sheets precoated with silica gel 60 F₂₅₄ (Merck). The TLC plates were visualized with Seebach stain (general), aq. KMnO₄ solution (for unsaturated compounds) and aq. FeCl₃ solution (for β ketoesters). Melting points were determined in Electrothermal IA9000 SERIES Digital Melting Point Aparatus and were uncorrected. Optical rotations were measured on a Perkin-Elmer 341 polarimeter at 20°C. IR spectra were recorded in KBr pellets with Perkin Elmer Spectrum BX spectrometer and are reported in cm⁻¹. ¹H and ¹³C NMR spectra were recorded on a Bruker DR400 and Varian Inova 300 spectrometer. Chemicals shifts are given in parts per million relative to TMS using the residual solvent peaks at δ = 7.27 (¹H NMR) and 77.16 (¹³C NMR) ppm in CDCl₃ and δ = 2.50 (¹H NMR) and 39.50 (¹³C NMR) ppm in DMSO-d₆. Enantiomeric excess was determined with a Perkin-Elmer Autosystem XL Gas Chromatograph using Alpha DEXTM 120 fused silica capillary column (30 m \times 0.25 mm \times 0.25 μ m film thickness). Elemental analyses were performed at A.Kolbe Mikroanalytisches Laboratorium, Germany or at the analytical laboratory of the Vilnius University.

VPO measurements were done on a KNAUER-7000 instrument equipped with EuroOsmo® v.1.5 software. The chamber temperature was set to 37°C and the head temperature to 38°C. The measurement time was from 2.5 min to 3.5 min. The baseline was obtained by adding drops of pure solvent on both thermistors and auto-zeroed after 30 min. All samples were prepared gravimetrically.

Chloroform was washed several times with water to remove ethanol, dried with anhydrous CaCl_2 and distilled from powdered 4Å molecular sieves. Analytical grade toluene was used as received. Benzil ($M_w=210.23$) was used as standard. For each solution at least 3 reproducible measurements were obtained. The calibration curve obtained with benzil solutions were used to calculate theoretical instrument reading values for each concentration of analyte. The degrees of association ($\langle N \rangle$) was calculated for each concentration of analyte by dividing theoretical values by experimental ones.

The electronic absorption spectra were recorded on a Perkin-Elmer Lambda 2 spectrometer. CD spectra were recorded on Jasco J-815 spectrometer with scanning rate of 50 nm/min. The stock solutions were prepared by weighting compound into volumetric flask and diluting with UV-grade solvents. All other solutions were obtained from stock solution by dilution. For DMSO titration experiment, the equal volumes of chloroform solution of analyte and of pure solvent were transferred into working and reference cell, respectively. The same amount of DMSO was added to both cells and the solutions were stirred for few minutes before the measurements.

Diffusion experiments were carried out using a 500 MHz Bruker Avance NMR spectrometer equipped with a BVT 3000 temperature unit and a GAB gradient unit calibrated to 54.9 Gauss/cm. All NMR experiments as well as all calculations were performed using standard applications in Bruker Topspin1.3 software. Diffusion was measured at 20 °C using a BPLED pulse sequence with a diffusion gradient, δ , set to 6 ms and the diffusion time, Δ , to 100 ms. The gradient pulses applied were sine shaped pulses ranging from 2%-60% of the maximum gradient output of 54.9 Gauss/cm. Conversion of the gradient strength from sine shaped pulses to square pulses was done by the NMR software and was calculated to the range of 0.692-22.835 Gauss/cm. At least three peaks were analyzed for each compound at three different concentrations. Viscosities were obtained experimentally. The diffusion experiments were

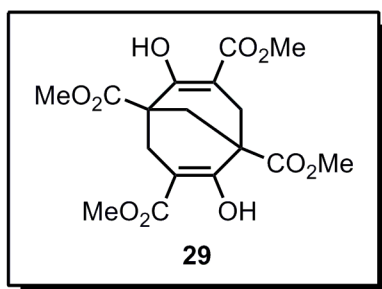
performed at least three times and only data for which the normalized residual sum of squares (RSS_{norm}) was lower than 0.001 were included.

X-ray analysis. Intensity data were collected at 293 K with an Oxford Diffraction Xcalibur 3 system using ω -scans and MoK α (λ 0.71073 Å). The structures were solved using direct methods and refined by full-matrix least-squares calculations on F² using SHELXTL 5.1.24. Non-H atoms were refined with anisotropic displacement parameters. Hydrogen atoms were constrained to parent sites, using a riding mode

Gel-permeation chromatography analysis of **81** was carried out at room temperature on a Viscotek system equipped with three Shodex columns in series (KF-805, KF-804 and KF-802.5), a refractive index detector and using chloroform as solvent at 1.0 mL/min. The concentration of the sample was 3mg/mL. Molecular weight and polydispersity were determined against monodisperse linear polystyrene standards. The PS standards had the following M_p : 2970, 30300, 96000. The molecular weights, M_n and M_w were determined using the calibration curve to 2910 and 3070, giving the polydispersity index $M_w/M_n = 1.05$. The calculated molecular weight for a tetramer is 4366 and for pentamer 5457, far from 3070. However, linear polystyrene might not be a good reference for cyclic structures such as the tetramer and pentamer. Monodisperse linear and cyclic polystyrene have been compared in GPC. It was shown that over a very large concentration range the M_w determined by GPC using linear polystyrene should be multiplied by a factor of 1.43.¹⁹⁹ Thus the corrected M_w for the aggregate of **81** is $1.43 \cdot 3070 = 4390$, a value clearly supporting the formation of a tetramer.

Molecular modelling was performed with MacroModel™ implemented in Maestro version 8.5 (Schrödinger Inc., Portland).

Meerwein's ester **29**

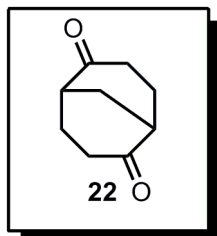


A 6 L round-bottomed flask equipped with a Dean–Stark trap was charged with benzene (2 L) and dimethyl malonate (1.32 kg, 10.0 mol). To this solution were added paraformaldehyde (0.25 kg, 8.35 mol) and piperidine (25.0 mL, 0.25 mmol) while stirring. The reaction mixture was stirred and heated under reflux for approximately 26 h until H₂O ceased to accumulate in the water trap (140 mL). The solvent was removed in vacuo at 60 °C using a rotary evaporator. It was also possible to distill off the solvent, which however was more laborious. The clear yellowish oil obtained can be stored overnight under vacuum although it is advisable to continue the synthesis directly since the oil darkens in color on prolonged storing. The yellowish and very viscous oil was added rapidly to a solution of anhyd MeOH (1.90 L) and NaOMe (395 g, 7.10 mol) under a N₂ flow and vigorous stirring. The residual oil was transferred to the reaction mixture using an additional portion of anhydrous MeOH (450 mL). Within 10 min, stirring was interrupted by formation of a solid mass. Stirring was continued by applying heat and crushing the solid using a spatula. The reaction mixture was heated overnight under reflux. During this time the solid mass dissolved and the sodium salt of **29** precipitated as a fine yellowish powder. The suspension was cooled on an ice bath for 2 h and then Et₂O (800 mL) was added to complete the precipitation. After additional 30 min cooling on an ice bath, the solid was collected by filtration using a Büchner funnel. The filter cake was washed with a cooled mixture of MeOH and Et₂O (v/v-1:1, 700 mL) yielding a white solid. The solid was dissolved in distilled H₂O (3.2 L) and the pH was adjusted to 4–5 using HCl (6 M, 645 mL). Upon acidifying, **29** precipitated as a white solid, which was collected by filtration using a Büchner funnel. Drying the solid overnight under vacuum at r.t. afforded **29** as a white solid; yield: 694 g (72%).

¹H NMR (400 MHz, CDCl₃) δ 2.33 (s, 2 H), 2.88 (s, 4 H), 3.77 (s, 6 H), 3.79 (s, 6 H), 12.18 (s, 2 H).

Anal. calcd for $C_{17}H_{20}O_{10} \cdot 1/6 CHCl_3$: C, 51.01; H, 5.03. Found: C, 51.20; H, 4.69.

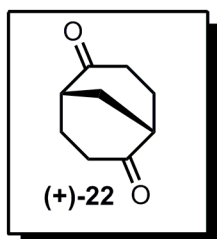
Bicyclo[3.3.1]nonane-2,6-dione **22**



A one-necked 5 L round-bottomed flask equipped with a reflux condenser topped with a dropping funnel was charged with a solution of **29** (412 g, 1.07 mol) and glacial AcOH (1.1 L). The reaction mixture was heated under reflux and HCl (743 mL, 6 M) was added dropwise over a period of 12 h. The mixture was heated under reflux for additional 12 h and then the solvent was removed under reduced pressure using water suction. The yellowish residue was dissolved in CH_2Cl_2 (500 mL) (Et_2O or EtOAc could also be used; however, much larger volumes are needed), washed with sat. $NaHCO_3$ (2×200 mL), brine (200 mL), and dried ($MgSO_4$). Upon concentration of the solution under reduced pressure, a pale yellow solid was obtained. The crude product was washed with ice-bath cooled Et_2O (~400 mL), which afforded **22** as a white solid; yield: 100.4 g (62%).

1H NMR (400 MHz, $CDCl_3$) δ 2.72–2.77 (br m, 2H), 2.60 (ddd, $J= 4.3$ Hz, $J= 6.6$ Hz, $J= 17.0$ Hz, 2H), 2.36–2.45 (m, 2H), 2.22 (br t, $J= 2.9$ Hz, 2H), 2.03–2.15 (m, 4H). Anal. calcd for $C_9H_{12}O_2$: C, 71.03; H, 7.95; Found: C, 71.03; H, 7.90.

(+)-(1*S*,5*S*)-Bicyclo[3.3.1]nonane-2,6-dione (+)-**22**

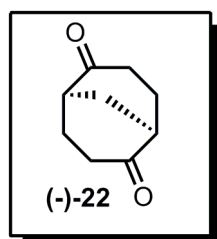


A 3 L round-bottomed flask was charged with a solution of *rac*-**22** (90.0 g) and H_2O (1.80 L). Stirring and heating was necessary to get *rac*-**22** in solution. Under gentle stirring and at r.t. was added Baker's yeast for sweet dough (153 g) in small portions. Sucrose (300 g) was added and the gentle stirring was continued for six days with further addition of sucrose (300 g) the second and the third day. The reaction mixture was centrifuged at 8000 rpm for 10 min. The slightly yellow supernate was decanted and saturated with excess NaCl. The precipitate was extracted with EtOAc (3×100 mL) until TLC did

not indicate the presence of **22**. The slightly yellow supernate was then extracted with CHCl_3 until TLC did not indicate the presence of **22** ($3\text{--}5 \times 400$ mL) in the aqueous phase. The combined organic phases were concentrated in vacuo yielding a yellowish semi-solid that was suspended in H_2O (1.80 L) and subjected to a second fermentation in accordance with the above procedure. After the second workup, enantiomerically pure (+)-**22** (ee >99%) was isolated by flash chromatography (petrol ether/ethyl acetate-2:1) as a white solid; yield: 21.7 g (48%).

$[\alpha]_D^{20} = 219.0$ (c 0.59 in CHCl_3). Anal. calcd for $\text{C}_9\text{H}_{12}\text{O}_2$: C, 71.03; H, 7.95; Found: C, 71.08; H, 7.91.

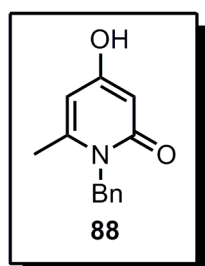
(-)-(1*R*,5*R*)-Bicyclo[3.3.1]nonane-2,6-dione (-)-**22**



A 50 mL round-bottomed flask was charged with 4 Å molecular sieves (0.150 g) and a solution of hydroxy ketones **22a-b** (0.100 g, 0.650 mmol), NMO (0.150 g, 1.24 mmol, 2 equiv) and CH_2Cl_2 (17.0 mL). To this mixture was added tetrapropylammonium perruthenate (TPAP) (11.8 mg, 32.5 mmol, 5 mol%) under stirring at r.t. The reaction mixture was stirred for 20 min and then Et_2O (10.0 mL) was added and the mixture was left to rest for 10 min without stirring to allow the catalyst to precipitate. The mixture was filtered through a pad of silica gel eluting with EtOAc. Upon concentration of the filtrate the product was obtained as a white solid in quantitative yield (ee = 75%).

Anal. calcd for $\text{C}_9\text{H}_{12}\text{O}_2$: C, 71.03; H, 7.95; Found: C, 71.05; H, 7.93.

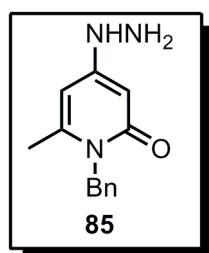
1-Benzyl-4-hydroxy-6-methyl-2(1*H*)-pyridinone **88**



To a stirred suspension of 4-hydroxy-6-methyl-2*H*-pyran-2-one **87** (10.0 g, 0.08 mol) in water (30 mL) benzyl amine (8.6 g, 0.08 mol) was added dropwise over a period of 30 min at 100 °C. The reaction mixture was then heated under reflux for 16 hrs. The reaction mixture was cooled; the solid was filtered, washed with water and dried in vacuum desiccator over CaCl_2 . The

crude reaction product was suspended in acetone (70 mL), heated under reflux for 1 h and filtered. The remaining solid was recrystallized from methanol to afford **88** (8.4g, 56%) as off-white solid, m.p. 215 °C. Analytical sample was obtained after three times crystallization from methanol, m.p. 216-217°C (lit. data m.p. 217 °C¹¹⁰).

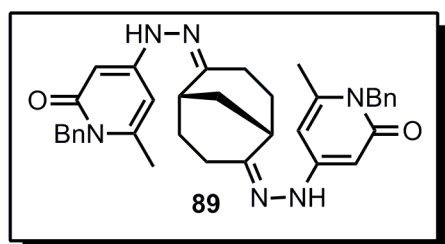
1-Benzyl-4-hydrazino-6-methyl-2(1*H*)-pyridinone **85**



Finely powdered **88** (100 mg, 0.46 mmol) and hydrazine hydrate (204 μL, 4.2 mmol) were placed into a 15 mL pressure tube. The reaction tube was placed in a beaker filled with vermiculite and irradiated in an ordinary domestic microwave oven (Zannusi ZM17M with rotate plate) for 6 min at 250W. The reaction mixture was cooled, the residue dissolved in methanol and collected. The procedure was repeated four more times (in total 500 mg, 2.3 mmol of **88**), combined solutions were evaporated to dryness the remaining solid was purified by flash chromatography (chloroform/methanol-10:1) to afford **85** (300 mg, 57 %) as brownish solid.

m.p. 218-220 °C; R_f 0.19 (chloroform/methanol-10:1); IR: ν 3259, 3194 (NH), 1652 (C=O), 1573, 1531, 818, 721; ¹H NMR (400 MHz, DMSO-*d*₆) δ 7.51 (s, 1H), 7.33-7.28 (m, 2H), 7.25-7.20 (m, 2H), 7.08-7.07 (m, 2H), 5.61 (bs, 1H), 5.49 (d, J = 2.1 Hz, 1H), 5.13 (s, 2H), 4.12 (bs, 2H), 2.07 (s, 3H); ¹³C NMR (100.3 MHz, DMSO-*d*₆) δ 163.8, 158.1, 145.2, 138.8, 128.7, 126.9, 126.3, 96.9, 87.6, 44.9 (2C), 20.2; MS, m/z (%): 231 ([*M*+2]⁺, 17), 230 ([*M*+1]⁺, 100), 229 ([*M*-1]⁺, 34), 154 (16), 136 (11), 91 (42); HRMS (FAB+) calcd for C₁₃H₁₆N₃O ([*M*+H]⁺): 230.1293; Found: 230.1292.

(1*S*,5*S*)-bicyclo[3.3.1]nonane-2,6-dione bis[(1-benzyl-6-methyl-2-oxo-1,2-dihydro-4-pyridinyl) hydrazone] **89**

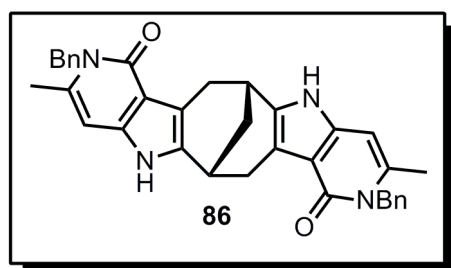


Hydrazine **85** (500 mg, 2.19 mmol) and (+)-**22** (150 mg, 1.00 mmol) were dissolved in methanol with heating. The resulting clear solution was refluxed for 5 h. The reaction

mixture was cooled, the precipitate was filtered, washed twice with cold solvent and dried in *vacuo* to afford the hydrazone as a mixture of *E,E* and *E,Z* isomers, which was used without further purification. Yield 550 mg (95%), white solid.

m.p. >320°C; IR: ν 3418, 3228 (NH), 1643 (C=O), 1564, 1531, 1236, 825; MS m/z (%): 575 ($[M+1]^+$, 23), 307 (47), 298 (18), 154 (100), 136 (74), 107 (22), 91 (28), 89 (22); HRMS (FAB+) calcd for $C_{35}H_{39}N_6O_2$ ($[M+H]^+$) 575.3134, found 575.3121; Anal. calcd for $C_{35}H_{38}N_6O_2$: C, 73.14; H, 6.66; N, 14.62; Found: C, 72.98; H, 6.58; N, 14.78.

Compound 86.

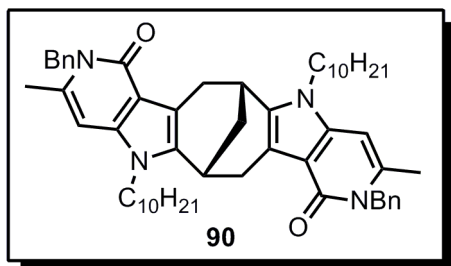


A round-bottomed flask equipped with an air condenser and rubber septum was charged with hydrazone **89** (500 mg, 0.87 mmol) and diphenyl ether (25 ml). The suspension was stirred and heated at reflux,

passing argon through the mixture via long cannula during the reaction time. After 7.5-8 hr the evolution of ammonia ceased and the reaction mixture was cooled, diluted with pentane and filtered. The precipitate was washed with diethyl ether and diethyl ether- methanol mixture (v/v-1:1). Yield 440 mg (94%), gray solid.

m.p. >320°C; IR: ν 3398, 3281 (NH), 1641 (C=O), 1575; 1H NMR (400 MHz $CDCl_3$ /TFA) δ 10.01 (s, 2H), 7.3-7.25 (m, 6H), 6.97-6.95 (m, 4H), 6.91 (s, 1H), 5.59 (d, $J= 16.2$ Hz, 2H), 5.47 (d, $J= 16.2$ Hz, 2H), 3.53 (d, $J= 2.6$ Hz, 2H), 3.34 (d, $J= 16.3$ Hz, 2H), 3.16 (dd, $J= 16.3, 5.0$ Hz, 2H) 2.48 (s, 6H), 2.17 (bs, 2H); ^{13}C NMR (100.3 MHz, $CDCl_3$ /TFA) δ 156.1, 142.1, 139.3, 139.2, 134.2, 129.1, 128.1, 125.8, 111.5, 110.8, 103.9, 49.6, 28.7, 28.3, 27.4, 20.7.

Compound 90

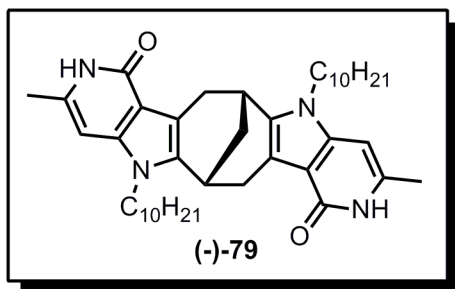


In a round bottomed flask NaH (22 mg, 0.56 mmol, 60% dispersion in mineral oil) was washed with dry hexane (2×2 mL) and solid **86** (100 mg, 0.185 mmol) was added. The flask was flushed with nitrogen and dry

DMF (25 mL) was added. The reaction mixture was stirred under nitrogen at r.t. until evolution of hydrogen ceased and clear solution was obtained (ca 2 h). To the resulting solution 1-iododecane (237 μ L, 1.1 mmol) in dry DMF (1 mL) was added dropwise and mixture was stirred for 24 h. DMF was removed by co-distillation with toluene, the obtained residue was suspended in chloroform and filtered through a short plug of silica gel eluting with chloroform. The filtrate was evaporated to dryness and the residue purified by flash chromatography to afford **90**. Yellow glass, yield 126 mg (83%).

m.p. 81-83 °C R_f 0.22 (heptane/ethylacetate-7:3); $[\alpha]_D^{20} = -244$ (c 0.073 in CHCl₃); UV (in CH₂Cl₂), λ_{max} (log ϵ): 319 (4.28, sh), 306 (4.36), 285 (4.23, sh), 220 (4.8, sh); CD (in CH₂Cl₂) λ_{max} ($\Delta\epsilon/\text{dm}^3\text{mol}^{-1}\text{cm}^{-1}$): 321 (-46.24), 310 (-43.28), 288 (0), 280 (11.86), 267 (0), 257 (-5.93); IR: 2925, 2853 (CH), 1654 (C=O), 1590, 729; ¹H NMR (400 MHz, CDCl₃) δ 7.27-7.23 (m, 4H), 7.19-7.16 (m, 2H), 7.12-7.11 (m, 4H), 6.09 (d, J = 0.5 Hz, 2H), 5.33 (br dd, 4H), 4.02 (dt, J = 15, 7.5 Hz, 2H) 3.89 (dt, J = 15, 7.5 Hz, 2H), 3.39 (bs, 2H), 3.31-3.21 (m, 4H), 2.26 (s, 6H), 2.15 (bs, 2H), 1.8-1.67 (m, 4H), 1.4-1.26 (m, 28H) and 0.88 (t, J = 7 Hz, 6H); ¹³C NMR (100.3 MHz, CDCl₃) δ 160.8, 138.2, 137.9, 137.5, 134.2, 128.5, 126.7, 126.4, 112.1, 111.3, 94.7, 46.0, 43.6, 31.9, 31.0, 30.4, 29.7, 29.5, 29.5, 29.3, 29.2, 27.1, 26.3, 22.7, 21.3, 14.1; MS, m/z (%): 822 ([M+2]⁺, 40), 821 ([M+1]⁺, 88), 820 ([M]⁺, 100), 819 ([M-1]⁺, 35), 429 (10), 339 (9), 91 (51); HRMS (FAB+) calcd for C₅₅H₇₂N₄O₂ ([M]⁺) 820.5655; Found 820.5666; Anal. calcd for C₅₅H₇₂N₄O₂: C, 80.44; H, 8.84; N, 6.82; Found: C, 80.77; H, 9.09; N, 6.69.

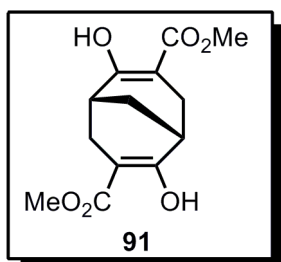
Compound (-)-79



The sodium was added to liquid ammonia (~25 ml) in small pieces until the dark blue colour persists. To the resulting solution, methanocyclooctadiindole **90** (25 mg, 0.03 mmol) in dry THF (15 ml) was added dropwise. After few minutes additional portion of dry THF (10 ml) was added and the mixture was stirred for 6 hr at -45 °C. The reaction mixture was quenched by the careful addition of excess of solid NH₄Cl. After evaporation of ammonia, the residue was suspended in water (10 mL), acidified with 2N HCl and extracted with CHCl₃. The combined organic phase was dried (Na₂SO₄), evaporated to dryness and the remaining solid was purified by flash chromatography (dichloromethane/methanol-95:5) to afford 16 mg (83%) of (-)-**79** as yellow glass.

m.p. >220°C (dec); *R_f* 0.26 (dichloromethane/methanol-95:5); $[\alpha]_D^{20} = -222$ (*c* 0.106 in CHCl₃); UV (*c* 0.4 mM, CH₂Cl₂), λ_{\max} (log ϵ): 314 (4.16, sh), 302 (4.28), 279 (4.24, sh), 220 (4.6); CD (*c* 0.4 mM, CH₂Cl₂), λ_{\max} ($\Delta\epsilon/\text{dm}^3\text{mol}^{-1}\text{cm}^{-1}$): 318 (-31.46), 307 (-32.2), 283 (0), 277 (7.77), 268 (0), 258 (-6.29); IR: ν 3419 (NH), 2925, 2853 (CH), 1648 (C=O); ¹H NMR (400 MHz, CDCl₃) δ 9.52 (bs, 2H), 5.97 (s, 2H), 4.0 (dt, *J* = 14.8, *J* = 7.5 Hz, 2H), 3.89 (dt, *J* = 14.8, 7.5 Hz, 2H), 3.37 (d, *J* = 2.6 Hz, 2H), 3.24 (dd, *J* = 16.0, 4.8 Hz, 2H), 3.16 (d, *J* = 16 Hz, 2H), 2.24 (s, 6H), 2.12 (bs, 2H), 1.85-1.62 (m, 4H), 1.39-1.2 (m, 28H) and 0.88 (t, *J* = 7 Hz, 6H); ¹³C NMR (100.3 MHz, CDCl₃) δ 161.2, 140.0, 135.3, 134.0, 111.5, 111.0, 93.0, 43.6, 31.8, 30.9, 30.4, 29.7, 29.6, 29.5, 29.3, 29.1, 27.1, 26.1, 22.6, 19.4, 14.1; MS, *m/z* (%): 642 ([M+2]⁺, 36), 641 ([M+1]⁺, 100), 640 ([M]⁺, 93), 639 ([M-1]⁺, 26), 499 (7), 339 (32), 211 (9); HRMS (FAB⁺) calcd for C₄₁H₆₀N₄O₂ ([M]⁺) 640.4716; Found 640.4725; Anal. calcd for C₄₁H₆₀N₄O₂: C, 76.83; H, 9.44; N, 8.74; Found: C, 77.26; H, 9.86, N, 8.44.

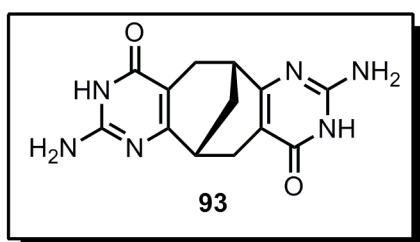
(+)-(1*S*,5*S*)-dimethyl 2,6-dihydroxybicyclo[3.3.1]nona-2,6-diene-3,7-dicarboxylate **91**



A solution of diketone (+)-**22** (7 g, 0.046 mol) in dimethyl carbonate (20 mL) was added dropwise over 2h to a suspension of NaH (11 g, 0.276 mol, 6 eq., 60% dispersion in mineral oil) in dry DMF (60 mL) under nitrogen atmosphere. The temperature of reaction mixture was kept below 40°C during the addition. Soon after first portions of **22** were added, evolution of hydrogen gas started and color of the reaction mixture turned to greenish and, later, to yellow. The mixture was stirred overnight, then carefully quenched with 10% HCl solution and extracted with EtOAc. The organic layer was dried with Na₂SO₄, evaporated to dryness and the residue is subjected to flash chromatography. After elution with petrol ether- ethyl acetate (10:1) the product **91** was isolated as a colorless solid (10.1 g). Contaminated fractions containing product were collected, evaporated under reduced pressure and the residue was recrystallized from petrol ether to afford additional portion of product (1.0 g). Total yield 11.1 g (90%).

m.p. 143.5- 144.5°C; $[\alpha]_D^{20}=120.2$ (*c* 0.0133 in CHCl₃); ¹H-NMR (400 MHz, CDCl₃) δ 12.09 (s, 2H), 3.75 (s, 6H), 2.73-2.66 (m, 2H), 2.58 (d, *J*= 16.1 Hz, 2H), 2.45 (dd, *J*= 16.1, 6.1 Hz, 2H), 1.84 (t, *J*=3.0 Hz, 2H); ¹³C-NMR (100.3 MHz, CDCl₃) δ 173.5, 173.2, 95.9, 51.7, 32.9, 28.0, 27.4; HRMS (ESI) calcd. for C₁₃H₁₇O₆ (M+H⁺): 269.1025; Found: 269.1013.

Compound 93

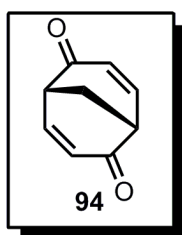


A mixture of **91** (53.7 mg, 0.20 mmol) and guanidinium carbonate (0.175 g, 0.98 mmol) in methanol (10 mL) were heated at 100 °C in a pressure vial for 24 hours. The solvent was removed under reduced pressure and the residue was triturated with water. The precipitate was filtered, washed

generously with water and diethyl ether. The solid material was dried under vacuum, which gave 45.8 mg (80%) of **93** as a white powder.

IR: ν 3438, 1652, 1539, 1496; ^1H NMR (400 MHz, d_6 -DMSO) δ 10.84 (br.s, 2H), 6.34 (br.s, 4H), 2.72 (br.s, 2H), 2.48-2.44 (m, 2H), 2.41-2.35 (m, 2H), 1.83 (m, 2H); ^{13}C -NMR (100.3 MHz, d_6 -DMSO) δ 164.6, 163.0, 106.2, 33.8, 28.4, 27.5; HRMS (ESI) calcd. for $\text{C}_{13}\text{H}_{15}\text{N}_6\text{O}_2$ (M+H): 287.1246; Found: 287.1246.

(+)-(1*R*,5*R*)-bicyclo[3.3.1]nona-3,7-diene-2,6-dione **94**



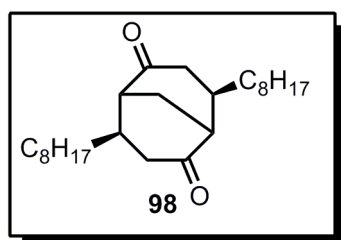
Large scale procedure: Under nitrogen, to a stirred suspension of sodium hydride (7.85 g, 0.20 mol, 60 % dispersion in mineral oil) in dry THF (30 mL) was added methyl benzenesulphinate (11.3 g, 9.50 mL, 77.0 mmol) at once. A solution of (+)-**22** (5.00 g, 32.9 mmol) in dry THF (40 mL) was added dropwise and the reaction mixture was stirred at room temperature overnight. The green-yellow suspension was quenched with 4% phosphoric acid until pH 3-4. After addition of water (50 mL), the aqueous phase was extracted with ethyl acetate (3 \times 25 mL). The combined organic fractions were washed with brine, dried (Na_2SO_4) and concentrated under reduced pressure, yielding 18.1 g of a crude yellow oil, which was subjected to flash chromatography (ethyl acetate) obtaining, beside unreacted methylbenzene sulfinate ($R_f=0.84$), two other fractions, consisting of the compounds 3,7-bis(phenylsulfinyl)bicyclo[3.3.1]nonane-2,6-dione ($R_f=0.28$) and 7-(phenylsulfinyl)bicyclo[3.3.1]non-3-ene-2,6-dione ($R_f=0.45$).

To the mixture of above compounds in toluene (80 mL), sodium carbonate (17.4 g, 0.16 mol) was added and the reaction mixture was brought to reflux. After 10 min., TLC (petrol ether/ethyl acetate-6:1) showed complete conversion and the reaction mixture was left to cool to room temperature and filtered. The filter cake was washed with toluene (60 mL) and the green clear filtrate was evaporated. The residue was purified by flash chromatography

(petrol ether/ ethyl acetate-6:1), yielding 3.9 g (80 %) of **94** as an off-white solid, which was stored at -18°C under nitrogen, protected from ambient light. m.p. 105°C (transition at 90°C); R_f 0.14 (petrol ether/ethyl acetate-6:1); $[\alpha]_D^{20}=2260$ (c 0.37 in EtOH); UV (EtOH) λ_{max} ($\log \epsilon$): 233(2.95), 260 (sh, 2.23), 346 (1.82); CD (EtOH) λ_{max} ($\Delta\epsilon/\text{dm}^3\text{mol}^{-1}\text{cm}^{-1}$): 342 (+10.2); IR: ν 3040 (C=C-H), 2941 (C-H), 1653 (C=O), 1559 (C=C); ^1H NMR (400 MHz, CDCl_3) δ 7.02 (dd, $J=10.0, 6.8$ Hz, 2H), 5.91 (d, $J=10.0$ Hz, 2H), 3.37, (dt, $J=6.8, 2.9$ Hz, 2H), 2.79 (t, $J=2.9$ Hz); ^{13}C NMR (100.3 MHz, CDCl_3) δ 192.4, 145.7, 125.6, 46.0, 34.8. HRMS (ES+) calcd. for $\text{C}_9\text{H}_8\text{O}_2$ ($M+H$): 149.0603; Found: 149.0208; Anal. calcd for $\text{C}_9\text{H}_8\text{O}_2$: C 72.94, H 5.45; Found: C 73.18, H 5.43.

Small scale procedure: The mixture of diketone (+)-**22** (50 mg, 0.33 mmol), PhIO_2 (0.39 g, 1.64 mmol), $(\text{PhSe})_2$ (5 mg, 0.0016 mmol) and catalytic amount of TsOH in dry toluene (10 mL) was heated under reflux for 3 h. The mixture was cooled to room temperature, filtered, washed with saturated NaHCO_3 solution, brine, and dried (MgSO_4). After evaporation under reduced pressure the residue was purified by flash chromatography (petrol ether/ethyl acetate 4:1) to afford 44 mg (90%) of **94**

exo,exo*-4,8-dioctylbicyclo[3.3.1]nonane-2,6-dione **98*



A solution of 1-iodooctane (0.60 g, 0.40 mL, 2.5 mmol) in dry *n*-pentane-diethyl ether (25 mL, 3:2) was cooled to -78°C (dry ice / acetone) under nitrogen and *tert*-butyllithium (4.2 mL, 5.5 mmol, 1.3 M in *n*-pentane) was added dropwise under occurrence of a fine white precipitate. After stirring for additional 5 min., the cooling bath was removed and the reaction mixture was left to warm up for 1h to consume unreacted *tert*-butyllithium, whereby the precipitate completely dissolved leading to a clear slightly yellow solution.

In another round-bottomed flask a suspension of copper cyanide (112 mg, 1.25 mmol) in dry diethyl ether (15 mL) was cooled to -40°C and the above obtained octyllithium solution was slowly added dropwise via syringe. After

stirring at -40°C for 40 min. copper cyanide completely dissolved. The reaction mixture was cooled to -78°C and **94** (50.0 mg, 0.338 mmol) in dry diethyl ether (5 mL) was added dropwise. At the same time the reaction mixture turned dark red. Stirring at -78°C was continued for 45 min. before the reaction mixture was quenched at the same temperature by careful addition of 5% aq. phosphoric acid (10 mL,) under formation of a white precipitate in the aqueous phase. The mixture was filtered through CELITE®. The phases were separated and the aqueous phase extracted with ethyl acetate (3×20 mL). The combined organic fractions were dried (Na_2SO_4), evaporated and the residue was purified by flash chromatography (petrol ether/ethyl acetate -16:1) yielding 105.5 mg (83%) of **98** as colorless oil.

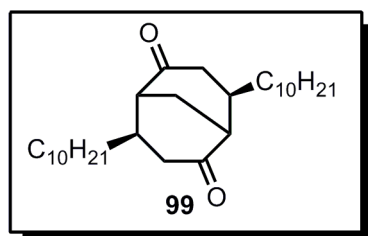
R_f 0.26 (petrol ether/ethyl acetate- 16:1); IR: ν 2925 (C-H), 2855 (C-H), 1708 (C=O). $^1\text{H-NMR}$ (400 MHz, CDCl_3) δ 2.48 (dd, $J=15.6, 6.7$ Hz, 2H), 2.45-2.41 (m, 2H), 2.23 (dd, $J= 15.6, 6.1$ Hz, 2H), 2.16-2.11 (m, 2H), 2.10-2.03 (m, 2H), 1.46-1.35 (m, 4H), 1.34-1.18 (m, 24H), 0.90-0.83 (m, 6H); $^{13}\text{C-NMR}$ (100.3 MHz, CDCl_3) δ 214.1, 48.3, 42.5, 36.6, 35.5, 32.0, 29.6, 29.6, 29.4, 26.9, 23.2, 22.8, 14.3; HRMS (FAB+) calcd. for $\text{C}_{25}\text{H}_{44}\text{O}_2$ ($\text{M}+\text{H}^+$): 377.3420; Found: 377.3425; Anal. calcd for $\text{C}_{25}\text{H}_{44}\text{O}_2$: C 79.73; H 11.78; O 8.50; Found: C 79.43; H, 11.71.

General procedure for 1,4-addition of decyl zinc bromide to enones

Zinc (0.33 g, 5 mmol) in dimethylacetamide (3 ml) was activated by stirring at room temperature with catalytic amount of iodine (64 mg, 0.25 mmol) until brown color disappeared. Decylbromide (0.747 g, 3.38 mmol) was added and mixture was heated at 80° for 5 h. The decyl zinc solution obtained was cooled to room temperature and added dropwise to a solution of $\text{CuCN}\cdot 2\text{LiCl}$ complex (0.363 g CuCN, 0.345 g LiCl, 4.06 mmol, dried at 140°C under high vacuum for 3 h prior to use) in dry THF (20 ml) at -30°C . After addition, the mixture was stirred at -30° for 5 min, and then the flask was removed from cooling bath and stirred for 15 min to complete transmetalation. The solution was cooled to -78° and solution of enone (0.676 mmol) and TMSCl (0.44 g,

4.06 mmol) in THF (3 mL) was added dropwise. The mixture was allowed to reach room temperature overnight. Then it was acidified with 10% HCl (8mL) and stirred at room temperature until silyl enol ether disappeared (TLC). The mixture was diluted with water and extracted with ethyl acetate. The combined organic extracts were mixed with equal amount of water and vigorously stirred to remove THF. The white precipitate formed was removed by filtration through CELITE®. The organic phase was separated, washed with sat. NaHCO₃ solution, brine and dried (Na₂SO₄). The solvent was evaporated under reduced pressure and the residue was purified by flash chromatography to afford decyl derivatives of carbonyl compounds.

***exo,exo*-4,8-didecylbicyclo[3.3.1]nonane-2,6-dione 99**

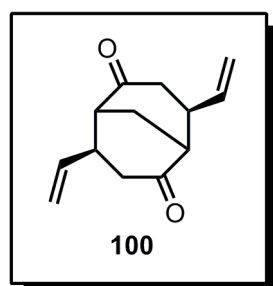


Prepared according to **General procedure for 1,4-addition of decyl zinc bromide to enones.**

Yield 0.092 g (95%), colorless oil. R_f 0.22 (petrol ether/ethyl acetate- 20:1); IR: ν 2925 (C-H), 2854 (C-H), 1709 (C=O); ¹H-NMR (400 MHz, CDCl₃)

δ 2.47 (dd, $J=15.6, 6.7$ Hz, 2H), 2.43-2.39 (m, 2H), 2.22 (dd, $J=15.6, 6.0$ Hz, 2H), 2.14-2.10 (m, 2H), 2.10-2.02 (m, 2H), 1.47-1.34 (m, 4H), 1.34-1.15 (m, 32H), 0.86 (t, $J=6.9$ Hz, 6H); ¹³C-NMR (100.3 MHz, CDCl₃) δ 214.0, 48.2, 42.5, 36.6, 35.5, 32.1, 29.7, 29.7, 29.7, 29.6, 29.5, 27.0, 23.2, 22.8, 14.3; HRMS (FAB+) calcd. for C₂₉H₅₂O₂ (M+H⁺): 432.3967; Anal. calcd for C₂₉H₅₂O₂: C 80.49; H 12.11; O 7.39; Found: C 80.36; H, 12.06.

***exo,exo*-4,8-divinylbicyclo[3.3.1]nonane-2,6-dione 100**

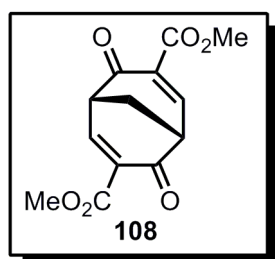


A solution of LiCl in THF (0.5M, 12.5 mL, 6.25 mmol) was added to a CuCN (0.272 g, 3.04 mmol) and the mixture was stirred under Ar at room temperature until all solid dissolved. The solution was cooled down to -30°C and vinyl magnesium bromide solution in THF (0.7M, 4.34 mL, 3.04 mmol) was added dropwise. The resulting dark brown mixture was warmed to -20°C and stirred for 30 min and then cooled to -78°C.

A solution of **94** (0.15 g, 1.01 mmol) and TMSCl (0.33 g, 3.04 mmol) in 3mL of THF was added dropwise and the reaction mixture was stirred until the temperature reached -20°C. The reaction was quenched with 10% HCl solution (20mL) and stirred at room temperature until the intermediate silylenol ether was hydrolyzed (TLC). The mixture was diluted with water and extracted with EtOAc . The combined organic phases were dried (Na₂SO₄), evaporated to dryness and the residue was purified by flash chromatography to afford 144.4 mg (70%) of **100** as colourless solid.

m.p. 65°C; R_f 0.22 (petrol ether/ethyl acetate- 20:1); IR: ν 2925 (C-H), 2854 (C-H), 1709 (C=O); ¹H-NMR (300 MHz, CDCl₃) δ 5.83 (ddd, *J*= 17.0, 10.4, 6.0 Hz, 1H), 5.17 (dd, *J*= 10.4, 1.6 Hz, 1H), 5.10 (dd, *J*= 17.0, 1.6 Hz), 2.93-2.83 (m, 2H), 2.62-2.2.53 (m, 6H), 2.19-2.14 (m, 2H); ¹³C-NMR (75 MHz, CDCl₃) δ 211.9, 139.3, 116.0, 48.1, 39.5, 22.8; Anal. calcd for C₁₃H₁₆O₂: C 76.44; H 7.90; Found: C 76.57; H, 8.02.

(+)-(1*S*,5*S*)-dimethyl 4,8-dioxobicyclo[3.3.1]nona-2,6-diene-3,7-dicarboxylate **108**

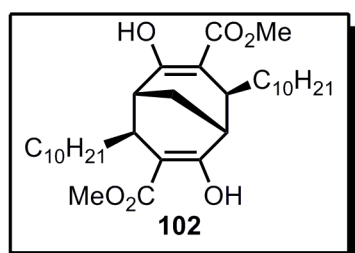


To a solution of ketoester **91** (3 g, 0.011mol) and pyridine (1.26 mL, 0.015 mol, 1.36 eq.) in CH₂Cl₂ (50 mL) was added phenylselenenyl chloride (2.79 g, 0.014 mol, 1.27 eq.) in one portion at 0°C under nitrogen. The orange mixture was stirred for 1h at 0°C and then 0.5 h at room temperature. The mixture was quenched with 10% HCl (40 mL) solution. Organic phase was separated, washed with additional portion of 10% HCl solution (40 mL), dried (Na₂SO₄) and filtered. The filtrate was cooled to 0°C and hydrogen peroxide (3.81mL, 0.037mol, 30%, 3.4 eq.) was added in one portion. After short time of induction, exothermic reaction begun and the mixture color changed from orange to greenish yellow. The mixture was stirred 20 min at 0°C and then 30 min at room temperature. The reaction mixture was quenched with water (50 mL). Organic phase was separated, washed with sat. NaHCO₃ (2×50mL), water (50 mL) and dried (Na₂SO₄). The solvent was

evaporated under reduced pressure and the residue was subjected to second selenation and selenoxide elimination sequence using exactly the same amounts of all reagents. The product was purified by flash chromatography eluting with petrol ether- ethyl acetate (1:1). The product was obtained as yellow solid (1.9 g, 64%).

m.p. 124.4-125.3°C; $[\alpha]_D^{20}=1380$ (*c* 0.0137 in CHCl₃); IR: ν 1734 (COOMe), 1684 (C=O), 1613 (C=C); ¹H-NMR (400 MHz, CDCl₃) δ 7.73 (d, *J*= 6.8 Hz, 2H), 3.82 (s, 6H), 3.67-3.57 (m, 2H), 2.79 (m, 2H); ¹³C-NMR (100.3 MHz, CDCl₃) δ 187.3, 163.6, 151.7, 129.1, 52.84, 47.1, 33.4; HRMS (ESI) calcd. for C₁₃H₁₂O₆ (M+H⁺): 265.0712; Found: 265.0713; Anal. calcd for C₁₃H₁₂O₆: C, 59.09; H, 4.58; O, 36.33; Found: C 59.26, H 4.78.

(+)-(1*R*,4*S*,5*R*,8*S*)-dimethyl-*exo,exo*-4,8-didecyl-2,6-dihydroxybicyclo[3.3.1]nona-2,6-diene-3,7-dicarboxylate **102**

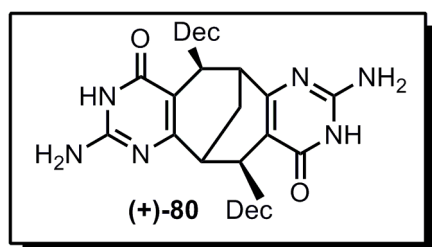


Prepared according to **General procedure for 1,4-addition of decyl zinc bromide to enones.**

Yield 0.333 g (90%), colorless oil. Eluent: petrol ether-ethyl acetate- 60:1. IR: ν 2926, 2856, 1654 (COOMe, hydrogen bonded), 1612, 1443, 1356,

1281, 1206; ¹H-NMR (400 MHz, CDCl₃) δ 12.28 (s, 2H), 3.75 (s, 6H), 2.67-2.56 (m, 2H), 2.52-2.43 (m, 2H), 1.85-1.76 (m, 2H), 1.72-1.57 (m, 2H), 1.50-1.16 (m, 34H), 0.89 (t, *J*= 6.5 Hz, 6H); ¹³C-NMR (100.3 MHz, CDCl₃) δ 174.11, 173.26, 100.81, 51.38, 37.43, 35.94, 33.62, 31.92, 29.66, 29.63, 29.54, 29.35, 27.91, 22.69, 18.11, 14.11; Anal. calcd for C₃₃H₅₆O₆: C, 72.22; H, 10.29; Found C, 72.57; H, 10.69.

Compound (+)-80

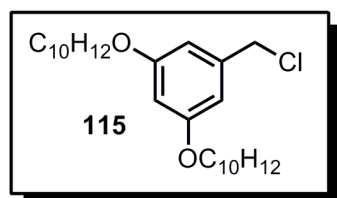


The mixture of ketoester **102** (0.107 g, 0.19 mmol) and guanidinium carbonate (0.175 g, 0.98 mmol) in methanol (10 mL) were heated at 100°C in pressure vial for 24 hr.

The solvent was removed under reduced pressure and the residue was triturated with water. The precipitate was filtered, washed generously with water and then dissolved in chloroform (the large amount of solvent is used to prevent the formation of gel). The solution was washed with water, dried (Na₂SO₄) and evaporated to small volume. Then, excess of methanol was added and the white precipitate formed was filtered and dried to obtain 0.07 g (65%) of (+)-**80** as a white powder.

m.p.130 (dec.); $[\alpha]_D^{20} = -34.1$ (*c* 0.00088 in CHCl₃); UV (*c* 0.88 mM, CHCl₃), λ_{\max} (log ϵ): 303 (4.16), 232 (4.21); UV (*c* 1.4 mM, DMSO), λ_{\max} (log ϵ): 290 (4.2), 238 (2.6); CD (*c* 0.88 mM, CHCl₃), λ_{\max} ($\Delta\epsilon/\text{dm}^3\text{mol}^{-1}\text{cm}^{-1}$): 293 (-9.3), 266 (0); 248 (37.6), 238 (0), 231 (-46.3); CD (*c* 1.4 mM, DMSO), λ_{\max} ($\Delta\epsilon/\text{dm}^3\text{mol}^{-1}\text{cm}^{-1}$): 228 (11.0); IR: ν 2925, 2855, 1640; ¹H NMR (400 MHz, d₆-DMSO-CDCl₃, 2:3 v/v) δ 10.46 (br.s, 2H), 5.92 (br.s, 4H), 1.80 (br.s, 2H), 1.77-1.67 (m, 2H), 1.50-1.37 (m, 2H), 1.37-1.10 (m, 36H), 0.82 (t, *J* = 6.8 Hz, 6H); HRMS (ESI) calcd. for C₃₃H₅₅N₆O₂(M+H⁺): 567.4387; Found: 567.4359.

1-(chloromethyl)-3,5-bis(decyloxy)benzene **115**

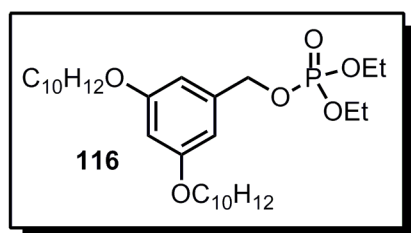


2,4,6-trichloro[1,3,5]triazine (TCT) (0.092 g, 0.50 mmol) was added to DMF (2 mL) and the mixture stirred at room temperature. After the formation of white solid, the reaction was periodically checked

by TLC until complete disappearance of TCT and then diluted with CH₂Cl₂ (10 mL) followed by addition of benzyl alcohol **113** (0.20 g, 0.48 mmol). After the addition, the mixture was stirred at room temperature for 5h and diluted with water (10 mL). Organic phase was washed with sat. NaHCO₃ solution followed by 10% HCl solution and brine. The organics were dried (Na₂SO₄), and the solvent evaporated under reduced pressure. The residue was purified by flash chromatography (petrol ether/ ethyl acetate- 20:1) to afford 0.207 g (99%) of **115** as colorless oil which solidifies slowly on standing.

m.p. <36°C; R_f 0.38 (petrol ether/ethyl acetate- 20:1); IR: ν 2923, 2852; 1599, 1467, 1172; ^1H NMR (300 MHz, CDCl_3) δ 6.53 (d, $J= 2.12$ Hz, 2H), 6.42 (t, $J= 2.12$ Hz, 1H), 4.51 (s, 2H), 3.95 (t, $J= 6.54$, 4H), 1.85-1.71 (m, 4H), 1.52-1.40 (m, 4H), 1.40-1.19 (m, 26H), 0.91 (t, $J= 6.6$ Hz, 6H); ^{13}C NMR (100.3 MHz, CDCl_3) δ 160.5, 139.3, 106.9, 101.3, 68.1, 46.4, 31.9, 29.7, 29.6, 29.4, 29.3, 29.2, 29.2, 26.0, 22.7, 14.1.

3,5-bis(decyloxy)benzyl diethyl phosphate 116

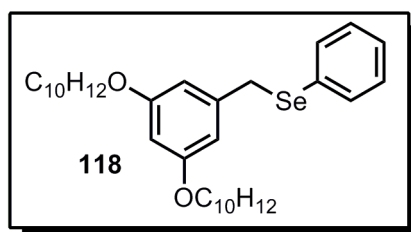


To the solution of benzyl alcohol **113** (0.420 g, 1.0 mmol), Et_3N (0.111 g, 1.1 mmol) and DMAP (0.0122 g, 0.1 mmol) was added diethyl chlorophosphate (0.190 g, 1.1 mmol)

dropwise at room temperature. The white precipitate forms very soon after addition. The mixture was stirred for 48 h at room temperature, and then quenched with sat. ammonium chloride solution and extracted with ethyl acetate (3 \times 20 mL). The combined organic extracts were dried (Na_2SO_4), evaporated under reduced pressure and purified by flash chromatography (petrol ether/ethyl acetate-4:1 to 3:1) to afford 0.233 g of starting benzyl alcohol and 0.247 g (45%, 99% brsm) of product as colorless oil.

IR: ν 2926, 2857, 1601, 1496, 1166; ^1H NMR (300 MHz, CDCl_3) δ 6.51 (d, $J= 2.12$ Hz, 2H), 6.41 (t, $J= 2.21$ Hz, 1H), 4.98 (d, $J= 7.79$ Hz, 2H), 4.17-4.04 (m, 4H), 3.93 (t, $J= 6.56$ Hz, 4H), 1.72-1.81 (m, 6H), 1.50-1.38 (m, 4H), 1.38-1.24 (m, 28H), 0.89 (t, $J= 6.73$, 6H); ^{13}C NMR (75 MHz, CDCl_3) δ 160.4, 138.0, 105.9, 101.2, 69.0, 68.9, 68.1, 63.9, 63.8, 31.9, 29.6, 29.5, 29.4, 29.3, 29.2, 26.0, 22.7, 16.1, 16.0, 14.1.

3,5-bis(decyloxy)benzyl phenyl selenide 118

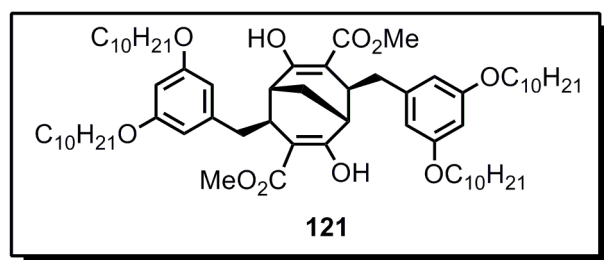


To a stirred suspension of NaH (2.13 g, 53.14 mmol, 1.4 eq.) and anhydrous THF (120 ml) was added diphenyl diselenide (9.16 g, 28.47 mmol, 0.75 eq.) in one portion. The reaction mixture was stirred at reflux for 1.5 h during which time the color changed

from yellow to greenish. The suspension was cooled to room temperature and benzyl bromide **113** was added all at once. The mixture was stirred for 2 h and then quenched with water (100 ml). The mixture was extracted with Et₂O (3 x 100 ml) and the combined organic phase was dried (Na₂SO₄) and concentrated *in vacuo*. The product was isolated with flash chromatography, first eluting excess diphenyl diselenide with petroleum ether (95% recovery of excess reagent) and then collecting the product with petroleum ether-dichloromethane (10:1) as slightly yellow oil (20.2 g, 95%).

IR: ν 2924 (C-H), 2853 (C-H), 1597 (C-Se); ¹H-NMR (400 MHz, CDCl₃) δ 7.59-7.43 (m, 2H), 7.36- 7.20 (m, 3H), 6.39 (br.t, J = 2.0 Hz, 2H), 6.36 (d, 1H), 4.13- 4.02 (m, 2H), 3.89 (t, J = 6.6 Hz, 4H), 1.85- 1.72 (m, 4H), 1.52- 1.42 (m, 4H), 1.34 (m, 24H), 0.95 (br.t, 6H); ¹³C-NMR (100.3 MHz, CDCl₃) δ 160.4, 140.8, 133.7, 130.8, 129.1, 127.4, 107.3, 100.4, 68.1, 32.7, 32.1, 29.8, 29.8, 29.6, 29.5, 29.4, 26.2, 22.9, 14.3; HRMS (FAB+) calcd. for C₃₃H₅₃O₂Se (M+H⁺): 561.3211; Found: 561.3224; Anal. calcd for C₃₃H₅₂O₂Se: C 70.68, H 9.53; Found: C 70.96, H 9.41.

(+)-(1*S*,5*S*)-dimethyl 4,8-*exo,exo*-bis(3,5-bis(decyloxy)benzyl)-2,6-dihydroxybicyclo[3.3.1]nona-2,6-diene-3,7-dicarboxylate **121**



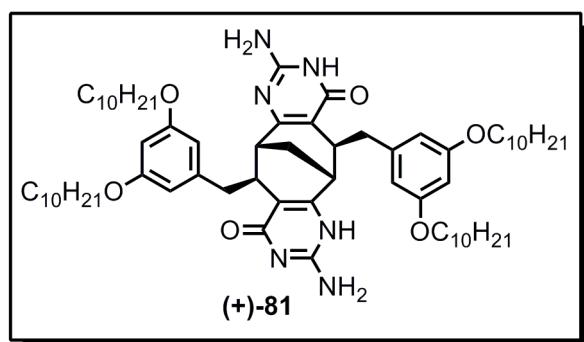
A solution of selenide **118** (10.59 g, 18.92 mmol, 5 eq.) and anhydrous THF (15 ml) was added rapidly to a solution of BuLi (9.45 ml, 1.6 M, 15.12

mmol, 4 eq.) and anhydrous THF (150 ml) at -110 °C under vigorous stirring. The reaction mixture gradually turned yellow as it was allowed to slowly reach -50 °C during a period of approximately 70 min. The solution was then transferred to a suspension of CuCN (1.35 g, 15.12 mmol, 4 eq.) and anhydrous THF (150 ml) precooled to -78 °C. The suspension was stirred for approximately 45 min letting the temperature rise to -35 °C. The temperature was then decreased to -78 °C again and a solution of **108** (1 g, 3.78 mmol),

freshly distilled TMSCl (2 ml) and anhydrous THF (15 ml) was added dropwise. The reaction mixture was stirred overnight without cooling bath, letting the temperature to increase to approximately - 10 °C. The reaction was quenched with aqueous 10 % HCl solution (40 mL), water (100 mL) and EtOAc (100 mL) was added and the suspension was filtered through CELITE®. The organic phase was separated and the water phase was extracted with EtOAc. The combined organic phase was dried (Na₂SO₄) and concentrated under reduced pressure yielding crude that was loaded on silica column. By-products were eluted with petroleum ether followed by petroleum ether-diethyl ether (70:1). The product was then collected as colorless oil (2.41 g, 59%) using petroleum ether-diethyl ether (50:1) as eluent.

$[\alpha]_D^{20}=40$ (c 0,010 in CHCl₃, ee >99%); IR: ν 2923 (C-H), 2854 (C-H), 1653 (COOMe, hydrogen bonded), 1601 (C=C); ¹H-NMR (400 MHz, CDCl₃) δ 12.26 (s, 2H), 6.37 (d, J = 2.1Hz, 4H), 6.33 (t, J = 2.1 Hz, 2H), 3.94 (t, J = 6.6 Hz, 8H), 3.78 (s, 6H), 3.09 (dd, J = 13.9, 3.4 Hz, 2H), 3.06-2.99 (m, 2H), 2.44 (d, J = 1.6 Hz, 2H), 2.35 (dd, J = 13.8, 11.0 Hz, 2H), 1.88 (d, J = 11 Hz, 2H), 1.84-1.72 (m, 8H), 1.41-1.21 (m, 48H), 0.89 (t, J = 6.9 Hz, 12H); ¹³C-NMR (100.3 MHz, CDCl₃) δ 175.1, 173.2, 160.6, 142.5, 107.7, 100.3, 99.2, 68.2, 51.8, 40.1, 39.0, 35.5, 32.1, 29.8, 29.8, 29.7, 29.6, 29.5, 26.3, 22.9, 17.8, 14.3; HRMS (ESI) calcd. for C₆₇H₁₀₉O₁₀ (M+H⁺): 1073.8021; Found: 1073.8038; Anal. calcd for C₆₇H₁₀₈O₁₀: C 74.96, H 10.14; Found: C 75.30, H 10.12.

Compound (+)-81



The mixture of **121** (2 g, 1.86 mmol), guanidinium chloride (0.89 g, 9.31 mmol) and potassium *tert*-butoxide (1.04 g, 9.31 mmol) in MeOH (30 mL) were heated at 100°C for 24 h in

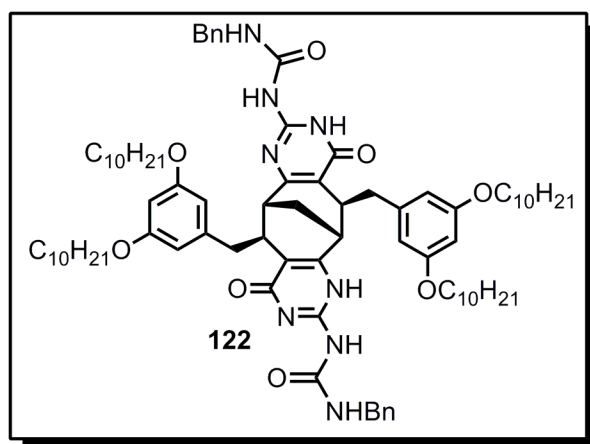
pressure vial. After quenching with excess of 10% HCl solution, the water

phase was extracted with CHCl_3 (3×40 mL) and the combined organics were washed with water (50 mL) and sat. NaHCO_3 solution and dried (Na_2SO_4). After evaporation under reduced pressure, the residue was purified by flash chromatography (ethyl acetate to dichloromethane/methanol- 16:1) to afford 1.86 g (92%) of (+)-**81** as a colorless glass which was converted to a white solid after addition of methanol and evaporation.

m.p.>130°C (decomp.); $[\alpha]_D^{20} = 18.6$ (*c* 0,0095 in CHCl_3 , *ee* >99%); UV (*c* 0.47 mM, CHCl_3), λ_{max} (log ϵ): 286 (5.6), 233 (5.3); UV (*c* 0.71 mM, DMSO), λ_{max} (log ϵ): 284 (4.0), 249 (4.24); CD (*c* 0.47 mM, CHCl_3), λ_{max} ($\Delta\epsilon/\text{dm}^3\text{mol}^{-1}\text{cm}^{-1}$): 307 (40.3), 294 (0), 281 (-30.3), 260 (0), 249 (27.9), 239 (0); CD (*c* 0.71 mM, DMSO), λ_{max} ($\Delta\epsilon/\text{dm}^3\text{mol}^{-1}\text{cm}^{-1}$): 285 (13.2), 254 (11.6), 248 (0), 244 (-11.8); IR: ν 2925 (C-H), 2855 (C-H), 1640 (C=O), 1598 (C=N); ^1H -NMR (400 MHz, CDCl_3) δ 14.33 (s, 2H), 12.23 (s, 2H), 7.58 (br.s, 4H); 6.51 (s, 2H), 6.37 (s, 3H), 6.18 (s, 1H), 4.83 (br.s, 4H), 3.98 (t, *J*= 5.70 Hz, 4H), 3.75 (t, *J*= 5.70 Hz, 4H), 3.28 (d, *J*= 11.7 Hz, 1H), 3.08-2.89 (m, 4H), 2.88-2.79 (m, 1H), 2.76 (br.s, 1H), 2.67-2.55 (m, 2H), 2.39 (t, *J*= 11.7 Hz, 1H), 2.11-1.92 (m, 2H), 1.88-1.74 (m, 4H), 1.67-1.54 (m, 4H), 1.54-1.43 (m, 4H), 1.43-1.07 (m, 52H), 0.98-0.75 (m, 12H); ^{13}C -NMR (100.3 MHz, CDCl_3) δ 167.5; 167.1, 165.8, 165.5, 160.3, 154.2, 153.4, 143.2, 141.8, 112.8, 109.8, 108.4, 108.2, 98.7, 98.6, 76.8, 68.1, 68.0, 40.5, 40.1, 38.7, 37.9, 36.9, 32.1, 32.0, 29.8, 29.8, 29.7, 29.6, 29.5, 29.3, 26.3, 26.2, 22.8, 22.8, 18.2, 14.27, 14.25; ^1H -NMR (400 MHz, d_6 -DMSO: CDCl_3 -5:1, v/v) δ 10.56 (s, 2H), 6.40 (d, *J*= 2.0 Hz, 4H), 6.28 (t, *J*= 2.0 Hz, 2H), 6.13 (br.s, 4H), 3.92 (t, *J*= 6.4 Hz, 8H), 3.02 (d, *J*= 11.1 Hz, 2H), 2.87 (d, *J*= 11.1 Hz, 2H), 2.46 (br.s, 2H), 2.07 (br.s, 2H), 1.73 (m, 8H), 1.42 (m, 8H), 1.27 (m, 56H), 0.87 (t, 12 H); ^{13}C -NMR (100.3 MHz, d_6 -DMSO: CDCl_3 -1:1 v/v) δ 163.12, 161.01, 158.24, 152.01, 141.78, 109.55, 106.37, 97.13, 77.36, 68.50, 65.93, 37.36, 29.95, 27.67, 27.62, 27.50, 27.46, 27.37, 24.22, 20.73, 12.41; HRMS (ESI) calcd. for $\text{C}_{67}\text{H}_{107}\text{N}_6\text{O}_6$ ($\text{M}+\text{H}^+$): 1091.8252; Found: 1091.8177; Anal. calcd for

$C_{67}H_{106}N_6O_6 \cdot 1.5CHCl_3$: C 72.36, H 9.60, N 7.53; Found: C 72.71, H 9.74, N 7.44.

Compound 122

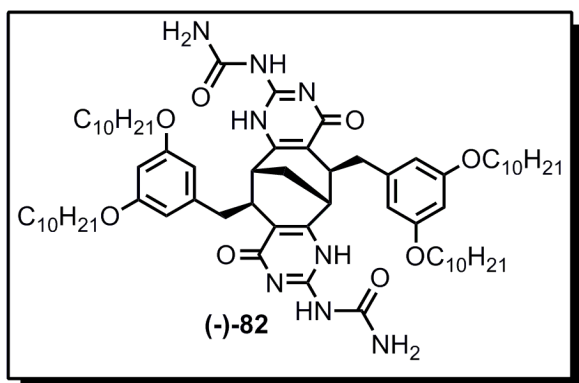


To pyridine (1.5 mL) solution of (+)-**81** (15 mg, 0.014 mmol) was added benzyl isocyanate (5.5 mg, 0.041 mmol) and the vial was tightly sealed. The mixture was irradiated in microwave reactor at 120°C for 15 min with stirring and after cooling to room

temperature, evaporated to dryness under reduced pressure. The residue was triturated with diethyl ether and filtered to remove dibenzyl urea precipitate. The diethyl ether solution was concentrated to small volume and excess of methanol was added. The white precipitate was filtered and dried *in vacuo* to give 15 mg (80%) of **122** as colorless solid.

¹H NMR (400 MHz, CDCl₃) δ 12.66 (s, 2H), 11.97 (s, 2H), 10.14 (s, 2H), 7.34 (d, *J* = 7.18 Hz, 4H), 7.16 (t, *J* = 7.53 Hz, 4H), 7.08-7.02 (m, 2H), 6.43-6.36 (m, 6H), 4.60 (dd, *J* = 6.84, 14.31, 2H), 4.24 (dd, *J* = 3.15, 14.05, 2H), 4.14 (dd, *J* = 6.42, 15.21 Hz, 4H), 3.98 (dd, *J* = 6.56, 15.28 Hz, 4H), 3.46 (d, *J* = 10.17 Hz, 2H), 3.04 (dd, *J* = 4.70, 11.11 Hz, 2H), 2.10 (t, *J* = 12.69, 2H), 1.95 (s, 2H), 1.85-1.74 (m, 8H), 1.53-1.41 (m, 8H), 1.41-1.14 (m, 50H), 0.88 (t, *J* = 6.86 Hz, 12 H); ¹³C NMR (100.3 MHz, CDCl₃) δ 171.9, 161.1, 156.3, 153.8, 148.3, 141.7, 138.1, 128.7, 128.5, 127.6, 115.9, 107.0, 100.3, 68.3, 44.1, 39.7, 37.7, 32.9, 32.2, 29.88, 29.85, 29.8, 29.6, 23.0, 17.3, 14.4; HRMS (ESI) calcd. for C₈₃H₁₂₁N₈O₈ (M+H⁺): 1357.9307; Found: 1357.9340; Anal. calcd for C₈₃H₁₂₀N₈O₈: C 73.41, H 8.91, N 8.25; Found: C 73.45, H 9.09, N 9.09.

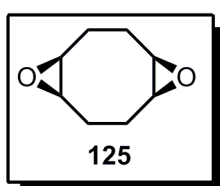
Compound (-)-82



(+)-81 (0.10 g, 0.092 mmol) was dissolved in dry pyridine (4 mL) under Ar and was added TMSCl (0.056 g, 0.52 mmol). The mixture was stirred for 3 h at room temperature was added phenyl chloroformate (0.081 g, 0.52 mmol) and stirring was continued for 5 h. The white precipitate formed just after addition. Aqueous ammonia (300 μL, 28%) solution was added and the mixture was stirred overnight. The reaction mixture was quenched with excess of 10% HCl solution and extracted with dichloromethane (3×30 mL). The combined organics were washed with water, dried (Na₂SO₄) and evaporated under reduced pressure. The glassy residue was triturated with methanol and an off-white precipitate that formed was filtered and dried in vacuo yielding 0.1 g (92%) of **82**.

m.p. 130 (dec.); IR: ν ; ¹H NMR (400 MHz, DMSO-d₆/CDCl₃- 1/1) δ 11.74 (s, 2H), 9.56 (s, 2H), 6.79 (br.s, 4H), 6.43 (s, 4H), 6.27 (s, 2H), 3.91 (t, J= 5.5 Hz, 8H), 3.10 (d, J= 12.5 Hz, 2H), 2.91 (d, J= 10.5 Hz, 2H), 2.61 (br.s, 2H), 2.35 (t, J= 11.8 Hz, 2H), 2.14 (br.s, 2H), 1.71 (m, 8H), 1.39 (m, 8H), 1.24 (m, 48H), 0.84 (m, 12H); ¹³C NMR (100.3 MHz, DMSO-d₆/CDCl₃- 1/1) δ 163.1, 160.5, 159.5, 155.7, 149.1, 142.8, 115.6, 107.5, 98.6, 67.3, 38.1, 35.9, 31.2, 28.92, 28.88, 28.76, 28.70, 28.63, 25.5, 22.0, 17.7, 13.7; HRMS (ESI) calcd. for C₆₉H₁₀₈N₈O₈ (M+H⁺): 1177.8368; Found:1177.8429; Anal. calcd for C₆₉H₁₀₈N₈O₈: C 70.31, H 9.51, N 7.53; Found: C 70.48, H 9.30, N 9.18.

syn-1, 5-diepoxyoctane 125

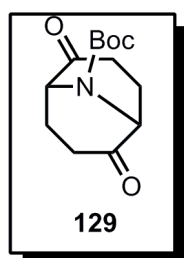


Procedure A. m-CPBA (5 g, 20 mmol, 72% dispersion with water) was dissolved with stirring in dichloromethane (100 mL). To the resulting solution anhydrous MgSO₄ was added

portionwise until clear solution was obtained. To the resulting mixture, cyclooctadiene (1g, 9.26 mmol) was added dropwise via syringe at slow addition rate to maintain the reaction temperature below solvent boiling point. The white precipitate (m-chlorobenzoic acid) formed soon after addition of diene. The mixture was stirred 2 h at room temperature and then filtered. The filter cake was washed with dichloromethane. The filtrate was washed successively with 2N NaOH solution, sat. solution of Na₂S₂O₅ and brine and dried (Na₂SO₄). After evaporation under reduced pressure, the oil obtained was subjected to flash chromatography (petrol ether/ethyl acetate- 3:1) to afford 0.88 g (68%) of **125** as colorless oil which slowly solidified.

Procedure B. To a 2.0 L three-necked flask equipped with mechanical stirrer, dropping funnel and thermometer, were added NaHCO₃ (30 g, 0.357 mol), water (400 mL), acetone (120 mL), ethyl acetate (400 mL), and cyclooctadiene (10 g, 0.093 mol) and the mixture was vigorously stirred. An aqueous Oxone (114 g, 0.186 mol, H₂O 440 mL) solution was added dropwise over 1 h at the rate to keep mixture temperature below 30°C. After addition, the mixture was stirred for an additional 1h. The organic layer was separated and washed with brine and dried (Na₂SO₄). The solvent was evaporated to leave 9.97 g (77%) of **125** as colorless oil, which slowly solidified. The product was TLC and NMR pure and was used for the next step without further purification.

tert*-butyl 2,6-dioxo-9-azabicyclo[3.3.1]nonane-9-carboxylate **129*



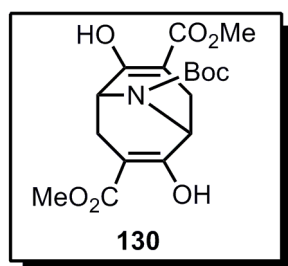
Procedure A. Oxalyl chloride (1.03 g, 8.11 mmol) was added dropwise to dichloromethane (20 mL) at -60°C followed by DMSO (1.26g, 16.2 mmol). The mixture was stirred for 2 min and a solution of **128** (0.94g, 3.67 mmol) in dichloromethane (6 mL) was added. After 15 min Et₃N (3.63 g, x mmol) was added and the mixture was left to stir for additional 5 min. Then, the cooling bath was removed and the mixture was allowed to reach room temperature. The reaction mixture was diluted with water (20 mL), the water phase was extracted with dichloromethane (3×20 mL). The organics were washed with 0.4 N HCl,

water, sat. NaHCO₃ solution and brine and dried (Na₂SO₄). After purification by flash chromatography, 0.77 g (83%) of dione **129** was obtained as colorless solid with characteristic smell (sulphides residues).

Procedure B. Diol **128** (0.257 g, 1 mmol) was dissolved in CCl₄/MeCN/H₂O (10.5 mL, 1:1:1.5-v/v) mixture and then NaIO₄ (0.853 g, 4 mmol) and RuO₂*H₂O (1.5 mg, 0.01 mmol) were added. The mixture was stirred 36 h at room temperature and then diluted with dichloromethane (20 mL) and water (10 mL). The water phase was extracted with dichloromethane (3× 15 mL). The combined organic extracts were dried (Na₂SO₄) and evaporated under reduced pressure. The yellowish solid residue was purified by flash chromatography (petrol ether/ethyl acetate- 2:1) to afford 0.242 g (96%) of **129** as a colorless solid.

m.p 88-89°C; R_f 0.79 (ethyl acetate); IR: ν 1715 (C=O), 1694 ((C=O)O*t*-Bu), 1404 (C-N), 1169 (CO-O-*t*Bu); ¹H NMR (300 MHz, CDCl₃) δ 4.8 (br.s, 1H), 4.74 (br.s, 1H), 2.56-2.69 (m, 2H), 2.38-2.5 (m, 4H), 2.15 (br.s, 2H), 1.51 (s, 9H); ¹³C NMR (75 MHz, CDCl₃) δ 209.1, 154.1, 81.9, 59.4, 35.3, 28.5, 25.8; Anal. calcd for C₁₃H₁₉NO₄: C 61.64, H 7.56, N 5.53; Found: C 61.82, H 7.59, N 5.81.

9-*tert*-butyl 3,7-dimethyl 2,6-dihydroxy-9-azabicyclo[3.3.1]nona-2,6-diene-3,7,9-tricarboxylate 130

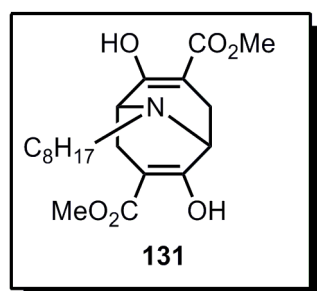


To a solution of LiHMDS (3.3 mL, 3.3 mmol, 1M solution in ethyl benzene) in THF (5 mL) cooled to -78°C was added dione **129** (0.350 g, 1.38 mmol) solution in THF (10 mL) dropwise. The mixture was stirred 30 min at -78°C and then 15 min at room temperature to complete enolization. The solution was then cooled back to -78°C under occurrence of white precipitate (lithium enolate) and were added neat HMPTA (0.48 mL, 2.75 mmol) and methyl cyanofomate (0.26 mL, 3.3 mmol). After stirring for 15 min, the precipitate dissolved and TLC showed complete conversion of starting material. The reaction was quenched at -78°C

with 0.1 M AcOH (10 mL) and allowed to reach room temperature. The organic layer was separated and water phase was extracted with dichloromethane (2×10 mL). The organic phase were dried with Na₂SO₄ and evaporated under reduced pressure. The residue is purified by flash chromatography (petrol ether/dichloromethane- 1:3.5 to dichloromethane/methanol- 150:1) to afford 0.46 g (91%) as colorless solid.

m.p. 133°C; R_f 0.81 (petrol ether/ethyl acetate- 1:1); IR: ν 1697 ((C=O)O*t*-Bu), 1662 ((C=O)OCH₃), 1620 (C=C-OH), 1417 (C-N), 1176 (CO-O-*t*Bu), 107 (CO-OCH₃); ¹H NMR (300 MHz, CDCl₃) δ 12.10 (s, 1H), 12.00 (s, 1H), 4.87 (d, *J*= 5.1 Hz, 1H), 4.71 (d, *J*= 5.4 Hz, 1H), 3.79 (s, 3H), 2.67-2.77 (m, 2H), 2.58 (dd, *J*= 4.2, 15.9 Hz, 2H), 1.49 (s, 9H); ¹³C NMR (75 MHz, CDCl₃) δ 172.7, 170.1, 169.3, 153.1, 95.9, 95.4, 81.3, 52.1, 50.2, 48.5, 28.6, 26.8, 26.5; Anal. calcd for C₁₇H₂₃NO₈: C 55.28, H 6.28 N 3.79; Found: C 55.64, H 6.42, N 3.79.

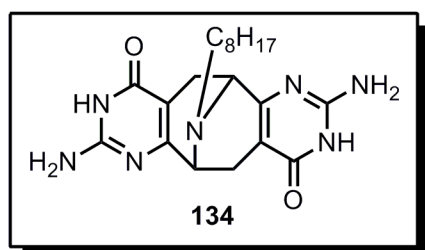
Representative procedure for the reductive amination of 130. Dimethyl 2,6-dihydroxy-9-octyl-9-azabicyclo[3.3.1]nona-2,6-diene-3,7-dicarboxylate 131.



Ketoester **130** (0.05 g, 0.135 mmol) solution dichloromethane (2 mL) was cooled in ice bath under Ar and to this solution was added trifluoroacetic acid (0.5 mL). After stirring for 3 h all volatiles were removed and the solid residue was dissolved in dichloromethane (5 mL) under Ar and were added n-octanal (27.4ml, 0.176 mmol), Et₃N (28.1 ml, 0.203 mmol) and NaHB(OAc)₃ (0.04 g, 0.189 mmol). Suspension was stirred for 25 min, then diluted with dichloromethane (5 mL) and sat. NaHCO₃ solution (5 mL). The water phase was extracted with dichloromethane (3×10 mL) and the combined organics were washed with brine and dried (Na₂SO₄). After evaporation under reduced pressure the residue was purified by flash chromatography (petrol ether/dichloromethane- 3:1) to afford 0.0433 g (84%) of **131** as colorless oil.

IR (**131**·HCl): ν 3436, 2430, 2305, 1667 (COOMe, hydrogen bonded), 1215 (CO-OMe); ^1H NMR (300 MHz, CDCl_3) δ 11.90 (s, 2H), 3.72 (s, 6H), 3.45 (d, J = 5.8 Hz, 2H), 2.62 (dd, J = 16.1, 6.44 Hz, 2H), 2.49 (dd, J = 14.0, 7.3 Hz, 2H), 2.39 (d, J = 16.3 Hz, 2H), 1.54-1.41 (m, 2H), 1.23 (m, 26H), 0.86 (t, J = 6.7 Hz, 3H); ^{13}C NMR (75 MHz, CDCl_3) δ 172.3, 170.6, 94.6, 54.2, 51.7, 51.5, 31.9, 29.64, 29.6, 29.55, 29.52, 29.5, 29.4, 29.3, 27.5, 27.2, 24.5, 22.6, 14.1; Anal. calcd for $\text{C}_{28}\text{H}_{47}\text{NO}_6\cdot\text{HCl}$: C, 63.44; H, 9.13; N, 2.64; Found: C, 63.78; H, 9.16; N, 2.89.

Compound 134

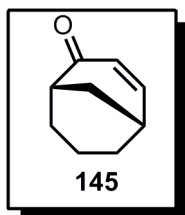


Ketoester **130** (0.05 g, 0.135 mmol) solution in dichloromethane (2 mL) was cooled in ice bath under Ar and to this solution was added trifluoroacetic acid (0.5 mL). After stirring for 3 h all volatiles were removed and the

solid residue was dissolved in dichloromethane (5 mL) under Ar and were added n-octanal (27.4 μl , 0.176 mmol), Et_3N (28.1 mL, 0.203 mmol) and $\text{NaBH}(\text{OAc})_3$ (0.04 g, 0.189 mmol). A suspension was stirred for 25 min, then diluted with dichloromethane (5 mL) and sat. NaHCO_3 solution (5 mL). The water phase was extracted with dichloromethane (3×10 mL) and the combined organics were washed with brine and dried (Na_2SO_4). After evaporation under reduced pressure the residue was purified by flash chromatography (petrol ether/dichloromethane-3:1) to afford 0.0433 g (84%) of **134** as colorless solid.

m.p. >300°C; IR: ν 3432, 2363, 1669 ((C=O) OCH_3), 1629 (C=OCH), 1444 (C-N), 1213 (CO- OCH_3); ^1H -NMR (300 MHz, CDCl_3) δ 0.87 (t, J = 6.69 Hz, 3H), 1.26 (bs, 10H), 1.45-1.54 (m, 2H), 2.40 (d, J = 16.1 Hz, 2H), 2.51 (dd, J = 14.21, 7.29 Hz, 2H), 2.63 (dd, J = 16.11, 6.51 Hz, 2H), 3.47 (d, J = 5.88 Hz, 2H), 3.74 (s, 6H), 11.92 (s, 2H); ^{13}C NMR (75 MHz, CDCl_3) δ 14.1, 22.6, 24.5, 27.3, 27.6, 29.2, 29.4, 31.8, 51.6, 51.8, 54.2, 94.7, 170.6, 172.3; Anal. calcd for $\text{C}_{13}\text{H}_{19}\text{NO}_4\cdot\text{HCl}$: C 57.42, H 7.72, N 3.35; Found: C 57.88, H 7.88, N 3.55.

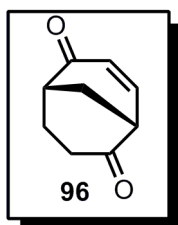
(+)-(1*S*,5*S*)-bicyclo[3.3.1]non-3-en-2-one **145**



The mixture of ketone **146** (60 mg, 0.43 mmol), PhIO₂ (0.28 g, 1.18 mmol), PhSeSePh (14 mg, 0.045 mmol) and catalytic amount of TsOH in dry toluene (10 mL) was heated under reflux for 3 h. The mixture was cooled to room temperature, filtered, washed with saturated NaHCO₃, brine and dried (MgSO₄). After evaporation under reduced pressure the residue was purified by flash chromatography (petrol ether/ethyl acetate-7:1) to afford 56 mg (95%) of **145** as white waxy solid (racemic **145**²⁰⁰)

$[\alpha]_D^{20}=115$ (*c* 0.76 in EtOH); CD: λ_{\max} ($\Delta\epsilon/\text{dm}^3 \text{ mol}^{-1} \text{ cm}^{-1}$): 341 (+0.95); ¹H NMR (300 MHz, CDCl₃) δ 1.50–1.70 (m, 6H), 1.60–1.80 (m, 1H), 2.17–2.26 (m, 1H), 2.45–2.54 (m, 1H), 2.57–2.68 (m, 1H), 6.17–6.21 (d, *J*= 9.9 Hz, 1H), 6.92–6.98 (ddd, *J* = 9.9, 6.5, 1.8 Hz, 1H); ¹³C NMR (100.3 MHz, CDCl₃) δ 203.3, 152.8, 132.0, 42.9, 34.2, 30.9, 28.2, 25.2, 17.5.

(+)-(1*S*,5*S*)-bicyclo[3.3.1]non-3-ene-2,6-dione **96**

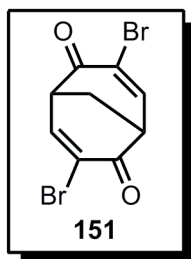


The mixture of diketone (+)-**22** (0.1 g, 0.66 mmol), PhIO₂ (0.34 g, 1.31 mmol), (PhSe)₂ (5 mg, 0.00165 mmol) and catalytic amount of TsOH in dry toluene (10 mL) was heated under reflux for 3-4 h. The mixture was cooled to room temperature, filtered, washed with saturated NaHCO₃, brine, and dried (MgSO₄). After evaporation under reduced pressure the residue was purified by flash chromatography (petrol ether/ethyl acetate 7:1) to afford 58 mg (60%) of **96** as white solid (racemic **96**¹²²).

m.p. 80°C (transition at 70°C); IR: ν 3048 (=C-H), 1711 (C=O), 1673 (C=O), 1608 (C=C); $[\alpha]_D^{20}=1569$ (*c* 0.204, EtOH); CD: λ_{\max} ($\Delta\epsilon/\text{dm}^3 \text{ mol}^{-1} \text{ cm}^{-1}$) 313 (+5.4), 254 (-2.4); ¹H NMR (300 MHz, CDCl₃) δ 7.12–7.05 (ddd, *J*= 9.9, 6.8, 2.1 Hz, 1H), 6.32 (d, *J*= 9.9 Hz, 1H), 3.40–3.30 (ddd, *J*= 6.8, 3.1 Hz, 1H), 2.39–2.77 (m, 2H), 2.71–2.63 (ddd, *J*= 13.2, 3.1 Hz, 1H), 2.37–2.11 (m, 4H);

^{13}C NMR (100.3 MHz, CDCl_3): δ 207.0, 200.8, 148.6, 133.1, 49.9, 41.9, 35.2, 34.3, 29.3; Anal. calcd. for $\text{C}_9\text{H}_{10}\text{O}_2$: C 71.79; H 6.75; Found: C 71.98; H 6.71.

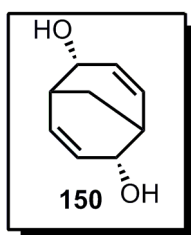
3,7-dibromobicyclo[3.3.1]nona-3,7-diene-2,6-dione **151**



Bromine (0.32 g, 2.0 mmol) was added dropwise to an ice-cold solution of dienone **94** (0.148 g, 1.0 mmol) in CCl_4 (10 mL), and the mixture was stirred at 0 °C for 1 h. To this mixture was added NEt_3 (0.22 g, 2.2 mmol) slowly and the mixture was stirring at room temperature overnight. A white precipitate was formed. The reaction mixture was diluted with CH_2Cl_2 , washed with a saturated $\text{Na}_2\text{S}_2\text{O}_5$ solution, water and brine, dried (Na_2SO_4), and evaporated. The residue was crystallised from a CH_2Cl_2 - CCl_4 mixture to afford 152 mg (50%) of **151** as a slightly yellow solid. Additional amount of product (10-15%) could be obtained from the mother liquor by flash chromatography (petrol ether/ethyl acetate- 5:1).²⁰¹

R_f 0.16 (petrol ether/ethyl acetate-5:1); ^1H -NMR (300 MHz, CDCl_3) δ 7.70 (d, J = 6.85 Hz, 2H), 3.68 (m, 2H), 5.26 (t, J = 2.90 Hz, 2H); ^{13}C NMR (75 MHz, CDCl_3) δ 185.1, 145.7, 122.0, 48.2, 34.2; Anal. calcd for $\text{C}_9\text{H}_6\text{Br}_2\text{O}_2$: C 35.33; H 1.98; Found: C 35.63; H 2.14.

endo,endo-bicyclo[3.3.1]nona-3,7-diene- 2, 6-diol **150**



To a solution of dienone **94** (50 mg, 0.34 mmol), $\text{CeCl}_3 \cdot 7\text{H}_2\text{O}$ (251,5 mg, 0.68 mmol) and MeOH (1,7 mL) was added NaBH_4 in portions (4 x 6,5 mg, 0,68 mmol) over a period of 2 minutes at ambient temperature. The reaction mixture was stirred for 20 minutes and then quenched with HCl (1 mL, 1 M) and concentrated under reduced pressure to a volume of approximately 1 mL. Brine (5 mL) was added and the mixture was extracted with diethyl ether (5 x 5 mL). The combined organic phase was dried (MgSO_4) and concentrated *in vacuo* yielding a white solid crude. The product was isolated with flash chromatography (ethyl acetate/ petroleum ether, 8:2) affording 49 mg of **149** in 95% yield. ^1H -NMR (400 MHz, CDCl_3) δ 5.88 (ddd, J = 10.2, 5.4, 1.8 Hz, 2

H), 5.75 (m, 2 H), 4.50 (m, 2 H), 2.60 (m, 2 H), 1.83 (m, 2 H), 1.60 (bs, 2H);
¹³C-NMR (100.3 MHz, CDCl₃) δ 132.3, 128.2, 78.9, 42.1, 29.2; Anal. calcd for
C₉H₁₂O₂: C 71.03; H 7.95; Found: C 70.92; H 7.84.

8 References

1. Peters, J.A. *Synthesis* **1990**, 1-25.
2. Butkus, E. *Synlett* **2001**, 1827-1834.
3. Cuesta-Rubio, O.; Padron, A.; Castro, H. V.; Pizza, C.; Rastrelli, L. *J. Nat. Prod.* **2001**, *64*, 973-975.
4. Gustafson, K. R.; Blunt, J. W.; Munro, M. H. G.; Fuller, R. W.; McKee, T. C.; Cardellina, J. H., II.; McMahon, J. B.; Cragg, G. M.; Boyd, M. R. *Tetrahedron* **1992**, *48*, 10093-10102.
5. Winkelmann, K.; Heilmann, J.; Zerbe, O.; Rali, T.; Sticher, O. *J. Nat. Prod.* **2001**, *64*, 701-706.
6. Granier, Th.; Hanhart, A.; Bajgrowicz, J.A. United States Patent, No 7482313, **2009**.
7. Boeckmann, R. K., Jr.; Bershas, J. P.; Clardy, J.; Solheim, B. *J. Org. Chem.* **1977**, *42*, 3630-3633.
8. Schultz, A. G.; Dittami, J. P. *J. Org. Chem.* **1984**, *49*, 2615-2618.
9. Zefirov, N.S. *Russ. Chem. Rev.* 1975, *44*, 196-212.
10. Peters, J.A.; Baas, J.M.A.; Graaf Van De, B.; Vand der Toorn, J.M.; Van Bekkum, H. *Tetrahedron* **1978**, *34*, 3313-3323 and references therein.
11. Butkus, E.; Kubilius, R.; Stončius, S.; Žilinskas, A. *J. Chem. Soc. Perkin. Trans. 1* **1999**, 1431-1436.
12. Stetter, H.; Cärtner, J. *Chem. Ber.* **1966**, *99*, 925-929.
13. Shea, K. *Tetrahedron* **1980**, *36*, 1683-1715.
14. Marshall, J.A.; Faubl, H. *J. Am. Chem. Soc.* **1967**, *89*, 5965-5966.
15. Wiseman, J.R. *J. Am. Chem. Soc.* **1967**, *89*, 5966-5968.
16. Butkus, E.; Stončius, S.; Žilinskas, A. *Chirality* **2001**, *13*, 694-698.
17. Berg, U.; Butkus, E. *J. Chem. Res. (S)* **1994**, 356-357.
18. Otomaru, Y.; Tokunaga, N.; Shintani, R.; Hayashi, T. *Org. Lett.* **2005**, *7*, 307-310.
19. Valik, M.; Strongin, R.M.; Kral, V. *Supramol. Chem.* **2005**, *17*, 347-367.

20. Naemura, K.; Matsumura, T.; Komatsu, M.; Hirose, Y.; Chikamatsu, H. *Bull. Chem. Soc. Jpn.* **1989**, *62*, 3523-3530.
21. Naemura, K.; Fukunaga, R.; Yamanaka, M. *J. Chem. Soc., Chem. Commun.* **1985**, 1560-1561.
22. Marjo, Ch.E.; Bishop, R.; Craig, D.C.; Scudder, M.L. *Eur. J. Org. Chem.* **2001**, 863-873.
23. Mori, K.; Nagano, E. *Biocatalysis* **1990**, *3*, 25-36.
24. Johanson, T.; Carlquist, M.; Olsson, C.; Rudolf, A.; Frejd, T.; Gorwa-Grauslund, M.F. *Appl. Microbiol. Biotechnol.* **2008**, *77*, 1111-1118.
25. Mori, K.; Takayama, Sh.; Kido, M. *Bioorganic & Medicinal Chemistry* **1994**, *2*, 395-401.
26. Hagaki, N.; Sugahara, T.; Iwabuchi, Y. *Org. Lett.* **2005**, *7*, 4181-4183.
27. Hoffmann, G.; Wiartalla, R. *Tetrahedron Lett.* **1982**, *23*, 3887-3888.
28. Mayr, M.; Bataille, C. J. R.; Gosiewska, S.; Raskatov, J. A.; Brown, J. M. *Tetrahedron -Asymmetry* **2008**, *19*, 1328-1332.
29. Lightner, D.A.; Paquette, L.A.; Chayangkoon, P.; Lin, H.S.; Peterson J.R. *J. Org. Chem.*, **1988**, *53*, 1969-1973.
30. Friberg, A.; Johanson, T.; Franzen, J.; Gorwa-Grauslund, M. F.; Frejd, T. *Org. Biomol. Chem.* **2006**, *4*, 2304-2312.
31. Meerwein, H.; Schurmann, W. *Ann.* **1913**, *398*, 196-242.
32. Schaefer, P.S.; Honig, L.M. *J. Org. Chem.*, **1968**, *33*, 2655-2659.
33. Quast, H.; Witzel, M. *Liebigs Ann.* **1993**, 699-700.
34. Henkel, J. G.; Faith, W. C.; Hane, J. T. *J. Org. Chem.* **1981**, *46*, 3483-3486.
35. Butkus, E.; Berg, U. *J. Chem. Res.(S)* **1993**, 116-117.
36. Mitsuo, M.; Masahiro, N.; Shigeaki, O.; Osamu, M.; Genzoh, T.; Hiromu, K. *J. Chem. Technol. Biot.* **1998**, 281-284.
37. Naemura, K.; Ida, H.; Fukuda, R. *B. Chem. Soc. Jpn.* **1993**, *66*, 573-577.
38. Gerlach, H. *Helv. Chim. Acta* **1978**, *61*, 2773-2776.
39. Snatzke, G.; Wolfram, B. *Tetrahedron* **1972**, *28*, 655-662.

40. Steed, J. W.; Atwood, J. L. *Supramolecular Chemistry*; John Wiley & Sons, Ltd: Chichester, **2000**.
41. Goshe, A.J.; Crowley, J.D.; Bosnich, B. *Helv. Chim. Acta.* **2001**, *84*, 2971-2985.
42. Jeffrey, G. *An introduction to Hydrogen Bonding*, Oxford University Press, **1997**.
43. Nieckarz, R.J.; Oldridge, N.; Fridgen, T.D.; Li, G.P.; Hamilton, I.P.; McMahon, T.B. *J. Phys. Chem. A* **2009**, *113*, 644-652 and references cited therein.
44. Rochet, J.C.; Lansbury, P.T. Jr. *Curr. Opin. Struct. Biol.* **2000**, *10*, 60-68.
45. Ghosh, S.; Li, X.-Q.; Stepanenko, V.; Würthner, F. *Chem.-Eur. J.* **2008**, *14*, 11343-11357.
46. Jorgensen, W.L.; Pranata, J. *J. Am. Chem. Soc.* **1990**, *112*, 2008.
47. Pranata, J.; Wierscke, S.G.; Jorgensen, W.L. *J. Am. Chem. Soc.* **1991**, *113*, 2810-2819.
48. Murray, T.J.; Zimmerman, S.C. *J. Am. Chem. Soc.* **1992**, *114*, 4010-4011.
49. Sartorius, J.; Schneider, H.J. *Chem.-Eur. J.* **1996**, *2*, 1446-1452.
50. Cram, D.J. *Angew. Chem. Int. Ed.* **1986**, *25*, 1039-1057.
51. Zimmerman, S.C.; Mrksich, M.; Baloga, M. *J. Am. Chem. Soc.* **1989**, *111*, 8528-8530.
52. Beijer, F.H.; Kooijman, H.; Spek, A.L.; Sijbesma, R.P.; Meijer, E.W. *Angew. Chem. Int. Ed.* **1998**, *37*, 75-78.
53. Beijer, F.H.; Sijbesma, R.P.; Kooijman, H.; Spek, A.L.; Meijer, E.W. *J. Am. Chem. Soc.* **1998**, *120*, 6761-6769.
54. Hamilton, A.D.; Pant, N. *J. Chem. Soc. Chem. Commun.* **1988**, 765-766.
55. Murray, T.J.; Zimmerman, S.C. *Tetrahedron Lett.* **1995**, *36*, 7627-7630.
56. Fenniri, H.; Deng, B.-L.; Ribbe, A.E.; Hallenga, K.; Jacob, J.; Thiyagarajan, P. *Proc. Natl. Acad. Sci.* **2002**, *99*, 6487-6492.
57. Zimmerman, S.C.; Corbin, P.S. *Struct. Bonding* **2000**, *96*, 63-94.
58. Watson, J.D.; Crick, F.H.C. *Nature*, **1953**; *171*, 964-967.

59. Topal, M.D.; Fresco, J.R. *Nature*, **1976**, *263*: 285–289.
60. Sztanke, K.; Fidecka, S.; Kędzierska, E.; Karczmarzyk, Z.; Pihlaja, K.; Matosiuk D. *Eur. J. Med. Chem.*, **2005**, *40*: 127–134.
61. Beak, P.; Covington, J.B.; Smith, S.G.; White, J.M.; Zeigler, J.M. *J. Org. Chem.* **1980**, *45*, 1354-1362.
62. Ducharme, Y.; Wuest, J. D. *J. Org. Chem.* **1988**, *53*, 5787-5789.
63. Gallant, M.; Phan Viet Minh, T.; Wuest, J. D. *J. Am. Chem. Soc.* **1991**, *113*, 721-723.
64. Jónsson, S.; Solano Arribas, C.; Wendt, O. F.; Siegel, J. S.; Wärnmark, K. *Org. Biomol. Chem.* **2005**, *3*, 996-1001.
65. Breit, B.; Seiche, W. *J. Am. Chem. Soc.* **2003**, *125*, 6608-6609.
66. Suarez, M.; Lehn, J. M.; Zimmerman, S. C.; Skoulios, A.; Heinrich, B. *J. Am. Chem. Soc.* **1998**, *120*, 9526-9532.
67. Mourran, A.; Ziener, U.; Möller, M.; Suarez, M.; Lehn, J.-M. *Langmuir* **2006**, *22*, 7579-7586.
68. Elvidge, J.A.; Redman, A.P. *J. Chem. Soc.* **1960**, 1710-1715.
69. American Veterinary Medical Association (AVMA), Press Release, May 1, **2007**.
70. Coghlan A.; Reuters *New Scientist*, **2008**, September 23.
71. Seto, C.T.; Whitesides, G.M. *J. Am. Chem. Soc.* **1993**, *115*, 1330-1340.
72. Timmerman, P.; Vreekamp, R.H.; Hulst, R.; Verboom, W.; Reinhoudt, D.N.; Rissanen, K.; Udachin, K.A.; Ripmeester, J. *Chem.-Eur. J.* **1997**, *3*, 1823-1832.
73. Drain, C.M.; Russell, K.C.; Lehn, J.-M. *Chem. Commun.* **1996**, 337-339.
74. Meyer, H.; Bossert, F.; Horstmann, H. *Liebigs Ann. Chem.* **1978**, 1476–1482.
75. Bühlmann, P.; Badertscher, M.; Simon, W. *Tetrahedron* **1993**, *49*, 595-598.
76. Watson, J. D.; Crick, F. H. C. *Nature* **1953**, *171*, 964-967.
77. Abe, H.; Takase, M.; ZDoi, Y.; Matsumoto, Sh.; Furusyo, M.; Inouye, M. *Eur. J. Org. Chem.* **2005**, *14*, 2931-2940.

78. Brunsveld, L.; Folmer, J.B.; Meijer, E.W.; Sijbesma, R.P. *Chem. Rev.* **2001**, *101*, 4071–4098.
79. Corbin, P.S.; Zimmerman, S.C. *J. Am. Chem. Soc.* **1998**, *120*, 9710-9711.
80. Laffite, V.G.H.; Aliev, A.E.; Horton, P.N.; Hursthouse, M.B.; Bala, K.; Golding, P.; Hailes, H.C. *J. Am. Chem. Soc.* **2006**, *128*, 6544-6545.
81. Baruah, P.K.; Gonnade, R.; Phalgune, U.D.; Sanjayan, G.J. *J. Org. Chem.* **2005**, *70*, 6461-6467.
82. Sun, H.; Steeb, J.; Kaifer, A.; *J. Am. Chem. Soc.* **2006**, *128*, 2820-2821.
83. Lehn, J.-M. *Chem.-Eur. J.* **1999**, *5*, 2455-2463.
84. Hof, F.; Craig, S.L.; Nuckolls, C.; Rebek, J.Jr. *Angew. Chem. Int. Ed.* **2002**, *41*, 1488-1508.
85. Lucking, U.; Tucci, F.C.; Rudkevich, D.M.; Rebek, J.Jr. *J. Am. Chem. Soc.* **2000**, *122*, 8880-8889.
86. Balbo Block, M.A.; Kaiser, Ch.; Khan, A.; Hecht, S. *Top. Curr. Chem.* **2005**, *245*, 89-150.
87. Hecht, S.; Huc, I.; *Foldamers: Structures, Properties, and Applications*, Wiley-VCH, Weinheim, **2007**.
88. Ghadiri, M.R.; Granja, J.R.; Milligan, R.A.; McRee, D.E.; Khazanovich, N. *Nature* **1993**, *366*, 324-327
89. De Santis, P.; Morosetti, S.; Rizzo, R. *Macromolecules* **1974**, *7*, 52-58.
90. Granja, J.R.; Ghadiri, M.R. *J. Am. Chem. Soc.* **1994**, *116*, 10785-10786.
91. Vollmer, M.S.; Clark, T.D.; Steinem, C.; Ghadiri, M.R. *Angew. Chem. Int. Ed. Engl.* **1999**, *38*, 1598-1601.
92. Seebach, D.; Matthews, J.L.; Meden, A.; Wessels, T.; Baerlocher, C.; McCusker, L.B. *Helv. Chim. Acta.* **1997**, *80*, 173-182.
93. Clark, T.D.; Buehler, L.K.; Ghadiri, M.R. *J. Am. Chem. Soc.*, **1998**, *120*, 651-656.
94. Gauthier, D.; Baillargeon, P.; Drouin, M.; Dory, Y.L. *Angew. Chem. Int. Ed.*, **2001**, *40*, 4635-4638.

95. Ranganathan, D.; Lakshim, C.; Karle, I.L. *J. Am. Chem. Soc.* **1999**, *121*, 6103-6107.
96. Semetey, V.; Didierjean, C.; Briand, J.-C.; Aubry, A.; Guichard, G. *Angew. Chem. Int. Ed.*, **2002**, *41*, 1895-1897.
97. Gattuso, G.; Menzer, S.; Nepogodiev, S.A.; Stoddart, J.F.; Williams, D.J. *Angew. Chem. Int. Ed. Engl.*, **1997**, *36*, 1451-1454
98. Dalgarno, S.J.; Cave, G.W.V.; Atwood, J.L. *Angew. Chem. Int. Ed.* **2006**, *45*, 570-575.
99. Sakai, N.; Mareda, J.; Matille, S. *Acc. Chem. Res.* **2008**, *41*, 1354-1365.
100. Das, G.; Talukdar, P.; Matille, S. *Science* **2002**, *298*, 1600-1602.
101. Sundquist, W. I.; Klug, A. *Nature* **1989**, *342*, 825-829.
102. Mezzina, E.; Mariani, P.; Itri, R.; Masiero, S.; Pieraccini, S.; Spada, G.P.; Spinuzzi, F.; Davis, J.T.; Gottarelli, G. *Chem.-Eur. J.* **2001**, *7*, 388-395.
103. González-Rodríguez, D.; van Dongen, L.J.J.; Lutz, M.; Spek, A.L.; Schenning, A.P.H.J.; Meijer, E.W. *Nature Chem.* **2009**, *1*, 151-155.
104. Fenniri, H.; Deng, B.-L.; Ribbe, A.E. *J. Am. Chem. Soc.* **2002**, *124*, 11064-11072.
105. Dan Pantos, G.; Pengo, P.; Sanders, J.K.M. *Angew. Chem. Int. Ed.* **2007**, *46*, 194-197.
106. Dan Pantos, G.; Wietor, J.-L.; Wietor, Sanders, J.K.M. *Angew. Chem. Int. Ed.* **2007**, *46*, 2238-2240.
107. Stončius, S.; Butkus, E.; Žilinskas, A.; Larsson, K.; Öhrström, L.; Berg, U.; Wärnmark, K. *J. Org. Chem.* **2004**, *69*, 5196-5203.
108. Pentfold, B.R. *Acta Crystallogr.* **1953**, *6*, 591-600.
109. Brienne, M.-J.; Gabard, J.; Leclercq, M.; Lehn, J.-M.; Cesario, M.; Pascard, C.; Cheve, M.; Dutruc-Rosset, G. *Tetrahedron. Lett.* **1994**, *35*, 8157-8160.
110. Castillo, S.; Ouadahi, H.; Herault, V. *Bull. Soc. Chim. Fr.* **1982**, *2*, 257-261.
111. Heber, D.; Stoyanov, E.V. *Synlett* **1999**, *11*, 1747-1748.

112. Martin, R. B. *Chem. Rev.* **1996**, *96*, 3043-3064.
113. Hammes, G. G.; Park, A. C. *J. Am. Chem. Soc.* **1969**, *91*, 956-961.
114. Hammes, G. G.; Spivey, H. O. *J. Am. Chem. Soc.* **1966**, *88*, 1621-1625.
115. Ts'o, P. O. P.; Chan, S. I. *J. Am. Chem. Soc.* **1964**, *86*, 4176-4181.
116. Rodger, A.; Nordén, B. *Circular Dichroism & Linear Dichroism*: Oxford University Press: Cambridge, UK, **1999**.
117. van Gestel, J.; Palmans, A.R.A.; Titulaer, B.; Vekemans, J.A.J.M.; Meijer, E.W. *J. Am. Chem. Soc.* **2005**, *127*, 5490-5494.
118. Zhao, D.; Moore, J. S. *Org. Biomol. Chem.* **2003**, *1*, 3471-3491.
119. Meerwein, H.; Schürmann, W. *Liebigs Ann.* **1913**, *398*, 196-242.
120. Beckmann, E.; Bahr, N.; Cullmann, O.; Yang, F.; Kegel, M.; Vogtle, M.; Exner, K.; Keller, M.; Knothe, L.; Prinzbach, H. *Eur. J. Org. Chem.* **2003**, 4248-4264
121. Knott, P.A.; Mellor, J.M. *J. Chem. Soc. C.* **1971**, 670-674.
122. Quast, H.; Becker, Ch.; Geißler, E.; Knoll, K.; Peters, E.-M.; Peters, K.; von Schnering, H.G. *Liebigs Ann.* **1994**, 109-120.
123. Nicolaou, K.C.; Montagnon, T.; Baran, P.S.; Zhong, Y.-L. *J. Am. Chem. Soc.* **2002**, *124*, 2245-2258.
124. Nicolaou, K.C.; Zhong, Y.-L.; Baran, P.S. *J. Am. Chem. Soc.* **2000**, *122*, 7596-7597.
125. Barton, D.H.R.; Godfrey, Ch.R.A.; Mozycki, J.W.; Motherwell, W.B.; Ley, S.V. *J. Chem. Soc. Perkin Trans. 1.* **1982**, 1947-1952.
126. Rappoport, Z.; Marek, I. *The chemistry of organozinc compounds: R-Zn*, Wiley-VCH, **2006**.
127. "Polyfunctional Zinc Organometallics for Organic Synthesis": P. Knochel, H. Leuser, L.-Z. Gong, S. Perrone, F. F. Kneisel, *Handbook of Functionalized Organometallics*, Vol. 1, Wiley-VCH, Weinheim, **2005**.
128. *Organozinc Reagents*, Oxford University Press, New York, **1999**.
129. Huo, S. Q. *Org. Lett.* **2003**, *5*, 423-425.

130. Knochel, P.; Rozema, M.J.; Tucker, C.E. *Organocopper reagents*, Oxford University press, Oxford, **1994**.
131. Knochel, P.; Yehn, N.C.P.; Berk, S.C.; Talbert, J. *J. Org. Chem.* **1988**, *53*, 2390-2392.
132. Quast, H.; Geißler, E.; Herkert, T.; Knoll, K.; Peters, E.-M.; Peters, K.; von Schnering, H.G. *Chem. Ber.* **1993**, *126*, 1465-1475.
133. House, H.O.; Auerbach, R.A.; Gall, M.; Peet, N.P. *J. Org. Chem.* **1973**, *38*, 514-522.
134. Mander, L.N.; Sethi, S.P. *Tetrahedron Lett.* **1983**, *24*, 5425-5428.
135. Crabtree, S.R.; Mander, L.N.; Sethi, S.P. *Organic Synthesis* **1998**, *Coll. Vol. 9*, 619.
136. House, H.O.; Fisher, W.F., Jr. *J. Org. Chem.* **1969**, *34*, 3615-3618.
137. Kim, S.; Park, J.H.; Jon, S.Y. *Bull. Korean Chem. Soc.* **1995**, *16*, 783-786.
138. Eriksson, M.; Iliefski, T.; Nilsson, M.; Olsson, Th. *J. Org. Chem.* **1997**, *62*, 182-187.
139. Kim, S.; Park, J.H. *Synlett*, **1995**, 163-164.
140. Kim, S.; Lee, J.M. *Tetrahedron Lett.* **1990**, *31*, 7627-7630.
141. Agami, C.; Platzer, N.; Puchot, C.; Sevestre, H. *Tetrahedron* **1987**, *43*, 1091-1098.
142. Garg, S.K.; Kumar, R.; Chakraborti, A.K. *Synlett* **2005**, *9*, 1370-1374.
143. Chu, Ch.-M.; Gao, Sh.; Sastry, M.N.V.; Yao, Ch.-F. *Tetrahedron Lett.* **2005**, *46*, 4971-4974.
144. Ito, H.; Takenaka, Y.; Fukunishi, Sh.; Iguchi, K. *Synthesis* **2005**, *18*, 3035-3038.
145. Krasovskiy, A.; Malakhov, V.; Gavryushin, A.; Knochel, P. *Angew. Chem. Int. Ed.* **2006**, *45*, 6040-6044.
146. Metzger, A.; Piller, F. M.; Knochel, P. *Chem. Commun.* **2008**, 5824-5826.
147. Clayden, J. *Organolithiums: Selectivity for Synthesis*, Pergamon, **2002**.
148. Clarebeau, M.; Krief, A. *Tetrahedron Lett.* **1985**, *26*, 1093-1096.
149. Dowd, P, Kennedy, P. *Synth. Commun.* **1981**, *11*, 935-941.

150. Schlessinger, R.H.; Beberitz, G.R.; Lin, P.; Poss, A.Y. *J. Am. Chem. Soc.* **1985**, *107*, 1777-1778.
151. Bull, S.D.; Davies, S.G.; Smith, A.D. *Tetrahedron: Asymmetry* **2001**, *12*, 2941-2945.
152. Chern, Ch.-Y.; Huang, Y.-P.; Kan, W.M. *Tetrahedron Lett.* **2003**, *44*, 1039-1041.
153. Ohgi, T.; Hecht, S.M. *J. Org. Chem.* **1981**, *46*, 1232-1234.
154. Webster, F.X.; Millar, J.G.; Silverstein, R.M. *Tetrahedron Lett.* **1986**, *27*, 4941-4944.
155. Hansen, M.M.; Harkness, A.R.; Khau, V.V.; Martinelli, M.J.; Deeter, J.B. *Tetrahedron: Asymmetry* **1996**, *7*, 2515-2518.
156. Keizer, H.M.; Sijbesma, R.P.; Meijer, E.W. *Eur. J. Org. Chem.* **2004**, 2553-2555.
157. Wilk, W.; Nören-Müller, A.; Kaiser, M.; Waldmann, H. *Chem.-Eur. J.* **2009**, *15*, 11976-11984.
158. Michel, P.; Rassat, A. *J. Org. Chem.* **2000**, *65*, 2572-2573.
159. Cope, A.C.; Fischer, B.S.; Funke, W.; McIntosh, J.M.; McKerverey, M.A. *J. Org. Chem.* **1969**, *34*, 2231-2234.
160. Rudolph, J.; Reddy, L.K.; Chiang, J.P.; Sharpless, K.B. *J. Am. Chem. Soc.* **1997**, *119*, 6189-6190.
161. Pillai, U.R.; Sahle-Demessie, E.; Varma, R.S. *Tetrahedron Lett.* **2002**, *43*, 2909-2911.
162. Xie, G.; Xu, L.; Hu, J.; Ma, Sh.; Hou, W.; Tao, F. *Tetrahedron Lett.* **1988**, *29*, 2967-2968. 163. Travis, B.R.; Sivakumar, M.; Hollist, G.O.; Borhan, B. *Org. Lett.* **2003**, *5*, 1031-1034.
164. Hashimoto, N.; Kanda, A. *Org. Proc. Res. Dev.* **2002**, *6*, 405-406.
165. Abdel-Magid, A.F.; Mehrman, S. *Org. Proc. Res. Dev.* **2006**, *10*, 971-1031.
166. Panchal, B.M.; Einhorn, C.; Einhorn, J. *Tetrahedron Lett.* **2002**, *43*, 9245-9248.

167. Samijlenko, S.P.; Potyahaylo, A.L.; Stepanyugin, A.V.; Hovorun, P.M. *Ukr. Biokhim. Zh.* **2003**, *75*, 42-48.
168. Tulub, A.A.; Semenov, S.G.; Stelsenko, A.I.; Yudovich, E.E. *Theor. Exp. Chem.* **1988**, *24*, 26-32.
169. Hélène, C.; Douzou, P.C.R. *Hebd. Seances Acad. Sci.* **1964**, *259*, 4853-4856.
170. Hélène, C.; Douzou, P.C.R. *Hebd. Seances Acad. Sci.* **1964**, *259*, 4387-4390.
171. Stewart, J. J. P. *J. Comput. Chem.* **1989**, *10*, 221-264.
172. Stewart, J. J. P. *J. Comput. Chem.* **1989**, *10*, 209-220.
173. Rocha, G. B.; Freire, R. O.; Simas, A. M.; Stewart, J. J. P. *J. Comput. Chem.* **2006**, *27*, 1101-1111.
174. Becke, A. D. *J. Chem. Phys.* **1993**, *98*, 5648-5652.
175. Rakotondradany, F.; Whitehead, A.; Lebuis, A. M.; Sleiman, H. F. *Chem.-Eur. J.* **2003**, *9*, 4771-4780.
176. Schalley, C. *Analytical Methods in Supramolecular Chemistry*; Wiley-VCH: Weinheim, **2007**.
177. Timmerman, P.; Weidmann, J. L.; Jolliffe, K. A.; Prins, L. J.; Reinhoudt, D. N.; Shinkai, S.; Frish, L.; Cohen, Y. *J. Chem. Soc. Perkin Trans. 2* **2000**, 2077-2089.
178. Mathias, J.P.; Seto, C.T.; Simanek, E.E.; Whitesides, G.M. *J. Am. Chem. Soc.* **1994**, *116*, 1725-1736.
179. Cates, M.E. *Macromolecules* **1987**, *20*, 2289-2296.
180. Frelek, J.; Szczepek, W.J.; Neubrech, S.; Schultheis, B.; Brechtel, J.; Kuball, H.-G. *Chem.-Eur. J.* **2002**, *8*, 296-305.
181. Grabowski, J.K.; "Conformations, Chiroptical and Related Spectral Properties of Enones", in *The Chemistry of Enones*, John Wiley and Sons, **1989**, pp. 55-105.
182. Doerner, T.; Gleiter, R.; Robbins, T.; Chayangkoon, P.; Lightner, D.A. *J. Am. Chem. Soc.* **1992**, *114*, 3235-3241.

183. Gawronski, J.K.; Liljefors, T.; Norden, B. *J. Am. Chem. Soc.* **1979**, *101*, 5515-5522.
184. Frelek, J.; Szczepek, W.J.; Weiß, H.P.; Reiß, G.J.; Frank, W.; Brechtel, J.; Schultheis, B.; Kuball, H.-G. *J. Am. Chem. Soc.* **1998**, *120*, 7010-7019.
185. Frelek, J.; Szczepek, W.J.; Weiss, H.P. *Tetrahedron: Asymmetry* **1995**, *6*, 1419-1430.
186. Francis, J.T.; Hitchcock, A.P. *J. Phys. Chem.* **1994**, *98*, 3650-3657.
187. Berova, N.; Di Bari, L.; Pescitelli, G. *Chem. Soc. Rev.* **2007**, *36*, 914-931.
188. Schmidt, G.M.J. *Pure Appl. Chem.* **1971**, *27*, 647-679.
189. Gavezzotti, A.; Filippini, G. *J Phy Chem* **1994**, *98*, 4831-4837.
190. Nangia, A.; Desiraju, G. *Top. Curr. Chem.* **1998**, *198*, 57-95.
191. Öhrström, L.; Larsson, K. *Molecular-Based Materials: The Structural Network Approach*; Elsevier B.V.:Amsterdam, **2005**.
192. Bishop, R. *Acc. Chem. Res.* **2009**, *42*, 67-78.
193. During the preparation of manuscript, a related study appeared in literature: Nguyen, V.T.; Chan, I.Y.H.; Bishop, R.; Craig, D.C.; Scudder, M.L. *New J. Chem.* **2009**, *8*, 1736-1741.
194. O’Keeffe, M.; Peskov, M.A.; Ramsden, S.; Yaghi, O.M. *Acc. Chem. Res.*, **2009**, *41*, 1782–1789.
195. O’Keeffe, M.; Yaghiand, O.M.; Ramsden, S. *Reticular Chemistry Structure Resource*, Australian National University Supercomputer Facility, <http://rcsr.anu.edu.au/>, **2009**.
196. Baburin, I.A.; Blatov, V.A.; Carlucci, A.; Ciani G.; Proserpio, D.M. *Cryst. Growth Des.* **2008**, *8*, 519–539.
197. Öhrström, L.; Larsson, K. *Dalton. Trans.* **2004**, *3*, 347-353.
198. Reddy, C. M.; Kirchner, M. T.; Gundakaram, R. C.; Padmanabhan, K. A.; G. R. Desiraju. *Chem. Eur. J.* **2006**, *12*, 2222-2234.
199. Geiser, D.; Höcker, H. *Polymer Bull.* 1980, *2*, 591-597.
200. Marwell, E.N.; Seubert, J.; Sturmer, D.; Federici, N. *J. Org. Chem.* 1970, *35*, 396-400.

201. Klimova, T. A.; Krayushkin, M. M.; Sevostyanova, V. V.; Novikov, S. S.; Karpenko, N. F. *Bulletin Of The Academy Of Sciences Of The USSR Division Of Chemical Science* **1975**, *24*, 1450-1453.